Alma Mater Studiorum - Università di Bologna

DOTTORATO DI RICERCA IN

CHIMICA

Ciclo XXXII

Settore Concorsuale: 03/C2

Settore Scientifico Disciplinare: CHIM/04

NEW FUNCTIONAL POLYTHIOPHENE BASED MATERIALS: FINE-TUNING OF PHOTOVOLTAIC OR CHIROPTICAL PROPERTIES

Presentata da: Martina Marinelli

Coordinatore Dottorato

Prof.ssa Domenica Tonelli

Supervisore

Prof.ssa Elisabetta Salatelli

Co-Supervisore

Prof. Massimiliano Lanzi

Esame finale 2020

Abstract

There is a remarkable level of interest in the development of π-conjugated polymers (ICPs) which have been employed, thanks to their promising optical and electronic properties, in numerous applications including photovoltaic cells, light emitting diodes and thin-film transistors. Although high power conversion efficiency can be reached using poly(3-alkylthiophenes) (P3ATs) as electron-donating materials in polymeric solar cells of the Bulk-Heterojunction type (BHJ), their relatively large band gap limits the solar spectrum fraction that can be utilized.

The research work described in this dissertation thus concerns the synthesis, characterization and study of the optical and photoactivity properties of new organic semiconducting materials based on polythiophenes. In detail, various narrow band gap polymers and copolymers were developed through different approaches and were characterized by several complementary techniques, such as gel permeation chromatography (GPC), NMR spectroscopy, thermal analyses (DSC, TGA), UV-Vis/PL spectroscopy and cyclic voltammetry (CV), in order to investigate their structural and chemical/photophysical properties. Moreover, the polymeric derivatives were tested as active material in air-processed organic solar cells.

My activity has also been devoted to investigate the behaviour of polythiophenes with chiral side chain, that are fascinating materials capable to assume helix supramolecular structures, exhibiting optical activity in the aggregated state. In this framework, part of a project concerning the study of chiral main chain conjugated block copolymers obtained by controlled polymerization mechanism, was carried out during a three-months stay at the Katholieke Universiteit of Leuven (Belgium).

The present thesis is organized in chapters the content which can be summarized as follows:

Chapter I. General introduction on the topic of conjugated polymers, followed by an overview on the synthesis and properties of polythiophenes, with a special focus on their application in organic solar cells.

Chapter II. New 4,7-bis(3-alkylthiophen-2-yl)benzo(2,1,3)thiadiazole monomers, functionalized with different alkyl side chains, have been synthesized through a palladium-catalyzed Suzuki cross-coupling reaction and then polymerized by oxidative coupling with

$FeCl_3$. These newly synthesized *main-chain* electron donor-acceptor systems have been characterized and tested as active media in single component organic solar cells.

Chapter III. Starting from soluble, regioregular and regiorandom homopolymeric precursors, new alkylthiophenic copolymers bearing the bromine atom and C_{60}-fullerene group at the end of a hexylic side chain inserted at position 3 of thiophene have been prepared. After investigation of the structural and photophysical properties of the above mentioned derivatives, the copolymers were also tested as photoactive layers in organic solar devices as *double-cable* materials.

Chapter IV. An investigation about the effect of regioregularity on the chiral behaviour of optically active polythiophenes bearing S or O as the connecting atom to the optically active side chain substituent was carried out. The polymers were obtained by regiospecific organometallic coupling (GRIM method) or non-regiospecific oxidative coupling with $FeCl_3$, starting respectively from chiral mono- or bithiophenic monomers; their optical activity has been evaluated by circular dichroism (CD), upon aggregation of the macromolecules by gradual addition of poor solvent to their chloroform solutions.

Chapter V. Three different conjugated PF-*b*-PT copolymers were synthesized via Suzuki Catalyst Transfer Condensative Polymerization (SCTCP) and characterized via GPC and ^{1}H-NMR spectroscopy. With the final aim to confirm the hypothesis that block copolymers can be designed to exhibit a unique set of properties by transferring the properties of one block to the other, the aggregation behaviour of the copolymers was studied by solvatochromism experiments.

Chapter VI. Overview of the main synthetic attempts and results obtained from the development of water-soluble conjugated polymers, bearing both neutral and ionic groups in the side chain, with the final purpose to test them as photoactive components in organic solar cells prepared through more sustainable process.

Table of contents

Chapter I

Chapter I: GENERAL INTRODUCTION

1. Conjugated polymers

1.1. Overview

Intrinsically conductive polymers (ICPs)[1,2,3] are an important subclass of materials which combine the intrinsic nature of polymers, such as lightness, flexibility and solution-processability, with the ability to conduct electrical current upon appropriate doping.
In fact, as a consequence of the extended π-conjugated system along their backbone, with alternating single and double bonds, these materials could be a real and promising alternative for the development of organic electronic devices. Moreover, in addition to have good charge transport and broad optical absorption properties, these polymers can be easily tuned by simple structural modifications. For example, the attachment of electron-donating and/or electron withdrawing functional groups along the conjugated polymer backbone can affect their ionization potential and therefore the HOMO and LUMO (the highest occupied and lowest unoccupied molecular orbitals, respectively) levels.

The first conductivity finding was obtained in the appropriately doped polyacetylene (PAc), whose polyene structure guarantees an extended conjugated system and conductivity values similar to a metal. However, since polyacetylene has no commercial application, due to its insolubility and high reactivity towards air and humidity, the attention has been focused on conjugated polymers derived from cycles and heterocycles.[4,5]

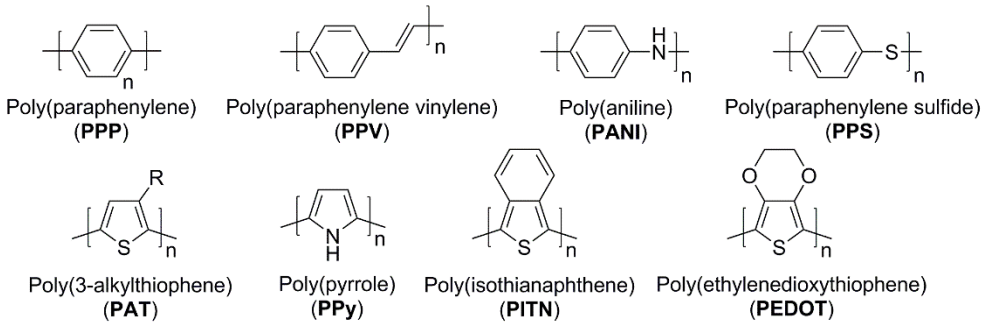

Figure 1. Structures of the main conjugated polymers used in organic electronics.

In these polyaromatic and polyheteroaromatic systems, the sp^2 hybridized carbon atoms in the backbone have unhybridized p_z orbitals perpendicular to them. The possibility to rotate

of the σ-bonds of the backbone leads the conjugated polymers to assume the most favored and planar conformation, in order to obtain the overlapping of the p_z orbitals of the major amount of single units and thus extends the conjugation segment, also called conjugation length, of these polymers.

An overview of the main ICPs, with their structures, is shown in Figure 1.

1.2. Conductivity and charge transport

As previously said, the phenomenon of semi-conductivity in polymers depends on their electronic structure and can be explained by the *"band model"* developed for inorganic semiconductors.

By increasing the number of conjugated bonds, an alternation of simple (σ) and double bonds (π) which - by means of a resonance effect - can be delocalized along the structure, the number of binding (π) and anti-binding (π*) orbitals increases until the formation of a two kind of quasi-isoenergetic levels: the valence and conduction band. This leads to a higher lying HOMO level and a lower lying LUMO level with a consequent reduction of the energy gap (Eg), that is the quantity of energy that separate the bands (Figure 2).[6]

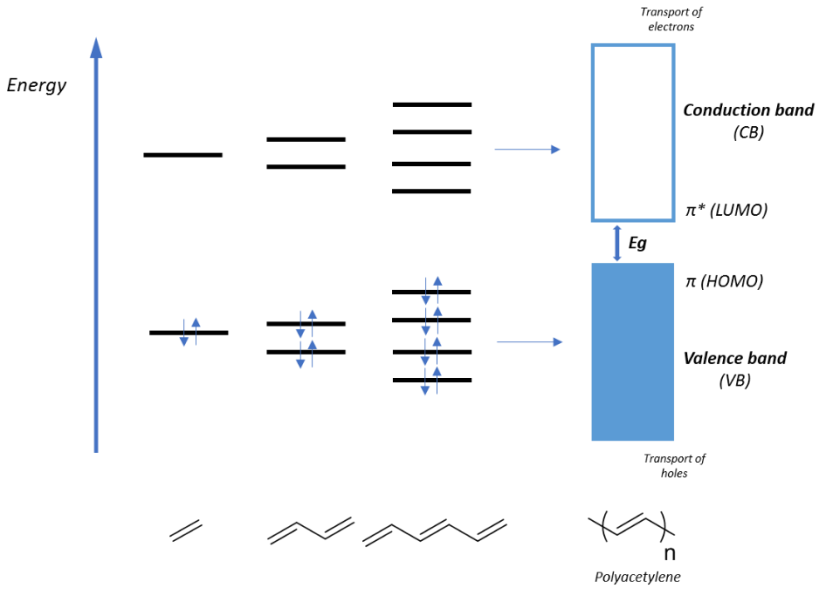

Figure 2. Formation of the valence (VB) and conduction band (CB) in conjugated polymers.

The decrease of the Eg, acting on the conjugation length and on the other factors that will be better discussed in the following chapters, is necessary to guarantee a

sufficiently high conductivity to favor and promote the passage of the excited electron from the valence to the conduction band. In the case of conducting metals, the Eg can be considered zero, as the two bands are basically overlapped, and therefore the maximum conductivity is achieved; while for insulating materials the values of Eg are too high to allow the promotion of the electrons to the conduction band. Even if the π-conjugated polymers are considered semiconductors, it is necessary to distinguish between their undoped and doped forms: in fact, the bandgap of undoped ICPs is still relatively large (~ 3 to 6 eV) and hence they show low conductivity (~ 10^{-7} to 10^{-11} $S \cdot cm^{-1}$) when compared to classic inorganic semiconductors. However, upon doping (paragraph 1.3), this gap can be reduced (~ 1 eV) and the conductivity increases by several orders of magnitude (~ 10^{-5} to 10^{3} $S \cdot cm^{-1}$).[7]

Since charges can be transported along the polymer backbone through the p_z orbitals, the charge transport in organic semiconducting materials generally takes place by an intra-chain mechanism. On the other hand, the tendency of supramolecular structures to self-assemble by π-π stacking also leads to inter-chain transport phenomena (hopping).[8]

Unfortunately, the conductivity of these materials is usually affected by the presence of a partially extended conjugation (presence of structural defects, i.e. sp^3 carbon), in addition to a limited planarity of the structure (free rotation of the simple bonds that allows the assumption of many conformations), with the presence of impurities and regio-irregularities (head-to-head and tail-to-tail junctions) along the chain.

1.3. Doping

The conductivity in organic compounds is usually enhanced by doping, a procedure which increases charge mobility through oxidation (p-doping) and reduction (n-doping) processes. Doping can be carried out by several methods, such as electrochemical doping, chemical doping, photo-doping and charge-injection doping.

First, the conductivity nature in polymers differs from that of inorganic semiconductors since the doping process is reversible and involves charge transfers, due to the partial or total oxidation/reduction of the macromolecule. In fact, in an inorganic semiconductor, where no charge transfers occur, doping involves the insertion of the doping species directly inside the semiconductor-lattice, forming electron-rich and electron-deficient sites. Furthermore, reversible ionization reactions of the polymer are possible because π-conjugated polymers have high values of electron affinity (EA) and low ionization

potentials (IP), that allow the insertion and removal of electrons with acceptable amounts of energy.

For this reason, acting as an electron source or electron sink, conjugated polymers can be easily p-doped (oxidized) and n-doped (reduced) by electrochemical doping. In chemical doping, instead, the partially oxidation or reduction of material is obtained by the use of oxidizing and reducing agents. The most commonly used p-doping species are Lewis acids ($AlCl_3$, $FeCl_3$), halogens (I_2, Br_2) and strong protonic acids, while alkaline metals in gas phase (Na, K) or liquid NH_3 are the most reductive dopants. However, we always obtain a charge complex in which the charge of polymers is balanced by a counter-ion.

As long as photo-doping in conjugated polymers involves locally oxidation/reduction by photo-absorption, it is also possible to generate – by application of appropriate potential – and inject charge carriers from suitable metal contact directly into the π and π* bands.[9]

Although in inorganic semiconductors the charge is directly transported by electrons, in π-conducting polymers charge carriers are radical cations/anions (in oligomers) or *polarons* and *bipolarons*, cationic or anionic, depending on the type of doping performed.

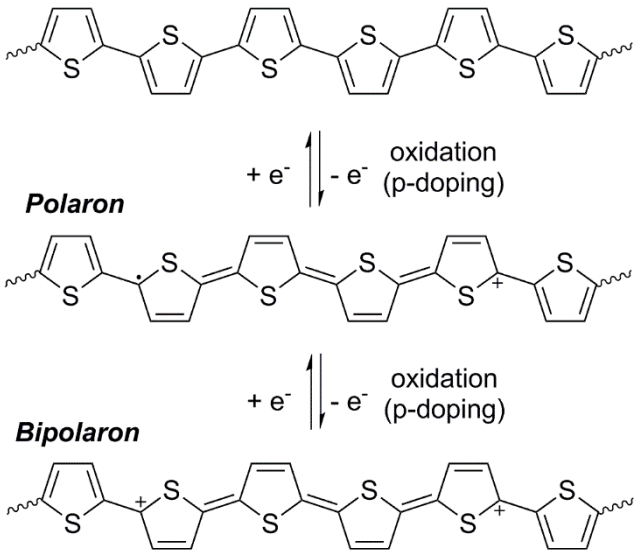

Figure 3. Formation of polaron and bipolaron in polythiophene.

For instance, when the polymer is oxidized (p-doping), a π electron is excited from VB to CB, leaving a hole and generating a radical cation. Being very unstable, the radical cation is delocalized by resonance, with charge separation and creation of a quinoid structure called polaron, which extends along four or five rings of the polymer. In case of high

doping, the formation of a di-cation known as bipolaron is also possible, caused by the interaction of two radical cations.

Both polaron and bipolaron can move along the polymer backbone producing delocalized structural deformations (quinoid forms), which result in the creation of real bipolaron bands and an overall reduction of the band gap.[10]

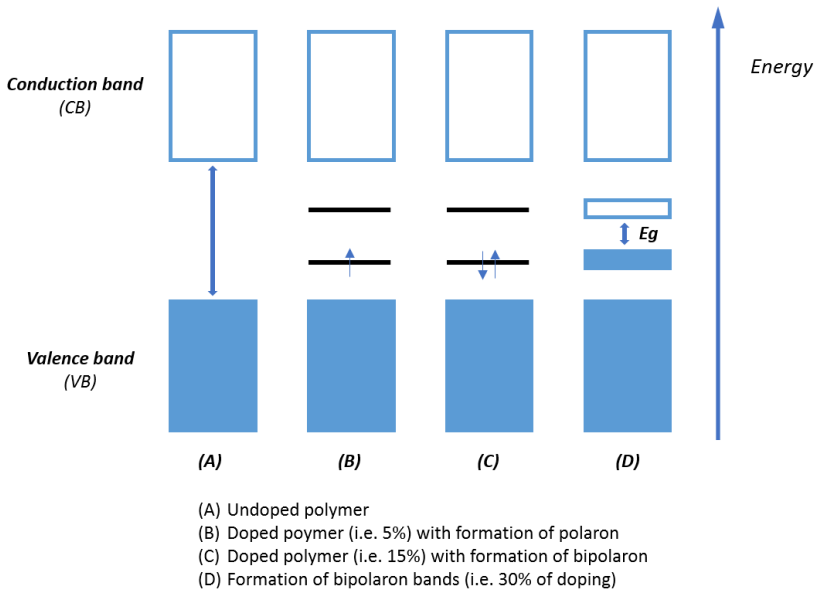

Figure 4. Change in band gap of a π-conjugated polymer upon doping.

Therefore, in addition to improve the conductivity of π-conjugated polymers by formation of charge carriers, polarons and bipolarons, the doping process also involves electrochromism in the material. The polymer, that shows different colours depending on its state of oxidation, has generally a red-orange colour in neutral form, turning in blue-green after doping, since the increase in planarization involves less energy and thus a red-shift of the absorption wavelength.

2. Polyalkythiophenes

2.1. Structures and characteristics

Among all the intrinsically π-conjugated polymers previously mentioned (paragraph 1.1), polythiophenes (PTs)[11] are definitely the most studied and used electroactive semiconducting materials.

Thiophene-based polymers are not only good electrical conductors in the doped state and light-emitters upon irradiation, but they are also materials combining low synthesis costs with unique properties, such as high stability, heat resistance and low toxicity.

Polythiophene is a polyheterocycle in which the rings are linked together through α positions and, depending on the synthesis method used, they can exist in different forms among which the semi-crystalline is the most common. However, polythiophene is infusible and cannot be processed, since it decomposes before melting and it is insoluble in the most common organic solvents. To ensure processability, β-thiophene alkyl side-chain functionalization is necessary to reduce the packing and the interaction between the polythiophene chains, obtaining the so-called poly(3-alkyl)thiophenes (P3ATs). On the other hand, the insertion of alkyl side chains determines a series of effects listed below.

Long and flexible side chains act as internal plasticizers and they determine an increase in solubility and therefore in processability, but the steric hindrance introduced by them leads to a decrease in the planarity of the aromatic structure and a reduction of the charge delocalization along the backbone. This affects the extension of the conjugation, modifying the redox behaviour, increasing the band gap value and, consequently, decreasing the polymer conductivity. For this reason, it is clear that is fundamental to choose the most suitable chain length, which have confirmed to be between 4-6 carbon atoms.

Since the asymmetric nature of 3-alkylthiophene monomer, α-α couplings between thiophene units are favored and three different isomeric forms are possible upon cross-coupling, obtaining head-to-tail (HT), head-to-head (HH) and tail-to-tail (TT) junctions (Figure 5). Poly(3-alkyl)thiophenes that contain significant amount of HH and TT couplings are called *regioirregular*, while polymers that contain only HT junctions are considered *regioregular*.

The presence or absence of regioregularity strongly affect properties and behaviour of the material, as the exclusive presence of HT couplings gives a higher conformational order

and, afterward, leads to an enhanced planarity, high crystallinity and, above all, better final electrical properties.

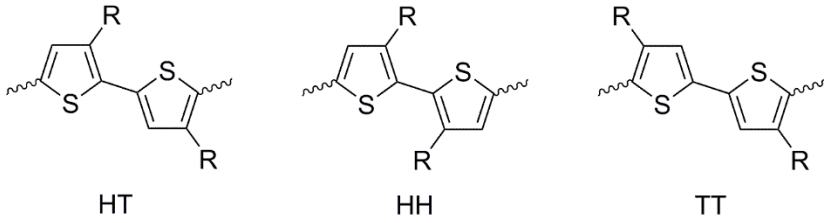

Figure 5. The three possible regioisomeric dyads in poly(3-alkyl)thiophenes.

2.2. Synthesis of PTs

Polythiophenes are obtained from β-substituted and α-functionalized thiophene monomers by electrochemical or chemical polymerization, including transition metal-catalyzed polymerization and oxidative polymerization. Furthermore, the synthesis routes can also be classified as regio or non-regiospecific, depending on whether head-to-tail polymers are obtained or not.[12]

The non-regiospecific *electrochemical polymerization*,[13] the first used in the production of polythiophenes, can be employed for monomers that in the presence of a potential give reactive radical ion intermediates as a consequence of their oxidation. Although it could be possible to cover conductive materials with controlled thicknesses of polymeric film, low yields and not well-defined structures are obtained.

The polymerization, which is usually carried out in a three-electrode system in a solution of the monomer, solvent and electrolyte, takes place directly on the electrode and leads to the complete exhaustion of the starting monomer since it is more easily oxidizable than the resulting polymer. The mechanism involves several steps of oxidation and formation of radical-cations, followed by coupling and re-aromatization - due to the loss of protons - with continuous oxidation of the neutral forms (Scheme 1).

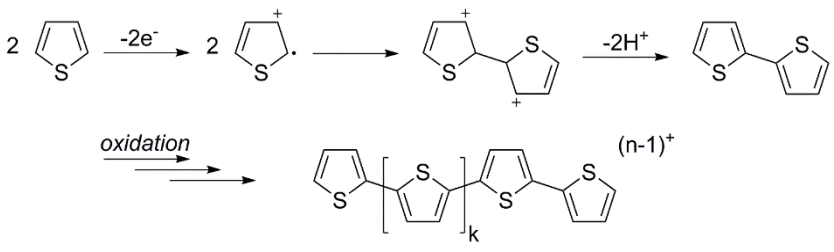

Scheme 1. Mechanism of electrochemical polymerization.

On the other hand, *chemical polymerization* involves the use of coupling reactions which allow more options to modify the backbone through different monomers. Not only is large-scale synthesis possible, it also allows to obtain low polydispersity index with desired molecular weights, as well as the possibility of post-polymerization by chemical modification.

2.2.1. Transition metal-catalyzed polymerizations

Despite many disadvantages are connected to the use of transition metal-catalyzed polymerizations,[14,15] such as low and strictly controlled temperatures, dry conditions and long times, their development introduced the regiochemical control of head-to-tail couplings in P3ATs.

In particular, starting from 2-bromo-5-bromomagnesium-3-dodecylthiophene, in presence of [1,3-bis(diphenylphosphino)propane]dichloronickel(II) [Ni(dppp)Cl_2] as a catalyst, the first synthesis of regioregular poly(3-alkyl)thiophene (~ 91% of HT dyads) has been carried out through Kumada coupling by ***McCullough and Loewe*** in 1992 (Scheme 2a). However, even though the regioregularity degree was further improved to ~ 98-100% by McCullough and coworkers, the working conditions need to be respected with extreme accuracy, as the final regioregularity depends on the isomeric purity of the two intermediates.

In the meanwhile, ***Rieke and Chen*** also developed another method which is based on the selective oxidative addition of 2,5-dibromo-3-alkylthiophene to an extremely reactive Zn (Zn *) known as Rieke zinc reagent (Scheme 2b). Satisfactory yields can be obtained but similarly to the McCullough method, the temperature control and above all the choice of the catalyst are of extremely importance, since the regiospecificity of the reaction is linked to its selectivity.

For this reason, a breakthrough variant of this polymerization, the ***Grignard Metathesis (GRIM) Method***,[16] has been developed by McCullough and coworkers in 1999. Since analytically pure and highly regioregular P3ATs can be obtained, GRIM method is indeed a clear improvement of the technique, due to its simplicity, cost-effectiveness and absence of cryogenic temperatures.

Starting from 2,5-dibromo-3-alkylthiophene, this method involves a magnesium-bromine exchange reaction (Grignard metathesis) - by treatment with alkylmagnesium bromide - and usually proceeds with the polymerization of the reaction mixture, in

presence of catalytic amount of Ni(dppp)Cl_2, at room temperature or at solvent reflux, (Scheme 2c).

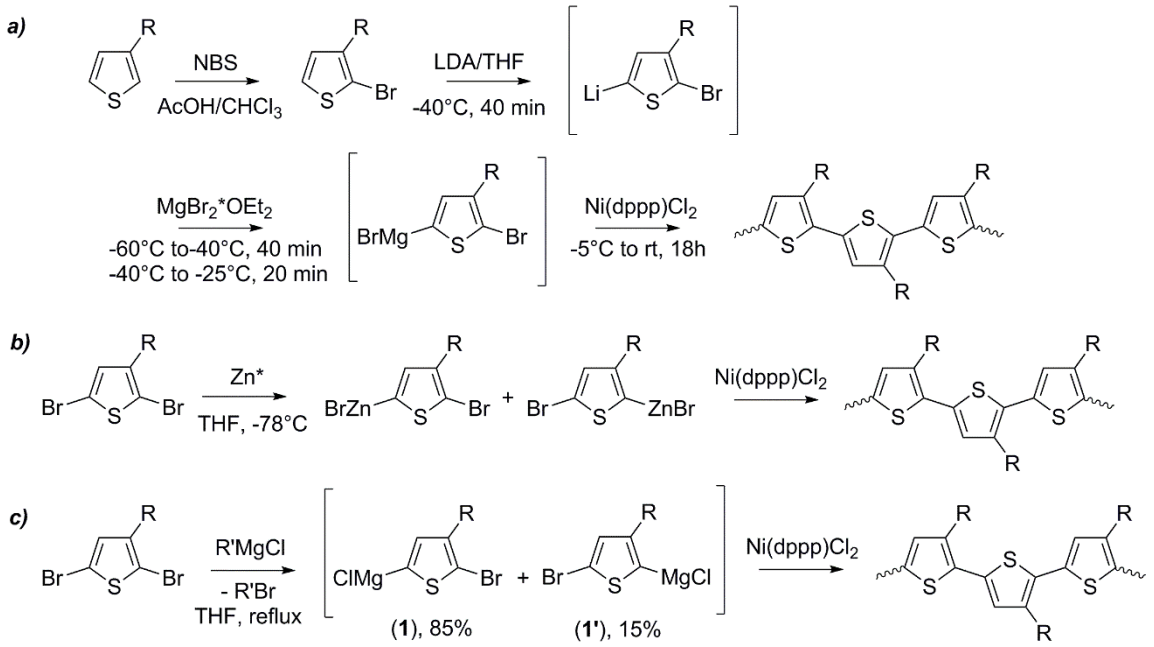

Scheme 2. (a) McCullough and Loewe, (b) Rieke and Chen, (c) GRIM Methods for the synthesis of regioregular P3ATs

Generally, when the Grignard metathesis is applied to 2,5-dibromo-3-alkylthiophene, some degree of regioselectivity is displayed, with exchange favored at the 5-position of the thiophene, leading to an 85:15 distribution of regiochemical isomers intermediates. In fact, even though only a moderate degree of regioselectivity is shown, independently from the Grignard reagent and reaction temperature used, it is noteworthy that 95-98% of HT couplings are always obtained.

A possible explanation to these results may be the steric congestion on the catalyst, provided by sterically demanding ligands (i.e. dpppe or dppp) and small metal centre (i.e. Ni), that could prevent the formation of HH coupling and favor HT and TT dyads. However, in addition to the nature of the catalyst, also a deep investigation of the mechanism of this kind of polymerization would certainly provide a better understanding of the observed behaviour.

In the first place, since a chain-growth mechanism is involved and the propagation step resulted to be a unique intramolecular catalyst-transfer process, the GRIM method has been discovered to be an example of catalyst transfer condensative polymerization (CTCP) and thus a controlled polymerization technique. In particular, as a matter of fact that couplings

between halide and Grignard function occur, the Grignard metathesis polymerization is also referred to *Kumada catalyst transfer condensative polymerization (KCTCP)*.[17,18,19]

To avoid the moisture and air sensitive problems, the KCTCP is generally initiated in situ (Scheme 3). Starting with the Grignard metathesis reaction, a tail-to-tail bithiophene-Ni complex (**3**) is formed via two transmetalation steps (TM), reductive elimination (RE) and subsequent intermolecular oxidative addition (OA) with one of the Br atoms. After a new TM reaction, that occurs between the initiating dimer (**3**) and a new monomer (**1**), chain growth starts and continues via iterative reductive elimination, oxidative addition and transmetalation steps, with the catalyst that remains always associated to the polymer backbone (**6**). In fact, due to this living character of CTCP, as a result of intramolecular transfer selectivity, transfer or termination reaction do not occur during the polymerization. Moreover, as chain-propagation occurs only via one-by-one addition of monomer molecules, only HT couplings are made during the propagation. However, if a completely regioregular polymer (100% HT dyads) is needed, an external situ initiation needs to be adopted, as the initiating TT-defect will be always present in the structure of the polymer. The obtainment of polymers with Br/H termination, caused by hydrolysis or quenching of the active Ni-complex, is a further proof of the living performance of the GRIM polymerization, as the catalyst ring-walking process does not change the termination pattern.

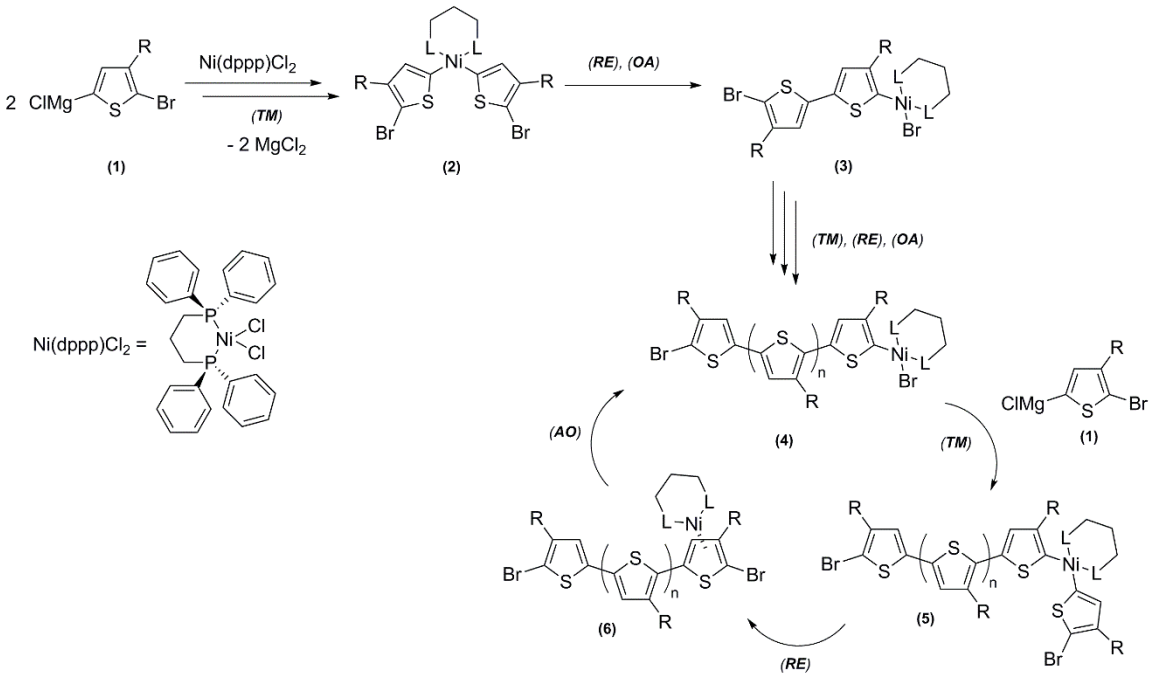

Scheme 3. Catalytic cycle of chain-growth KCTP or GRIM method.

The regio-specific synthesis of polythiophenes is also possible through Pd-catalyzed cross-coupling reactions, by the use of organometallic intermediates. Over the last two decades, the most employed cross-coupling reactions have been for sure the ***Stille*** and the ***Suzuki-Miyaura*** reactions. Both reactions consist in the coupling of a nucleophilic tin or boron thienyl derivatives with thienyl halides, generally in the presence of palladium (zero) complexes (Scheme 4). Although cryogenic conditions are required for the preparation of the intermediates, which moreover must be isolated and purified, high HT couplings percentages are still obtained, in addition to have boronic esters/acids that are much more moisture stable and compatible with a great variety of functional groups.

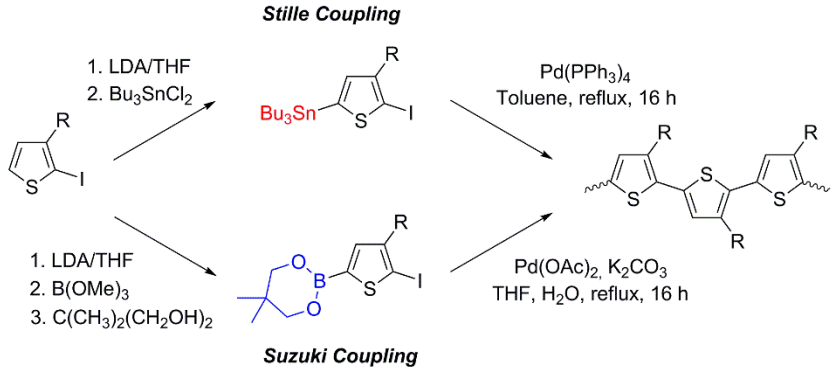

Scheme 4. Stille and Suzuki cross-coupling polymerizations.

Similarly to the KCTCP, also the *Suzuki catalyst transfer condensative polymerization* (SCTCP) has been developed, to prepare polythiophenes, polyfluorenes and polyphenylenes. Indeed, the first living Suzuki polymerization has been carried out by Yokozawa, using external Pd/t-Bu_3P based initiator to synthesize polyfluorene.[20]

To promote the intramolecular transfer of Pd that occurs in the oxidative addition step, SCTCP mechanism is best performed via a Pd catalyst in the presence of a small amount of water. Not only does a faster intramolecular transfer offer less chance of dissociation, it also promotes a better control of the polymerization.[21] In fact, the adoption of this method resulted to be particularly intriguing for the controlled synthesis of block copolymers.

2.2.2. Oxidative polymerizations

Among oxidative polymerizations, the non-regiospecific ***oxidative synthesis with ferric trichloride***[22] is probably the most promising and interesting method, since it is simple, cost-effective and it can be adopted on a large scale. The non-toxic and low-cost ferric trichloride, thanks to its Lewis acid character, acts both as a polymerizing and doping agent. However, to ensure coordination and subsequent polymerization-oxidation, it is necessary to work with anhydrous solvents (i.e. $CHCl_3$), in which $FeCl_3$ is insoluble (Scheme 5).

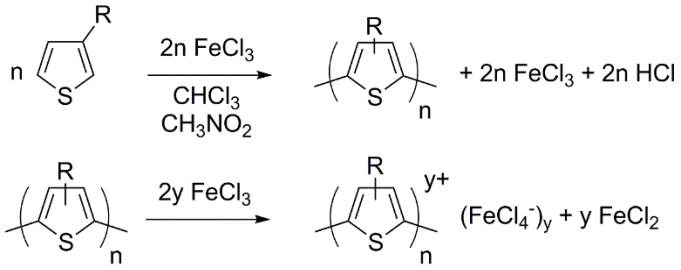

Scheme 5. Oxidative polymerization with $FeCl_3$.

The reaction is carried out under inert conditions, to avoid interference with the radical-cationic mechanism, and in the presence of a strong excess of oxidizing agent that allows to obtain the material directly in the doped form.

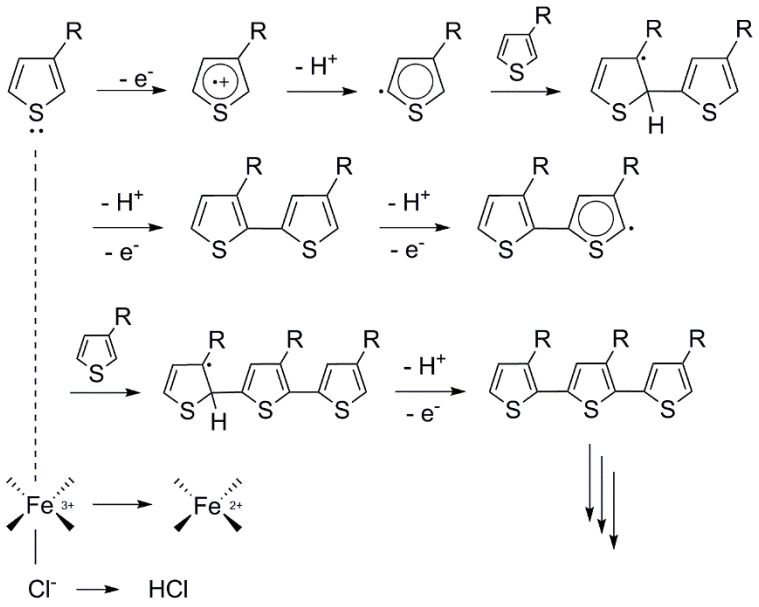

Scheme 6. Mechanism of oxidative polymerization with $FeCl_3$.

Similarly to the electrochemical polymerization, the mechanism involves the coordination of the thiophene ring, through the sulphur atom, to the empty *d*-orbital of Fe^{3+}, creating a radical-cation. This evolves to 5-thienylradical, couples with another monomer molecule and produces a dimer, as a consequence of the aromatization by output of protons and further oxidations. The start of an oxidation-cycle leads to the growth and doping of the chains (Scheme 6).

Polymers in the most-conductive form, with high weights and good yields are obtained. Although only around 75% of HT dyads can be usually obtained with this method, an interesting characteristic of this polymerization is the possibility to synthesize regioregular polyalkylthiophenes starting from symmetrically substituted monomers.[23]

This aspect of the oxidative coupling, in addition to the GRIM Method, the Suzuki cross-coupling reaction and SCTCP, as methods mainly adopted for the synthesis of the compounds presented in this dissertation, will be further discussed in the following chapters.

2.3. Optical and chiroptical properties

The interesting electrical and optical properties of intrinsically π-conjugated polymers depend on the conformation assumed by their backbone, both in the ground and in the excited state, and by the orientation in the space of the side chains.

Moving from a single isolated polymer chain to a self-assembled material, the optical properties will change as a consequence of the intermolecular interactions that appear in the solid form. The self-assembly of π-conjugated polymers, in solution or in film, gives chromism phenomena. Chromism usually consists in the reversible change of colour due to the action of an external stimulus, which can be a change in the polarity of the solvent (solvatochromism) or a change in temperature in the solid state (thermochromism).[24]

Several studies showed that the polymer, in the presence of a non-solvent or low temperatures assumes a planar and ordered conformation at lower internal energy; on the contrary, the use of a good solvent or a temperature increase induce the assumption of a more disordered and distorted structure, thus reducing the extension of conjugation.

Therefore, these structural changes involve a modification of the energy of the π-π* orbitals and thus an overall change of the energy gap, which result in a visible change of the colour of the polymer. Polythiophenes, in the presence of a non-solvent or at low temperatures absorb at longer wavelengths assuming a blue-green colour (red-shift), while

they are red-orange if dissolved in a good solvent or brought to high temperatures (blue-shift).[11]

In general, the opportunity to easy-tune the optical properties of these materials, simply by inserting substituents in the side chain or modifying the length of the chain, is one of their most attractive features. For example, the insertion of electron donor groups with the heteroatom directly linked to the thiophene in position 3, is expected to produce a decrease of the band gap and oxidation potential, caused by a higher lying HOMO level.[14]

On this basis, the introduction of chiral substituents in position 3 on the thiophene ring also involves modifications of this packing, up to the possibility of inducing chiral activity in the main chain.

The chirality, however, is only evident when the polymer shows an ordered aggregated form prepared in an enantioselective way, i.e. by inserting enantiomerically pure side chains. Furthermore, other external parameters such as temperature and the type of solvent, the electronic and hindrance nature of the main/side chain, as well as the distance of the chiral centre from the backbone and the degree of regioregularity, strongly affect this phenomenon. In fact, optical activity is not usually observed if the polymer is dissolved in a good solvent or at high temperatures - conditions which favor a disordered random coil conformation - but only in case of aggregated form (i.e. thin film at room temperature or by addition of a poor solvent).[24,25]

In these conditions, the assumption of a *helical conformation* as an *intramolecularly organization*, is commonly believed to be the origin of the optical activity in polythiophenes. On the other hand, other studies connect the origin of the high optical activity in these materials to the *intermolecular* supramolecular self-assembly of several rigid and planar chains as shown in Figure 6.

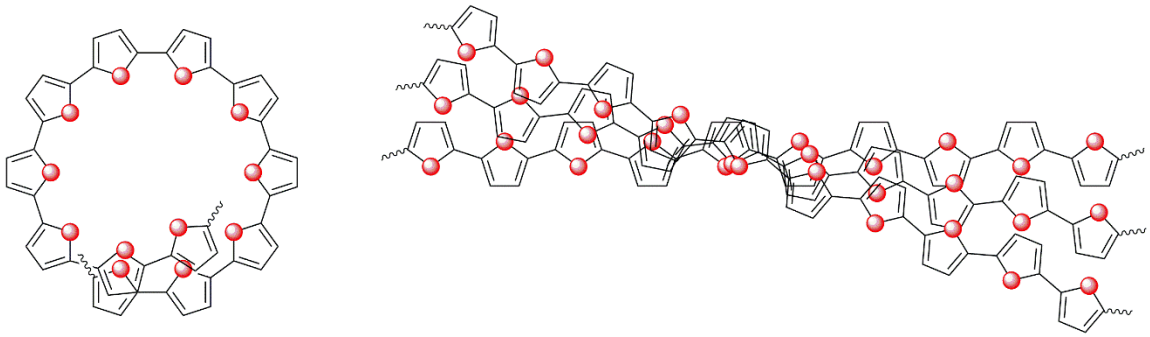

Figure 6. Helical conformation of one single chain (left) and chiral supramolecular self-assembly (right).

Fortunately, a difference between these two situations can be made by their different concentration dependence. As intramolecular process, the formation of helices is only dependent on the solvent quality, without regard to the concentration; the intermolecular phenomena, on the contrary, is affected by dilution of the solution.[26,27]
However, it is important to underline that a complete structural interpretation of the origin of the chiral activity in the polymer, at this moment, has not yet been reached.

2.3.1. Circular dichroism spectroscopy

The behaviour of chiral polythiophenes is studied by circular dichroism (CD).[28] CD spectroscopy is based on the fact that chiral optically active substances have the ability to absorb left- and right-circularly polarized light differently.

In the first place, to fully understand the phenomenon, it is necessary to know that a monochromatic radiation consists of electric and magnetic fields whose vectors, respectively E and H, are perpendicular to each other and with respect to the direction of propagation. If in a not-polarized ray the oscillation of E and H is in infinite planes, in a linearly polarized ray (i.e. in a plane) the vibration of the vectors is limited to a single surface, as shown in Figure 7. In the case of circularly polarized radiation, on the other hand, the vectors E and H oscillate and at the same time rotate with respect to the direction of propagation creating an helix: this radiation can be circularly polarized clockwise (right-handed) or in the sense counter-clockwise (left-hand) (Figure 7). Left- and right-circularly polarized light are therefore two components of linearly polarized light.

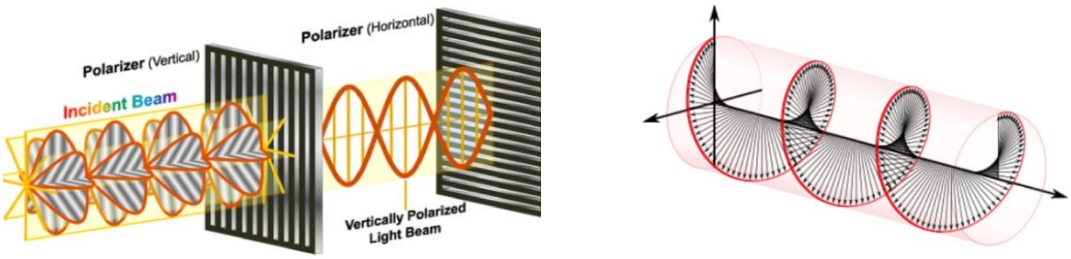

Figure 7. Linear polarization of the light (left) and circularly polarized radiation (right).

When such radiation is sent through a chiral sample a phase difference is created, caused by the diversity of the two refraction indices ($n_L \neq n_R$) which produce a rotation of the polarization plane over a certain angle. Moreover, it is possible an unequal absorption of

the two components, as they also have different molar extinction coefficients ($\varepsilon_L \neq \varepsilon_R$), which produce an elliptically polarization of the emergent light (Figure 8).

When this phenomenon of rotation of the plane of a circularly polarized light is evaluated at the maximum absorption wavelength, we refer to circular dichroism (CD). The optical rotation can also be determined as a function of the wavelength of the incident light and the technique is known as rotary optical dispersion (ORD).

A circular dichroism spectra, in correspondence of the maximum absorption, usually shows a trend known as Cotton effect: a positive Cotton effect is obtained when, at the decrease of λ, the ORD curve passes first for a maximum and then for a minimum or when a circular dichroism spectrum shows a positive band. A negative cotton effect is obtained when an opposite behaviour occurs.

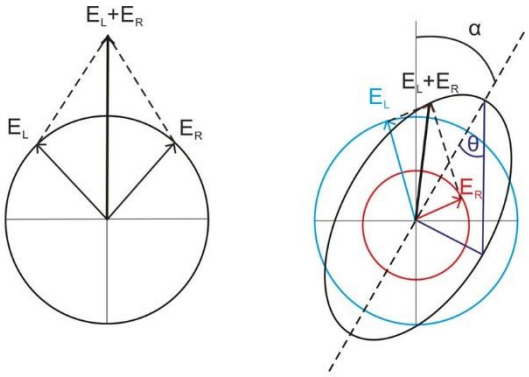

Figure 8. Circularly (left) and elliptically (right) polarized light.

3. Application of ICPs

3.1. Overview

In a near future, inorganic electronics are expected to be replaced by organic ones, thanks to their advantages in terms of processability, good mechanical properties (flexibility and film ability), cost-effectiveness, environmentally benign manufacturing and easy tunability of electrical properties via chemical synthesis. Among several intrinsically π-conjugated polymers, polyaniline, polypyrrole and polythiophenes are probably the most described and investigated candidates for this purpose.

Indeed, the left part of this introductive chapter will be focused on a brief description of the main energy/electronic applications which involve those type of organic semiconductors. In particular, the operational principle of organic solar cells as energy harvesting application and the use of polythiophenes for their development will be especially discussed.

3.2. Organic solar cells (OSCs)

Due to the reduced availability of fossil fuels and a better understanding of the long-term effects of CO_2 and other greenhouse gas, a long-standing intensification and diversification of research on renewable energy sources need to be done.

Solar light, that can be used either as a source of heat or converted into electrical energy by photovoltaic cells, is one of the most promising clean energy resources since it is unlimited and at zero-cost. Although photovoltaic electricity is presently dominated by a deeply studied and well-developed silicon technology, which combines good conversion efficiency (~ 25%) and durability, it is too expensive in terms of production, purchase and installation costs.[29] On the other hand, organic solar cells are strongly potentially advantageous since can be rolled out onto large-area, light weight and flexible substrates, by means of simple and low-environmental-impact solution processing. In fact, efficiencies increasing from 1.0 % to 13-15% in twenty years have been produced, thanks to an intensive multidisciplinary research effort.[30,31]

A photovoltaic device is based on the so-called *photovoltaic effect* and the mechanism of solar energy conversion into electrical energy differs from silicon to organic semiconductors. In a silicon solar cell, since it has high dielectric constant, the photo-

absorption directly generates free-charge carriers (electrons and holes) able to separate at the interface of a p-n junction and diffuse, by action of a field, to the respective opposite charge electrodes. On the contrary, because of the low dielectric constant, organic semiconductors upon photo-absorption create *excitons*, i.e. hole-electron pairs strongly bounded by Coulombic attraction, which require high electric field to dissociate. In order to be useful, the exciton needs to be dissociated into free charges and does not decay to the ground state, as it would involve the loss of the absorbed energy. In OPVs, the dissociation takes place in presence of a two-component system, which consists of an electron-donor and an electron-acceptor material, that behaves similarly to the p-n junction. Generally, the donor and acceptor components are typically characterized by a large ionization potential (IP) and high electronic affinity (EA), respectively.[32,33]

As described in the literature, the photovoltaic process (Figure 9) consists of four fundamental steps.[34]

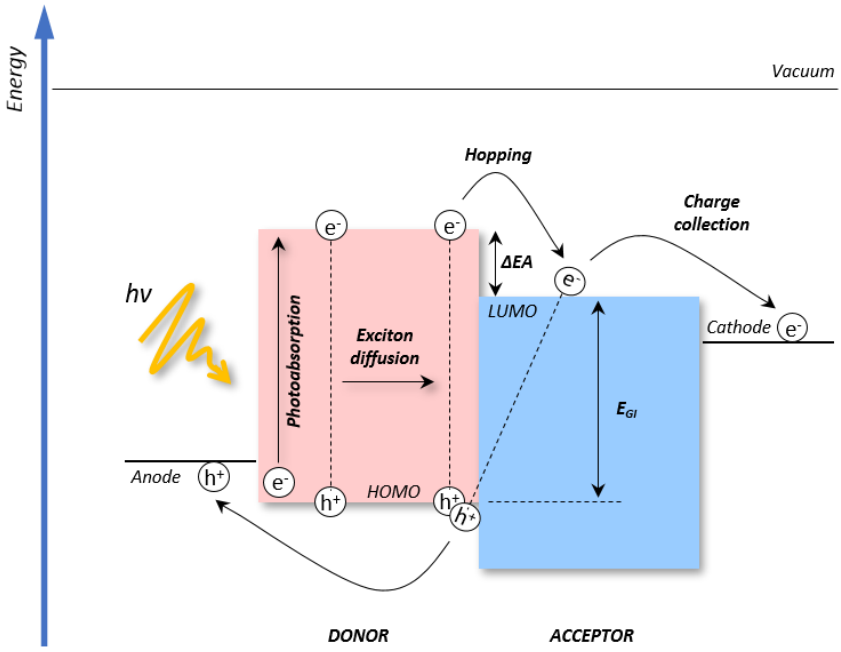

Figure 9. Scheme of the device operating principles.

Upon ***photo-absorption***, an electron can be excited from the donor HOMO to its LUMO, forming an exciton which, due to the difference in energy levels of the electronic states, must then ***diffuse*** to the donor/acceptor interface via a chemical potential gradient. When the energy difference between the donor and acceptor LUMO (ΔEA) is greater than the binding energy of the exciton - otherwise there would be *geminate recombination* of the

two charges causing a decrease in efficiency - the electron is transferred to the LUMO of the acceptor material by ***hopping*** and a charge transfer (CT) complex can be formed.
If the distance between electron and hole becomes greater than Coloumb's range of attraction, the CT complex can become free charges. Any dissociated charges can then be transported through p- or n-type domains to the electrodes, with holes and electrons being ***collected*** respectively at the anode and at the cathode, where they can be used to do work in an external circuit. A further decrease in efficiency can also occur since free charge carriers may recombine with other unassociated charge carriers present in the device (*charge recombination*).

There are different types of organic solar cells but all of them consist of sandwich structures, where the photo-active layer is always enclosed between two electrodes; in particular, two fundamental architectures of active layer have been developed (Figure 10). The first *bilayer heterojunction structure*, reported with a power conversion efficiency of ~ 1% by Tang in 1986,[35] was obtained by a separate deposition of donor and acceptor materials, resulting in two layers with a sharp and well-defined interface. Even though bilayer architectures are still deeply investigated, the short diffusion length of excitons in organic materials (typically 10-20 nm) drastically limits the maximum thickness of the active layer and, consequently, the fraction of the incident light that can be absorbed and thus converted. This problem has been partially solved with the realization of a ***bulk heterojunction (BHJ) structure***, in which a large-area and continuous network of donor and acceptor materials is created, minimizing the exciton traveling distance and therefore increasing the number of excitons dissociated.[35,36]

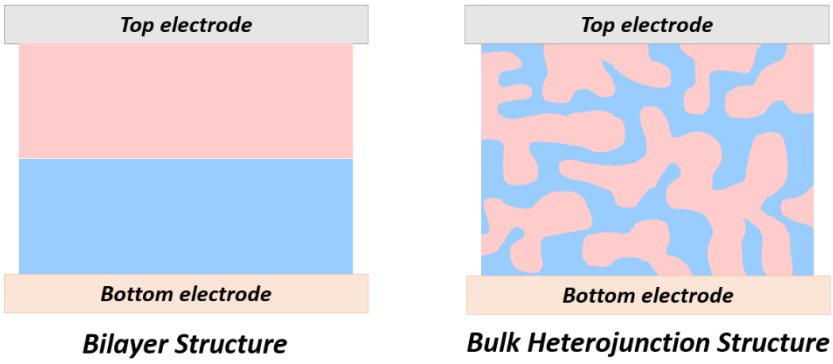

Figure 10. Fundamental architectures of photoactive layer.

Three device geometries, that include standard BHJ, inverted BHJ and tandem devices, are currently identified for this type of OSC.

In the conventional *standard* geometry (Figure 11a), the photoactive blend is usually built on the top of a semi-transparent layer of ITO (tin-doped indium oxide), which is modified with a thick hole-transport layer of poly(3,4-ethylenedioxythiophene):poly(styrene-sulfonate) (PEDOT:PSS), and enclosed by a layer of electron transport and a layer of Al. In this system, holes and electrons are transported, respectively, to the anode (ITO) and to the cathode (Al).

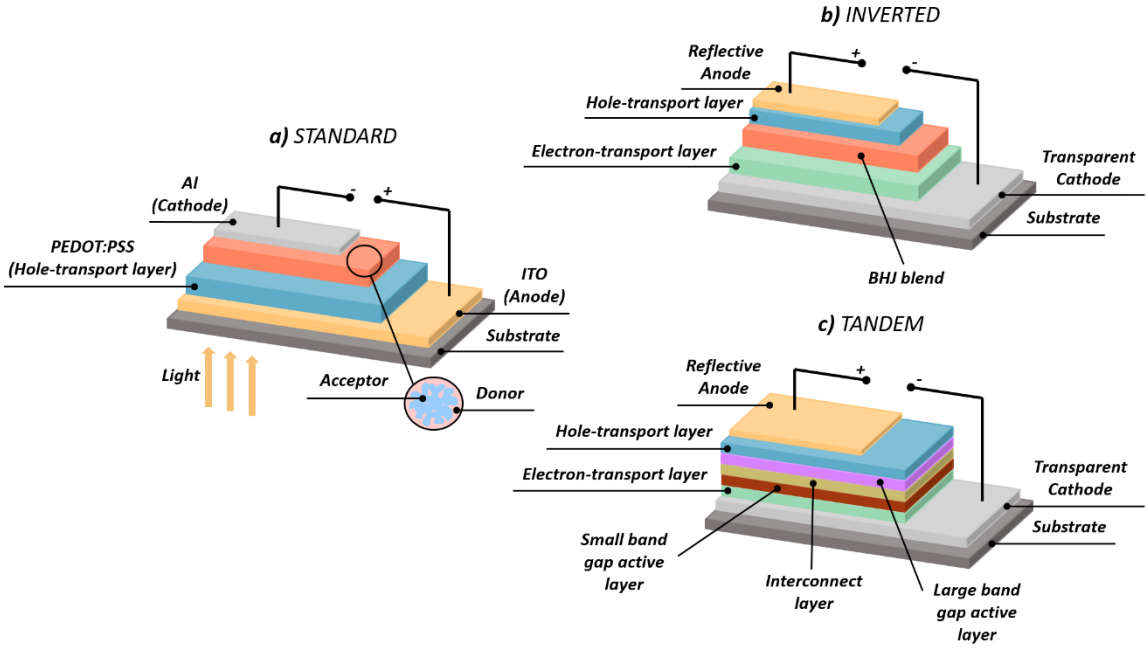

Figure 11. Device geometry of (a) standard, (b) inverted and (c) tandem OSC.

Instead, in the *inverted* type geometry (Figure 11b), the order of the layers is reversed and there is therefore a change of the roles of the charge collecting nature of the electrodes, since the top metal electrode is now the hole-collecting anode. While the cathode is made by ITO but coated with ZnO or other oxides, in order to reduce its work function, the anode typically consists of a stable metal such as Ag or Au, functionalized with V_2O_5 or MoO_3. This geometry, compared to the previous one, tends to be more stable to external oxidation and to be more compatible with high scale-up conditions.

The *tandem* geometry (Figure 11c) has been developed to address two typical problems of organic solar cells. As previously mentioned, the first issue is the limit of the thickness of the active layer which does not allow the maximum absorption; on the other hand, a second problem concerns how the active layer absorbs light, since part of the light is not absorbed but is transmitted by the cell, getting lost. Composed of a greater number of layers, it presents at least two photo-active layers placed one above the other but separated by an

interconnect layer: the first active layer absorbs high-energy photons and transmits those with lower energy, which can be absorbed by the second active layer. The intermediate layer allows the holes of a substrate to recombine with the electrons of the other. It is quite evident that in this way the cell is able to absorb more light without affecting the thickness of the layers.[32,37]

Photovoltaic systems are photodiodes connected in forward-bias that generate reverse current only upon photoabsorption: a typical current density-voltage (J-V) curve of an organic solar cell is shown in Figure 12.

The ***power conversion efficiency (PCE)***, the ratio of the maximum electrical power generated by the device to the total incident optical power (photons), usually is the main parameter of evaluation of OSCs and is proportional to short circuit density current (J_{sc}), open circuit voltage (V_{oc}) and fill factor (FF), according to the following equation:

$$PCE = \frac{P_m}{P_{in}} \cdot 100\% = \frac{V_{oc} \cdot J_{sc} \cdot FF}{P_{in}} \cdot 100\%$$

J_{sc}, which is the maximum amount of current that could pass through the cell surface when the resistance and thus the voltage is zero, mainly depends on the efficiencies of each single step involved in the photogeneration mechanism. On the contrary, the maximum voltage of the cell that could be obtained in the absence of current (V_{oc}) is proportional to the energy level difference between the LUMO of the acceptor and the HOMO of the donor material (E_{GI}). *FF*, instead, is the factor that takes into account the non-ideality of the system and graphically represents the "squareness" of the J-V curve.[38]

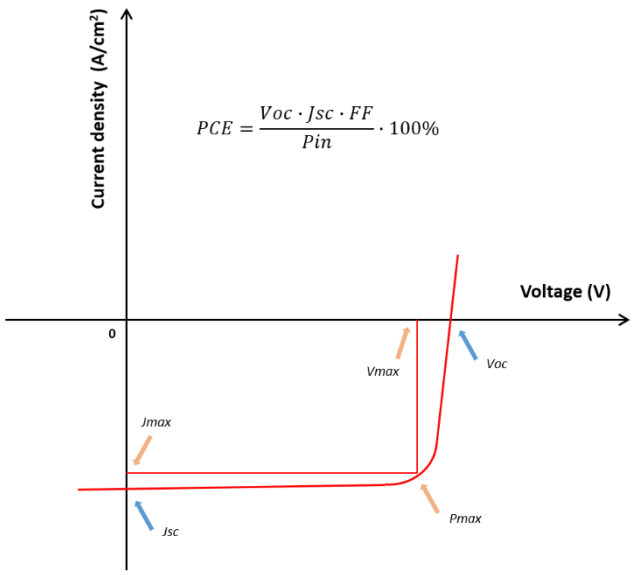

Figure 12. J-V curve of an organic solar cell.

Therefore, it is quite clear that the optical-electrical properties of the components of the active layer and their energy level alignment play a crucial role on the performance of the device. For instance, a larger value of E_{GI} certainly leads to a higher V_{oc} but, as said before, an adequate LUMO-LUMO offset (ΔEA) between donor/acceptor materials needs to be provided as a driving force to split the excitons. In fact, it is of primary importance the development of stable but still processable donor/acceptor materials that guarantee reasonable band gaps and good charge mobility.[39]

During the past two decades, oligo- and poly(3-alkylthiophenes) – in the first place poly(3-hexylthiophene) (P3HT) – have certainly been the centre of the synthetic chemistry of electron-donor polymers. On the other hand, soluble derivatives of fullerenes – [6,6]-phenyl-C61-butyric acid methyl ester ($PC_{61}BM$) and $PC_{71}BM$ – were the standard acceptor materials for many years. However, despite the many well-known advantages of π-conjugated systems as donor domain, narrow bandwidth of absorption spectra and poor values of V_{oc} are obtained, as a consequence of their large optical band gap (~ 1.9 eV) and their often high HOMO level. Moreover, the optimized bulk heterojunction morphology is not thermodynamically stable and leads to the formation of a electron-donor (D) or acceptor (A) cluster-phase separation.[40,41,42]

In this context, in addition to the aforementioned substituents effects – i.e. by attachment of electron donating group such as alkoxy group (paragraph 2.3) – several other factors, such as intermolecular interactions, aromaticity or increased intra-chain resonance and charge transfer, can be adopted to tune and design low band gap polythiophenes.[37,43] In particular, the synthesis of a single ambivalent active material, with donor and acceptor domains chemically linked to each other, could be the most promising solution to these questions, providing the fabrication of ***single material organic solar cells (SMOSCs)***.[44]

Thanks to the combinations of D and A units in the same molecule/polymer, in order to create and promote an internal charge transfer, SMOSCs may considerably simplify the device fabrication. Furthermore, not only could they provide a possible definitive solution to the morphological instability of multicomponent BHJs, but they should also erase the issue connected to the short exciton diffusion length in organic semiconductors, since the light absorption and charge separation would occur at the same molecule.

However, in spite of these major potential advantages – i.e. conceptual simplicity – SMOSCs have, until now, met with very limited success and attracted much less attention than BHJs. In addition to the fact that the design of those type of active materials is indeed a very complex problem, it is a widespread idea that single material organic solar cells

cannot reach high PCEs, probably due to the fast charge recombination and inefficient charge hopping/transport which can happen.

Fortunately, research on SMOSCs has recently witnessed important progress and the best PCE, which has remained around 1.50% for several years,[45] has now increased up to values of 4.0–5.0%.[46]

3.2.1. Single material organic solar cells (SMOSCs)

The complex design and synthesis of active materials for SMOSCs[44] should guarantee all the functions usually achieved by a classic BHJ blend.

In fact, although thermal treatments and additives can be effective, it is the chemical structure of the active material to primarily affect the morphology of SMOSCs. Therefore, the different fabrication of SMOSCs can be essentially envisioned taking into account the nature of the electron-donor (polymer or molecule) and electron-acceptor material (fullerene or not-fullerene) and most of all, their mode of connection. Generally, the D and A units are covalently linked to each other by a flexible insulating spacer (L), which needs to be long enough to allow the self-organization into separated domains (Figure 13). It is quite clear that the nature and length of these flexible linkers would determine the nanophase separation and morphology of the material.

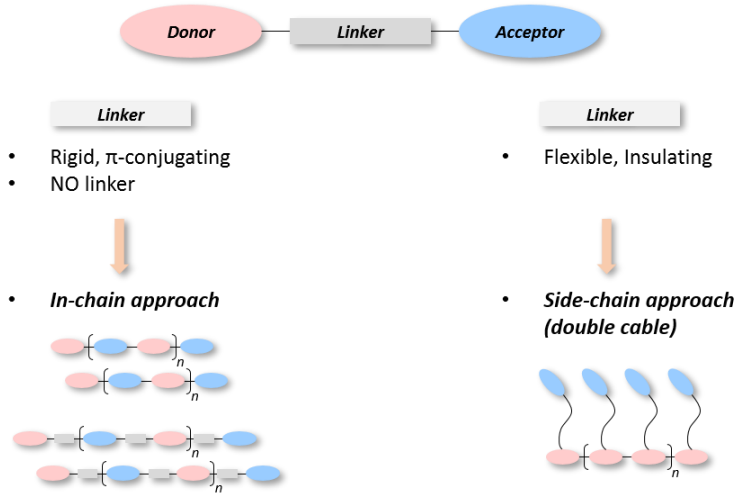

Figure 13. Development of polymeric electron-donor and acceptor materials.

Among all possible synthetic approaches for the development of photoactive materials for SMOSCs, the attention will be focused only on two types of those systems, since they will be objects of a further discussion in the following chapters of this dissertation.

"In-chain" donor/acceptor systems[32] are polymers or block-polymers characterized by the alternation of electron-rich and electron-poor units, typically heterocycles, along the polymer backbone.

In those type of materials, the band gap reduction is due to an orbital mixing of these internal units, with particular regard to the high HOMO and low LUMO level of the D and A domains, respectively. As highly conjugated systems, "in-chain" donor/acceptor polymers usually exist in two ground state resonance structures that are the *aromatic* and the *quinoidal* forms. Although the second one is less energetically stable and so has a smaller band gap than the aromatic resonance, the quinoidal form is usually promoted by the structure as it provides better planarity of the backbone and enhances the charge carrier mobility. However, since these polymers are often difficult to purify and their properties tend to suffer from batch to batch variation, SMOSCs based on small molecular "in-chain" D-A systems have emerged as promising alternative. In fact, despite the major difficulty to create donor/acceptor microdomains due to their small dimensions, the reproducibility of design/purification and a straightforward analysis of their structure-properties result to be quite advantageous.

On the other hand, the synthesis of ***"double-cable" polymers***,[45,47] that are π-conjugated systems (donor) with acceptor (i.e. fullerene) pendant units, can also be possible.

In those type of materials, which are typically obtained starting from precursors that have ω-bromoalkyl reactive groups, it is reasonable to assume the existence of "channels" that could contribute to limit the charge recombination, as they promote a rapid migration and collection of holes and electrons. Indeed, even though positive charges and electrons are expected to be transported, respectively, by the polymer backbone and the C_{60} groups attached to it by flexible spacers, the charge transport should be considered in a 3D material, where it occurs by a hopping mechanism.

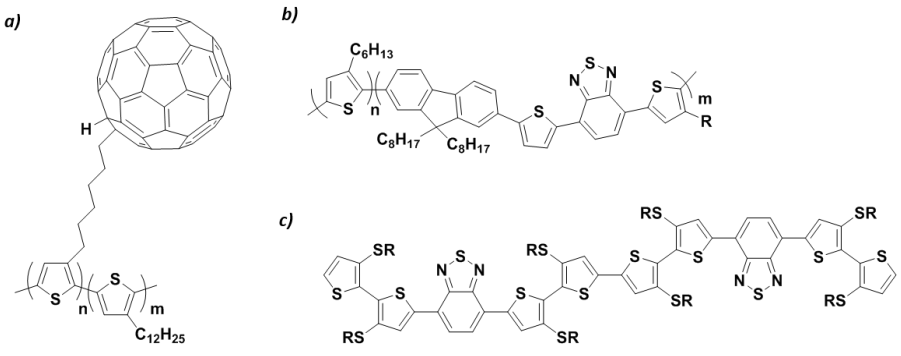

Figure 14. Example of (a) double-cable system, (b) in-chain donor/acceptor polymer and (c) molecule.

3.2.2. Morphology control of active layer

Independently from the type of architecture or geometry adopted, it should be clear from now that the morphology control of the active layer is one of the main issues related to the production of organic solar cells.[32,43]

As previously mentioned, in order to guarantee continuous charge transport but also exciton dissociation, the ideal morphology should be a continuous and interpenetrating network of donor and acceptor materials, with domain size similar to the exciton diffusion length (~ 10/20 nm).

The active layer morphology, especially for thiophene based material, can be affected by several parameters such as the solvent, the use of additives, the donor/acceptor concentrations, the deposition method and, most of all, the type of annealing performed. In fact, due to a self-reorganization of the material, thermal and/or solvent-vapor annealings are particularly important since they improve charge transport and extend the optical absorption into the red. Furthermore, not only is the stability of the blend definitely improved by pre-thermal treatment (when devices are annealed prior to cathode deposition), but also the lifetime of devices is especially enhanced. On the contrary, solvent annealing promotes both better crystallization of the thiophene-based donor material and leads to a better diffusion/segregation of PCBM.

3.2.3. Conclusion and outlook

A great progress has been made in the development and understanding of this new and interesting technology, but it is clear how important is to continue the research on this topic. In addition to find valid alternatives to PCBM as acceptor materials, as well as to try to extend the absorption spectrum to the entire visible region, the idea of large-scale production of OSCs should be strongly pursued. In fact, in spite of the numerous potential advantages of those systems (i.e. flexibility, processability etc.), the low PCE values are still the major drawback of this technology. However, the research should not focus only on the increase of PCE but it should also provide a solution to many issues as environmental impact, scalability and stability of materials/device.

3.3. Other energy/electronics applications

The development of rechargeable batteries as ***charge storage devices***[48] is one of the most important goal that can be pursued with intrinsically conductive polymers.

In addition to the possibility to create light, easy to shape and flexible electrodes, it is noteworthy the potential of polythiophenes as overcharge protection for lithium-ion batteries. Thanks to the reversible electrochemical behaviour of PTs, which converts the cell into resistor upon over-charging, permanent degradation and, above all, exothermic conditions that might lead to explosion can be avoided. In fact, in Li-polymer batteries (Figure 15), that are usually made of metallic Li and a conductive material (i.e. polypyrrole) as anode and cathode, those electroactive polymers act as solid supports electrolyte that can be impregnated with non-aqueous electrolytes, typically a lithium salt (i.e. $LiClO_4$, $LiBF_4$). Moreover, since only physical and not-chemical processes of charge and discharge are involved – as electrodes made with these materials undergo doping or de-doping process when they are charged and discharged – there is no aging of the system.

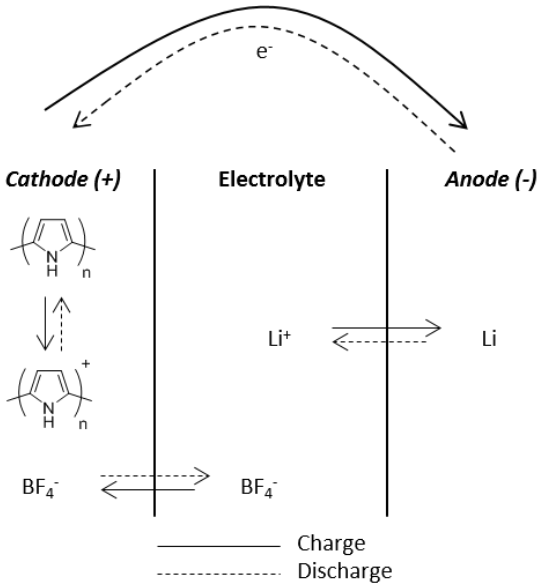

Figure 15. Scheme of a Li-PPy battery.

Conjugated polymers, especially polythiophenes, are also particularly useful in ***electrochromic device applications (ECDs)***.[49]

As previously said, electrochromism is the colour variation induced by a reversible electrochemical process (doping) and ICPs are therefore intrinsically electrochromic materials. The device consists of a polymeric multilayers structure that changes colour due

to a variation of the energy gap, and therefore of the maximum absorption, caused by a reversible switch from neutral to the oxidized form.

Low oxidation potentials and stability, as well as high contrast ratio and fast switching times, are necessary requirements to have good electrochromic materials, which can find application in "smart windows" and displays.

As opposite phenomena to photovoltaic effect, also electroluminescence – the direct conversion of electrical energy into light – can occur in semiconductor materials.

In particular, among the various electroluminescent devices, a great interest is focused on ***OLEDs (organic light emitting diodes)***.[50] In those p-n junctions, by application of a potential to the device, electrons and positive charges are injected into the system, generating photons and thus emitting light. To obtain different colour, since the emission wavelength depends on the Eg of the semiconductor material, a multilayer structure of different types of materials would be necessary. In OLEDs several layers of different organic semiconductors are usually built on the top of a layer of metal cathode - which has been modified with a thick electron-transport layer – and enclosed by a layer of hole transport and a semi-transparent anode/glass substrate (Figure 16).

However, although OLEDs can be used to realize flexible, light and easy shape displays, they have short lifetime and higher costs.

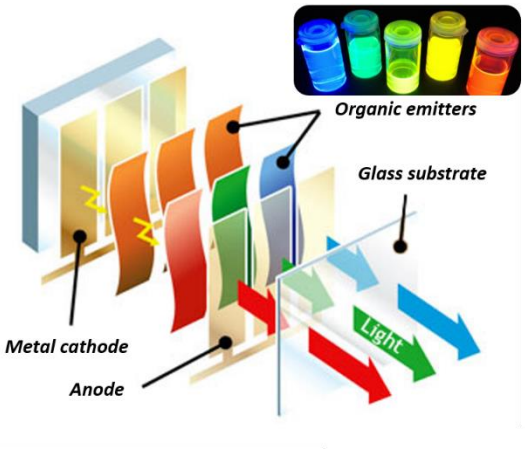

Figure 16. OLED structure.

References

[1] S. Gunes, H. Neugebauer, N. S. Sariciftci, *Chem. Rev.* **107** (2007) 1324-1338.
[2] J. Roncali, *Macromol. Rapid. Commun.* **28** (2007) 1761-1775.
[3] A. Di Terje, A. Skotheim, J. R. Reynold, *Handbook of Conducting Polymers* (2007) CRC Press.
[4] C. K. Chiang, C. R. Fincher, Y. W. Park, A. J. Heeger, H. Shirakawa, E. J. Louis, S. C. Gau, A. G. MacDiarmi, *Phys. Rev. Lett.* **39** (1977) 1098–1101.
[5] S. C. Rasmussen, *ACS Symposium Series* **1080** (2011) 147–163.
[6] A. Moliton, R. C. Hiorns, *Polym. Int.* **53** (2004) 1397–1412.
[7] P. Kar, *John Wiley & Sons* (2013) 1–18.
[8] P. Stanetty, G. Hattinger, M. Schnürch, M. D. Mihovilovic, *J. Org. Chem.* **70** (2005) 5215-5220.
[9] M. C. Petty, *Springer Handbook of Electronic and Photonic Materials* (2007) Springer: Boston, 1219-1239.
[10] G. Horowitz, P. Delannoy, *Handbook of Oligo- and Polythiophenes* (2007) Wiley: Weinheim.
[11] I. F. Perepichka, D. F. Perepichka, *Handbook of Thiophene-based Materials* (2009) Wiley.
[12] H.S. Nalwa, *Handbook of Organic Conductive Molecules and Polymers* (1997) Wiley.
[13] J. Heinze, B. A. Frontana-Uribe, S. Ludwigs, *Chem. Rev.* **110** (2010) 4724-4771.
[14] I. Osaka, R. McCullough, *Acc. Chem. Res.* **41** (2008) 1202-1214.
[15] T. M. S. K. Pathiranage, D. S. Dissanayake, C. N. Niermann, Y. Ren, M. C. Biewer, M. C. Stefan, *Journal of Polymer Science, Part A: Polymer Chemistry* **55** (2017) 3327–3346.
[16] R. S. Loewe, P. C. Ewbank, J. Liu, L. Zhai, R. McCullough, *Macromolecules* **34** (2001) 4324-4333.
[17] M. C. Iovu, E. E. Sheina, R. R. Gil, R. D. McCullough, *Macromolecules* **38** (2005) 8649-8656.
[18] R. Miyakoshi, A. Yokoyama, T. Yokozawa, *J. Am. Chem. Soc.* **127** (2005) 17542-17547.
[19] A. Kiriy, V. Senkovskyy, M. Sommer, *Macromol. Rapid Commun.* **32** (2011) 1503-1517.
[20] C. G. Dong and Q. S. Hu, *J. Am. Chem. Soc.* **127** (2005) 10006–10007.
[21] K. Kosaka, Y. Ohta, T. Yokozawa, *Macromol. Rapid Commun.* **36** (2015) 373–377.
[22] J. M. G. Cowie, *Polymers: Chemistry and Physics of Modern Materials* (1991) CRC Press.
[23] L. Angiolini, V. Cocchi, L. Guadagnini, A. Mignani, E. Salatelli, D. Tonelli, *Synthetic Metals* **202** (2015) 169-176.
[24] B. M. W. Langeveld-Voss, R. A. J. Janssen, E. W. Meijer, *Journ. Molec. Structure* **521** (2000) 285-301.
[25] F. J. M. Hoeben, P. Jonkheijm, E. W. Meijer and A. P. H. J. Schenning, *Chem. Rev.* **105** (2005) 1491-546.
[26] Z. B. Zhang, M. Fujiki, M. Motonaga, C. E. McKenna, *JACS* **125** (2003) 7878-7881.

[27] G. Longhi, S. Abbate, G. Mazzeo, E. Castiglioni, P. Mussini, T. Benincori, R. Martinazzo, F. Sannicolò, *J. Phys. Chem. C* **118** (2014) 16019-16027.
[28] L. Moggi, A. Juris, M.T. Gandolfi, *Manuale del Fotochimico-Tecniche e Metodologie* (2006) Bononia University Press.
[29] A. Hagfeldt, G. Boschloo, L. Sun, L. Kloo, H. Pettersson, *Chem. Rev.* **110** (2010) 6595–663.
[30] S. Zhang, Y. Qin, J. Zhu, J. Hou, *Adv. Mater.* **30** (2018) 1800868.
[31] X. Che, Y. Li, Y. Qu, S. R. Forrest, *Nat. Energy* **3** (2018) 422-427.
[32] K. A. Mazzio, C. K. Luscombe, *Chem. Soc. Rev.* **44** (2015) 78-90.
[33] J. E. Donaghey, A. Armin, P. L. Burn, P. Meredith, *Chem. Commun.* **51** (2015) 14115-14118.
[34] T. M. Clarke, J. R. Durrant, *Chem. Rev.* **110** (2010) 6736–6767.
[35] C. W. Tang, *Appl. Phys. Lett.* **48** (1986) 183-185.
[36] G. Yu, J. Gao, J. C. Hummelen, F. Wudl, A. J. Heeger, *Science* **270** (1995) 1789–1791.
[37] H. Wang, C. Chen, R. Jeng, *Materials* **7** (2014) 2411-2439.
[38] J. H. Hou, H. Y. Chen, S. Zhang, G. Li, Y. Yang, *JACS* **130** (2008) 16144-16145.
[39] R. Street, K. Song, J. Northrup, S. Cowan, *Phys. Rev. B* **83** (2011) 165207.
[40] E. Bundgaard, F. Krebs, *Sol. Energy Mater. Sol. Cells* **91** (2007) 954–985.
[41] P. Cheng, X. Zhan, *Chem. Soc. Rev.* **45** (2016) 2544-2582.
[42] N. Li, J. D. Perea, T. Kassar, M. Richter, T. Heumueller, G. J. Matt, Y. Hou, N. S. Guldal, H. Chen, S. Chen, S. Langner, M. Berlinghof, T. Unruh, C. J. Brabec, *Nat. Commun.* **8** (2017) 1-9.
[43] U. Mehmood, A. Al-Ahmed, I. A. Hussein, *Renewable and Sustainable Energy Reviews* **57** (2016) 550-561.
[44] J. Roncali, I. Grosu, *Adv. Sci.* **6** (2019) 1801026.
[45] J. Roncali, *Adv. Energy Mater.* **1** (2011) 147-160.
[46] F. Pierini, M. Lanzi, P. Nakielski, S. Pawłowska, O. Urbanek, K. Zembrzycki, T. A. Kowalewski, *Macromolecules* **50** (2017) 4972-4981.
[47] A. Cravino, N. S. Sariciftci, *J. Mater. Chem.* **12** (2002) 1931-1943.
[48] G. Chen, T. J. Richardson, *Electrochem. Solid State Lett.* **7** (2004) A23-26.
[49] P. M. Beaujuge, J. R. Reynolds, *Chem. Rev.* **110** (2010) 268-320.
[50] K. T. Kamtekar, A. P. Monkman, M. R. Bryce, *Adv. Mat.* **22** (2010) 572-582.

Chapter II

Chapter II: SMOSCs - SYNTHESIS AND CHARACTERIZATION OF "IN-CHAIN" DONOR/ACCEPTOR SYSTEMS

1. Introduction

2.1. Overview

As previously stated, organic solar cells (OSCs) are generally constituted by a bicontinuous interpenetrating network - made of a conjugated polymer and fullerene derivative that acts respectively as electron donor (D) and as an electron acceptor (A) material - that is able to absorb sunlight, produce excitons and thus generate charges which can migrate to the electrodes. The structure of this blend, defined as bulk heterojunction (BHJ), is presently adopted as the standard architecture for organic polymeric devices.[1] Despite regioregular poly(3-alkylthiophene)s have been the most studied and promising electron-donor materials in BHJ, further improvements are currently searched through the synthesis of narrow band gap polymers with higher carrier mobility and wider absorption of the solar spectrum in the near infrared region.

Indeed, the synthesis of conjugated copolymers combining donor and acceptor units in the same macromolecule has proved to be a well-known and powerful strategy to obtain low band gap materials for application in OSCs,[2,3,4] as the intramolecular charge transfer mechanism allows extension of the conjugation length and affects the band gap values by formation of new high-lying HOMO and low-lying LUMO energy levels.[5,6,7,8] However, even though all the required performances normally achieved by BHJ cells could be provided by a molecularly based blend,[4,9] it is important to remember that the charge transfer mechanism - since the electron donor ability is increased - may also be enhanced by the presence of S- or O-alkyl groups linked to the position 3 of thiophene rings.[10]
On the other hand, the benzothiadiazole moiety covalently inserted in the macromolecular structure in place of fullerene, is considered to be one of the best electron-acceptor moiety because, due to its highly coplanar and rigid geometry, it favors electronic conjugation and convenient physical arrangement of the material in the solid state.[2]

Therefore these (co)polymers appear particularly intriguing since they can be directly employed as single photoactive materials in organic solar cells (SMOSCs), the D and A moieties being present in the same molecule, as well as they improve the cell stability and simplify the device fabrication.[11]

On the other side, in order to improve the possibility of application of these materials, it appears of relevant interest to adopt relatively simple synthetic routes as complex and demanding procedures for the preparation of monomers and polymers are presently typically requested for this type of materials.[7]

1.2. Aim of the chapter

In this context, poly[4,7-bis(3-oxyhexylthiophen-2-yl)benzo[c][2,1,3]thiadiazole] (**P3a**) - based on electronically conjugated 3-alkoxythiophene and benzothiadiazole as electron-donor and acceptor building blocks, respectively - has been prepared starting from the related symmetrical head-to-head trimeric monomer. The monomer was obtained through an acceptably smooth reaction path and polymerized by the poorly demanding $FeCl_3$ oxidative coupling (Scheme 1).

In order to compare the effect of the presence of oxygen on the optical-electrical properties, as well as on the solid-state morphology and photovoltaic properties of the material, poly[4,7-bis[3-(6-methoxyhexyl)thiophen-2-yl]benzo[c][2,1,3]thiadiazole] (**P3b**) - having the oxygen atom in a position which is electronically isolated from the donor thiophene rings - was also prepared.

The structural, electrochemical, and photophysical properties of the prepared polymers were investigated by gel permeation chromatography (GPC), thermal analyses (TGA and DSC), ^{1}H-NMR, ultraviolet-visible (UV-Vis) and photoluminescence (PL) spectroscopy, as well as cyclic voltammetry (CV), X-ray diffractometry and reflectivity (XRR-XRD), external quantum efficiency (EQE), atomic force microscopy (AFM) and Kelvin probe atomic force microscopy (KPFM).

Both the aforementioned polymeric derivatives were finally tested as active media in air-processed SMOSCs. For comparison, the performance of the polymeric derivative with a 3-hexyl side chain (**P3c**), lacking of any oxygen atom, was also intentionally prepared by $FeCl_3$ polymerization - that is a simpler method than that reported in the literature[12] - and tested for photovoltaic activity. Moreover, being the deposition method of the film relevant to the final performance of the solar cells, a further technique such as the spray

coating was also tested in the sample preparation for the application as solar cell and the results compared to those obtained by the usual doctor-blade deposition procedure.

This chapter is based on adapted content from "Single-Material Organic Solar Cells with Conjugated Electron-Donor Alkoxy Substituted Bithiophene Units and Electron-Acceptor Benzothiadiazole Moieties in the Main Chain" M. Marinelli, M. Lanzi, A. Liscio, A. Zanelli, M. Zangoli, F. Di Maria, E. Salatelli, which has been submitted to *Journal of Material Chemistry C*.

All synthetic results, polymerizations and measurements represented in this chapter were obtained by Andrea Crocetta under the supervision of the author, or by the author herself.

2. Results and discussion

2.1. Synthesis

The monomers 4,7-bis(3-oxyhexylthiophen-2-yl)benzo[c][2,1,3]thiadiazole (**3a**) and 4,7-bis[3-(6-methoxyhexyl)thiophen-2-yl]benzo[c][2,1,3]thiadiazole (**3b**) for the synthesis of polymeric derivatives, **P3a** and **P3b**, were respectively obtained starting from 3-oxyhexylthiophene (**1a**)[7] and 3-(6-methoxyhexyl)thiophene (**1b**)[13] (details in experimental section). Polymer **P3c** was obtained from monomer **3c**, prepared starting from commercial 3-hexylthiophene (**1c**) (Scheme 1).

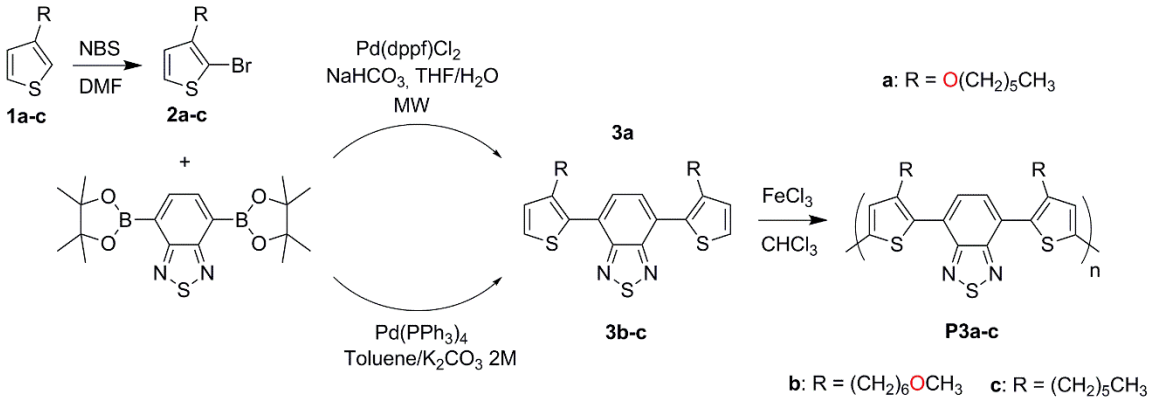

Scheme 1. Synthetic route to monomers and polymers.

In particular, compounds **1a-c** were firstly treated with N-bromosuccinimide[14] to give the corresponding 2-bromo derivatives **2a-c**, respectively.

The presence of the oxygen directly linked to the thiophene ring makes delicate the monomer synthesis (**3a**) as the starting monobrominated derivative is unstable, undergoing autopolymerization if stored in the absence of solvent. Indeed, as reported in the literature,[15] the presence of alkoxy and bromo group ortho to each other in the thiophene ring favors the interaction with the α-hydrogen of another molecule, generating a proton and activating an acid-catalyzed polymerization that leads to branched polymeric derivatives (Figure 1). The obtained by-product (**P2a**), which presumably had an overall regiorandom structure, has been anyway partially characterized.

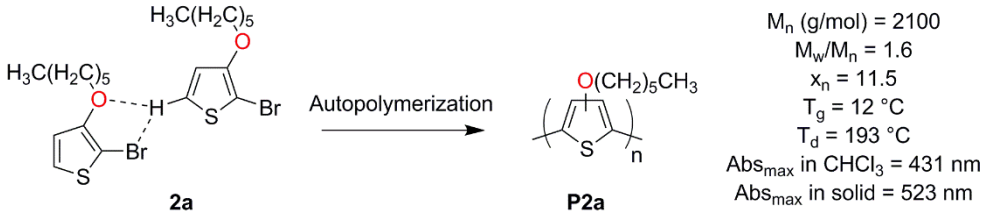

Figure 1. Autopolymerization of 2-bromo-3-alkoxyhexylthiophene (**P2a**).

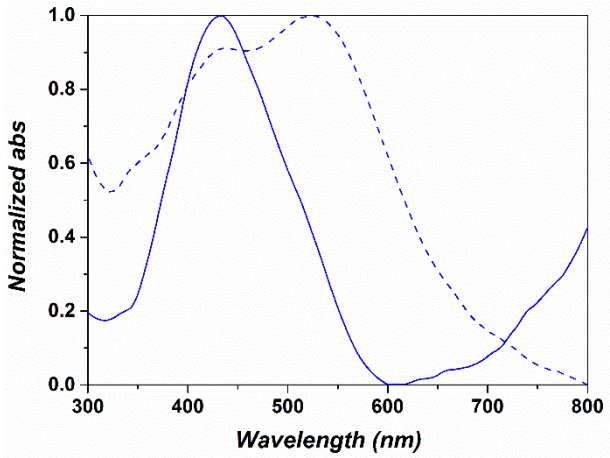

Figure 2. Normalized absorption spectra of **P2a** in $CHCl_3$ (solid line) and thin film (dotted line).

However, despite its instability, the alkoxyhexyl-derivative gives almost no reaction in the classic Suzuki-Miyaura cross-coupling reaction, which was already successfully used with the other two bromo-derivatives. For this reason, the synthesis of **3a** from **2a** was carried out following the synthetic protocol based on microwave (MW) assistance,[16] recently adopted for similar benzothiadiazole derivatives,[4] with a bis(boronic acid pinacol ester) of 2,1,3-benzothiadiazole and Pd(dppf)Cl_2 as catalyst.

In general, the Suzuki-Miyaura reaction[17,18,19] is a cross-coupling reaction between halides and boron derivatives that allows, through a palladium-based catalytic cycle, the formation of carbon-carbon bonds.

In the first place, palladium (**1**) oxidatively adds to the halide (**2**) to form the organo-palladium species (**3**); then the palladium (II) complex (**4**) - where the base was added in the prior step - gives transmetalation with the boron-ate complex (**6**) to form the new organopalladium species (**8**). In fact, despite the real mechanism involved in the transmetalation remains undiscovered, organoboron compounds have confirmed to do not undergo transmetalation in the absence of base. The third and last step in the cycle is the reductive elimination of the desired product, with the formation of the C-C bond between

the aromatic ligands and consequent regeneration of the catalyst: in our case, since a trimer needs to be obtained, the cycle is repeated twice on the same starting material (Scheme 2). The MW assistance allowed to obtain **3a** in similar yields as **3b** and **3c**, but with a remarkable improvement of rate (30 min compared to 24 h), accompanied by a significant reduction of the reaction temperature (80°C vs. 110°C), with a consequent lower production of by-products.

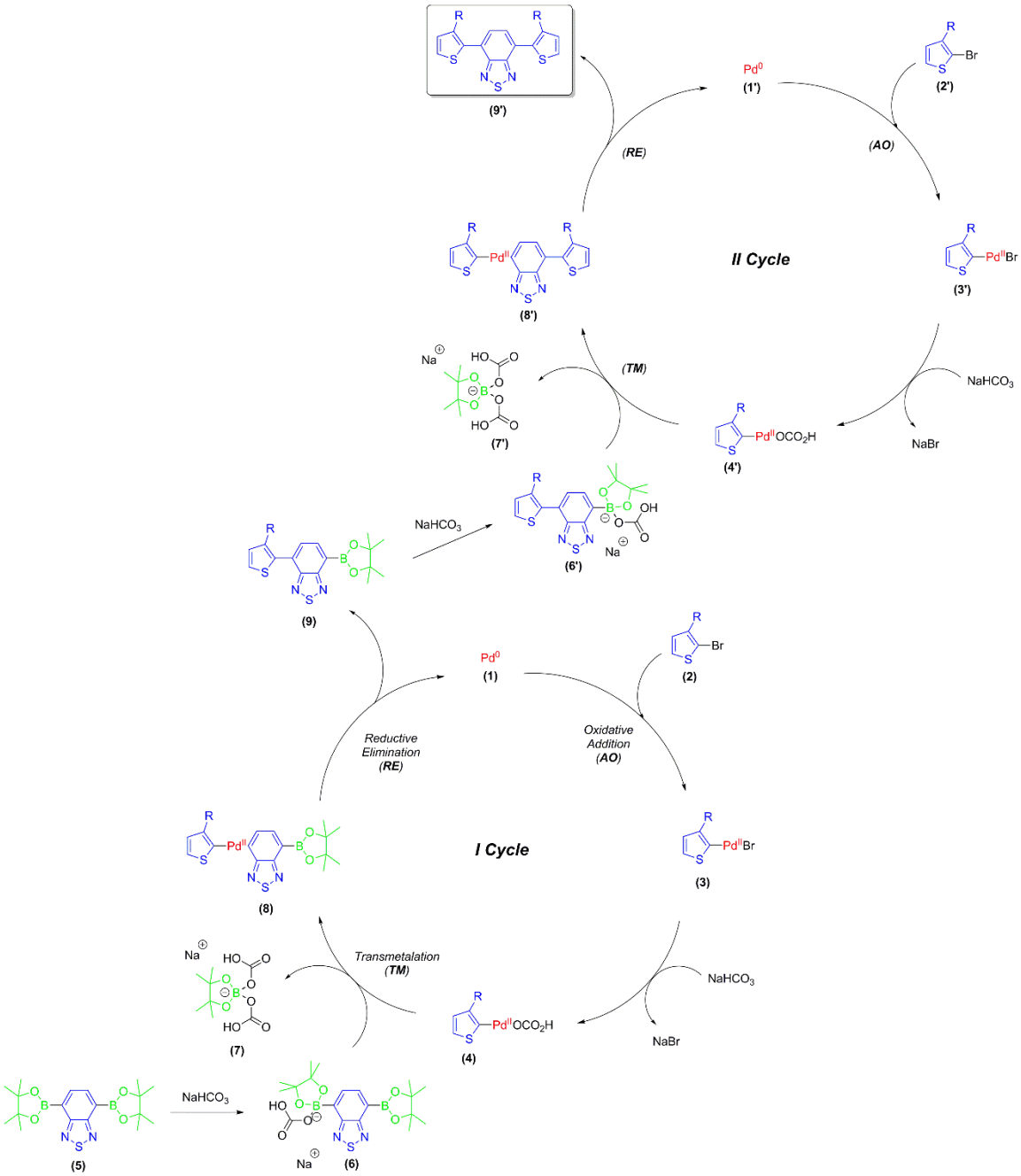

Scheme 2. Mechanism of Suzuki-Miyaura cross-coupling reaction used for the synthesis of monomers.

The polymerization of **3a** and **3b** to the corresponding **P3a** and **P3b** derivatives was performed with good yields through the well-established and straightforward procedure of oxidative coupling with $FeCl_3$.[20] In fact, even though this procedure is a non-regiospecific method when applied to 3-alkylthiophenes, in this case exclusively tail-to-tail (TT) junctions between the thiophene rings are obtained, due to the symmetrical structure and chemical equivalence of the coupling positions in the monomers.[21] As mentioned in the Introduction section of this chapter, the polymerization of **3c** to **P3c** was also carried out in the presence of $FeCl_3$ in order to obtain a product comparable to the related **P3a** and **P3b** derivatives (Table 1), since the synthetic procedure reported by El-Shehawy[12] through Stille coupling gave a product with higher molecular mass and polydispersity index.

The chemical structure of monomers (**3a-c**) and polymers (**P3a-c**) was confirmed by ^{1}H-NMR (Figure 11 and 12, experimental section), displaying a significant downshield shift of the aryl protons in both the oxyhexyl derivatives when compared to the corresponding protons of **3b-c** and **P3b-c**, indicating an increased electron delocalization in the benzothiadiazole moiety due to the presence of the oxygen directly linked to thiophene ring.

Table 1. Yields and characterization data of polymeric derivatives.

Polymers	*Yield (%)* [a]	M_n *(g/mol)* [b]	M_w/M_n [c]	x_n [d]	T_g *(°C)* [e]	T_d *(°C)* [f]
P3a	98	8600	1.1	17.3	43	238
P3b	79	15700	1.1	29.8	3	144
P3c	54	11800	1.2	25.3	1	139

[a] Weight of polymer/weight monomer x 100; [b] Average molecular weight determined by GPC in $CHCl_3$; [c] Polydispersity index; [d] Average polymerization degree; [e] Glass transition temperature determined by DSC (second heating cycle); [f] Decomposition temperature determined by TGA.

2.2. Thermal properties

As far as the thermal properties are concerned (Table 1 and Figure 3), since both polymers have the hexyl moiety directly linked to the thiophene ring, the behaviour of **P3b** resulted quite similar to that of **P3c**, thus evidencing that the presence of methoxy group in the side chain does not substantially affect the T_g and T_d values in the bulk. By contrast, **P3a** exhibited more pronounced thermal properties, reasonably ascribable to an increased

aromatic conjugation that favors a more compact arrangement of the macromolecules in the solid state, which could be of interest for future applications.

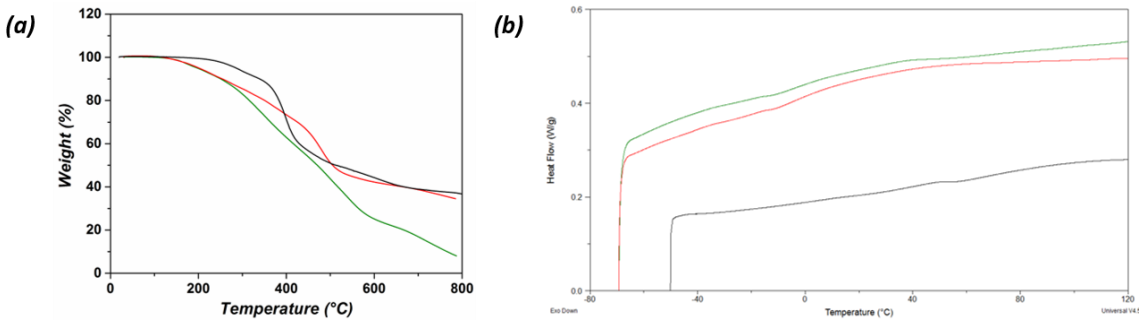

Figure 3. (a) TGA and (b) DSC thermograms of **P3a** (black line), **P3b** (red line) and **P3c** (green line).

However, as only glass transitions were displayed in the DSC thermograms, it is reasonable to assume that all the examined polymeric samples are substantially in the amorphous state, although X-ray reflectivity (XRR) and X-ray diffraction (XRD) measurements carried out on **P3a-c** samples as powders - in collaboration with Dr. Massimo Gazzano (CNR-ISOF, Bologna) - display the presence of a small amount of crystallinity in the material (Figure 4). This can be justified on the basis that the small amount of crystal phase is below the detection limit of DSC analysis.

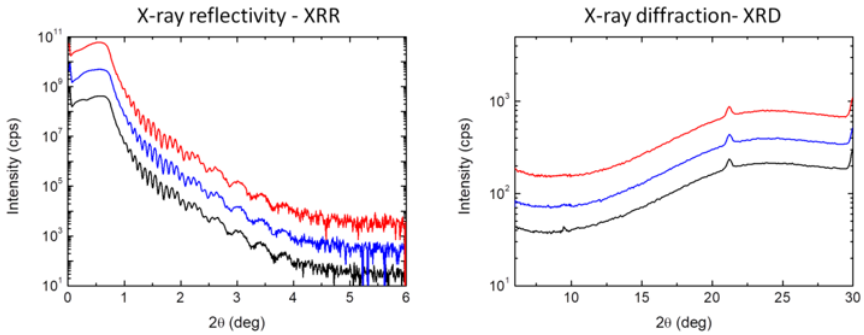

Figure 4. X-ray reflectivity and X-ray diffraction of thin films of **P3a** (red line), **P3b** (blue line) and **P3c** (black line).

2.3. Optical properties

The UV-Vis spectra of the monomers (Table 2 and Figure 5a) show a noticeable bathochromic shift of the absorption and emission maxima of **3a** with respect to **3b** and **3c**, with a slightly lower value of the related Stokes shift for **3a** in the PL spectrum, probably ascribable to the increased coplanarity of the aromatic rings with respect to

thiophene moieties. On the other hand, the absence of any electronic effects on the aromatic system by the side chain methoxy group in **3b** was further confirmed, since the absorption spectra of **3b** and **3c** appear actually identical.

Table 2. Maximum absorption (λ_{max}) and emission (λ_{em}) wavelengths (nm) of monomers and polymers in $CHCl_3$ solution.

Monomers	*λ_{max} (nm)*	*λ_{em} (nm)*	*Stokes shift*	*Polymers*	*λ_{max} (nm)*	*λ_{em} (nm)*	*Stokes shift*
3a	477	612	135	***P3a***	570	677	107
3b	406	554	148	***P3b***	487	650	163
3c	403	554	151	***P3c***	453	629	176

As commonly observed for alternating electron donor-acceptor (co)polymers, the UV-Vis spectra of the polymeric samples in solution (Figure 5a) are characterized by multiple absorptions; the one at lower wavelength, in the region below 400 nm, can be assigned to the π–π* electronic transition of bithiophene donor units, whereas the high-wavelength band (453–570 nm) is related to the intramolecular π–π* transition between the ground and the excited states of the donor-acceptor charge transfer complex.[12]

In addition to the expected red shift to higher wavelength of the absorption maximum of **P3a-c** in comparison with **3a-c**, due to an enhanced electronic conjugation in the main chain, it is noteworthy to observe the remarkable bathochromic effect in **P3a** which, despite its lower polymerization degree, can be probably induced by the presence of oxygen directly linked to thiophene ring (Table 2).

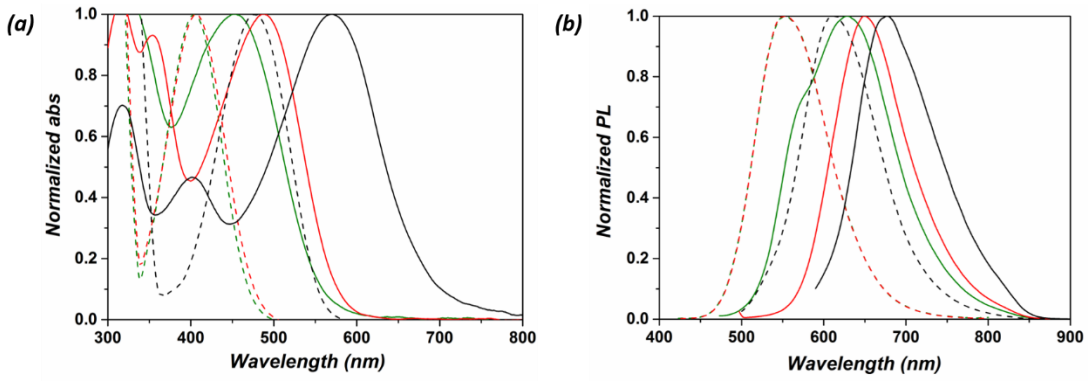

Figure 5. (a) Normalized absorption and (b) photoluminescence spectra in $CHCl_3$ of monomers (dashed line) and polymers (solid line): **3a-P3a** (black), **3b-P3b** (red) and **3c-P3c** (green).

Similarly to the absorption behaviour, the photoluminescence spectrum of **P3a** (Figure 5b) exhibits an emission maximum at higher wavelength if related to **P3b** and **P3c**. The lower Stokes shift value, which is indicative of reduced energy level of the excited state, could be associated to the presence of more ordered conformations of the macromolecules in solution promoted by the increased resonance in the main chain. Otherwise, the higher absorption and emission λ_{max} values of **P3b** compared to **P3c** may be attributed to higher polymerization degree of the aforementioned sample.

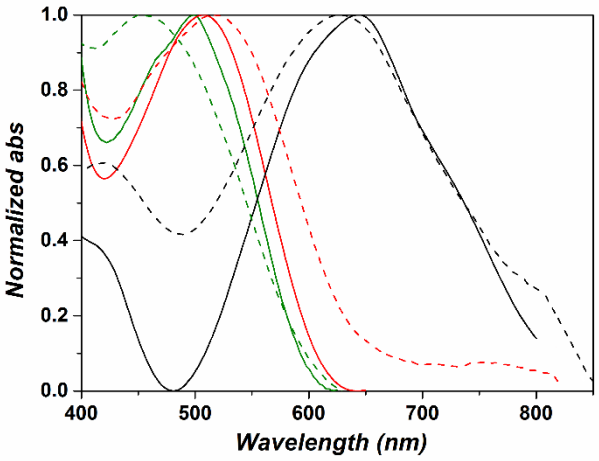

Figure 6. Normalized absorption spectra of polymers as films cast from chlorobenzene by the doctor-blade technique (solid line) and spray coating (dashed line): **P3a** (black), **P3b** (red) and **P3c** (green).

The UV-Vis spectra of thin films of the polymers, obtained by the doctor-blade technique from chlorobenzene solution, are reported in Figure 6 and the related data in Table 3. The absorptions of all samples appear significantly red-shifted and exhibit broader bands than the corresponding absorptions in solution. Again, **P3a** displays a larger bathochromic effect (74 nm), with respect to solution, than **P3b** and **P3c**.

Being the deposition method of the film relevant to the preparation and performance of the solar cells, the spray coating from chlorobenzene as additionally technique was also tested. As reported in Figure 6, the spray coating technique produces thin films with some further absorptions at higher wavelength, especially for **P3a** and **P3b**. However, in agreement with the XRR and XRD measurements, they do not appear particularly structured.

In order to have a better and adequate understanding of the electrochemical behaviour of the synthesized materials, also the optical band gap values E_g^{opt} of the polymeric derivatives have been calculated[22] by the corresponding onset absorption wavelengths in the solid state. As reported in Table 3, the lowest energy gap value of 1.48 eV was found for the thin film of **P3a** prepared by spray coating, whereas **P3b** and **P3c** displayed a

similar behaviour, with E_g^{opt} close or superior to that reported for P3HT (ca. 1.90 eV),[23] regardless the deposition procedure adopted.

Table 3. Maximum absorption (λ_{max}) wavelengths and optical band gap (E_g^{opt}) of thin films of **P3a-c** deposited by doctor-blade technique or spray coating from chlorobenzene.

Filming method:	*Doctor-blade*		*Spray coating*	
Polymers	λ_{max} *(nm)*	E_g^{opt} *(eV)*	λ_{max} *(nm)*	E_g^{opt} *(eV)*
P3a	644	1.53	629	1.48
P3b	507	2.03	561	1.93
P3c	500	2.10	454	2.07

2.4. Electrochemical properties

Cyclic voltammetry measurements - in collaboration with Dr. Alberto Zanelli (CNR-ISOF, Bologna) - were carried out on thin films of **P3a-c** obtained by doctor-blade or spray coating deposition technique from chlorobenzene solutions. The results are reported in Table 4 and the related voltammograms in Figure 7.

Table 4. Redox potentials[a], HOMO/LUMO energy levels[b] and electrochemical energy gap values[b] of the polymers deposited by doctor-blade (in black) or spray coating (in red) technique.

Polymers	E_{ox}^{on}	E_{red}^{on}	*HOMO*	*LUMO*	E_g
P3a	0.66	-1.17	-5.34	-3.51	1.83
	0.62	-1.05	-5.30	-3.63	1.67
P3b	0.87	-1.16	-5.55	-3.52	2.03
	0.86	-1.04	-5.54	-3.64	1.90
P3c	1.02	-1.05	-5.70	-3.63	2.07
	1.03	-1.07	-5.71	-3.61	2.10

[a] In V vs. SCE; [b] In eV.

It can be noted that, regardless the deposition method adopted, the presence of oxygen in the side chain of thiophene rings reduces the oxidation potential of the macromolecules, more significantly for **P3a** with respect to **P3b**. Whereas, despite the values of reduction potential appear rather insensitive to the chemical structure of the side chain substituent, the deposition by spray coating seems to favor less negative values of this potential, thus leading to lower energy gaps, especially for **P3a**, in agreement with the results obtained from the absorption spectra.

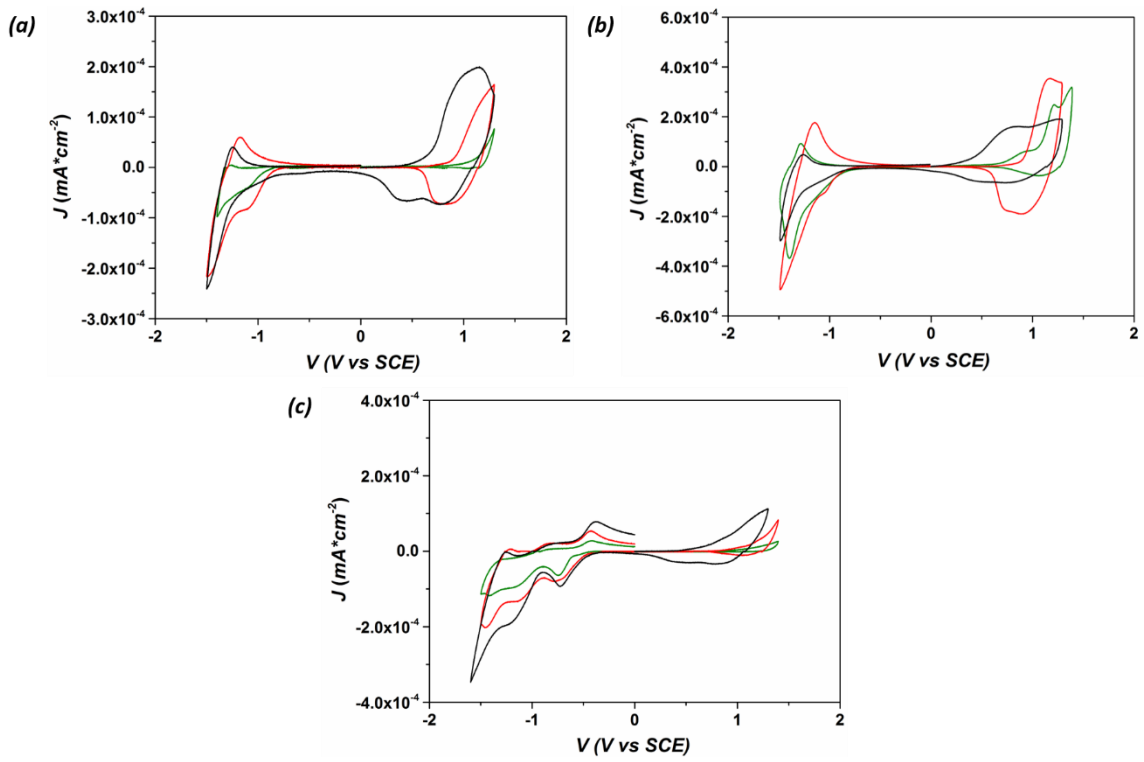

Figure 7. Second cyclic voltammograms in the solid state at 0.1 V s^{-1} of **P3a** (black line), **P3b** (red line) and **P3c** (green line) films prepared by doctor-blade deposition (a), spray coating deposition (b) and as blends with **$PC_{61}BM$** (c) prepared by doctor-blade deposition.

Although the poly[4,7-bis(3-alky-2-yl)benzo[c][2,1,3]thiadiazole] (**P3a-c**) have been prepared with the purpose to test them as active media in single material organic solar cells (SMOSCs), cyclic voltammetry measurements were also made on blends of **P3a-c** with **$PC_{61}BM$** (1/1 w/w) prepared by doctor-blade deposition. In fact, independently from the way of application, it could be useful to gain information about the behaviour of the material when in the presence of additional electron acceptor derivatives.

Again, **P3a** showed the lowest value of oxidation potential and reduction potential similar to **P3b** (Table 5 and Figure 7c), thus confirming to be a low band-gap polymer (< 2 eV) with promising potential for application as active material in photovoltaic cells.

Table 5. Redox potentials[a], HOMO/LUMO energy levels[b] and electrochemical energy gap values[b] of **P3a-c** blends with **$PC_{61}BM$** deposited by doctor-blade.

Blends	E_{ox}^{on}	E_{red}^{on}	*HOMO*	*LUMO*	E_g
P3a:PC$_{61}$BM	0.39	-1.00	-5.07	-3.68	1.39
P3b:PC$_{61}$BM	1.01	-1.01	-5.69	-3.67	2.02
P3c:PC$_{61}$BM	0.84	-[c]	-5.52	-[c]	-

[a] In V vs. SCE; [b] In eV; [c] Not determined.

2.5 Photoactivity

The J−V features of the best performing SMOSCs, with structure ITO/PEDOT:PSS/photoactive polymer/Al, are reported in Figure 8a and 8b with the related photovoltaic parameters listed in Table 6.

Table 6. Properties of organic solar cells prepared with polymeric derivatives **P3a-c** prepared by doctor-blade or spray coating technique (average values collected from ten devices).

Polymers	J_{sc} *(mA/cm²)* [a]	J_{sc} *(EQE)*	V_{oc} *(V)* [b]	*FF* [c]	*PCE (%)* [d]
P3a [e]	2.63±0.09	2.59	0.41±0.01	0.51±0.02	0.55±0.04
P3b [e]	0.83±0.04	0.81	0.44±0.01	0.44±0.01	0.16±0.01
P3c [e]	0.11±0.01	0.11	0.45±0.01	0.41±0.01	0.02±0.01
P3a [f]	3.72±0.15	3.65	0.39±0.01	0.53±0.02	0.77±0.03
P3b [f]	1.16±0.09	1.07	0.42±0.01	0.43±0.02	0.21±0.02
P3c [f]	0.11±0.08	0.11	0.45±0.01	0.42±0.02	0.02±0.01

[a] Short circuit current density; [b] Open circuit voltage; [c] Fill factor; [d] Photovoltaic cell efficiency; [e] By doctor-blade technique; [f] By spray coating deposition.

As expected on the base of energy gap values determined from optical spectra and cyclic voltammetry, the devices containing the photoactive component **P3a** and **P3b** deposited by spray coating show the best efficiency results, achieving the maximum value of 0.77% with **P3a** and 0.21% for **P3b**; differently, **P3c** shows the lowest PCE value.

It can be assumed that these results are primarily originated by the J_{sc} values, which are dependent on factors related to the efficiencies of each stage in the photovoltaic process - efficiency of photoabsorption, diffusion and dissociation of excitons, transport and collection of charge - and appear generally enhanced, mainly for **P3a**, by the spray coating procedure with respect the doctor-blade deposition.

However, even if the V_{oc} values seem to be independent from the deposition method and the nature of the compound, they are in good agreement with the trend observed for the electrochemical experiments carried out on the polymer thin films. Indeed, when the Eg value decreases, the V_{oc} - as being this parameter dependent to a first approximation on the difference between the HOMO of the donor and the LUMO of the acceptor - accordingly decreases.

The overall cell performances of **P3a** and **P3b**, result to be improved by the spray coating deposition, suggesting a more favourable arrangement of the macromolecules to exciton diffusion and charge transport. Moreover, although not directly involved in the aromatic

conjugation, it is also noteworthy that the presence of oxygen in the side chain of **P3b** favors to some extent the photoconversion efficiency with respect to **P3c**.

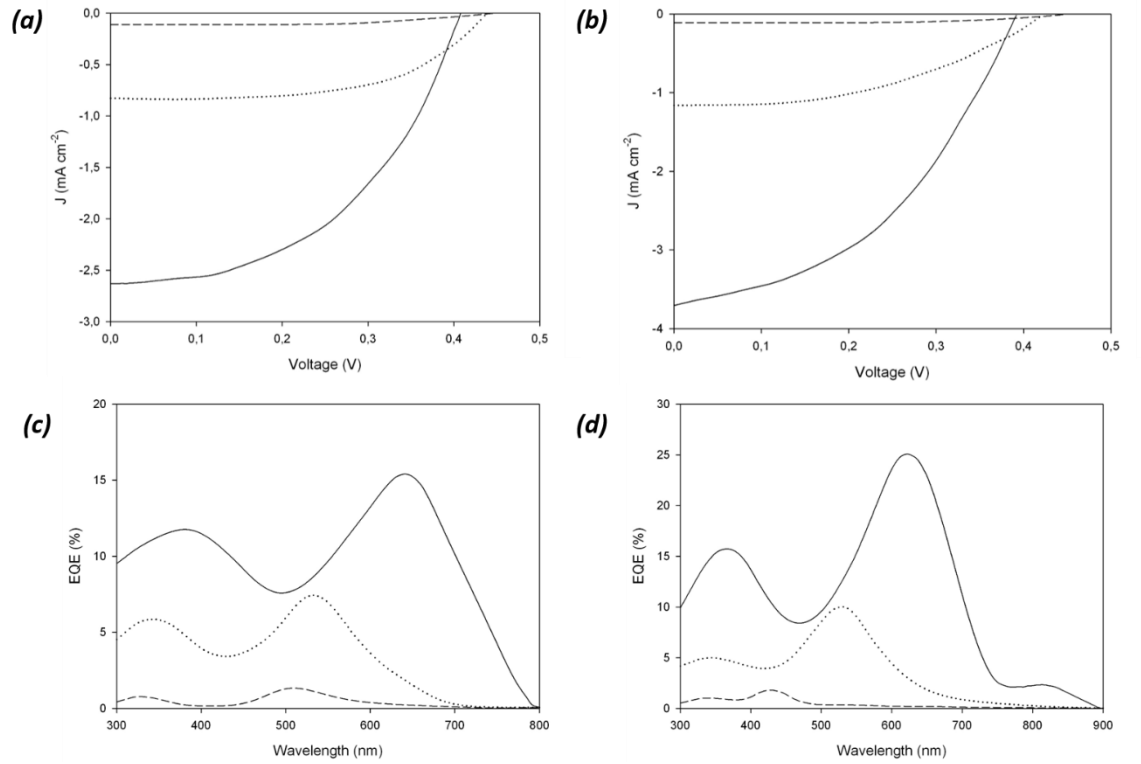

Figure 8. J-V characteristics under white light illumination of **P3a** (solid line), **P3b** (dotted line) and **P3c** (dashed line) cells prepared by doctor-blade (a) or spray coating (b) deposition; EQE of the **P3a-c** cells prepared by doctor-blade (c) or spray coating (d) deposition.

The external quantum efficiencies (EQE) of the cells optimized for thickness (Figure 8c and 8d) - which were carried out in collaboration with Dr. Filippo Pierini (IPPT-PAN, Warsaw) - display maxima ranging from 15% (doctor blade) to 28% (spray coating). The EQE values in the examined range were used for calculation of J_{sc}, obtaining data (Table 6) that are consistent with the experimental findings, thus confirming the best performance of the device prepared with **P3a** by spray coating. Furthermore, the EQE profiles follow the trend observed in the UV-Vis spectra of polymers in thin film, indicating that the whole absorption effectively contributes to the photocurrent. It is also particularly noteworthy the wide range of absorption obtained for **P3a** deposited by spray coating, that could be one of the factors on the basis of the high observed value of J_{sc}.

In according to the idea of a deepest investigation of the electrochemical behaviour, blends of **P3a-c** with $PC_{61}BM$ (1/1 w/w) were also tested by doctor-blade deposition in bulk heterojunction organic solar cells (Table 7 and Figure 9).

Table 7. Properties of organic solar cells prepared with blends of **P3a-c** with **$PC_{61}BM$**, prepared by doctor-blade technique (average values collected from ten devices).

Blends	J_{sc} *(mA/cm²)* [a]	J_{sc} *(EQE)*	V_{oc} *(V)* [b]	*FF* [c]	*PCE (%)* [d]
P3a:PC₆₁BM	1.81±0.09	1.73	0.43±0.01	0.43±0.02	0.33±0.02
P3b:PC₆₁BM	1.19±0.07	1.12	0.45±0.01	0.41±0.01	0.22±0.02
P3c:PC₆₁BM	0.83±0.06	0.81	0.50±0.01	0.41±0.02	0.17±0.01

[a] Short circuit current density; [b] Open circuit voltage; [c] Fill factor; [d] Photovoltaic cell efficiency.

The efficiency of **P3a** does not improve when tested in the presence of PCBM as an additional electron acceptor. Although the electrochemical E_g of the mixture with PCBM appears reduced by the presence of the additional electron acceptor, the V_{oc} value of the cell containing **P3a** results substantially unaffected if compared to the sample obtained by the doctor-blade deposition technique; while both the J_{sc} and fill factor (FF) values are reduced, presumably as a consequence of the hindering action of PCBM towards the intermolecular current photogeneration inside the macromolecular aggregates.

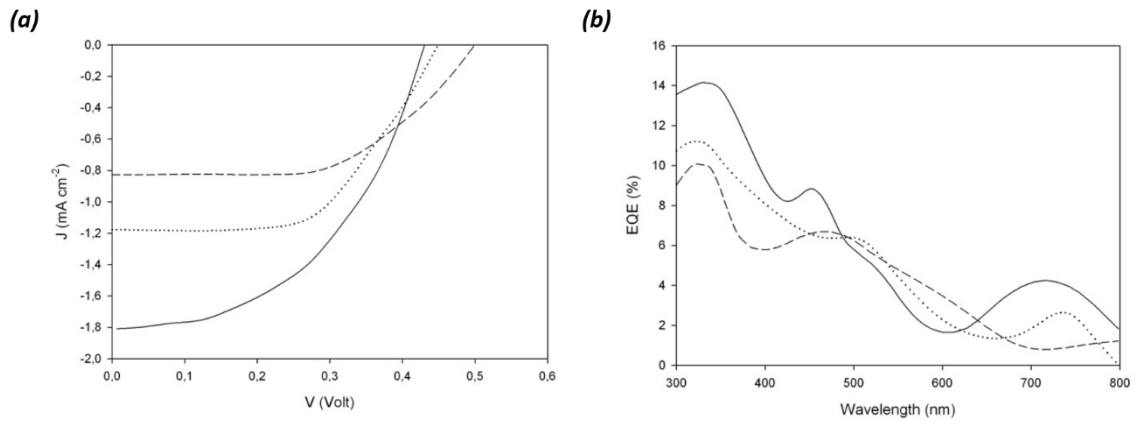

Figure 9. (a) J-V curves under white light illumination and (b) EQE of cells prepared by doctor-blade deposition with blends of **P3a-c/$PC_{61}BM$**. **P3a**: solid line, **P3b**: dotted line; **P3c** dashed line.

2.6. Investigation of morphology

Since the electrical properties of the films strongly depend on their structure, the surface morphology and the corresponding surface photo-voltage were investigated by AFM and KPFM techniques (Table 8) in collaboration with Dr. Andrea Liscio (CNR-IMM, Rome). The morphology study was only carried out on films of polymers **P3a-c** deposited by spray coating, due to their best photoactivity results.

Table 8. KPFM data for **P3a**, **P3b** and **P3c**.

Polymers	R_{RMS} *(nm)*	*SPV roughness (mV)*	*ΔSPV (V)*
P3a	40*	480 ± 40	1.4 ± 0.2
P3b	100*	170 ± 20	0.2 ± 0.1
P3c	100*	100 ± 20	0.1 ± 0.1

* Standard deviation = 10%.

All three materials exhibit a quite rough surface (R_{RMS}) - ranging from ~ 40 nm (**P3a**) to ~ 100 nm (**P3b** and **P3c**) - as outlined in the AFM images (Figure 10). Furthermore, micrometric structures are also present on the surfaces with different sizes, in the range of 0.2 – 2 µm for **P3a**, larger than 5 µm for **P3b** and smaller than 1 µm for **P3c**.

Maps of the surface density of photogenerated charges were measured by KPFM, making a comparison of two different parameters: SPV roughness and ΔSPV. The first one corresponds to the dispersivity of the measured data - since as higher is the SPV roughness, as lower is the homogeneity of the photo-charge density - while the latter is the difference between the charge density measured after and before illumination.

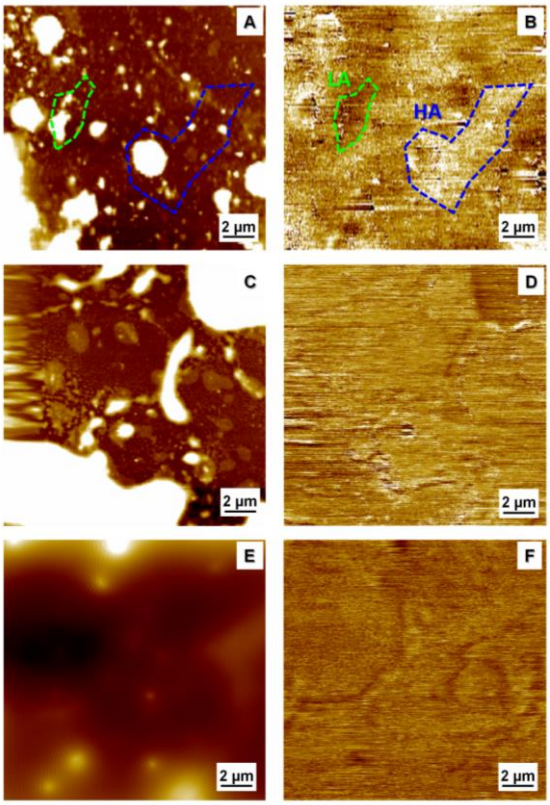

Figure 10. AFM (left) and KPFM (right) images of **P3a** (A, B), **P3b** (C, D) and **P3c** (E, F). Z- range: AFM images (A, C) 100 nm, (E) 300 nm; KPFM images (B, D, F) 1.2 V.

As observed, higher both SPV roughness and ΔSPV values are displayed by **P3a** film than the other two samples, **P3b** and **P3c**. KPFM measurements are performed illuminating continuously all the samples (i.e. steady-state). Thus, the presence of patches with larger SPV indicates a larger lifetime of the photo-charges with a corresponding increase of the recombination time. This inhomogeneity in the photo-charges reflects an overall higher ΔSPV value clearly showing a better intrinsic performance of the system respect to the other two materials.

2.7. Conclusions

Intrinsically regioregular, linear polymeric single-component photoactive materials for solar cells containing 3-substituted bithiophene and benzothiadiazole moieties in the main chain as electron donor and acceptor moieties, respectively, have been prepared in good yields through a straightforward oxidative polymerization process employing $FeCl_3$.

The side-chain substituent linked to the bithiophene moieties plays an important role, significantly affecting the optical properties as well as the energy gap values of the material. In particular, the sample bearing the side chain 3-oxyalkyl group displays enhanced electron donor properties allowing to achieve the best performances in term of sunlight photoconversion efficiency, in line, or even better, with respect to currently reported values.

Moreover, in all cases the deposition of the polymers through spray coating allowed to improve the PCE values, if compared to deposition by doctor blade technique.

3. Experimental section

3.1. Materials

All commercial reagents and solvents were used as received unless otherwise stated. *N*-Bromosuccinimide (NBS) (Sigma-Aldrich) was recrystallized from hot water. Anhydrous solvents were prepared following literature procedures[24] and stored over molecular sieves. All manipulations involving air- or moisture-sensitive reagents were performed under nitrogen in dried glassware.

3.2. Synthesis of monomers

*3.2.1. 3-Hexyloxythiophene (**1a**)*

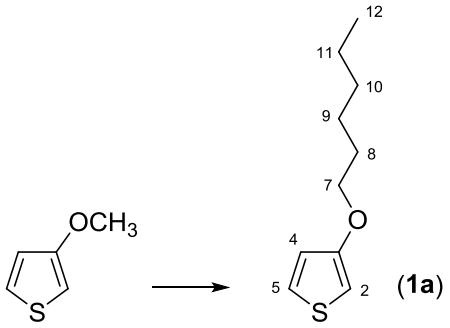

To a three-neck flask, containing a solution of 3-methoxythiophene (Sigma-Aldrich, 2.00 g, 17.4 mmol) in 16.8 ml of toluene, 1-hexanol (4.4 mL, 34.8 mmol) and p-toluenesulfonic acid monohydrate (0.60 g, 2.6 mmol) were sequentially added under stirring and inert atmosphere. The mixture was heated to 120 °C under N_2 for 20 h. After cooling, the reaction mixture was then poured into water (150 ml) and extracted with CH_2Cl_2. The organic phase was washed with water, dried with Na_2SO_4 and the solvent removed by evaporation under reduced pressure. The crude product was finally purified by column chromatography on silica gel with cyclohexane/CH_2Cl_2 4:1 v/v as eluent to afford 2.21 g (12.0 mmol, 68% yield) of **1a** as a colorless liquid.

^{1}H NMR ($CDCl_3$, ppm): δ 7.16 (dd, 1H, 5-H), 6.78 (dd, 1H, 4-H), 6.22 (dd, 1H, 2-H), 3.98 (t, 2H, 7-H), 1.75 (m, 2H, 8-H), 1.50-1.32 (m, 6H, 9-H, 10-H and 11-H), 0.91 (t, 3H, 12-H).

*3.2.2. 3-(6-Methoxyhexyl)thiophene (**1b**)*

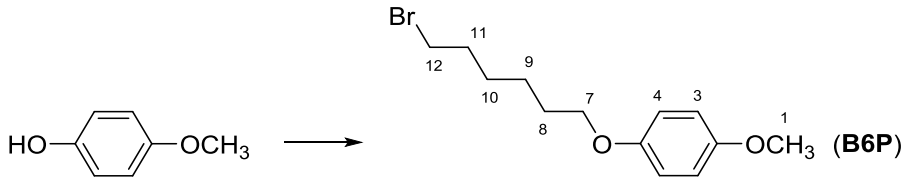

A solution of KOH (32.32 g, 576.1 mmol) and p-methoxyphenol (Sigma-Aldrich, 49.46 g, 399.8 mmol) in 80 ml of methanol was added in 90 minutes to a solution of 1-6-dibromohexane (Sigma-Aldrich, B6B, 200.0 g, 819.7 mmol) in 160 ml of acetone and then heated under stirring and reflux for 1 h. After cooling to room temperature and removal of KBr as a solid by filtration, the reaction mixture was evaporated under reduced pressure. The crude product was dissolved in Et_2O (100 ml) and firstly washed with NaOH 2% wt. and then with water. After drying with Na_2SO_4 and concentration at reduced pressure, the crude product was purified by vacuum distillation (P=0,5 mbar, T=52°-54°C) in order to eliminate the excess of B6B and afford 89.56 g (311.8 mmol, 78% yield) of 1-bromo-6-(p-methoxyphenoxy)hexane (**B6P**) as a white solid.

^{1}H-NMR ($CDCl_3$, ppm): δ 6.83 (s, 4H, 3-H and 4-H), 3.91 (t, 2H, 7-H), 3.77 (s, 3H, 1-H), 3.42 (t, 2H, 12-H), 1.89 (m, 2H, 8-H), 1.77 (t, 2H, 11-H), 1.53-1.46 (m, 4H, 9-H and 10-H).

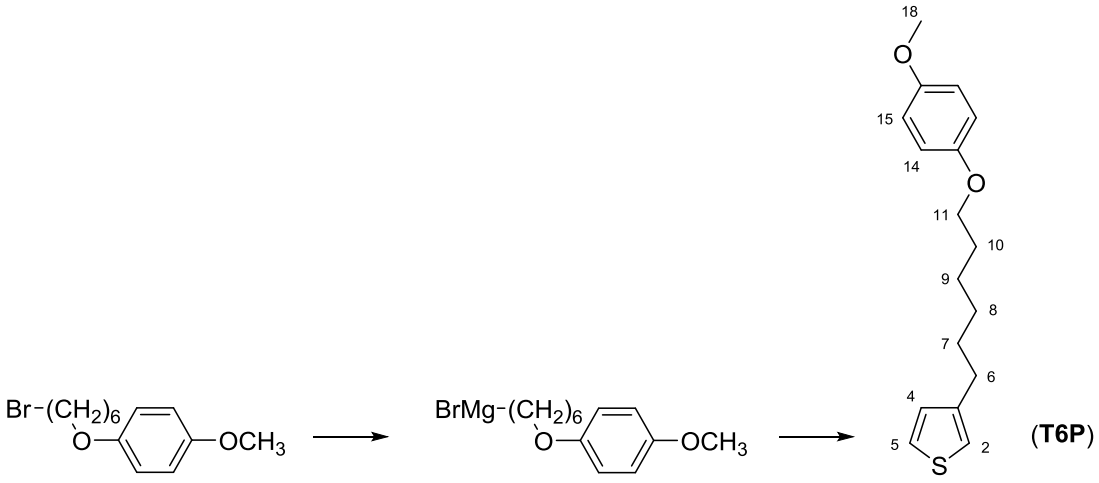

To a three-neck flask, containing B6P (20.0 g, 69.6 mmol) and Mg° (1.75 g, 72.0 mmol), anh. Et_2O (150 mL) was added under stirring and nitrogen atmosphere; the reaction mixture was then heated to 35°C for 5 h. The Grignard compound of B6P was subsequently transferred via cannula to a second flask and added drop by drop at low temperature (-5/-8°C) to a suspension of 3-bromothiophene (Sigma-Aldrich, 9.62 g, 59.0 mmol) and

$Ni(dppp)Cl_2$ (Sigma-Aldrich, 0.056 g, 0.104 mmol). The mixture was heated under reflux for 16 h and afterwards poured in HCl 2% wt. (200 ml) followed by extraction with Et_2O. The organic phase was washed with water, dried with Na_2SO_4 and the solvent removed by evaporation under reduced pressure. The crude product was finally purified by recrystallization from ligroin, followed by column chromatography on silica gel with hexane/Et_2O 97:3 v/v as eluent to obtain 8.49 g (29.32 mmol, 42% yield) of 3-[6-(p-methoxyphenoxy)hexyl]thiophene (**T6P**) as a white solid.

^{1}H-NMR ($CDCl_3$, ppm): δ 7.24-7.22 (m, 1H, 5-H), 6.94-6.90 (m, 2H, 2-H and 4-H), 6.82 (s, 4H, 14-H and 15-H), 3.90 (t, 2H, 11-H), 3.76 (s, 3H, 18-H), 2.64 (t, 2H, 6-H), 1.82-1.70 (m, 2H, 10-H), 1.70-1.58 (m, 2H, 7-H), 1.54-1.38 (m, 4H, 8-H and 9-H).

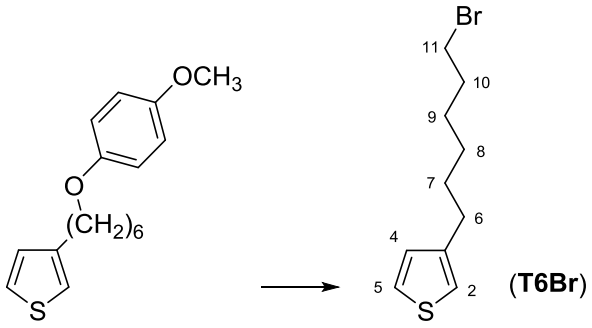

A mixture of acetic anhydride (19.5 ml) and HBr 48% wt. (14.1 ml) was added to T6P (6.00 g, 20.69 mmol) and the reaction mixture was heated at 90°C for 24 h. After cooling and dilution with water, the mixture was extracted with petroleum ether and then washed with saturated $NaHCO_3$ solution and finally water to neutrality. After drying with Na_2SO_4 and concentration at reduced pressure, the crude product was purified by column chromatography on silica gel with cyclohexane as eluent to afford 3.92 g (15.93 mmol, 77% yield) of 3-(6-bromohexyl)thiophene (**T6Br**) as a colorless oil.

^{1}H-NMR ($CDCl_3$, ppm): δ 7.24-7.22 (m, 1H, 5-H), 6.94-6.90 (m, 2H, 2-H and 4-H), 3.40 (t, 2H, 11-H), 2.63 (t, 2H, 6-H), 1.90-1.82 (m, 2H, 10-H), 1.68-1.60 (m, 2H, 7-H), 1.50-1.32 (m, 4H, 8-H and 9-H).

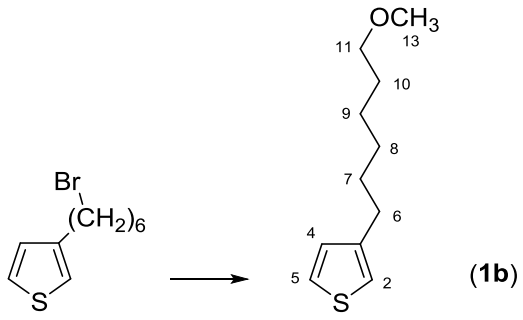

(**1b**)

A solution of T6Br (0.3 M, 3.83 g, 15.5 mmol) in 52 ml of anh. MeOH was added to a solution of MeONa in MeOH 30% wt. (Sigma-Aldrich, 16.4 ml) under stirring and nitrogen atmosphere. The reaction mixture was refluxed for 4 h, afterwards poured into water and extracted with Et_2O. The crude product was dried with Na_2SO_4 and concentrated at reduced pressure obtaining 2.78 g (14.1 mmol, 90% yield) of 3-(6-methoxyhexyl)thiophene (**1b**) as a colorless liquid.

^{1}H-NMR (ppm): δ 7.24-7.22 (m, 1H, 5-H), 6.94-6.90 (m, 2H, 2-H and 4-H), 3.36 (t, 2H, 11-H), 3.33 (s, 3H, 13-H), 2.63 (t, 2H, 6-H), 1.68-1.54 (m, 4H, 7-H and 10-H), 1.42-1.32 (m, 4H, 8-H and 9-H).

*3.2.3. 2-Bromo-3-hexyloxythiophene (**2a**)*

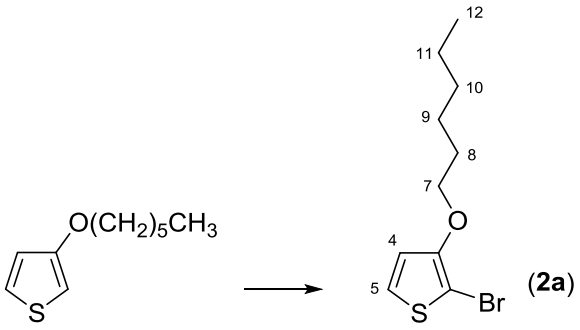

(**2a**)

N-Bromosuccinimide (NBS) (386 mg, 2.2 mmol) dissolved in 3 ml of N,N-dimethylformamide (DMF) was added in 1h to a solution of 3-hexyloxythiophene (400 mg, 2.2 mmol) in 3 ml of DMF at 0°C, under stirring and protection from light. The mixture was stirred for 24h at room temperature in the dark and then poured into water (50 ml) and extracted with Et_2O. After drying on Na_2SO_4 and solvent evaporation at reduced pressure, the crude product was purified by column chromatography on silica gel with cyclohexane/ethyl acetate 19:1 v/v as eluent to afford 560 mg (98% yield) of **2a** as a yellowish liquid. *Caution! The product appears to be unstable, undergoing exothermic autopolymerization if stored in the absence of solvent even in the cold.*

^{1}H-NMR ($CDCl_3$, ppm): δ 7.18 (d, 1H, 5-H), 6.78 (d, 1H, 4-H), 3.98 (t, 2H, 7-H), 1.75 (m, 2H, 8-H), 1.50-1.32 (m, 6H, 9-H, 10-H and 11-H), 0.91 (t, 3H, 12-H).

*3.2.4. 2-Bromo-3-(6-methoxyhexyl)thiophene (**2b**)*

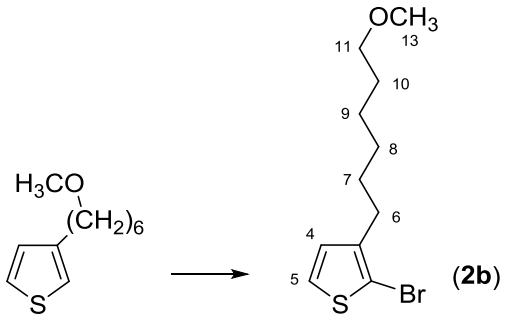

The same procedure described for 2a was followed starting from 3-(6-methoxyhexyl)thiophene (262 mg, 1.32 mmol) and NBS (235 mg, 1.32 mmol) in DMF obtaining 325 mg (89% yield) of pure **2b** as a yellowish oil, without need of chromatographic purification.

^{1}H-NMR ($CDCl_3$, ppm): δ 7.18 (d, 1H, 5-H), 6.78 (d, 1H, 4-H), 3.36 (t, 2H, 11-H), 3.33 (s, 3H, 13-H), 2.56 (t, 2H, 6-H), 1.64-1.54 (m, 4H, 7-H and 10-H), 1.44-1.34 (m, 4H, 8-H and 9-H).

*3.2.5. 2-Bromo-3-hexylthiophene (**2c**)*

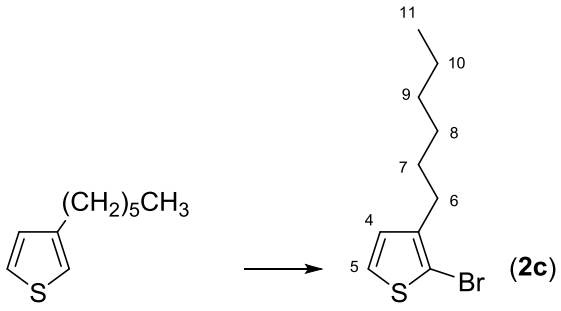

The same procedure described for 2a was followed starting from 3-hexylthiophene (Sigma-Aldrich) (1.00 g, 0.006 mol) in 7 ml of DMF and NBS (1.06 g, 0.006 mol) dissolved in 7 ml of DMF. The crude product was purified by column chromatography on silica gel with cyclohexane as eluent to obtain 1.21 g (77% yield) of **2c** as a colorless liquid.

^{1}H-NMR ($CDCl_3$, ppm): δ 7.17 (d, 1H, 5-H), 6.78 (d, 1H, 4-H), 2.56 (t, 2H, 6-H), 1.60-1.54 (m, 2H, 7-H), 1.36-1.26 (m, 6H, 8-H, 9-H and 10-H), 0.88 (t, 3H, 11-H).

*3.2.6. 4,7-Bis(3-hexyloxythiophen-2-yl)benzo[c][2,1,3]thiadiazole (**3a**)*

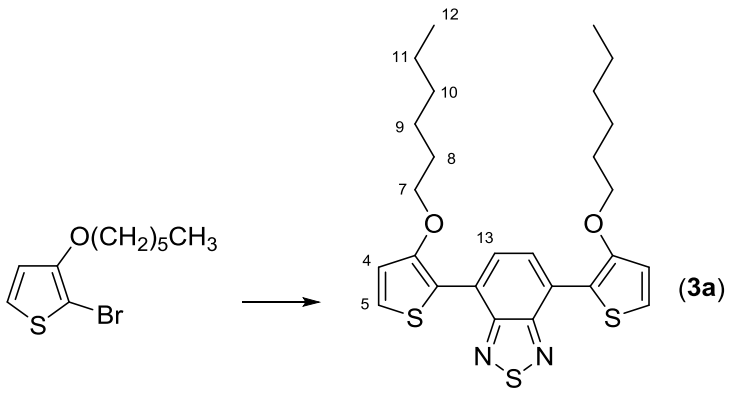

A mixture of 2-bromo-3-hexyloxythiophene (120 mg, 0.46 mmol), 2,1,3-benzothiadiazole-4,7-bis(boronic acid pinacol ester) (Sigma-Aldrich) (106 mg, 0.27 mmol), $PdCl_2$dppf (Sigma-Aldrich) (19mg, 5% mol), $NaHCO_3$ (115 mg, 1.37mmol) in THF/water 2:1 v/v (4.5 ml) was kept under MW irradiation at 80°C for 30 min. The reaction mixture was cooled to room temperature and poured into water (100 ml), extracted with CH_2Cl_2 and finally washed with water. After drying (Na_2SO_4) and solvent evaporation at reduced pressure, the crude product was purified by flash chromatography with increasing amounts of CH_2Cl_2 in cyclohexane as eluent (85:15 v/v) to afford 106 mg (0.21 mmol, 56% yield) of **3a** as a dark red oil.

^{1}H-NMR ($CDCl_3$, ppm): δ 8.46 (s, 2H, 13-H), 7.44 (d, 2H, 5-H), 6.99 (d, 2H, 4-H), 4.15 (t, 4H, 7-H), 1.82 (m, 4H, 8-H), 1.50-1.32 (m, 12H, 9-H, 10-H and 11-H), 0.91 (t, 6H, 12-H).

*3.2.7. 4,7-Bis[3-(6-methoxyhexyl)thiophen-2-yl]benzo[c][2,1,3]thiadiazole (**3b**)*

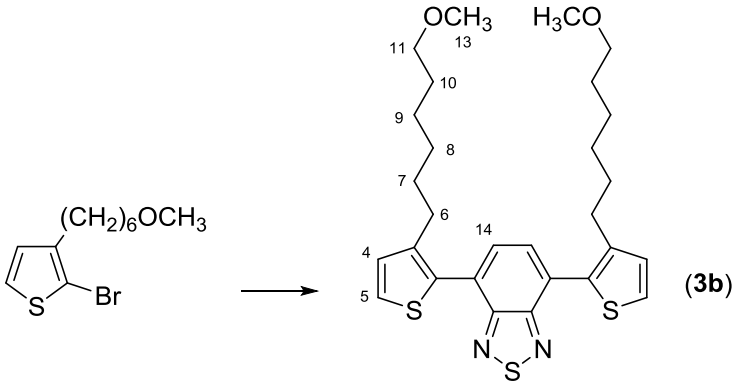

To a solution of 2-bromo-3-(6-methoxyhexyl)thiophene (300 mg, 1.08 mmol) in 6.0 ml of degassed toluene, 2,1,3-benzo[c]thiadiazole-4,7-bis(boronic acid pinacol ester) (168

mg, 0.43 mmol) was added, followed by the sequential addition of $Pd(PPh_3)_4$ (Sigma-Aldrich) (65 mg, 7% mol) and aq. 2M K_2CO_3 (5 ml), at room temperature under N_2 atmosphere. The mixture was vigorously stirred and degassed for 30 min and then heated under reflux (110°C) for 24h. After cooling, the mixture was treated with toluene and water, the organic layer dried on Na_2SO_4 and the solvent evaporated at reduced pressure. The crude product was finally purified by column chromatography on silica gel with cyclohexane/ethyl acetate 10:2 v/v as eluent to afford 297 mg (0.56 mmol, 52% yield) of **3b** as a fluorescent orange oil.

^{1}H-NMR ($CDCl_3$, ppm): δ 7.64 (s, 2H, 14-H), 7.44 (d, 2H, 5-H), 7.10 (d, 2H, 4-H), 3.30 (t, 4H, 11-H), 3.28 (s, 6H, 13-H), 2.66 (t, 4H, 6-H), 1.70-1.58 (m, 4H, 10-H), 1.52-1.44 (m, 4H, 7-H), 1.34-1.24 (m, 4H, 8-H and 9-H).

*3.2.8. 4,7-Bis(3-hexylthiophen-2-yl)benzo[c][2,1,3]thiadiazole (**3c**)*

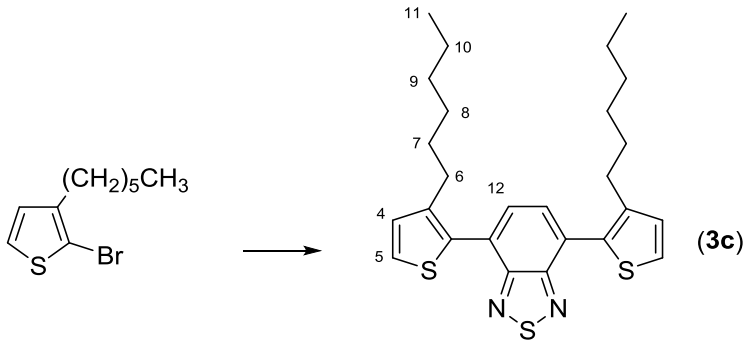

The same procedure described for 3b was followed starting from 2-bromo-3-(hexyl)thiophene (250 mg, 1.01 mmol) and 2,1,3-benzothiadiazole-4,7-bis(boronic acid pinacol ester) (157 mg, 0.40 mmol) in toluene (6 ml) to obtain 255 mg (0.54 mmol, 54% yield) of **3c** as a fluorescent yellow oil. The crude product was purified by column chromatography on silica gel with increasing amounts of CH_2Cl_2 in cyclohexane as eluent (85:15 v/v) to obtain 275 mg (0.59 mmol, 58% yield) of **3c** as a fluorescent yellow oi1.

^{1}H-NMR ($CDCl_3$, ppm): δ 7.64 (s, 2H, 12-H), 7.44 (d, 2H, 5-H), 7.10 (d, 2H, 4-H), 2.66 (t, 4H, 6-H), 1.64-1.59 (m, 4H, 7-H), 1.28-1.16 (m, 12H, 8-H, 9-H and 10-H), 0.81 (t, 6H, 11-H).

3.3.Synthesis of polymers

*3.3.1. Poly[4,7-bis(3-hexyloxythiophen-2-yl)benzo[c][2,1,3]thiadiazole] (**P3a**)*

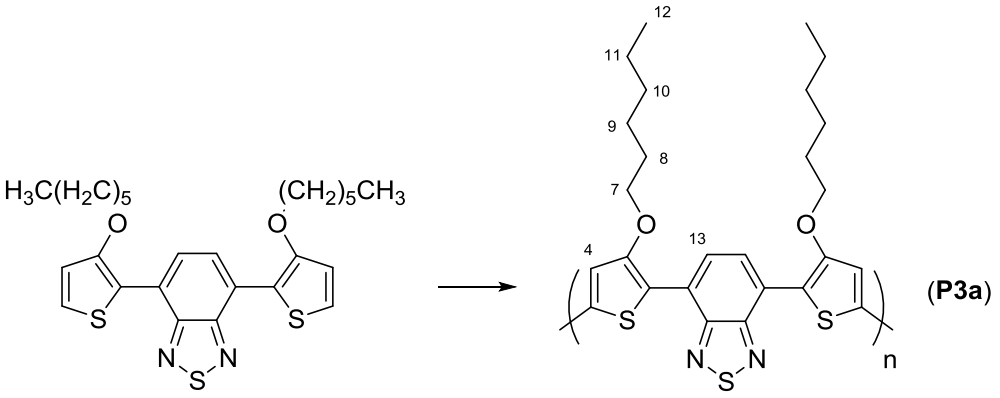

To a three-necked flask containing a suspension of $FeCl_3$ (137 mg, 0.85 mmol) in anh. $CHCl_3$ (5 ml), a solution of 3a (106mg, 0.21mmol) in anh. $CHCl_3$ (5 ml) was slowly added (20 min) under inert atmosphere at room temperature. The mixture was left under stirring for 24 h, turning from greenish to dark blue/black colour. Then, 50 ml of THF and 100 ml of $CHCl_3$ were added and the mixture washed with 2% aq. HCl up to exhaustive extraction of the iron (III) ion (negative essay with NH_4SCN). The crude product was washed with water to neutrality, dried (Na_2SO_4), concentrated to small volume and finally treated with MeOH to give 0.102 g (0.21 mmol, 98% yield) of **P3a** as a dark blue solid.

^{1}H-NMR ($CDCl_3$, ppm): δ 8.55 (bs, 2H, 13-H), 7.00 (bs, 2H, 4-H), 4.25 (bt, 4H, 7-H), 1.90 (bm, 4H, 8-H), 1.64-1.18 (m, 12H, 9-H, 10-H and 11-H), 0.97 (bt, 6H, 12-H).

*3.3.2. Poly[4,7-bis[3-(6-methoxyhexyl)thiophen-2-yl]benzo[c][2,1,3]thiadiazole] (**P3b**)*

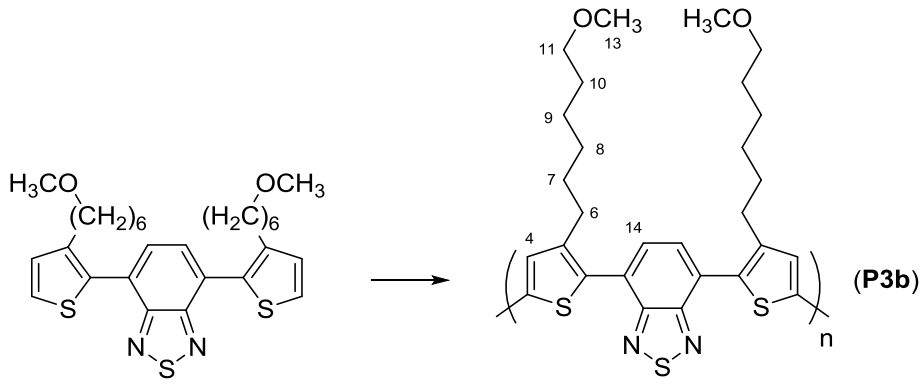

The same procedure described for P3a was followed starting from $FeCl_3$ (147 mg, 0.91 mmol) and 3b (120 mg, 0.23 mmol) to give 96 mg (0.18 mmol, 79% yield) of **P3b** as a purple/black solid.

^{1}H-NMR ($CDCl_3$, ppm): δ 7.71 (bs, 2H, 14-H), 6.98 (s, 2H, 4-H), 3.31 (bs, 6H, 11-H and 13-H), 2.72 (m, 4H, 6-H), 1.72 (m, 4H, 10-H), 1.52 (m, 4H, 7-H), 1.46-1.22 (m, 4H, 8-H and 9-H).

*3.3.3. Poly[4,7-bis(3-hexylthiophen-2-yl)benzo[c][2,1,3]thiadiazole] (**P3c**)*

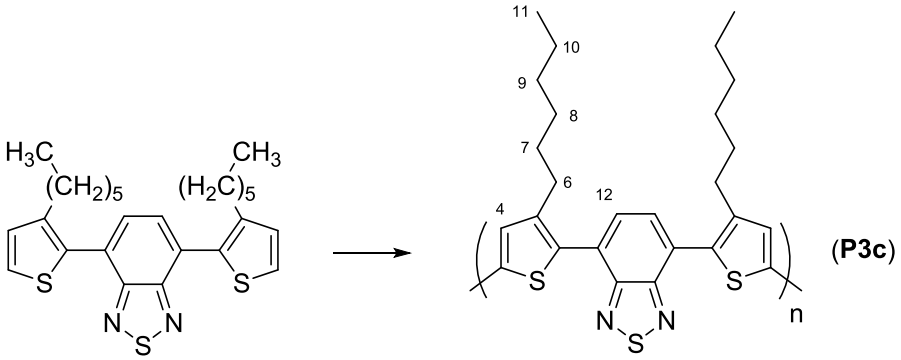

The same procedure described for P3a was followed starting from $FeCl_3$ (138 mg, 0.85 mmol) in anh. $CHCl_3$ (5 ml) and 3c (100 mg, 0.21 mmol) in anh. $CHCl_3$ (5 ml) to give 52 mg (0.11 mmol, 54% yield) of **P3c** as a dark red solid.

^{1}H-NMR ($CDCl_3$, ppm): δ 7.65 (s, 2H, 12-H), 6.92 (s, 2H, 4-H), 2.64 (m, 4H, 6-H), 1.70-1.06 (m, 16H, 7-H, 8-H, 9-H and 10-H), 0.90-0.84 (bt, 6H, 11-H).

3.4. Methods and characterizations

Microwave (MW) irradiation was performed in a Milestone Microsynth Labstation operating at 2450 MHz and equipped with pressure and temperature sensors.

^{1}H-NMR spectra were recorded on a Varian Mercury 400 (400 MHz) spectrometer at room temperature in $CDCl_3$ solutions with TMS as the internal standard. Chemical shifts are given in ppm.

Molecular mass and polidispersity of the polymers were determined in $CHCl_3$ by gel permeation chromatography (GPC) on a HPLC Lab Flow 2000 apparatus equipped with a Rheodyne 7725i injector, a Phenomenex Phenogel mixed bed 5μ MXL type column and an RI K-2301 KNAUER detector. The calibration curve was obtained using monodisperse polystyrene standards.

Thermogravimetric analysis (TGA) of the polymers (mass samples ~10 mg) was carried out by a TGA TA Instruments Q600 apparatus operating under nitrogen atmosphere in the 20÷800°C temperature range at a heating scan rate of 20°C/min. A DSC TA Instruments Q2000 operating in the –50÷200°C temperature range at a heating rate of 10°C/min under nitrogen atmosphere was used for the thermal analyses by differential scanning calorimetry (DSC) (mass samples ~10 mg).

UV-Vis and photoluminescence (PL) spectra were run by using a Perkin Elmer Lambda 20 and Perkin Elmer LS50B spectrophotometer, respectively, at room temperature on 1.3 10^{-3} M chloroform solutions in 0.1 and 1 cm quartz cells. Solid state measurements were made on polymer samples cast from chlorobenzene solutions (5 mg/mL) on quartz slides by the doctor-blade technique or spray-coating.

Cyclic voltammetry measurements were performed at 0.1 V/s on an AMEL model 5000 potentiostat/galvanostat controlled by the software Corrwere 2.9 for Windows. A home-made three-compartments electrochemical cell equipped with a Pt wire auxiliary electrode and an aq. KCl Saturated Calomel reference Electrode (SCE), both connected to the working compartment with a liquid bridge, was purged with Ar and maintained under Ar pressure during the measurements. The supporting electrolyte was 0.1 M $(C_2H_5)_4NBF_4$ (Sigma-Aldrich, puriss. vacuum dried) in anh. propylene carbonate (Sigma-Aldrich, stored under Ar pressure) where the oxidation potential of ferrocene resulted 0.50 V vs. SCE. Polymeric thin films were made by doctor-blade technique or spray-coating from chlorobenzene solutions (5 mg/mL) on ITO electrodes (2.25 cm^2) at room temperature. HOMO, LUMO and band gap (E_g) energies, expressed in eV units, were estimated on the basis of the following relationships: $E_{HOMO} = -(E_{ox} + 4.68)$, $E_{LUMO} = -(E_{red} + 4.68)$, $E_g = -(E_{HOMO} - E_{LUMO})$.[25]

Organic solar cells were fabricated on commercial ITO-coated glass substrates (2.5 × 2.5 cm, surface resistance 20 Ω/sq) according to the following procedure: the ITO layer was partially etched with acid (aq. HCl 10% wt.) and heated at 60°C for 15 min in order to obtain a final area of 1.5 x 1.0 cm covered by indium tin oxide. The substrate was then cleaned using distilled water followed by 2-propanol, and finally dried by a gentle nitrogen flow. A conductive thin layer of poly(3,4-ethylenedioxythiophene):polystyrene sulfonic acid (Sigma-Aldrich, PEDOT:PSS, 2.8% wt., dispersion in water), diluted 1:1 v/v with isopropanol, was deposited using the doctor blade technique over the previously treated ITO glass and subsequently heated in a Büchi GKR-50 glass oven at 120°C for 2h under vacuum. The active layer constituted by the synthesized polymer sample was cast from

chlorobenzene solution (5 mg/ml) by doctor-blade technique or spray-coating and then annealed under vacuum at 120°C for 30 min. The device fabrication was completed by thermal evaporation of the Al electrode over the active layer through a shadow mask using an Edwards 6306A coating system operating at 10^{-6} mmHg (final active area of 1.0 × 1.0 cm). The current-voltage (I-V) characteristics and PCE were measured in air at room temperature using a Keithley 2401 source meter under the illumination of an Abet Technologies LS150 Xenon Arc Lamp Source AM 1.5 Solar Simulator (100 mW/cm^2), calibrated with an ILT 1400-BL photometer. The final structure of the device was: ITO (~ 80 nm)/PEDOT:PSS (~ 120 nm)/active layer (~ 100 nm)/Al (~ 50 nm).

The external quantum efficiency (EQE) was measured by a 7-SC Spec III Modularized Solar Cell Spectral Test System (SevenStar Optics, Beijing, PRC). The J_{sc} values were calculated from the EQE curves according to Open Photovoltaics Analysis Platform.[26] The reported photoconversion efficiency results were averaged from three different devices, prepared under the same operating conditions, with a standard deviation of about 5%.

AFM and KPFM measurements were performed in air by employing a commercial digital microscope Bruker MultiMode 8. In order to obtain a sufficiently large and detectable mechanical deflection, we used (k = 2.8 N/m) Pt/Ir coated Si ultra-levers (SCM-PIT, Bruker) with oscillating frequencies in the range between 60-90 kHz. AFM and KPFM images were acquired in the same measurement; a topographic line scan is first obtained by AFM operating in semicontact mode and then that same line is rescanned in lift mode with the tip raised to a lift height of 20 nm. Raw AFM data were filtered to remove experimental artifacts by using histogram flattening procedures.[27] The KPFM technique provides a voltage resolution of about 5 mV and a lateral resolution of a few tens of nanometres.

X-ray diffraction analysis (XRD) was performed using a PANalytical X'Pert diffractometer equipped with a copper anode (λ_{mean} = 0.15418 nm) and a fast X'Celerator detector on polymer samples deposited from chlorobenzene solutions on ITO (5 mg/mL) by the doctor-blade technique or spray coating.

3.5. ^{1}H-NMR spectra

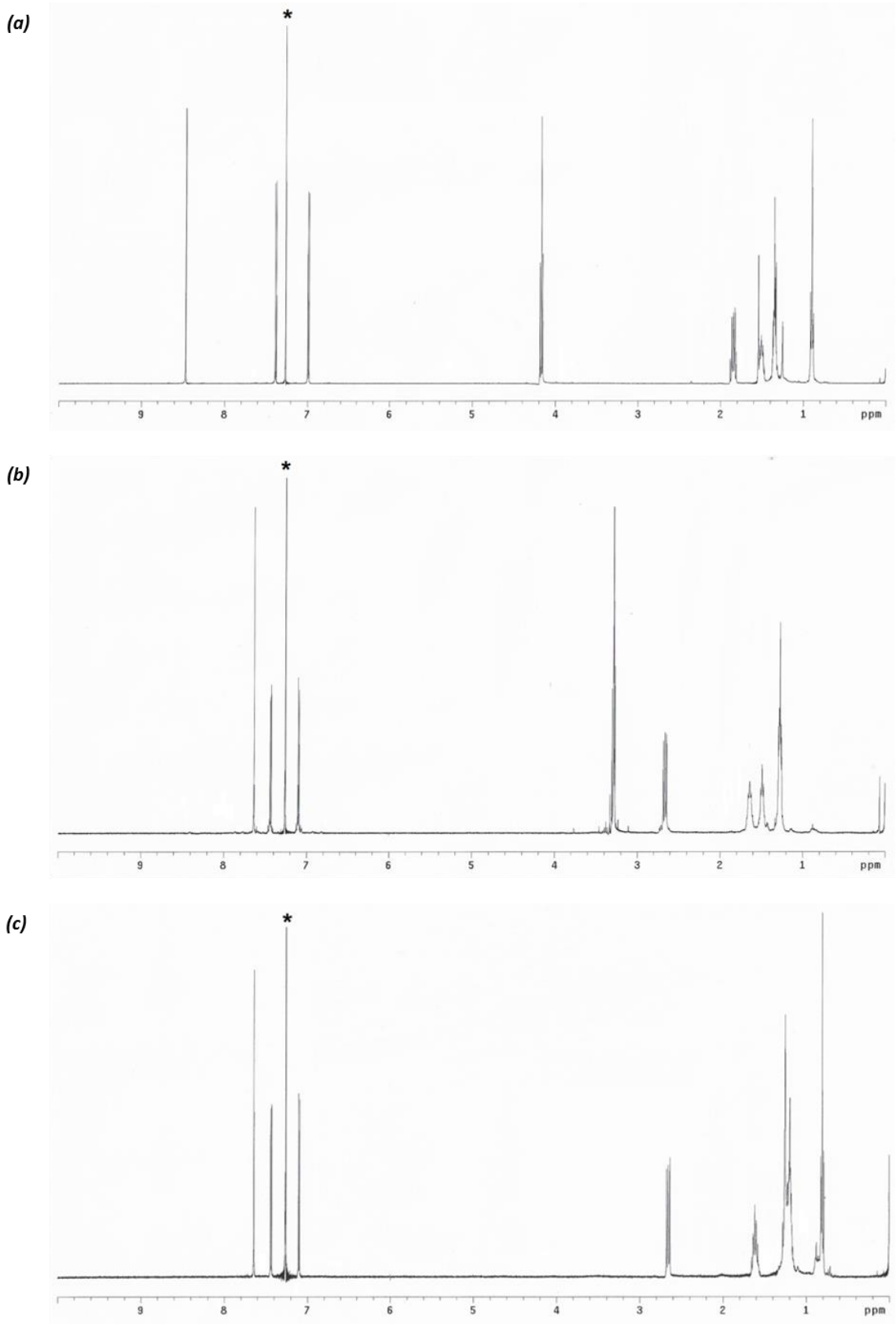

Figure 11. ^{1}H-NMR spectra of monomers **3a** (a), **3b** (b) and **3c** (c). Asterisk: solvent resonance ($CDCl_3$).

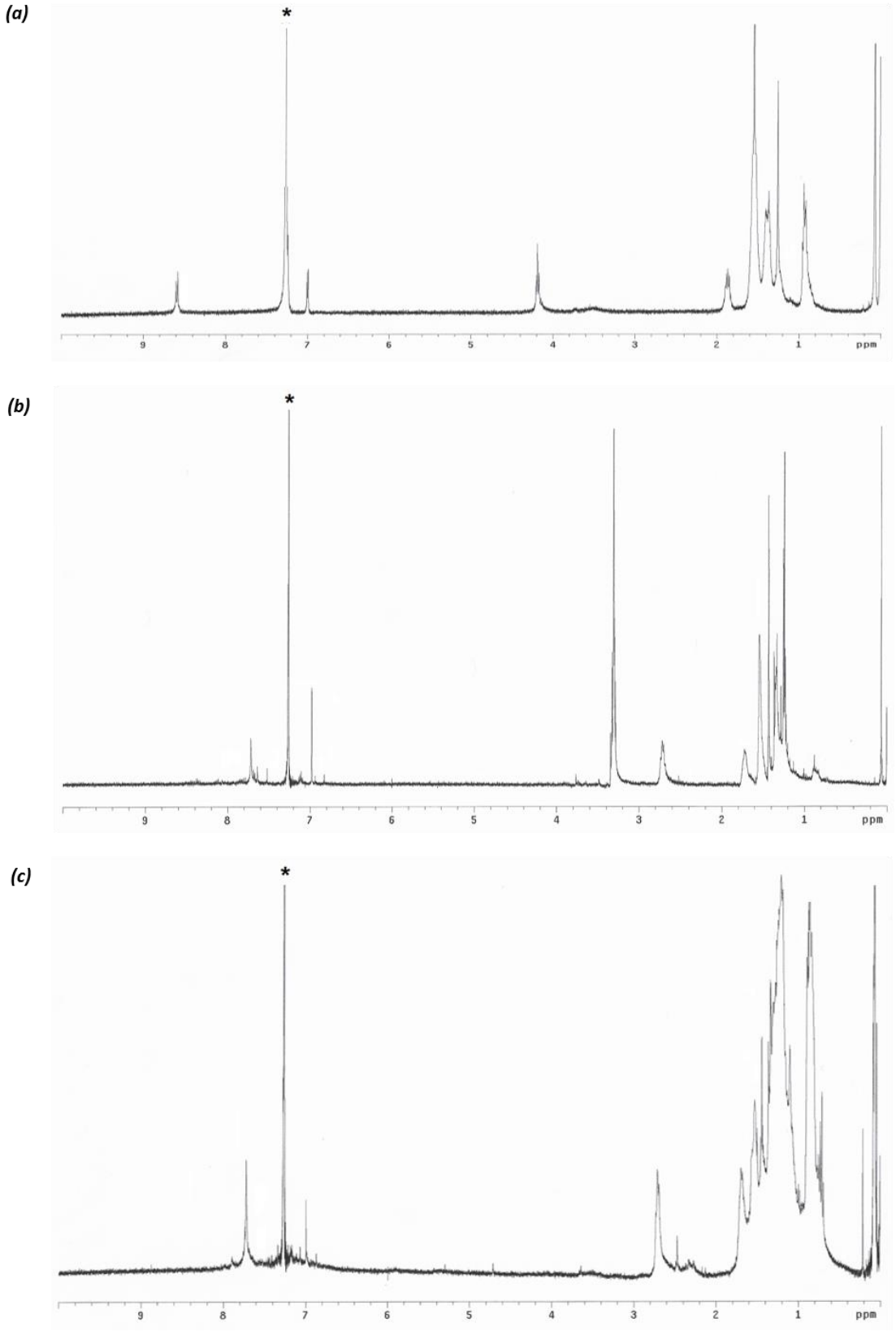

Figure 12. ^{1}H-NMR spectra of polymers **P3a** (a), **P3b** (b) and **P3c** (c). Asterisk: solvent resonance ($CDCl_3$).

Reference

[1] L. Lu, T. Zheng, Q. Vu, A. M. Schneider, D. Zhao, L. Yu, *Chem. Rev.* **115** (2015) 12666-12731.
[2] P. Zhou, Z. Zhang, Y. Li, X. Chen, J. Qin, *Chem. Mater.* **26** (2014) 3495-3501.
[3] Y. F. Li, *Acc. Chem. Res.* **45** (2012) 723-733.
[4] F. Di Maria, M. Biasiucci, F. P. Di Nicola, E. Fabiano, A. Zanelli, M. Gazzano, E. Salatelli, M. Lanzi, F. Della Sala, G. Gigli, G. Barbarella, *J. Phys. Chem. C* **119** (2015) 27200-27211.
[5] R. Kroon, M. Lenes, J. C. Hummelen, P. W. M. Blom, B. De Boer, *Polym. Rev.* **48** (2008) 531–582.
[6] Y. W. Li, L. L. Xue, H. Li, Z. F. Li, B. Xu, S. P. Wen, W. J. Tian, *Macromolecules* **42** (2009) 4491–4499.
[7] B. Xu, S. Noh, B. C. Thompson, *Macromolecules* **47** (2014) 5029-5039.
[8] K. A. Mazzio, C. K. Luscombe, *Chem. Soc. Rev.* **44** (2015) 78-90.
[9] Y. Tamai, H. Ohkita, H. Benten, S. J. Ito, *Phys. Chem. Lett.* **6** (2015) 3417-3428.
[10] S. Chenjun, Y. Yao, Y. Yang, P. Qibing, *J. Am. Chem. Soc.* **128** (2006) 8980-8986.
[11] T. L. Nguyen, T. H. Lee, B. Gautam, S. Y. Park, K. Gundogdu, J. Y. Kim, H. Y. Woo, *Adv. Funct. Mater.* **27** (2017) 1702474.
[12] A. A. El-Shehawy, N. I. Abdo, A. A. El-Barbary, J. Lee, *Eur. J. Org. Chem.* **25** (2011) 4841-4852.
[13] C. Della Casa, P. Costa Bizzarri, M. Lanzi, F. Bertinelli, *Acta Polym* **48** (1997) 251-255.
[14] R.H. Mitchell, Y.H. Lai, R.V. Williams, *J. Org. Chem.* **44** (1979) 4733-4735.
[15] P. Wagner, K. W. Jolley, D. L. Officer, *Aust. J. Chem.* **64** (2011) 335–338.
[16] F. Di Maria, G. Barbarella, *J. Sulfur Chem.* **34** (2013) 627-637.
[17] N. Miyaura and A. Suzuki, *J. Chem. Soc. Chem. Commun*. **19** (1979) 866-867.
[18] N. Miyaura and A. Suzuki, *Chem. Rev*. **95** (1995) 2457-2483.
[19] A. Suzuki, *Angew. Chem. Int. Ed*. **50** (2011) 6722-6737.
[20] C. Della Casa, F. Bertinelli, P. Costa Bizzarri, E. Salatelli, *Adv. Mater.* **7** (1995) 1005-1009.
[21] L. Angiolini, V. Cocchi, L. Guadagnini, A. Mignani, E. Salatelli, D. Tonelli, *Synthetic Metals* **202** (2015) 169-176.
[22] R. Holze, *Organometallics* **33** (2014) 5033-5042.
[23] W. Zhao, S. Li, H. Yao, S. Zhang, Y. Zhang, B. Yang, J. J. Hou, *Am. Chem. Soc.* **139** (2017) 7148.
[24] D. D. Perrin, W. L. F. Armarego, D. R. Perrin, *Purification of Laboratory Chemicals*, Pergamon Press: Oxford, 1966.
[25] S. Trasatti, *Pure Appl. Chem.* **58** (1986) 955-966.
[26] Web site: http://opvap.com/eqe.php.
[27] A. Liscio, *Chem. Phys. Chem*. **14** (2013) 1283-1292.

Chapter III

Chapter III: SMOSCs - SYNTHESIS AND CHARACTERIZATION OF "DOUBLE-CABLE" SYSTEMS

1. Introduction

1.1. Overview

After the interesting results achieved with the main-chain donor-acceptor polymers previously investigated (chapter II), the research project was oriented to the development and study of similar systems but having the acceptor units in the side chain, known as double-cable materials.

In OSCs, a blend of a conjugated polymer as electron-donor and a fullerene derivative as electron acceptor material – and thus a bulk heterojunction structure – usually provides a large interface area among the components, in addition to promote the efficient generation of free charge carriers and their subsequent fast transport to the respective electrode.[1] However, an optimized three-dimensional nanomorphology of the photoactive blend is difficult to obtain, as both the electron-donor and electron-acceptor components spontaneously tend to segregate. Indeed, the blend morphology typically arises from the reduced miscibility of the two components that, due to the deposition process, often leads to the formation of fullerene clusters within the conjugated polymer matrix. Since the charge transport through the electrodes is hindered by the phase separation which creates some "voids", the random nature of the interpenetrating electron-donor and acceptor network spontaneously formed during the deposition of the blend could be undoubtedly considered an efficiency-limiting factor.[2,3]

In order to produce optimized phase-separated structures for charge generation while maintaining a continuous path in each phase for the adequate transport of charges, some techniques have been recently proposed. In addition to the aforementioned insertion of the acceptor group in the main chain polymer backbone,[4] the use of additives,[5] compatibilizers[6] and, above all, the covalent linkage of the electron acceptor units as pendants in the side-chain of the donor polymer appears particularly intriguing.[7,8,9,10,11,12]

In fact, thanks to the idea of creating "molecular heterojunctions" by covalently grafting the fullerene to the polythiophene backbone - which provides a limited spontaneous phase separation and clustering phenomena - double-cable (co)polymers could be a suitable alternative to the conventional BHJ architecture.[13] Anyhow, as the efficiency of the devices using the fullerene in the side or main chain is strongly related to the electron acceptor amount, it is then important to synthesize the double-cable material with the appropriate fullerene content, while preserving an adequate solubility of the final material in common organic solvents.

With regard to this aspect, the synthesis of these derivatives by using a post-polymerization approach may be considered an extremely fascinating opportunity. Not only could the properties be easily tuned by insertion of controlled and specific moieties, but the thermal stability could also be improved by inserting photo-crosslinkable moieties in the conjugated polymer side chains. Indeed, since low thermal stability is often shown by most of BHJ organic solar cells, as the photoactive blend spontaneously separates in the micrometer scale[14] when exposed to the solar irradiation, the presence of photo-crosslinkable moieties could stabilize the film morphology without affecting the chain-packing, the number and dimension of D/A domains and thus the final efficiency of the photovoltaic cell.[15]

1.2. Aim of the chapter

In this framework, the synthesis of some new thiophenic copolymers bearing both a C_{60}-fullerene moiety and a photocrosslinkable bromine group at the end of a hexamethylenic side chain are presented.

Fullerene-substituted copolymers have been prepared with a simple and straightforward post-polymerization functionalization procedure based on Grignard coupling, which has been demonstrated to facilitate the synthetic procedures required for the obtainment of polymers with the desired functional groups.[16] As the conductivity is affected by the regioregularity degree, soluble regiorandom (**PT6Br**) and regioregular (**rrPT6Br**) homopolymeric precursors having similar molecular weights were synthesized by using two different polymerization methods. In order to study the effect of the photoactive layer on the final performance, the materials were functionalized with different contents of fullerene, to give **PT6Br/F** and **rrPT6Br/F**, respectively (Scheme 1).

The copolymers have been carefully characterized by means of chemical and spectroscopic techniques. In addition to examine the molecular arrangement of their films by atomic force microscopy (AFM) measurements, the effects of the regioregularity and fullerene content on the power conversion efficiency when employed as photoactive single materials in organic solar cells (SMOSCs) have been investigated.

Furthermore, the insertion of a thin layer of Au nanoparticles (AuNPs) as anode interlayer has also been tested, leading to a remarkable PCE value of 5.68% with the best performing device, in addition to study the stability over time of the photocrosslinked cells as compared to the uncrosslinked counterparts.

This chapter is based on adapted content from "Effect of Photocrosslinking of D-A Thiophene Copolymers on the Performance of Single-Material Solar Cells" M. Lanzi, E. Salatelli, M. Marinelli, Filippo Pierini, *Macromol. Chem. Phys.* (**2019**) 1900433.
All synthetic results, polymerizations and measurements represented in this chapter were obtained by Debora Quadretti under the supervision of the author, or by the author herself. The electrochemical and morphological characterization, in addition to the measurements of external quantum efficiency (EQE), were carried out in collaboration with Dr. Filippo Pierini of the IPTT-PAN Institute of Warsaw.

2. Results and discussion

2.1. Synthesis

Starting from 3-(6-bromohexyl)thiophene (**T6Br**), the key intermediate previously adopted for the synthesis of 4,7- bis[3-(6-methoxyhexyl)thiophen-2-yl]benzo[c][2,1,3]thiadiazole (chapter I), homopolymers **PT6Br** - **rrPT6Br** and their corresponding double-cable copolymers **PT6Br/F** - **rrPT6Br/F** have been prepared according to the procedure shown in Scheme 1.

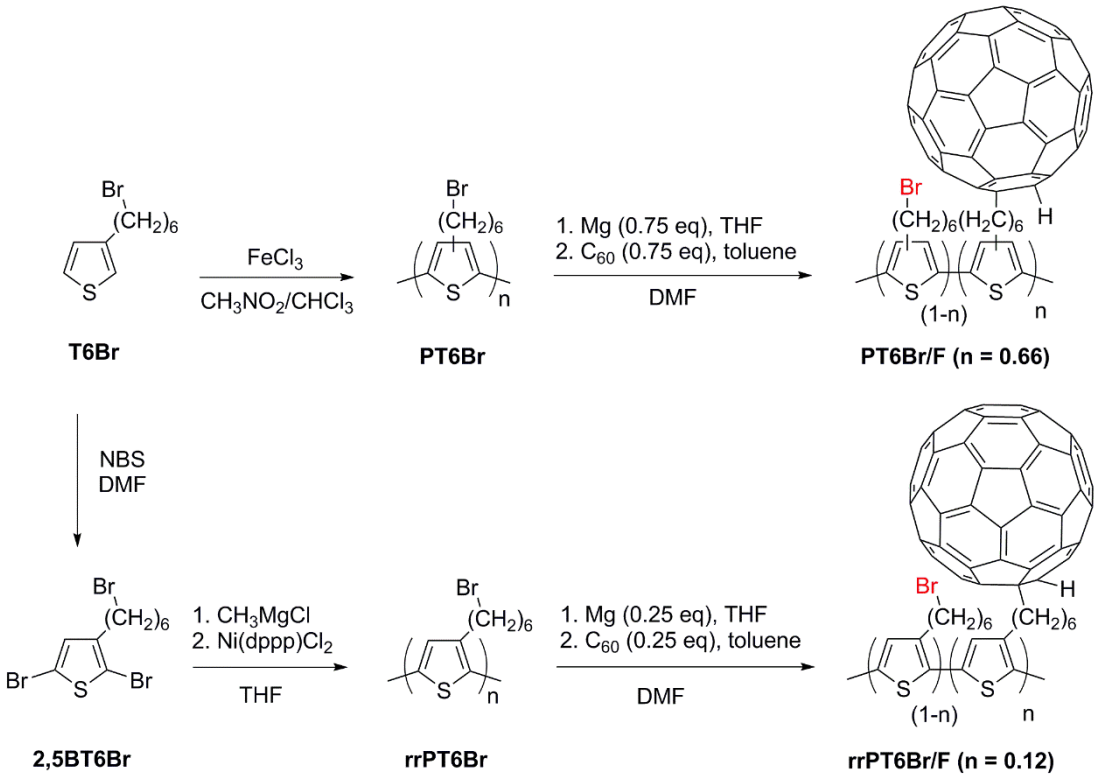

Scheme 1. Synthesis of homopolymers and double-cable copolymers.

In a first approach, as reported by Stokes,[17] several attempts of synthesis of **T6Br** through lithiation (Figure 1) have been made; in fact, in addition to the use of commercially available reagents, this method should provide a more direct and fast route of synthesis with respect to the one previously adopted.[18]

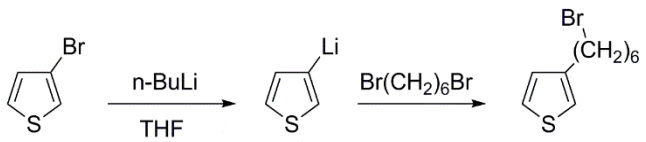

Figure 1. Synthesis of **T6Br** by Stokes.

However, although the desired product has been anyway obtained, the formation of a large amount of by-products - probably due to the easy conversion of 3-lithiothiophene into 2-lithiothiophene at room temperature -[19] and the constant presence of unreacted starting material always led to unsatisfactory yields, making necessary to adopt again the aforementioned conventional procedure.[18]

Since previous investigations[20] showed solubility and reactivity problems when a fullerenate monomer was directly used, the non-regioregular **PT6Br** was synthesized by reacting 3-(6-bromohexyl)thiophene with iron trichloride in $CH_3NO_2/CHCl_3$ mixture. Thanks to the dissolution of the oxidizing agent in nitromethane, this procedure involves the precipitation of $FeCl_3$ in a highly active microcrystalline form that leads to a better control of the polymer molecular weight thus minimizing the insoluble fraction content.[21] On the other hand, regioregular poly[3-(6-bromohexyl)thiophene] (**rrPT6Br**) was polymerized by means of a regiospecific procedure, the Grignard Metathesis (GRIM) polymerization,[22] which involved the cross-coupling of the organomagnesium intermediate - prepared by reacting 2,5-dibromo-3-(6-bromohexyl)thiophene (**2,5BT6Br**) with a pre-formed Grignard reactant (CH_3MgCl) - in the presence of $Ni(dppp)Cl_2$ as a catalyst.

The brominated homopolymeric precursors, whose characteristics are reported in Table 1, were well soluble in common organic solvents and this was particularly true for the regioirregular sample (up to 50 mg/ml and 20 mg/ml in THF for **PT6Br** and **rrPT6Br**, respectively).

Table 1. Characteristics of homopolymers and double-cable copolymers.

Samples	*Yield (%)* [a]	*HT dyads* [b]	M_n *(g/mol)* [c]	M_w/M_n [c]	*Fullerene content (% mol)* [d]
PT6Br	40	70	26000	1.4	0
rrPT6Br	47	97	24000	1.3	0
PT6Br/F	75	70	54700 [e]	1.4 [e]	66
rrPT6Br/F	95	97	28800 [e]	1.3 [e]	12

[a] In fractionated polymer; [b] Regioregularity from ^{1}H-NMR expressed as head-to-tail dyads percentage; [c] Determined by GPC relative to polystyrene standards; [d] Determined by ^{1}H-NMR; [e] Calculated from the molecular mass of the corresponding homopolymers.

The homopolymers were then dissolved in anhydrous THF and added with Mg turnings to obtain the corresponding ω-bromomagnesium derivatives which were directly reacted with a solution of fullerene in toluene.

Although the obtained double-cable copolymers were well soluble in chlorobenzene, 1,2-dichlorobenzene and pyridine up to 10 mg/ml they resulted only partially soluble in $CHCl_3$ and THF (around 0.5 mg/ml). Moreover, the solubility of **rrPT6Br/F** in common organic solvents is almost the same as its regioirregular counterpart, despite the lower molecular weight and fullerene content. This could be ascribed to its higher molecular packing that, due to the higher degree of regioregularity, strongly hinders the solvation of the macromolecular structure.

2.2.NMR and FT-IR characterization

The chemical structure, regioregularity degree and fullerene content of the synthesized materials have been evaluated by NMR spectroscopy.

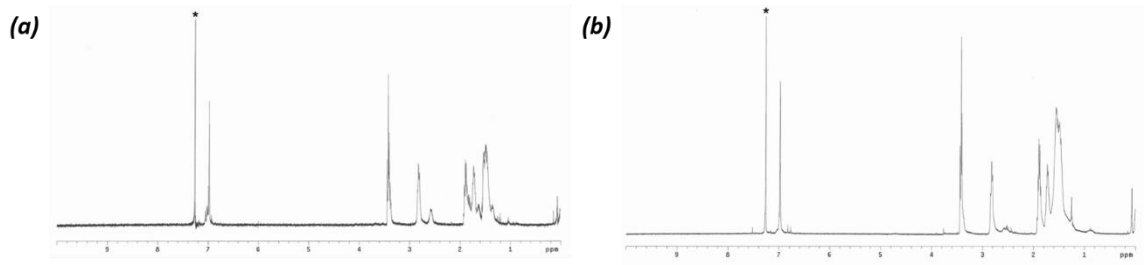

Figure 2. ^{1}H-NMR spectra of **PT6Br** (a) and **rrPT6Br** (b) in $CDCl_3$. Asterisk: solvent resonances.

The spectra of **PT6Br** (Figure 2a) and **rrPT6Br** (Figure 2b) display a major singlet at 6.98 and 6.97 ppm, respectively, which can be assigned to the 4-H protons of the backbones; not only does the exclusive presence of these signals in the aromatic region indicate the effective polymerization of T6Br, but it also gives further confirmation of the good molecular weights obtained by GPC analysis. In fact, no other signals related to terminal protons of oligomeric chains are observed.

Moving to upfield, both of them show a multiplet/triplet at 3.43 ppm related to the -CH_2- directly linked to the bromine atom; on the other hand, since **PT6Br** and **rrPT6Br** are homopolymers with different regioregularity degrees - and therefore contain HT, TT and HH couplings - the resonance of the methylenic protons α to thiophene ring is split into two multiplets/triplets, at 2.83 and 2.57 ppm for **PT6Br** and 2.82 and 2.52 for **rrPT6Br**,

respectively. As the resonance at lower field may be assigned to head-to-tail (HT) junctions, while the other one to head-to-head and tail-to-tail (HH, TT) junctions, the regioregularity degree of both the homopolymers is thus given by the ratio of their integrated intensities: 70% HT for **PT6Br** and 97% HT for **rrPT6Br**, in agreement with the values usually reported for oxidative polymerization and GRIM polymerization of alkylthiophene monomers.[23]

Finally, the last signals in the 1.95-1.30 ppm range are related to the central methylene groups of the alkylic side chain.

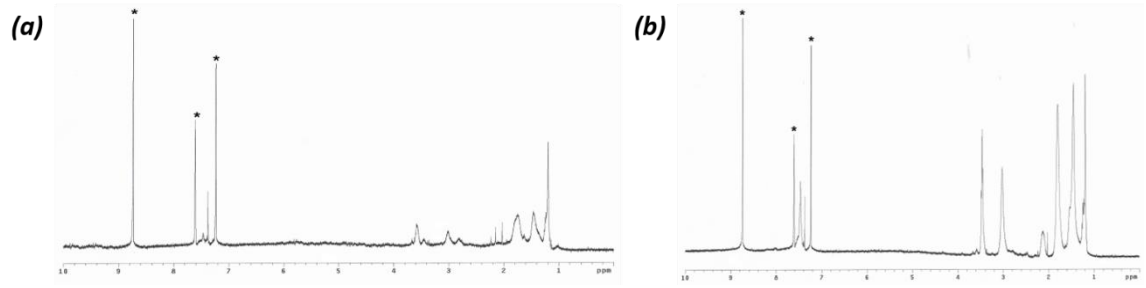

Figure 3. ^{1}H-NMR spectra of double-cable copolymers, **PT6Br/F** (a) and **rrPT6Br/F** (b), in d_5-pyridine. Asterisk: solvent resonances.

Concerning the double-cable copolymers, both the spectra of **PT6Br/F** (Figure 3a) and **rrPT6Br/F** (Figure 3b) show two signals in the aromatic region, at 7.47 and 7.38 ppm, which are respectively ascribable to the 4-H proton of the thiophenic backbone and to the proton directly linked to the fullerene group. Similarly to what have been done with homopolymers, the signals at 3.58 and 3.45 (3.47 for **rrPT6Br/F**) ppm – related to the methylenic protons in α-position to C_{60} and Br group – were used to calculate the fullerene content: 66% and 12% molar ratio in **PT6Br/F** and **rrPT6Br/F**, respectively.

Since the synthesis of these materials has been carried out by a post-polymerization approach, which does not involve the main chain backbone in the reaction, the regioregularity degree of the synthesized double-cable materials can be assumed as the same of the starting homopolymeric precursors.

The ^{13}C-NMR spectra of **PT6Br/F** and **rrPT6Br/F** are reported in Figure 4; they were recorded in d_5-o-dichlorobenzene (ODCB), whose signals can be found at 127.19, 130.04 and 132.39 ppm.

The prevalence of one kind of configurational sequence (HT-HT) in **rrPT6Br/F** copolymer, as already observed by ^{1}H-NMR analysis, was further confirmed by the presence of only four evident signals related to thiophenic carbons in the ^{13}C-NMR

spectrum (Figure 4b). Moreover, as detailed in the experimental section, in addition to show the signals ascribable to the 3-(6-bromohexyl)thiophene and 3-(6-fullerenylhexyl)thiophene units, a lower intensity of the signals of the latter unit is displayed, according to its lower fullerene content.

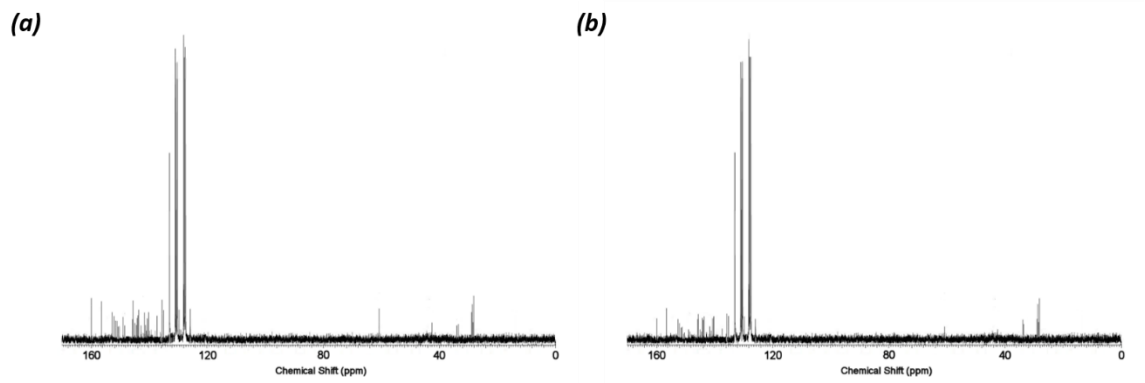

Figure 4. ^{13}C-NMR spectra of **PT6Br/F** (a) and **rrPT6Br/F** (b).

According to NMR characterization, also FT-IR spectroscopy on Ge or KBr disks gave extra confirm of the identity of all synthesized material: the IR absorption bands of homopolymers and copolymers as well as their assignments are reported in Table 2.

Table 2. Main IR absorption bands of homo- and double-cable copolymers.

Assignment	***PT6Br***	***rrPT6Br***	***PT6Br/F***	***rrPT6Br/F***
νC-H β thiophene	3055	3055	3053	3056
ν_{as} CH_2	2929	2929	2929	2930
ν_{sym} CH_2	2854	2854	2852	2852
ν_{as} C=C thiophene	1509	1505	1506	1513
ν_{as} C=C thiophene	1457	1432	1455	1456
fullerene	-	-	1429	1428
νC-C thiophene-thiophene	1259	1258	1260	1259
fullerene	-	-	1182	1182
δC-H thiophene	1090	1071	1034	1031
γC-H thioph. 2,3,5-trisubstituted	827	826	834	836
γC-H side chain	727	724	747	749
νC-Br (aliphatic)	645, 562	642, 561	649, 560	646, 562
fullerene	-	-	576, 522	576, 525

ν = stretching; γ = out of plane bending; δ = in plane bending.

The absence of the bands at 3104 cm^{-1} (νC-H in α to thiophene ring), 768 cm^{-1} (γC-H 3-substituted thiophene) and at 1001 cm^{-1} (νC-Br aromatic), further confirms the formation

of **PT6Br** and **rrPT6Br** of high molecular weight (Figure 5). On the other hand, the desired post-functionalization with C_{60}-fullerene in the side chains, is confirmed by the presence of the absorptions at 1429, 1182, 576 and 522 cm^{-1} in **PT6Br/F** and at 1428, 1182, 576 and 525 cm^{-1} in **rrPT6Br/F** spectra. Furthermore, it can also be observed that the intensity of fullerene absorptions is roughly proportional to its content in the copolymer.

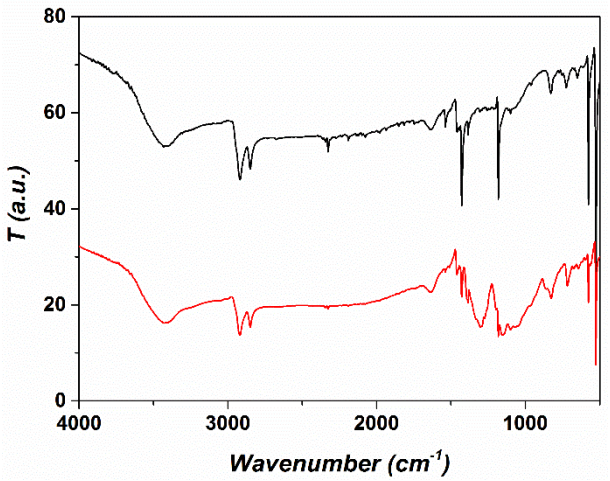

Figure 5. FT-IR spectra of **PT6Br/F** (black line) and **rrPT6Br/F** (red line).

2.3. Thermal properties

The thermal stability of copolymers was determined by TGA, under oxidizing atmosphere (air) and at a heating scan of 10°C/min (Figure 6a). While the polythiophenic main chains are stable up to about 500°C, a weight loss which can be ascribed to HBr and CH_2Br losses is observed at 271°C and 236°C for **PT6Br/F** and **rrPT6Br/F**, respectively (Table 3). In particular, probably as a consequence of its higher bromine content, a more evident loss is observed for the regioregular sample.

Table 3. Glass-transition (T_g), melting (T_m), crystallization (T_c) and decomposition (T_d) temperatures of double-cable copolymers.

Samples	*T_g (°C)*	*T_m (°C)*	*T_c (°C)*	*T_d (°C)*
PT6Br/F	26	82	-	271
rrPT6Br/F	31	96	92	236

The DSC analysis was carried out under nitrogen atmosphere at a heating rate of 5°C/min (Figure 6b). Although glass transitions and melting points at temperatures increasing with the bromine content are shown by the polymeric samples, only **rrPT6Br/F** shows a clear first order crystallization transition. In fact, it appears that the presence of a high amount of the sterically-hindering fullerene, combined with a lower degree of configurational regularity, promotes a higher formation of amorphous structures in **PT6Br/F**.

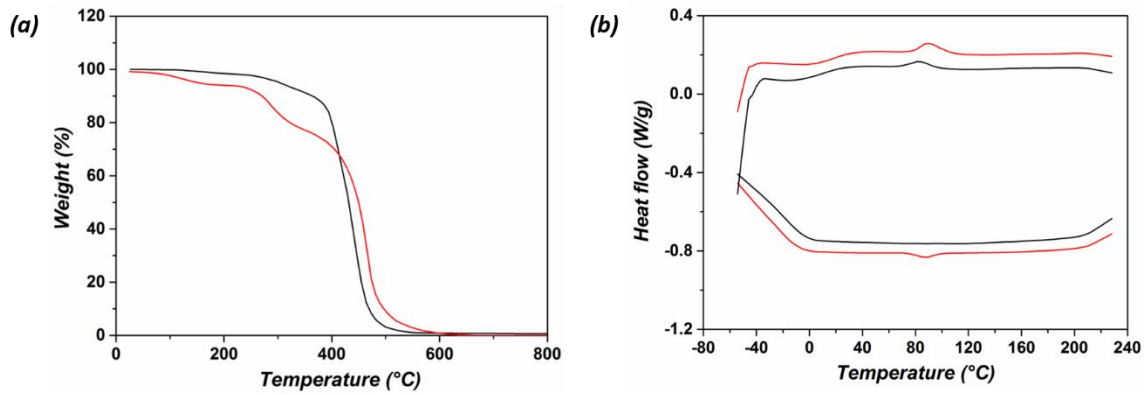

Figure 6. (a) TGA and (b) DSC (second scan) thermograms of copolymers **PT6Br/F** (black line) and **rrPT6Br/F** (red line).

2.4. Optical properties

The optical properties of homopolymers **PT6Br** and **rrPT6Br** and double-cable copolymers **PT6Br/F** and **rrPT6Br/F** were evaluated in thin film on quartz slide, obtained by doctor-blade deposition, respectively from chloroform and chlorobenzene solution.

Table 4. Maximum absorption (λ_{max}) of homo- and double-cable copolymers in thin film from chloroform and chlorobenzene solutions, respectively.

Samples	λ_{max} *(nm)*
PT6Br	532
rrPT6Br	555
PT6Br/F	448
rrPT6Br/F	468

Both the homopolymers display a clear film-formation ability and reorganization of the macromolecules in a fully planar and ordered system typical of the solid state (Figure 7). Moreover, despite the lower molecular weight, **rrPT6Br** showed an evident red shift of the maximum wavelength absorption (Table 4) with respect to the regiorandom derivative (**PT6Br**), probably due to its higher degree of regioregularity.

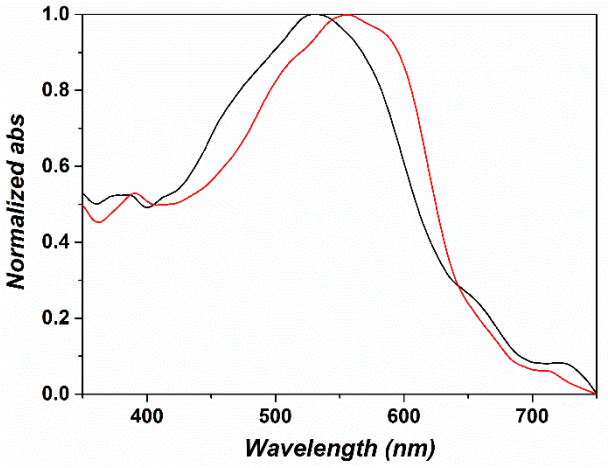

Figure 7. Normalized UV-Vis spectrum of homopolymers in thin film: **PT6Br** (black line) and **rrPT6Br** (red line).

Otherwise, although a comparison between the two double-cable copolymers could be inappropriate, having both of them a different regioregularity degree and fullerene content, the evaluation of their optical properties in the solid state is particularly interesting in view of their application as single materials in OSCs.

First of all, the UV-Vis spectrum of pure fullerene was recorded in chlorobenzene solution and then subtracted from the copolymers spectra, with the aim of better evaluate the absorption of the polythiophenic moieties at high wavelengths, as fullerene - which is a very efficient chromophore particularly at lower wavelengths - displays a strong overlapping absorption around 350 nm.[24] Observation of the resulting subtracted spectra (Figure 8) allows to determine the absorption maximum for the polythiophenic component at 448 nm and 468 nm for **PT6Br/F** and **rrPT6Br/F**, respectively, that also corresponds to an average conjugation length of 6 and 8 thiophenic rings.[25]

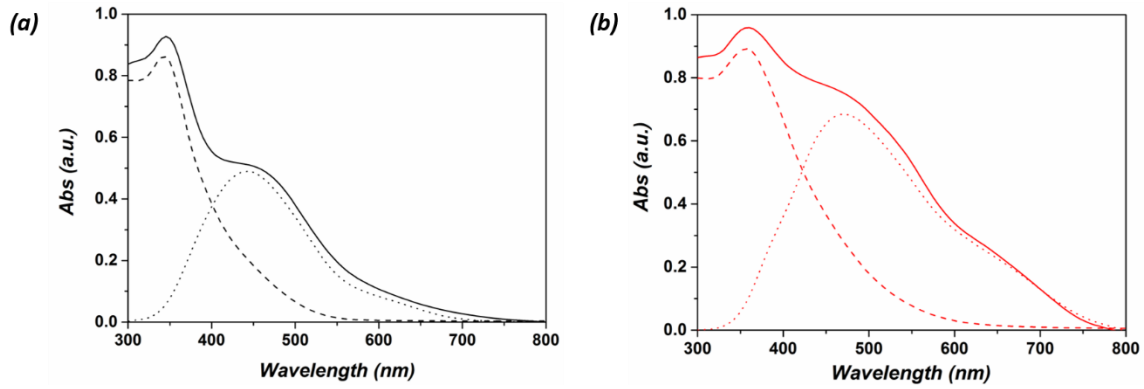

Figure 8. UV-Vis spectrum (dotted line) of **PT6Br/F** (a) and **rrPT6Br/F** (b) in thin film, obtained by subtraction of fullerene spectrum (dashed line) to original copolymer spectrum (solid line).

A strong blue-shift of the absorption maxima wavelengths of the thiophene system, reasonably caused by the bulky and hindering nature of the fullerene units inserted in the side chain, is displayed by the double-cable copolymers with respect to the homopolymers (Table 4). Indeed, the maximum absorption wavelength obtained for **rrPT6Br/F** could be related to the presence of a lesser content of fullerene in the material, although this finding may also be attributed to its higher regioregularity degree. However, since generally no large difference in the absorption values has been obtained for the copolymers, it is reasonable to suppose that the contribution of regioregularity is counter-balanced by the different fullerene content.

Moreover, as a consequence of interchain π-π stacking in the solid state, the spectrum of **rrPT6Br/F** also shows a shoulder at 632 nm - and at around 620 nm in **PT6Br/F** spectrum - that is ascribable to the 0-0 pure electronic transition and is only evident in conformationally ordered polythiophenic chains.[26] The presence of this absorption is especially interesting since the copolymer morphology can be partially analysed by Yamamoto and coworkers method.[27] In fact, according to their theory, the UV-Vis film spectrum of functionalized polyalkylthiophenes can be separated in two essential contributions: the absorption at around 450 nm (A_a), that is ascribable to the amorphous domains, and the vibrational absorption shoulders at around 620-630 nm (A_c), which are caused by the π-π stacking of polymer chains in crystalline domains.

The degree of crystallinity, related to the degree of order of the polymer chains in the film state, could be therefore roughly estimated by using the following equation:

$$\chi_c = \frac{(\varepsilon_a/\varepsilon_c)A_c}{(\varepsilon_a/\varepsilon_c)\,A_c + A_a}$$

where $\varepsilon_a/\varepsilon_c$ (0.719) is the extinction coefficient ratio between the amorphous and crystalline poly(3-hexylthiophene).[27]

From the reported spectra, a crystallinity degree of 11% and 22% can be estimated for **PT6Br/F** (A_c = 0.08 and A_a = 0.47) and **rrPT6Br/F** (A_c = 0.26 and A_a = 0.68); as expected, the regioregular double-cable copolymer is more prone to assume ordered conformations which lead to aggregates suited to give crystallization.

2.5. Electrochemical characterization

In view of their application in single material organic solar cells (SMOSCs), the copolymers **PT6Br/F** and **rrPT6Br/F** have been electrochemically characterized by cyclic voltammetry (CV) making use of a polymer-coated Pt disk as the support electrode, acetonitrile containing TBAPF6 (0.1 M) as supporting electrolyte, Pt wire as counter electrode and SCE (saturated calomel electrode) as reference electrode.

Copolymers films display an onset of the p-doping process at 0.83 V and 1.22 V for **PT6Br/F** and **rrPT6Br/F**, respectively, with a faster increase of the oxidation current for the regioregular sample, suggesting a better conductivity and thus an improved performance when employed as electron-donor polymer (Table 5 and Figure 9).

Table 5. Electrochemical characteristics of copolymers.

Samples	E_{ox}^{onset} *(V)*	E_g^{opt} *(V)*	*HOMO (eV)*	*LUMO (eV)*
PT6Br/F	0.83	2.04	-5.23	-3.19
rrPT6Br/F	1.22	1.90	-5.62	-3.72

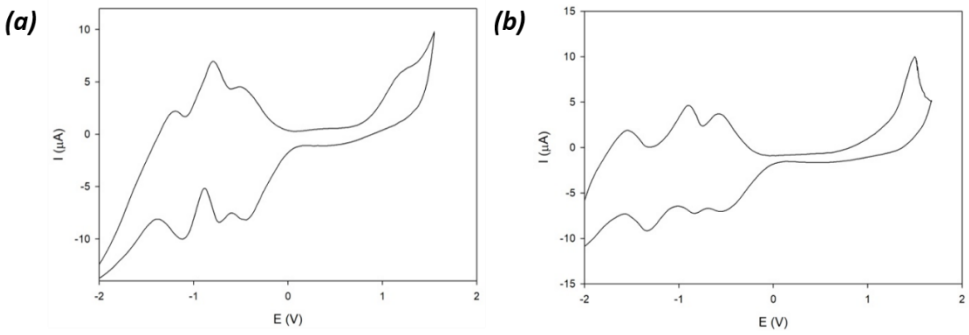

Figure 9. CV curves (third cycle) of **PT6Br/F** (a) and **rrPT6Br/F** (b).

Whereas the HOMO level of the copolymers was measured by CV, the LUMO energy had to be indirectly calculated. Indeed, since several waves related to the multiple

reduction processes of the fullerene group[28] dominate the negative potentials zone of the voltammograms, the reduction potential of the polythiophenic component of the films is impossible to evaluate. However, the electrochemical behaviour of the films indicates that both the fullerene pendant group and the conjugated polythiophene chain retain their individual electrochemical properties.

Therefore, considering that the SCE reference electrode has a potential of 4.40 eV relative to vacuum,[29] the energy of the HOMO levels was estimated according to the relation (**1**); on the other hand, by means of the relation (**2**), the energy of the LUMO levels was calculated from the aforementioned HOMO values and the values of the optical bandgaps (E_g^{opt}), which were obtained from the UV-Vis spectra of films:

$$(\mathbf{1}) \qquad I_p(HOMO)(eV) = -e(E_{ox}^{onset} + 4.40)$$

$$(\mathbf{2}) \qquad LUMO = HOMO + E_g^{opt}(eV)$$

As reported in Table 5, it is especially noteworthy the low HOMO level energy and thus the low bandgap value obtained for **rrPT6Br/F**, that could have positive potential implications on the conversion efficiency of the cell.[30] In fact, not only does the bandgap show a remarkably low value, if compared to the standard reference P3HT (-4.8 eV),[31] but allows to predict a high open-circuit voltage value of the cell, since the V_{oc} of a BHJ solar cell is directly proportional to the absolute value of I_p(HOMO).[32]

2.6.Morphological analysis

It is well-known that investigation, and thus control, of the morphology of the active layer is a factor of primary importance in the production of organic solar cells. For this reason, X-rays diffraction (XRD) patterns of **PT6Br/F** and **rrPT6Br/F** in film, before and after the annealing procedure, carried out under the same experimental conditions adopted for the preparation of solar cells – i.e. heating in the glass oven under vacuum at 120°C for 30 min – have been evaluated (Figure 10).

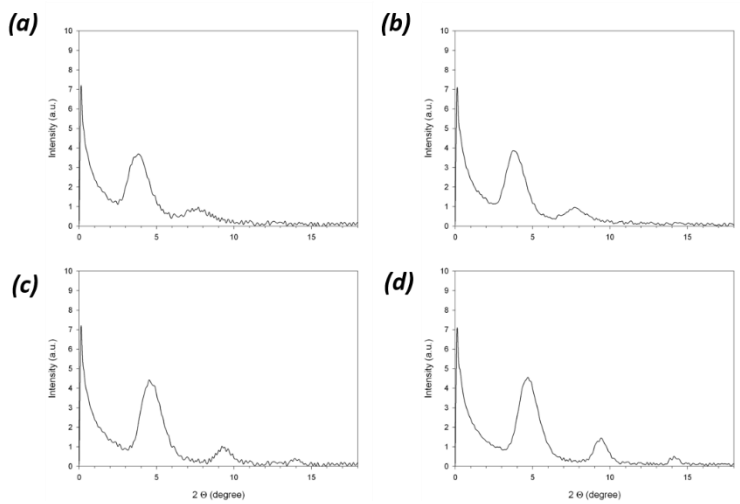

Figure 10. X-rays diffractograms of **PT6Br/F** (a-b) and **rrPT6Br/F** (c-d), before (left) and after (right) annealing.

Firstly, as expected, the annealing procedure confirms to be an effective method in the enhancement of the structural order of the material, since the annealed samples show slightly sharper and more intense peaks than the native ones. Small angle reflections in the 2ϑ=3.75-4.67 range, corresponding to the first order reflections (100) ascribable to the distance between polythiophenic chains lying on the same plane, are shown by all the examined samples (Table 6). Even though both **PT6Br/F** and **rrPT6Br/F** films further show the second order reflections (200), determined by the multiple X-ray reflections on the film, the third order reflections (300) can be found only for the regioregular sample, probably due to an improved structural order induced by the higher regioregularity degree. Moreover, since the interlayer d_1 spacings distances are notably lower in the annealed samples, the positive effect of the annealing procedure on the structural order and on the packing degree of the copolymer films are furtherly confirmed.

Table 6. Structural parameters of the synthesized copolymers in film.

Samples	*Low-angle diffractions (2ϑ, degree)*	*On plane PT chain distances (Å)*
PT6Br/F	3.75; 7.63	23.55
PT6Br/F annealed	3.84; 7.72	22.98
rrPT6Br/F	4.61; 9.31; 13.90	19.13
rrPT6Br/F annealed	4.67; 9.38; 14.12	18.92

In addition to XRD measurements, the surface morphology of the double-cable copolymers was also examined by AFM. Films of similar thickness (~ 100 nm), obtained from chlorobenzene solutions, were obtained on ITO glasses by doctor-blade technique; similarly to XRD analysis, the samples were also thermally annealed.

As expected from this type of molecular architecture, which involves direct covalent linking of the electron-acceptor group to the electron-donor conjugated backbone, the AFM images (Figure 11) display the formation of an homogeneous bi-continuous network between the polythiophene- (brighter areas) and the fullerene-rich phases (darker areas).

The effect of the annealing procedure on the film morphology can be also evaluated considering the root-mean-square (RMS) roughness of the different samples, which increases from 0.89 to 1.05 nm for **PT6Br/F** and from 1.08 to 1.13 nm for **rrPT6Br/F**. Upon annealing, the films surface becomes rougher since the controlled heating enhances the crystallinity of the polythiophenic component of the double-cable polymer,[33,34] with positive effects on the hole-carrier transport.[35] Furthermore, a rougher film surface could also lead to an increase of the contact area between the photoactive layer and the metal cathode, that results in a more efficient charge-collection at the interface.

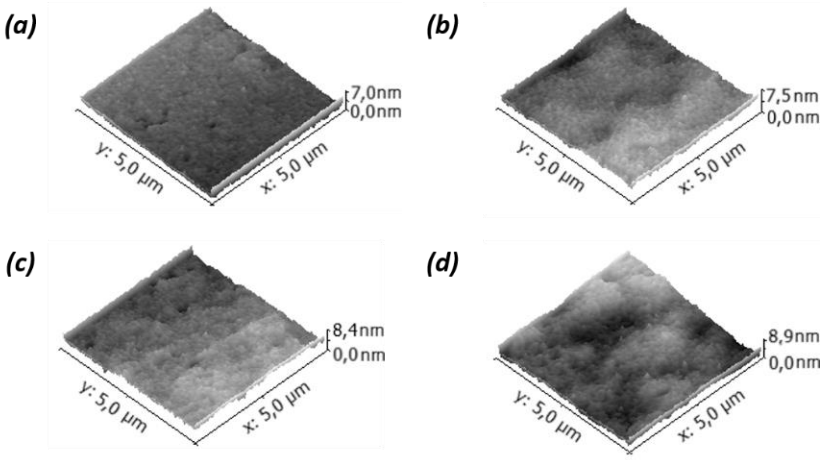

Figure 11. AFM images of **PT6Br/F** (a-b) and **rrPT6Br/F** (c-d) before (left) and after (right) annealing.

2.7. Organic solar cells

2.7.1. Photovoltaic properties

The performance of the synthesized copolymers as photoactive layers, deposited from chlorobenzene solutions by doctor-blade technique, has been investigated by fabricating a series of single material organic solar cells (SMOSCs) having the following structure: ITO (80 nm)/PEDOT:PSS (100 nm)/double-cable copolymer (150 nm)/Al (50 nm).
In addition to the current density-voltage (J/V) curves of the devices, which are shown in Figure 12, the main photovoltaic parameters such as short-circuit current density (J_{sc}), open-circuit voltage (V_{oc}), fill factor (FF) and above all power conversion efficiency (PCE), are summarized in Table 7.

As a result of its increased crystallinity and reduced bandgap, the regioregular copolymer **rrPT6Br/F** shows a PCE notably higher than its regioirregular counterpart **PT6Br/F** (5.21 vs 3.55%). Indeed, despite a lower fullerene content, structural regularity clearly appears to be a key-parameter in the promotion of the formation of efficient bi-continuous interpenetrating networks which, as demonstrated by the higher value of J_{sc} obtained with regioregular sample, is able to enhance the charge transport and their subsequent collection to the electrodes. Moreover, not only is a higher value of V_{oc} shown by **rrPT6Br/F**, originated by its lower HOMO level energy, but the obtained results are also in good agreement with the findings reported by Ansari and coworkers in a recent study.[36] Since the authors observed that highly regioregular electron-donor polymers typically show an enhanced mobility of excitons and thus a compressed bandgap, the importance of structural regioregularity in the donor polymer need to be evidenced, with the purpose of improving and promoting the absorption efficiency of the solar spectrum.

Table 7. Properties of organic solar cells prepared with double-cable copolymers (average values collected from ten devices).

Copolymers	*J_{sc} (mA/cm^2)*	*V_{oc} (V)*	*FF*	*PCE (%)*
rrPT6Br/F	11.6±1.2	0.68±0.01	0.64±0.03	5.21±0.09
rrPT6Br/F*	12.2±1.3	0.68±0.01	0.67±0.04	5.68±0.12
PT6Br/F	10.4±1.1	0.62±0.01	0.55±0.06	3.55±0.13
PT6Br/F*	10.9±1.2	0.63±0.01	0.60±0.05	4.12±0.08

* Samples with AuNPs interlayer.

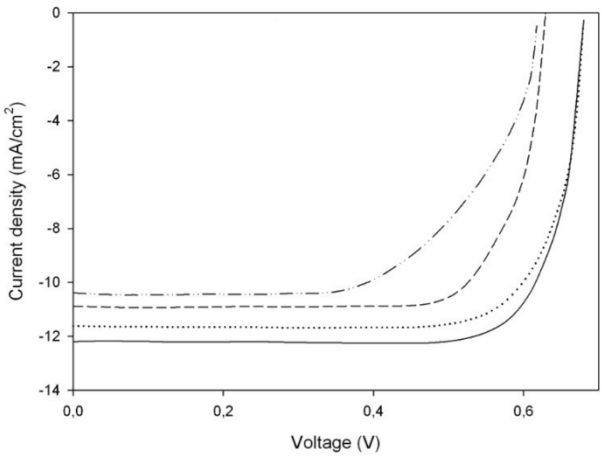

Figure 12. Current density-voltage for the best-performing cells fabricated with **PT6Br/F** (solid-dotted line), **rrPT6Br/F** (dotted line), **PT6Br/F*** (dashed line) and **rrPT6Br/F*** (solid line).

In order to further enhance the current density of the prepared devices, a thin layer of gold nanoparticles (AuNPs) - prepared according to ref.[37,38] - has also been inserted as anode interlayer, between the PEDOT:PSS and the photoactive blend layers. It is well known that the series resistance could be reduced by the presence of a highly-conductive interlayer in BHJ organic solar cells.[39,40]

Similarly to those previously described, the solar cells with the AuNPs interlayer (**PT6Br/F*** and **rrPT6Br/F***) were thermally-treated and measured to give the J/V curves reported in Figure 12 and the main photovoltaic features reported in Table 7. The final architecture of the device resulted to be: ITO (80 nm)/PEDOT:PSS (100 nm)/AuNPs (30 nm)/double-cable copolymer (150 nm)/Al (50 nm).

After incorporating AuNPs interlayer, as a consequence of the increased J_{sc} and FF values, an increase of the PCE by about 11% was produced. In addition to prove the effectiveness of the metal nanoparticles insertion in reducing the series resistances, the obtained results also suggest a simple method to increase the charge mobility and thus enhance the efficiency of polymeric BHJ solar cells.

Taking into account that the wavelengths of photocurrent response for fabricated SMOSCs range from 300 to 710 nm, the curve of the device based on **PT6Br/F** and **rrPT6Br/F** sample has, respectively, two feature peaks at 330 and 540 nm and two main peaks at 350 and 560 nm (Figure 13).

The quantum efficiency (EQE) profiles substantially follow the trend observed in the absorption spectra of copolymers in film, suggesting that the harvested photons over the whole absorption spectrum can effectively contribute to the final photocurrent. Furthermore, in agreement with previous findings showing higher value of J_{sc} when

rrPT6Br/F is used as photoactive layer in BHJ solar cell, an enhanced EQE is observed (EQE_{max} 68% vs 59%), indicating an improved charge collection efficiency for the regioregular double-cable copolymer.

The parameters derived from EQE measurements[41] (J_{sc}, $J_{sc\,max}$ with a theoretical 100% EQE and HOMO-LUMO bandgap) are in good agreement with the above reported values (12.1 mA cm^{-2}, 19.4 mA cm^{-2}, 1.85 eV for **rrPT6Br/F** and 10.8 mA cm^{-2}, 18.3 mA cm^{-2}, 1.96 eV for **PT6Br/F**, respectively).

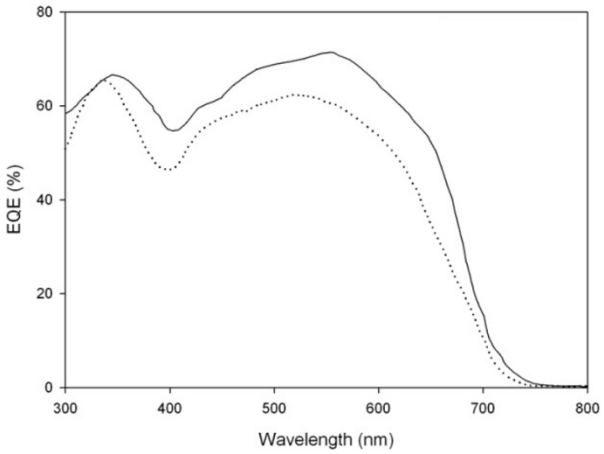

Figure 13. EQE spectra of copolymer devices: **PT6Br/F** (solid line) and **rrPT6Br/F** (dotted line).

2.7.2. Photocrosslinking of photoactive layers

The importance of thermal annealing aimed to the optimization of photoactive layer morphology was first reported by Padinger and coworkers[42] on P3HT/PCBM blends. In fact, when the active layer of the OSC is heated to a temperature higher than T_g or T_m (if detectable), the polymer chains are able to reorganize themselves in a more crystalline structure - while the fullerene molecules diffuse into the blend - and a thermodynamically favored reorganization is allowed. Therefore, annealing generally results in higher conversion of photons to charges and in an enhanced mobility of the latters.[43]

However, as previously noted, the bicontinuous network with nanometer-scale phase segregation created in the blend after the annealing procedure is not thermally stable over time. Indeed, as the polymer-fullerene nanoclusters are created by kinetically trapping of the electron donor/acceptor nanostructures, during the light exposition of the final devices (or after long storage times) a spontaneously segregation of the components to the original macrophase separation is produced. Although the adoption of thermally cross-linkable moieties on the polymer chains have been proposed to enhance the phase stability of the

BHJ solar cells,[44,45] a decrease of PCE was observed, probably due to the achievement of a more disordered blend morphology during the thermal crosslinking procedure. In this context, since the synthesized double-cable copolymers are functionalized with bromine groups, a photocrosslinking at room temperature can be performed as a promising and really interesting alternative to thermal crosslinking.

Via a radical mechanism, initiated by the photochemical break of C-Br bonds under UV-light,[46,47] the photocrosslinking was carried out on the just annealed BHJ cells before the Al cathode deposition. By firstly exposing the films to UV-light (3.2W @ 250 nm, λ_{max} at 253.7 nm, distance of irradiation 5 cm) for different times and subsequent immersion of the film in chlorobenzene for 15 min, the right time of exposure (30 minutes) was determined. By comparison of the films weights before and after solvent treatment, the copolymers films resulted to be totally insoluble in the chlorinated solvent already after 15 minutes of UV exposure, proving the effectiveness of the crosslinking procedure.

The thermal stability was studied using the most performing cells - samples **PT6Br/F*** and **rrPT6Br/F*** - and a conventional P3HT:PCBM blend device as a reference cell [ITO/PEDOT:PSS/AuNPs/P3HT(M_n = 36 KDa, PDI = 1.25, 96% HT):PCBM (1:1 w/w)/Al]; the cells were submitted to constant heating at 150°C under vacuum for different times (up to 80 h) in order to simulate an accelerated aging (Figure 14).

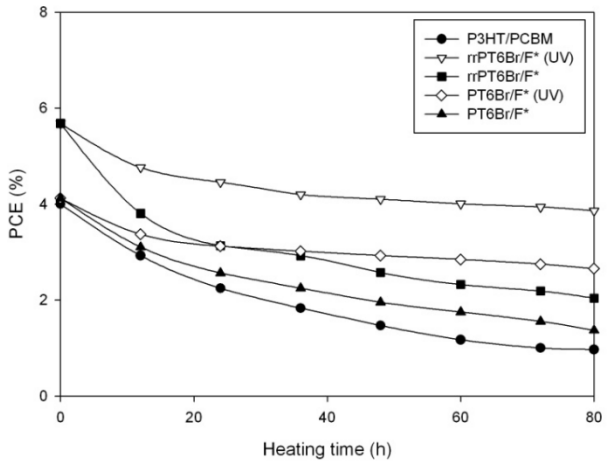

Figure 14. Efficiencies of OSCs heated at 150°C vs. time.

The PCE of the unexposed samples decreases to a 36% (**rrPT6Br/F***) and 34% (**PT6Br/F***) of the initial value after 80 h at 150°C, whereas a faster decrease is exhibited by the reference cell which reach the 25% of the initial efficiency.

These data are especially significant as they are a further confirm of the intrinsic higher stability of the double-cable copolymers, when used as photoactive layers in SMOSCs,

with respect to the classic blend BHJ architecture. Indeed, the covalent attachment of the electron-acceptor fullerene-moiety to the donor polymer backbone provides a beneficial impact on duration and thermal properties of the final device, due to a reduced mobility of the components.

On the other hand, the effectiveness of the photocrosslinking procedure is evidenced by the results obtained with the UV-exposed samples, which showed very stable device performances even after 80 h of annealing at 150°C: the 68% and 65% of the initial efficiency for the regioregular **rrPT6Br/F*** and the regiorandom **PT6Br/F*** copolymer, respectively, are still observed. The obtained results clearly evidence that the photocrosslinking procedure is particularly promising for the achievement of thermally stable high performance devices.

2.8. Conclusions

Two double-cable and photocrosslinkable thiophene-based copolymers, with different regioregularity degree, have been prepared with the aim to prepare high performance single material organic solar cells (SMOSCs).

In particular, the newly electron-donor and acceptor double-cable materials have been successfully synthesized through a simple and straightforward post-polymerization approach on poly[3-(6-bromohexylthiophene)] (**PT6Br**) by means of a Grignard coupling reaction with C_{60}-fullerene. In addition to confirm the successful anchorage of C_{60} to the PT6Br backbone, FT-IR and NMR spectroscopy and elemental analysis also provided the extent of substitution degree. Since the two precursor polymers showed similar molecular weights but different degrees of regioregularity (**PT6Br** and **rrPT6Br**), they were functionalized with different amounts of fullerene according to their different solubility.

The regioregular double-cable copolymer (**rrPT6Br/F**) showed the most performing properties, despite its lower content of electron-acceptor group, thus confirming the decisive effect of the structural regularity on the electronic characteristics of the photoactive blend. It is particularly noteworthy that a notable increase in power conversion efficiency was also obtained by interposing a thin layer of Au nanoparticles as anode interlayer, allowing to reach a PCE of 5.68% with the regioregular sample.

Finally, the presence of brominated side chains allowed the photocrosslinking at room temperature of the prepared SMOSCs in order to improve their temporal stability.

3. Experimental section

3.1. Materials

All reagents were purchased from Sigma-Aldrich and used without further purification unless otherwise stated. All solvents used were dried and purified by normal laboratory procedures, stored over molecular sieves and handled in a moisture-free atmosphere.

3.2. Synthesis of monomers

*3.2.1. 3-(6-Bromohexyl)thiophene (**T6Br**) by lithiation*

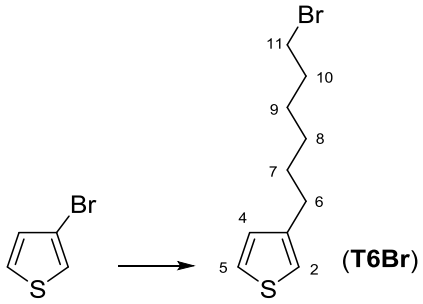

73.6 ml (0.184 mol) of a 2.5 M solution of *n*-butyl-lithium in hexane was added dropwise to a solution of 3-bromothiophene (30.0 g, 0.184 mol) in 250 ml of *n*-hexane previously cooled down to -80°C. After stirring for 10 min under argon atmosphere, 25 ml of anhydrous THF was added and the mixture was stirred for 90 min and then warmed up to -10°C. 38 ml (0.247 mol) of 1,6-dibromohexane in 10 ml of anhydrous THF were then dropped and the mixture stirred for further 2 h at room temperature under inert atmosphere. The mixture was quenched with 200 ml of distilled water and extracted with 4 × 150 ml of diethyl ether. The organic phase was then washed to neutrality, dried over $MgSO_4$ and evaporated under reduced pressure to give 12.68 g of crude product which was purified by vacuum distillation to give 4.09 g of **T6Br** (8% yield), b.p. 96°C, 0.5 mmHg.

^{1}H-NMR ($CDCl_3$, ppm): δ 7.24 (m, 1H, 5-H), 6.93 (m, 2H, 2-H and 4-H), 3.41 (t, 2H, 11-H), 2.64 (t, 2H, 6-H), 1.86 (m, 2H, 10-H), 1.64 (m, 2H, 7-H), 1.47 (m, 2H, 9-H), 1.37 (m, 2H, 8-H).

*3.2.2. 2,5-Dibromo-3-(6-bromohexyl)thiophene (**2,5BT6Br**)*

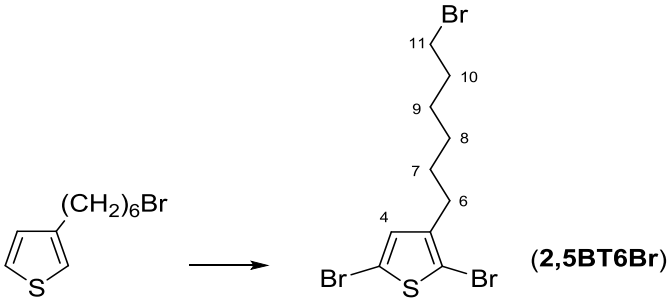

0.715 g (4.02 mmol) of N-bromosuccinimide (NBS) in 4.0 ml of N,N-dimethylformamide (DMF) were added dropwise – under stirring and in an inert atmosphere – to a solution of 1.00 g (4.02 mmol) of T6Br in 4.0 ml of DMF. The mixture was reacted for 6 h at room temperature in the dark and under a gentle argon flux. 1.07 g (6.02 mmol) of NBS in 6.0 ml of DMF were added dropwise and the mixture was reacted for another 24 h. The reaction mixture was then poured into 130 ml of an aqueous solution of NaCl and the organic phase was extracted with 5 × 100 ml of petroleum ether. The collected organic phases were washed with water to neutrality, dried and concentrated at reduced pressure giving 1.60 g of **2,5BT6Br** (98% yield).

^{1}H-NMR ($CDCl_3$, ppm): δ 6.77 (s, 1H, 4-H), 3.41 (t, 2H, 11-H), 2.52 (t, 2H, 6-H), 1.86 (m, 2H, 10-H), 1.57 (m, 2H, 7-H), 1.47 (m, 2H, 9-H), 1.35 (m, 2H, 8-H).

3.3. Synthesis of homo- and copolymers

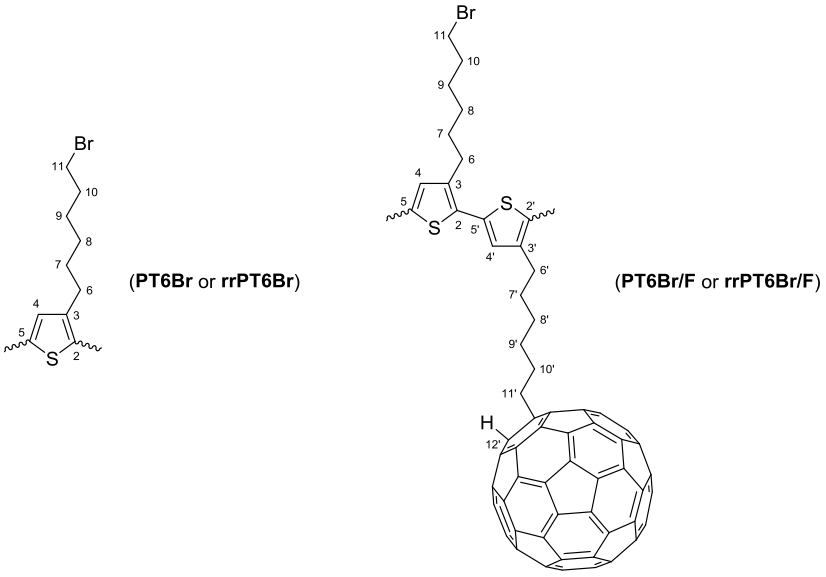

Figure 13. Atoms numbering for homopolymers and double-cable copolymers.

*3.3.1. Poly[3-(6-bromohexyl)thiophene] (**PT6Br**) by oxidative polymerization*

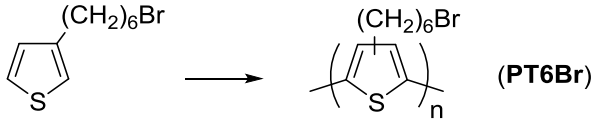

(**PT6Br**)

2.68 g (16.5 mmol) of iron trichloride in 17 ml of anhydrous nitromethane was dropped in 20 min, under argon and at room temperature, into a solution of 1.00 g (4.02 mmol) of T6Br in 48 ml of anhydrous $CHCl_3$. After the addition was completed, the reaction mixture was stirred for 2 h at room temperature and then added to 50 ml of THF. The mixture was then poured into 250 ml of a 5% methanolic solution of HCl and the resulting precipitate filtered on a PTFE membrane (0.45 µm pore size) and washed several times with further MeOH. The recovered polymer was then re-dissolved in 150 ml of $CHCl_3$ and the obtained solution washed with 2% aqueous HCl, up to exhaustive extraction of the iron (III) ion (negative essay with NH_4SCN), and with distilled water to neutrality. The organic phase was dried with $MgSO_4$ and concentrated at reduced pressure. The final polymer was fractionated using a 1:10 (v/v) $CHCl_3$/MeOH mixture giving 0.392 g (40% yield) of dark-red **PT6Br**.

^{1}H-NMR ($CDCl_3$, ppm): δ 6.98 (m, 1H, 4-H), 3.43 (m, 2H, 11-H), 2.83 and 2.57 (2m, 2H, 6-H), 1.94-1.32 (bm, 8H, 7-H, 8-H, 9-H and 11-H).

^{13}C-NMR ($CDCl_3$, ppm): δ 143.71, 143.01, 141.03, 140.28 (C3), 136.94, 135.88, 134.61, 134.77 (C5), 131.32, 130.85, 130.23, 129.85 (C2), 129.04, 128.65, 128.32, 127.63 (C4), 34.55 (C11), 33.81 (C10), 30.94 (C6), 29.96 (CH_2), 29.15 (CH_2), 28.53 (CH_2).

FT-IR (Ge, cm^{-1}): 3055, 2929, 2854, 1509, 1457, 1259, 1090, 827, 727, 645, 562.

*3.3.2. Poly[3-(6-bromohexyl)thiophene] (**rrPT6Br**) by GRIM (Grignard Metathesis) polymerization*

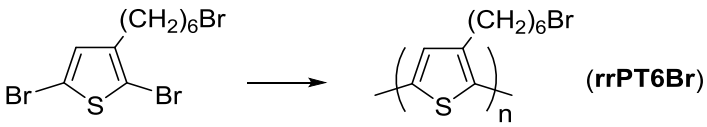

(**rrPT6Br**)

1.40 ml of a 3.0M CH_3MgCl solution (4.20 mmol) in n-butyl ether was added to 1.60 g (3.96 mmol) of 2,5BT6Br in 32 ml of anhydrous THF. The mixture was refluxed for 2 h under stirring and in inert atmosphere and then 10.7 mg (0.0198 mmol) of [1,3-bis(diphenylphosphino)propane] Nickel (II) chloride ($Ni(dppp)Cl_2$) was added and the

reaction refluxed for 75 min. After cooling down to room temperature, the mixture was poured in 400 ml of MeOH and the resulting suspension was centrifuged at 3000 rpm for 20 min. The recovered polymer was dissolved in 20 ml of $CHCl_3$, filtered on a PTFE membrane (0.20 µm pore size) and fractionated using a 1:5 (v/v) $CHCl_3$/MeOH mixture. After solvent evaporation at reduced pressure, 0.452 g (1.85 mmol) of reddish **rrPT6Br** were obtained (47% yield).

^{1}H-NMR ($CDCl_3$, ppm): δ 6.98 (s, 1H, 4-H), 3.43 (t, 2H, 11-H), 2.84 (m, 2H, 6-H), 1.94-1.38 (bm, 8H, 7-H, 8-H, 9-H and 10-H).

^{13}C-NMR ($CDCl_3$, ppm): δ 140.31 (C3), 134.91 (C5), 131.23 (C2), 129.01 (C4), 34.59 (C11), 33.97 (C10), 30.61 (C6), 29.83 (CH_2), 29.17 (CH_2), 28.55 (CH_2).

FT-IR (Ge, cm^{-1}): 3055, 2929, 2854, 1505, 1432, 1258, 1071, 826, 724, 642, 561.

*3.3.3. Poly[3-(6-bromohexyl)thiophene-co-3-(6-fullerenylhexyl)thiophene] (**PT6Br/F**)*

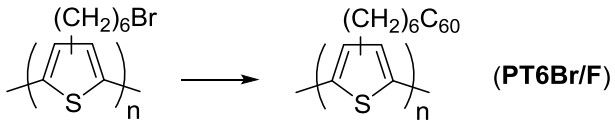

0.200 g (0.816 mmol) of PT6Br in 5 ml of anhydrous THF was added dropwise to 14.87 mg (0.612 mmol) of Mg turnings under stirring and in an inert atmosphere. The mixture was refluxed for 20 h, cooled down to room temperature, and then transferred via cannula to a solution of 0.441 g (0.612 mmol) of C_{60}-fullerene in 300 ml of anhydrous toluene and 1.3 ml of anhydrous N,N-dimethylformamide (DMF). The reaction mixture was stirred for 90 min under inert atmosphere and then 2.5 ml of a 1.87 M aqueous solution of NH_4Cl and 100 ml of brine was added. The organic phase was washed several times with distilled water, dried with $MgSO_4$ and concentrated. The copolymer was dissolved in 100 ml of $CHCl_3$ and the obtained solution dropped into 350 ml of *n*-heptane. After filtration on a PTFE membrane (0.45 µm pore size), 0.407 g (0.609 mmol) of fractionated **PT6Br/F** was obtained (75% yield).

^{1}H-NMR (pyridine-d_5, ppm): δ 7.47 (m, 4-H and 4'-H), 7.38 (s, 12-H), 3.58 (m, 11-H), 3.45 (m, 11'-H), 3.01 and 2.81 (m, 6-H and 6'-H), 1.91-1.14 (bm, 7-H, 8-H, 9-H, 10-H and 7'-H, 8'-H, 9'-H, 10'-H).

^{13}C-NMR (ODCB-d_4, ppm): δ 160.03, 156.28, 151.67, 149.29, 148.36, 147.94, 147.81, 147.38, 146.99, 146.12, 146.01, 145.89, 145.55, 145.38, 145.24, 145.01, 144. 77, 144.12, 143.79, 143.47, 142.66, 142.14, 142.03, 141.91, 141.73 and 141.22 (C_{60}), 143.48, 142.96, 141.12 and 140.57 (C3 and C3'), 140.29, 140.04, 137.75 and 136.04 (C_{60}), 136.65, 136.02, 135.55 and 134.95 (C5 and C5'), 129.82, 129.78, 129.52 and 129.26 (C2 and C2'), 129.11, 128.88, 128.36 and 128.03 (C4 and C4'), 61.76 (C11), 42.95 (C10), 34.73 (C11'), 34.02 (C10'), 30.68 (C6 and C6'), 29.95 (C9 and C9'), 29.32 (C7 and C7'), 28.73 (C8 and C8').
FT-IR (KBr, cm^{-1}): 3053, 2929, 2852, 1506, 1455, 1429, 1260, 1182, 1034, 834, 747, 649, 576, 560, 522.

*3.3.4. Poly[3-(6-bromohexyl)thiophene-co-3-(6-fullerenylhexyl)thiophene] (**rrPT6Br/F**)*

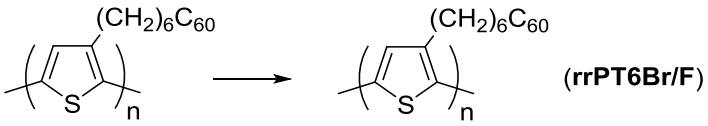

The adopted procedure was the same as for PT6Br/F, using 0.200 g (0.816 mmol) of rrPT6Br in 10 ml of anhydrous THF and 4.90 mg (0.202 mmol) of Mg turnings for the Grignard formation, and 0.147 g (0.204 mmol) of C_{60}-fullerene in 100 ml of anhydrous toluene and 0.5 ml of anhydrous N,N-dimethylformamide (DMF) for the coupling step. 0.250 g (0.776 mmol) of fractionated **rrPT6Br/F** was obtained (95% yield).

^{1}H-NMR (pyridine-d_5, ppm): δ 7.47 (s, 4-H and 4'-H), 7.38 (s, 12-H), 3.58 (m, 11-H), 3.47 (m, 11'-H) 3.02 and 2.78 (m, 6-H and 6'-H), 1.89-1.12 (bm, 7-H, 8-H, 9-H, 10-H and 7'-H, 8'-H, 9'-H, 10'-H).

^{13}C-NMR (ODCB-d_4, ppm): δ 159.89, 156.26, 151.59, 149.24, 148.32, 147.89, 147.80, 147.37, 146.95, 146.08, 145.99, 145.77, 145.42, 145.26, 145.18, 145.00, 144. 74, 144.11, 143.76, 143.43, 142.64, 142.11, 142.01, 141.86, 141.69 and 141.18 (C_{60}), 140.55 (C3 and C3'), 140.21, 140.00, 137.77 and 136.02 (C_{60}), 134.93 (C5 and C5'), 129.81 (C2 and C2'), 128.88 (C4 and C4'), 61.75 (C11), 42.93 (C10), 34.72 (C11'), 34.00 (C10'), 30.67 (C6 and C6'), 29.95 (C9 and C9'), 29.30 (C7 and C7'), 28.71 (C8 and C8').

FT-IR (KBr, cm^{-1}): 3056, 2930, 2852, 1513, 1456, 1428, 1259, 1182, 1031, 836, 749, 646, 576, 562, 525.

3.4.Preparation of gold nanoparticle layer

3.30 mg (8.4 μmol) of Gold (III) chloride hydrate ($HAuCl_4 \cdot 3H_2O$, Aldrich Cod. 254169) were dissolved in 10 ml of distilled water and added with 2 ml of H_2O_2 (30% w/v). The volume of the solution was halved by heating and the obtained solution was sonicated, filtered on a PTFE septum (0.20 μm pore size) and 400 μl of the resulting solution was deposited using a BLE Spin Coater operating at 2000 rpm on the ITO glass slide previously spin-cast using the PEDOT:PSS solution and allowed to dry into a temperature-controlled oven at 75°C. The final thickness of the AuNPs layer was around 30 nm.

3.5.Methods and characterizations

Molecular weights were determined by gel permeation chromatography (GPC) by using THF solutions on a HPLC Lab Flow 2000 apparatus equipped with a Rheodyne 7725i injector, a Phenomenex Mixed bed column 5μ MXL and a RI K-2301 KNAUER detector. The calibration curve was recorded using monodisperse polystyrene standards.

A DSC TA Instruments Q2000 was used for the thermal analysis by varying the temperature from -50°C to 230°C at a rate of 5°C min^{-1} in a nitrogen atmosphere (mass samples ~10 mg). A TGA TA Instruments Q600, operating in air flux, was used to determine the decomposition temperatures of the samples (mass samples ~10 mg) by heating from 30°C to 900°C at a scan rate of 10°C min^{-1}.

^{1}H- and ^{13}C-NMR were recorded on a Varian Mercury Plus (400 MHz) spectrometer using TMS as a reference.

IR spectra were taken on Ge and KBr disks using a Perkin Elmer Spectrum One or a Bruker Alpha Platinum spectrophotometer.

UV-Vis spectra were recorded on a Perkin Elmer Lambda 19 spectrophotometer using about 10^{-5} M polymer solutions in spectroquality solvents in Suprasil quartz cuvettes (1 cm × 1 cm) or films on quartz slides.

Cyclic voltammograms were recorded using an Autolab PGSTAT204 (Metrohm) potentiostat/galvanostat at a potential scan rate of 100 mV/s on polymer films deposited on Pt electrodes from chlorobenzene solutions. The working electrode (polymer coated Pt disk), the counter electrode (Pt wire) and the reference electrode (aqueous saturated calomel electrode) were immersed in an acetonitrile solution with tetrabutylammonium

hexafluorophosphate (TBAPF6) 0.1 M as supporting electrolyte using a single compartment three-electrode cell.

AFM measurements were made on a Burleigh Vista 100 atomic force microscope in a semicontact tapping mode using high resolution silicon nitride tips. X-ray diffraction data of polymer films were recorded at room temperature by using a CuKα (λ = 1.5406 Å) radiation source (Philips PW 1050) and a Bragg-Brentano diffractometer (Philips PW 1710) equipped with a graphite monochromator in the diffracted beam. The 2θ range between 2.0 and 90.0° was scanned by 881 steps of 0.1° with a counting time of 15 s for each step.

Single material organic solar cells (SMOSCs) were prepared according to the following procedure: the ITO glass substrate (1 cm × 1 cm, surface resistance 21 Ω/sq) was etched on one side by using a 10% wt aqueous solution of HCl and heated at 60°C for 15 min in order to obtain an area of 0.75 × 1 cm covered by indium tin oxide. The glass was then cleaned in an ultrasonic bath (Elmasonic S30H) using acetone and then treated at 60°C for 20 min with a solution of aqueous NH_3 (0.8 M) and H_2O_2 (0.5 M), rinsed with distilled water, 2-propanol and dried with a nitrogen flow. The final resistance of the ITO glass was 12 Ω/sq. Poly(3,4-ethylenedioxythiophene):polystyrene sulfonic acid (PEDOT:PSS, 2.8 wt% dispersion in water, viscosity 20 cps) was diluted 1:1 v/v with 2-propanol, sonicated, filtered on a Gooch G2 and the resulting solution (viscosity 12 cps) deposited over the previously treated ITO glass by the doctor blading technique using a Sheen Instrument Model S265674, leaving only a small (0.25 × 1 cm) area uncovered at the opposite side of the previously etched area. The PEDOT:PSS film was heated in a Büchi GKR-50 glass oven at 130°C for 2 h under vacuum (10^{-3} mmHg). A solution made by mixing 5 mg of double-cable copolymer (PT6Br/F or rrPT6Br/F) in 1 ml of chlorobenzene was sonicated for 15 min, filtered on a PTFE septum (0.25 μm pore size) and deposited by doctor blading on the slide in order to cover the PEDOT:PSS layer. The sample was then annealed in the glass oven under vacuum (10^{-3} mmHg) at 120°C for 30 min. Finally, a 50 nm thick Al electrode was deposited over the polymeric layer through a shadow mask using an Edwards 6306A coating system operating at 10^{-6} mmHg. The active area of the cell was 0.25 × 0.25 cm^2. The current-voltage characteristics were measured in air using a Keithley 2401 source meter under the illumination of an Abet Technologies LS150 Xenon Arc Lamp Source AM 1.5 Solar Simulator (100 mW/cm^2) calibrated with an ILT 1400-BL photometer. The structure of the final devices were: ITO (80 nm)/PEDOT:PSS (100 nm)/active layer (150

nm)/Al (50 nm). The spectral response of the solar cells was measured using a 7-SC Spec III Modularized Solar Cell Spectral Test System (SevenStar Optics, Beijing, PRC). Layer thicknesses were measured using a Film Thickness Probe FTPAdvances FTPadv-2 (Sentech GmbH, Germany) equipped with the FTPExpert software.

References

[1] J. You, L. Dou, K. Yoshimura, T. Kato, K. Ohya, T. Moriarty, K. Emery, C. C. Chen, J. Gao, G. Li, *Nat. Commun.* **4** (2013) 1-10.
[2] C. Y. Yang, A. J. Heeger, *Synth. Met.* **83** (1996) 85-88.
[3] M. T. Dang, L. Hirsch, G. Wantz, *Adv. Mater.* **23** (2011) 3597-3602.
[4] R. C. Hiorns, E. Cloutet, E. Ibarboure, L. Vignau, N. Lemaitre, S. Guillerez, C. Absalon, H. Cramail, *Macromolecules* **42** (2009) 3549-3558.
[5] G. A. Bernardin, N. A. Davies, C. E. Finlayson, *Materials Science in Semiconductor Processing* **71** (2017) 174-180.
[6] K. Sivula, Z. T. Ball, N. Watanabe, J. M. J. Fréchet, *Adv. Mater.* **18** (2006) 206-210.
[7] G. T. Feng, J. Y. Li, F. J. M. Colberts, M. M. Li, J. Q. Zhang, F. Yang, Y. Z. Jin, F. L. Zhang, R. A. J. Janssen, C. Li, W. W. Li, *J. Am. Chem. Soc.* **139** (2017) 18647-18656.
[8] M. Chen, M. Li, H. Wang, S. Qu, X. Zhao, L. Xie, S. Yang, *Polym. Chem.* **4** (2013) 550-557.
[9] J. U. Lee, A. Cirpan, T. Emrick, T. P. Russell, W. H. Jo, *J. Mater. Chem.* **19** (2009) 1483-1489.
[10] Y. Murata, M. Suzuki, K. Kamatsu, *Org. Biomol. Chem.* **1** (2003) 2624-2625.
[11] T. Yamazaki, Y. Murata, K. Komatsu, K. Furukawa, M. Morita, N. Maruyama, T. Yamao, S. Fujita, *Org. Lett.* **6** (2004) 4865-4868.
[12] M. Lanzi, L. Paganin, F. Errani, *Polymer* **53** (2012) 2134-2145.
[13] E. D. Glowacki, N. S. Sariciftci, C. W. Tang, *Solar Energy*, Springer: New York, 2013, 97-128.
[14] B. C. Thompson, J. M. J. Fréchet, *Angew. Chem. Int. Ed.* **47** (2008) 58-77.
[15] B. J. Kim, Y. Miyamoto, B. Ma, J. M. J. Fréchet, *Adv. Funct. Mater.* **19** (2009) 2273-2281.
[16] M. H. Li, P. Xu, J. G. Yang, S. F. Yang, *J. Mater. Chem.* **20** (2010) 3953-3960.
[17] K. K. Stokes, K. Heuzé, R. D. McCullough. *Macromolecules* **36** (2003) 7114-7118.
[18] C. Della Casa, P. Costa Bizzarri, M. Lanzi, F. Bertinelli, *Acta Polym* **48** (1997) 251-255.
[19] X. Wu, T. Chen, L. Zhu, R. D. Rieke, *Tetrahedron Letters* **35** (1994) 3673-3674.
[20] M. Lanzi, E. Salatelli, T. Benelli, D. Caretti, L. Giorgini, F. P. Di Nicola, *J. Appl. Polym. Sci* (2015) 42121.
[21] P. Costa Bizzarri, F. Andreani, C. Della Casa, M. Lanzi, E. Salatelli, *Synth. Met.* **75** (1995) 141-147.
[22] R. S. Loewe, P. C. Ewbank, J. Liu, L. Zhai, R. McCullough, *Macromolecules* **34** (2001) 4324-4333.
[23] M. Lanzi, L. Paganin, *Eur. Polym. J.* **44** (2008) 3987-3996.
[24] B. W. Bondouris, F. Molins, D. A. Blank, C. D. Frisbie, M. A. Hillmyer, *Macromolecules* **42** (2019) 4118-4126.
[25] R. Qian, *Makromol. Chem. Macromol. Symp.* **33** (1990) 327-339.
[26] J. Clark, C. Silva, R. H. Friend, F. C. Spano, *Phys. Rev. Lett.* **98** (2007) 206406.
[27] S. Yamamoto, H. Yasuda, H. Ohkita, H. Benten, S. Ito, S. Miyanishi, K. Tajima, K. Hashimoto, *J. Phys. Chem. C* **118** (2014) 10584-10589.

[28] L. Echegoyen, L. E. Echegoyen, *Acc. Chem. Res.* **31** (1998) 593-601.
[29] J. Pommerehne, H. Westweber, W. Guss, R. F. Mahrt, H. Bassler, M. Porsch, J. Daub, *Adv. Mater.* **7** (1995) 551-554.
[30] P. Schilinsky, C. Waldauf, J. Hauch, C. J. Brabec, *J. Appl. Phys.* **95** (2004) 2816-2819.
[31] T. V. Richter, C. H. Braun, S. Link, M. Scheuble, E. J. W. Crossland, F. Stelzl, U. Wuerfel, S. Ludwigs, *Macromolecules* **45** (2012) 5782-5788.
[32] M. C. Scharber, D. Muehlbacher, M. Koppe, P. Denk, C. Waldauf, A. J. Heeger, C. J. Brabec, *Adv. Mater.* **18** (2006) 789-794.
[33] W. B. Lai, C. Li, J. Q. Zhang, F. Yang, F. J. M. Colberts, B. Guo, Q. M. Wang, M. M. Li, A. D. Zhang, R. A. J. Janssen, M. J. Zhang, W. W. Li, *Chem. Mater.* **29** (2017) 7073-7077.
[34] H. W. Tang, G. H. Lu, L. G. Li, J. Li, Y. Z. Wang, X. N. Yang, *J. Mater. Chem.* **20** (2010) 683-688.
[35] A. Lange, A. Hollaender, M. Wegener, *Materials Science and Engineering B* **178** (2013) 299–305.
[36] M. A. Ansari, S. Mohiuddin, F. Kandemirli, M. I. Malik, *RSC Adv.* **8** (2018) 8319-8328.
[37] B. R. Panda, A. Chattopadhyay, *J. Nanosci. Nanotechnol.* **7** (2007) 1911-1915.
[38] A. Chou, K. C. Vernon, L. Piro, B. Radi, E. A. Jaatinen, T. J. Davis, *J. Phys. Chem. C*, **116** (2012) 26517-26522.
[39] D. U. Karatay, M. Salvador, K. Yao, A. K. Y. Jen, D. S. Ginger, *Appl. Phys. Lett.* **105** (2014) 033304.
[40] L. Lu, Z. Luo, T. Xu, L. Yu, *Nano Lett.* **13** (2013) 59-64.
[41] Y. Li, W. Huang, H. Huang, C. Hewitt, Y. Chen, G. Fang, D. L. Carroll, *Solar Energy* **90** (2013) 51-57.
[42] F. Padinger, R. S. Rittberger, N. S. Sariciftci, *Adv. Funct. Mater.* **13** (2003) 85-88.
[43] V. D. Mihailetchi, H. Xie, B. de Boer, L. J. A. Koster, P. W. M. Blom, *Adv. Funct. Mater.* **16** (2006) 699-708.
[44] M. Drees, H. Hoppe, C. Winder, H. Neugebauer, N. S. Sariciftci, W. Schwinger, F. Schaffler, C. Topf, M. C. Scharber, Z. Zhu, R. Gaudiana, *J. Mater. Chem.* **15** (2005) 5158-5163.
[45] Z. Zhu, S. Hadjikyriacou, D. Waller, R. Guadiana, *J. Macromol. Sci. Part A* **41** (2004) 1467-1487.
[46] K. S. Lee, K. Y. Yeon, K. H. Jung, S. K. Kim, *J. Phys. Chem. A.* **112** (2008) 9312-9317.
[47] Y. Tang, L. Ji, R. S. Zhu, Z. R. Wei, B. Zhang, *J. Phys. Chem. A* **109** (2005) 11123-11126.

Chapter IV

Chapter IV: OPTICAL ACTIVITY – EFFECT OF REGIOREGULARITY ON CHIRAL POLY(3-HETEROALKYLTHIOPHENE)S

1. Introduction

1.1. Overview

Due to the combination of chirality with electrical conductivity, chiral conjugated polymers are potentially useful in many areas such as polarization-sensitive electroptical devices, polarized photo- and electroluminescence or chiral enantioselective sensors.[1]

As mentioned in the Introduction, chirality in the main chain of a polymer can be possibly induced by attachment of enantiomerically pure side chains to the backbone. Indeed, referring to chiral polythiophenes, the first optically active derivative bearing a chiral substituent covalently attached to the 3-position of the thiophene ring was obtained - by electrochemical polymerization - and then investigated since 1988 by Lemaire and coworkers.[2,3]

However, as the chirality is only evident when the polymer shows an ordered aggregated form, a decisive breakthrough in the research was definitely represented by the possibility to prepare regioregular derivatives by regiospecific polymerization routes, such as those reported by Mc Cullough, Chen and Rieke.[4,5] In fact, in early investigations, the frequent obtainment of optically active derivatives as a mixture of regioisomers involving steric interactions, as in the case of head-to-head (HH) coupling, usually determined a decrease of the conjugation length as well as reduced chiroptical properties. Thus, the achievement of regioregular head-to-tail (HT) couplings gave access to a wide range of chiral P3ATs with markedly enhanced chiroptical properties.

Circular dichroism (CD) studies allowed to demonstrate that in HT P3ATs the aggregation involves essentially planar polymer chains that have a helical *interchain order*, rather than an *intramolecular* helical conformation. In particular, HT poly{3-[(*S*)-(2-methylbutyl)]thiophene} (PMBT) was deeply investigated and was found to display chiral anisotropy factor g values as high as $1.0\ 10^{-2}$ at 612 nm[6] and high degree of crystallinity (65%)[7,8] upon aggregation from the solution by gradual addition of a poor solvent. In fact,

the aggregation of π-conjugated polymers results to be a multichain event - even in the case of very dilute solutions - as a consequence of a kind of sergeants-and-soldiers principle which occurs during the ordering process.[9]

More recently, starting from the bithiophenic monomer 3,3'-bis[(*S*)-(2-methylbutyl)]thiophene, the synthesis of the regioregular head-to-head/tail-to-tail (HH/TT) isomeric homologue of PMBT has been reported by the research group where I carried out my PhD.[10] In particular, it was observed that the polymer showed an helical structure limited to some chain sections, both in solution and in the solid state, and this was probably due to the steric interactions between side chain alkyl groups, that disfavor coplanarity of thiophene rings and thus the obtainment of supramolecular chiral aggregates upon aggregation from the solution. For this reason, the introduction of a heteroatom between the thiophene ring and the chiral alkyl group should provide a reduction of the steric hindrance and, therefore, promote conformations suitable to produce a better rings coplanarity and then a longer extent of conjugation in the main chain, even in the HH-TT regioregular polymeric derivatives. However, if compared to chiral P3ATs, relatively less research concerning optically active 3-sulfanyl or 3-alkoxy thiophene polymeric derivatives can be found in the literature.[2]

As far as 3-sulphanyl thiophene derivatives are concerned, 4,4'-bis[*(S)*-2-methylbutylsulphanyl]2,2'-bithiophene was polymerized in the presence of ferric chloride to give the related TT-HH polythiophene. Starting from a random, optically inactive monomolecular phase of the polymer in solution, conversion into a chiral monomolecular (or loosely aggregated) phase was provided by treatment with poor solvent or by casting as film.[11] On the other hand, chiral regioregular HT poly(3-alkoxythiophene) bearing the optically active 3,7-dimethyloctyloxy moiety in the side chain displayed a different behaviour, since a spin-coated film CD spectra exhibited a large bisignate Cotton effect with a high g factor of 10^{-2} at 745 nm, originated by the formation of coplanar strands, stacked in a chiral way.[12] Similar results were also obtained with diblock copolymers constituted by 3-alkyl- and 3-alkoxy polythiophene blocks bearing the (*S*) and/or (*R*)-3,7-dimethyloctyl moiety linked directly to the ring and/or through the oxygen atom, upon addition of poor solvent to the chloroform solution, giving rise to aggregation as helical supramolecular structures characterized by high g values.[13]

Strong activity ($g \sim 8\ 10^{-2}$) in the aggregated phase was also exhibited by regioregular poly[3,4-bis((*S*)-2-methylbutoxy)thiophene], probably originated from a helical packing of predominantly planar chains, rather than from a helical intrachain conformation.[14] On

the contrary, the chiral analogue 3,4-alkylthio bisubstituted polythiophene displayed no optical activity in poor solvent or in the solid state, even though aggregate formation was evidenced,[15] thus suggesting that the presence of chiral thio-substituents produces aggregated forms without chiral preference.

1.2. Aim of the chapter

In this framework, starting from mono- and bithiophene monomers, novel optically active polythiophenes bearing electron-donating chiral side chains have been prepared by synthetic methods suitable to achieve, respectively, regioregular HT (**P2a-b**) and HH-TT (**P4a-b**) derivatives (Scheme 1).

In particular, the same (*S*)-(2-methyl)butyl moiety was used as the chiral component - in order to obtain results comparable to those reported for the above mentioned optically active P3ATs -[6,10] and linked at position 3 of the thiophene ring through heteroatoms, such as S or O, in order to evaluate their effect on aggregation and, consequently, on the chiroptical properties.

The polymers have been fully characterized and investigated by optical and chiroptical methods upon aggregation both from the solution, by gradual addition of poor solvent, and as cast films. Moreover, a comparison with the related HT and HH/TT poly(3-alkyl)thiophene derivatives bearing the same optically active substituent directly linked to the ring but without heteroatom has been made, providing insight into the role of intra-interchain interactions.

This chapter is based on adapted content from "Chiral behavior of regioregular head-to-tail and head-to-head/tail-to-tail poly(heteroalkyl)thiophenes" M. Marinelli, L. Angiolini, M. Lanzi, F. Di Maria, E. Salatelli, submitted to *Synthetic Metals*.

All synthetic results, polymerizations and measurements represented in this chapter were obtained by Letterio Giannino under the supervision of the author, or by the author herself.

2. Results and discussion

2.1. Synthesis

The mono- (**2a-b**) and bithiophene monomers (**4a-b**) used for the preparation of the corresponding HT and HH polymeric derivatives were obtained by the starting materials 3-[(*S*)-(2-methylbutyl)sulphanyl]thiophene (**1a**) and 3-[(*S*)-2-methylbutoxy]thiophene (**1b**) (Scheme 1).

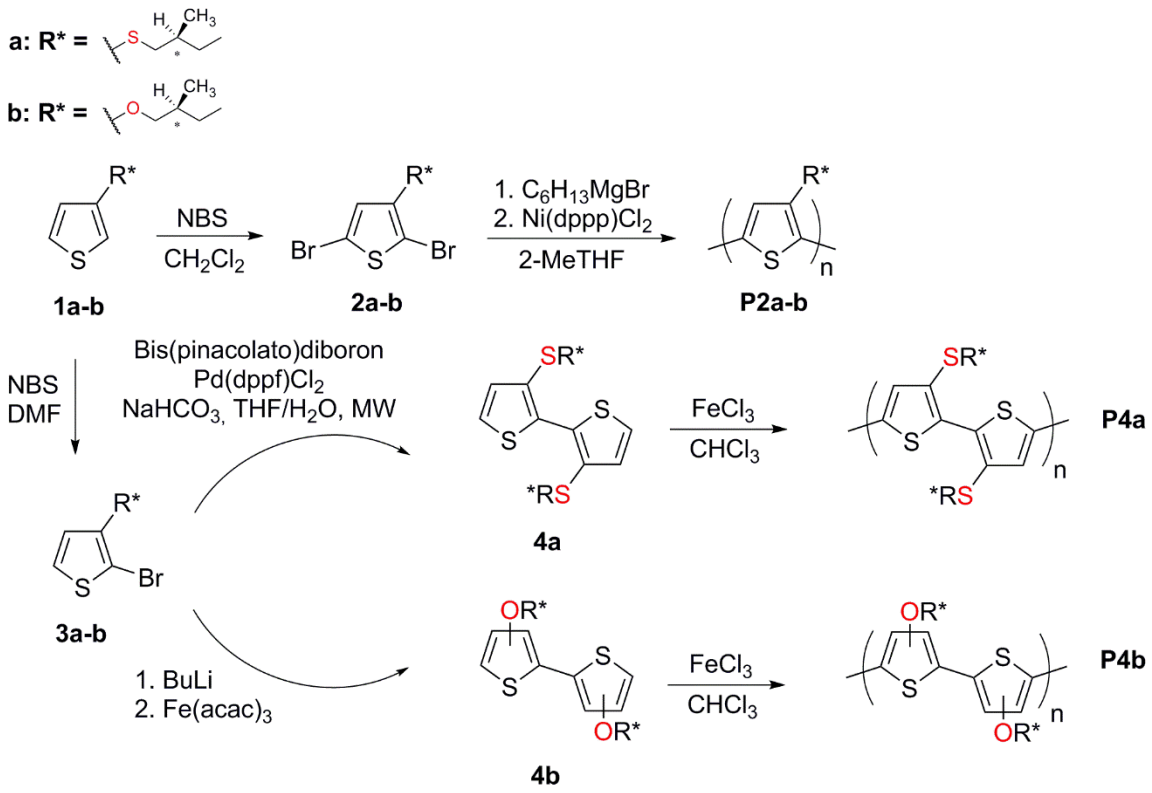

Scheme 1. Synthetic route to optically active S- and O-alkyl substituted thiophene monomers and polymers.

In particular, similarly to the method reported for the synthesis of the related 3-S-hexyl thiophene,[16] **1a** was obtained by nucleophilic reaction of 3-mercaptothiophene[16] with (+)-(*S*)-1-bromo-2-methylbutane, which have been prepared by reaction with LiBr of the *p*-toluensulfonate ester of enantiomerically pure (–)-(*S*)-2-methyl-1-butanol[17,18] (details in experimental section). (+)-3-[(*S*)-(2-Methylbutoxy)]thiophene (**1b**) was instead obtained by transetherification of commercial 3-methoxythiophene with (–)-(*S*)-2-methyl-1-butanol, in according to the procedure reported by Xu and coworkers and already adopted for the related 3-O-hexyl thiophene derivative (chapter II).[19]

Compounds **1a-b** were then submitted to treatment with N-bromosuccinimide[20,21] to obtain the corresponding 2,5-dibromo derivatives (**2a-b**), as well as the 2-bromo derivatives (**3a-b**) subsequently used for the preparation of the HH bithiophene monomers (**4a-b**).

(+)-3,3'-bis[(S)-(2-methylbutyl)sulphanyl]-2,2'-bithiophene (**4a**) was obtained in high yield following the successful synthetic protocol based on microwave-assisted Suzuki-Miyaura cross-coupling reaction, already used for the synthesis of 4,7-bis(3-oxyhexylthiophen-2-yl)benzo[c][2,1,3]thiadiazole (chapter II) and more recently for similar, optically inactive, derivatives.[22] By contrast, not only was the preparation of the related oxyalkyl disubstituted bithiophene monomer (**4b**) through this route unsatisfactory, but also the synthesis by oxidative coupling with BuLi/$CuCl_2$[22] was inconclusive. This situation results to be particularly interesting because it is a further confirm of the behaviour already observed for the aforementioned synthesis of previous oxygen compounds (chapter II).

However, (+)-3,3'-bis[(S)-(2-methylbutoxy)-2,2'-bithiophene (**4b**) could only be obtained as mixture of HH-HT 60:40 regioisomers, whose molar composition has been established by ^{1}H-NMR spectroscopy (Figure 8, experimental section), starting from the 2-bromo-3-oxyalkyl thiophene precursor (**3b**) by the use of BuLi and $Fe(acac)_3$.[23]

The optically active mono- and bithiophene monomers were then polymerized, respectively, by regiospecific organometallic coupling and not-regiospecific oxidative coupling, since these procedures allow to obtain the corresponding polymeric derivatives with well-defined HT or HH-TT regioregularity.

In detail, thanks to the selectivity of the sterically hindranced catalyst Ni(dppp)Cl_2, regioregular HT polythiophenes (**P2a-b**) have been synthesized through the GRIM (Grignard Metathesis) method,[24,25] by firstly treating the dibromo derivatives (**2a-b**) with a Grignard reagent that involves a magnesium/bromine exchange.

On the other hand, the polymerization of **4a** and **4b** to the corresponding **P4a-b** derivatives was carried out with good yields following the simple and well established oxidative coupling with iron (III) trichloride. As already mentioned, the symmetrical structure and chemical equivalence of the starting monomer allows to obtain a completely regioregular polymer, which displays only HH-TT junctions between the thiophene rings, despite the use of the aforementioned not-regiospecific method.

Even though (+)-3,3'-bis[(*S*)-(2-methylbutoxy)-2,2'-bithiophene was not obtained as pure but only as a mixture of the HH:HT regioisomers (60:40 molar ratio), it has been anyway

polymerized by oxidative coupling with $FeCl_3$, in order to obtain **P4b** at least partially comparable to the related sulphanyl derivative **P4a**.

2.2.Physical and thermal properties

All the polymeric derivatives were characterized by gel permeation chromatography (GPC) and thermal analysis, to obtain molecular mass and thermal properties (Table 1 and Figure 1).

Table 1. Yields and characterization data of polymeric derivatives.

Polymers	*Yield (%)* [a]	M_n *(g/mol)* [b]	M_w/M_n [c]	x_n [d]	T_g *(°C)* [e]	T_d *(°C)* [f]
P2a	73	2600	1.8	14.3	1	288
P2b	53	3600	2.0	21.4	7	263
P4a	97	1300	1.2	7.0	-25	139
P4b	95	1100, 3400	1.1, 1.3	6.5, 20.2	-15	114

[a] Weight of polymer/weight monomer x 100; [b] Average molecular weight determined by GPC in THF; [c] Polydispersity index; [d] Average polymerization degree expressed as monothiophenic repeating units; [e] Glass transition temperature determined by DSC (second heating cycle); [f] Decomposition temperature determined by TGA.

As reported in Table 1, the average polymerization degrees of **P2a** and **P2b** are comparable, whereas that of **P4a** appears significantly lower, being substantially constituted by a mixture of oligomers, as confirmed also by the ^{1}H-NMR spectrum (Figure 3a). By contrast, although the presence of an oligomeric fraction accompanying the main product is detected by GPC, it is particularly noteworthy the fact that **P4b** displays higher average molecular mass than **P4a**, despite it was obtained with similar yield, probably due to the positive role towards polymerization played by the electron donating nature of the alkoxy group.

Concerning thermal properties, both **P2a** and **P2b** display similar behaviour, with a slightly higher value of the glass transition temperature and a lower decomposition temperature for the oxyalkyl derivative with respect to the thioalkyl one. Reasonably due to an increased flexibility induced by the presence of HH junctions, the glass transition temperatures of the bithiophene derivatives **P4a-b** appear lower with respect to their counterparts **P2a-b**.

Furthermore, since a larger conjugation extent in the backbone is induced by the alkoxy group, which increases the polarity of the aromatic system and thus favors a more compact arrangement of the macromolecules in the solid state, the alkoxy derivatives **P2b** and **P4b** confirm their slightly higher rigidity than **P2a** and **P4a**. Both the HH bithiophenic derivatives show lower thermal stability with respect to the related HT regioregular samples - to be again attributed to HH junctions - while the oxygen-containing derivatives, **P2b** and **P4b**, result to be more unstable upon heating with respect to **P2a** and **P4a**.

An overall amorphous character in the solid state of all the polymeric derivatives is suggested by the absence of endothermic peaks, related to melting, and by the presence of only glass transitions in the DSC thermograms (Figure 1b).

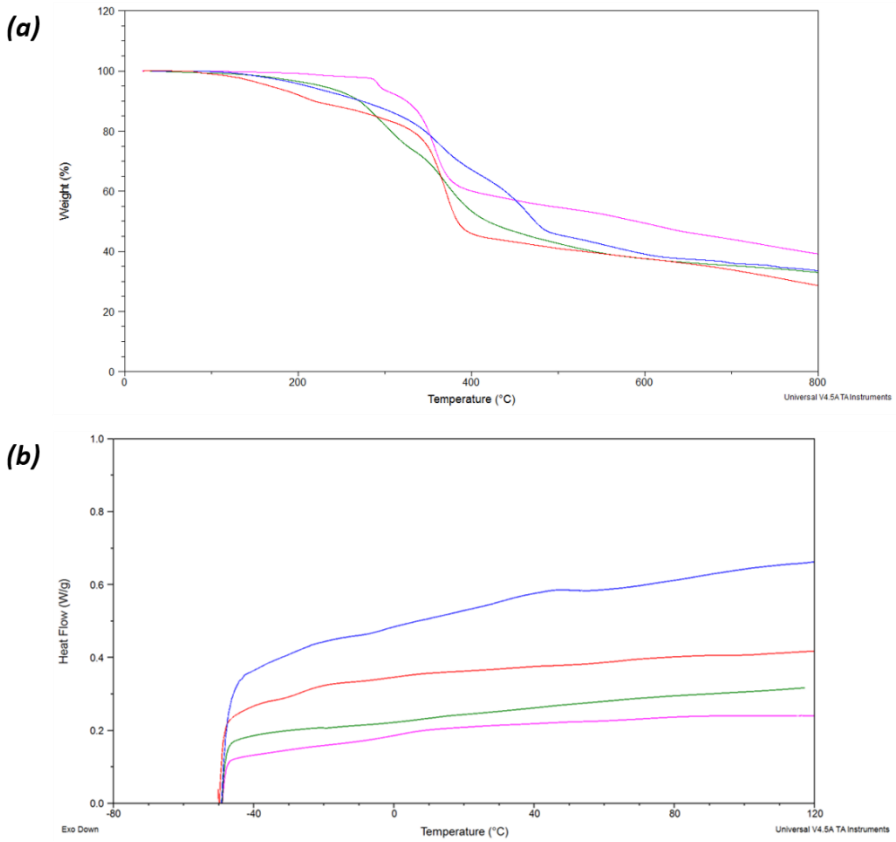

Figure 1. (a) TGA and (b) DSC thermograms of **P2a** (fuchsia line), **P2b** (green line), **P4a** (red line) and **P4b** (blue line).

2.3. ^{1}H-NMR and FT-IR characterizations

The chemical structure and regioregularity degree of synthesized materials have been evaluated by ^{1}H-NMR spectroscopy in $CDCl_3$.

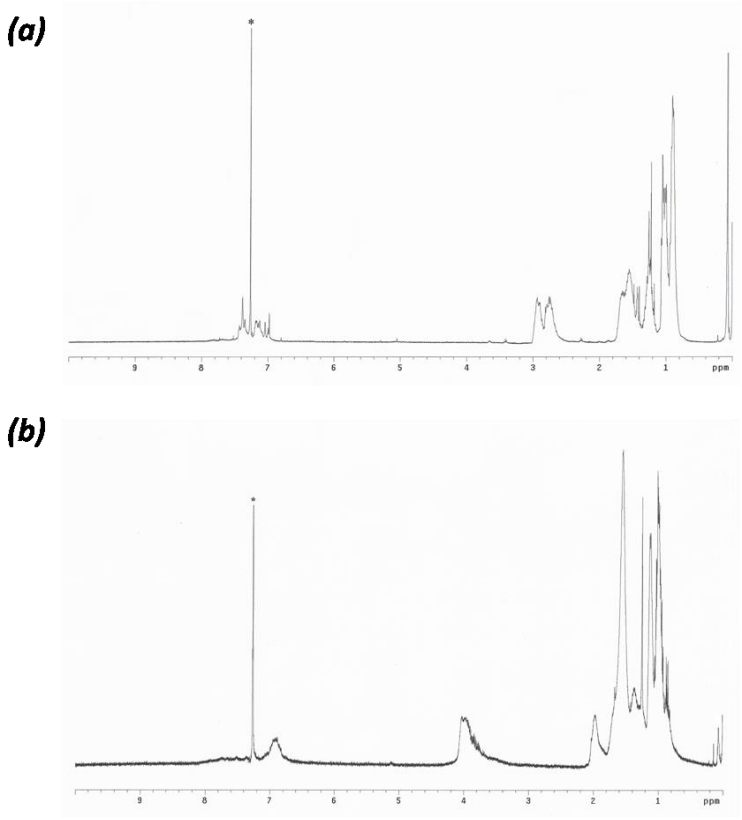

Figure 2. ^{1}H-NMR spectra of **P2a** (a) and **P2b** (b). Asterisk: solvent resonances.

Starting from the HT regioregular polymers, **P2a** (Figure 2a) displays a major singlet at 7.38 ppm which can be assigned to 4-H proton of the backbone. The minor signals at around 7.2 ppm could be assigned to minor HH-TT connections that thus lower the HT regioregularity degree to about the 90%, as measured by integration.

On the other hand, the spectrum of **P2b** (Figure 2b) shows a broad resonance of the polymer backbone 4-H proton at 7.02-6.80 ppm, upfielded with respect to the corresponding proton of **P2a**, reasonably due to an increased electron density induced by the oxygen atom directly linked to thiophene ring. Taking into account the resonances of the 4-H proton related to the four possible triad sequences (HT-HT, TT-HT, HT-HH and TT-HH) - which range in the intervals of 7.04-6.84 ppm[26] or 6.95-6.83 ppm[27] as reported for various poly(3-alkoxythiophene)s obtained under not regiospecific conditions - no reasonable evaluation of the regioregularity degree can be made for **P2b**, since signals are

clearly overlapped. However, the prevalence of the HT configuration is confirmed by the maximum intensity of the 4-H resonance that is centred at 6.90 ppm[26] and corresponds to the value reported for the HT-HH triad.

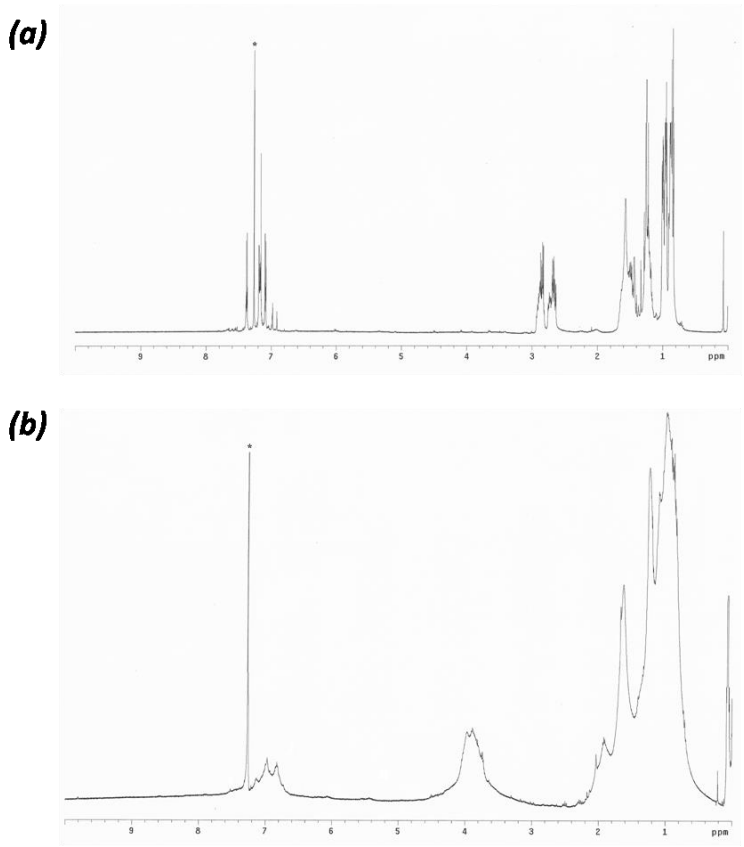

Figure 3. ^{1}H-NMR spectra of **P4a** (a) and **P4b** (b). Asterisk: solvent resonances.

As previously mentioned, according to the GPC analysis that indicated a low molecular mass of this sample, the expected oligomeric structure for **P4a** is further confirmed by the ^{1}H-NMR spectrum (Figure 3a). Indeed, in addition to the resonance of the 4-H proton of the backbone displayed at 7.2 ppm, signals related to the 4-H and 5-H hydrogens of the terminal thiophene rings are also clearly present at 7.08 and 7.38 ppm, respectively, suggesting that the polymerization of **4a** actually occurred only to a limited extent, yielding a mixture of material particularly rich in oligomeric derivatives.

The ^{1}H-NMR spectrum of **P4b** (Figure 3b) confirms the obtainment of a polymer having a substantially regiorandom structure, with the presence of three broad signals centred at 7.13, 6.97 and 6.83 ppm related, respectively, to the presence of prevalently HH-TT oligomeric chains, HH-TT-HT and HT-HT junctions.[26,27]

According to ^{1}H-NMR characterization, also FT-IR spectroscopy on Ge gave a further confirmation of the identity of all synthesized materials.

The IR spectrum of **P2a** shows the expected absorptions characteristic of 2,5-coupled 3-substituted polythiophenes: aromatic C-H stretching at 3071 cm^{-1} and one out-of-plane deformation of aromatic C-H at 803 cm^{-1} due to the trisubstituted ring. The alkyl chain gives stretching vibrations in the region 2963-2854 cm^{-1} and deformation modes below 1475 cm^{-1}. In the IR spectrum of thioalkyl bithiophene polymeric derivative **P4a**, the alkylsulfanyl chain gives rise to C-H stretching vibrations in the region 2963-2846 cm^{-1} and to deformation modes around 1478, 1458, 1434 (S-CH_2) and 1378 cm^{-1}. The aromatic C-H stretching and out-of-plane deformation are found at 3079 and 814 cm^{-1}, respectively. The alkoxy pendants of **P2b** give C-H stretching at 2959-2850 cm^{-1} (CH_2 and CH_3). Ring vibrational modes are seen at 1523, 1446 and 1350 cm^{-1}. The band at 1068 cm^{-1} is assigned to C(ring)-O-C stretch. The vibrational band at 802 cm^{-1} is attributable to C-H_β out-of-plane deformation mode of thiophene rings. Similarly, **P4b** gives the corresponding absorptions at 2966-2850, 1523, 1398, 1353 cm^{-1}. The C(ring)-O-C stretch. appears at 1064 cm^{-1} and the C-H_β out-of-plane deformation mode of thiophene rings at 802 cm^{-1}.

2.4. Optical properties

The UV-Vis spectra of the monomers in chloroform solutions (Table 2 and Figure 4a) show, as expected, a remarkable bathochromic shift of the absorption maxima of the alkoxy derivatives (**1b** and **4b**) with respect to **1a** and **4a**. Accordingly, this red-shift effect is more evident in the bithiophene compounds (35 nm **1a-b** vs. 52 nm **4a-b**), being the enhancement of aromatic conjugation - originated by connecting two thiophene rings - higher in the alkoxy derivatives with respect to the sulphanyl ones (28 nm **1-4b** vs. 11 nm **1-4a**). However, a certain electron donating ability is also displayed by the sulphanyl monomers compared to the related 3-alkylthiophene and 3,3'-dialkyl bithiophene derivatives, since they absorb, respectively, at 241 nm[28] and 248 nm,[10] thus at lower wavelengths.

Table 2. Maximum absorption (λ_{max}) of monomers and absorption/emission (λ_{em}) wavelengths (nm) of polymers in $CHCl_3$ solution and as films obtained from chlorobenzene solution.

Solution						*Film*
Monomers	λ_{max} *(nm)*	*Polymers*	λ_{max} *(nm)*	λ_{em} *(nm)*	*Stokes shift*	λ_{max} *(nm)*
1a	265	***P2a***	483	601	118	509
1b	300	***P2b***	574	665	91	580
4a	276	***P4a***	416	582	166	469
4b	328	***P4b***	522	612	90	529

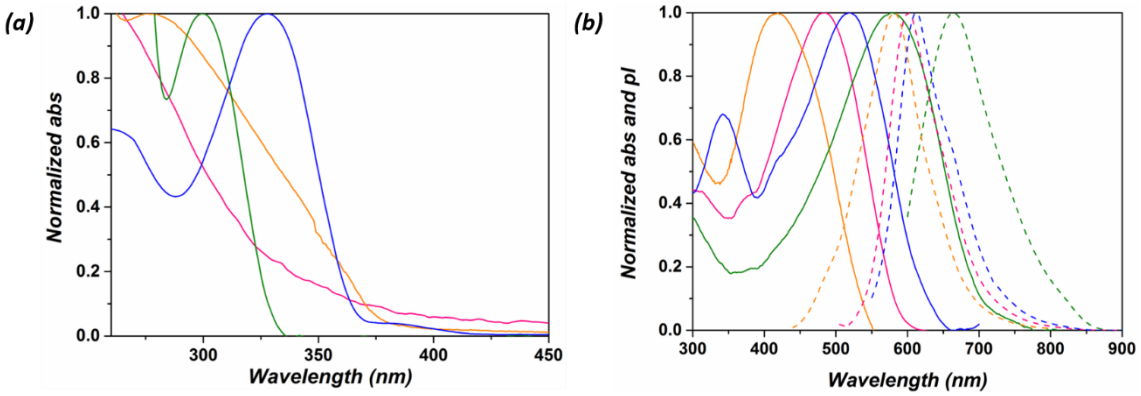

Figure 4. Normalized absorption spectra of monomers (a) and normalized absorption (solid line)/photoluminesce (dotted line) spectra of polymers (b) in $CHCl_3$ solutions (pink line: **1a** and **P2a**; green line: **1b** and **P2b**; orange line: **4a** and **P4a**; blue line: **4b** and **P4b**).

Concerning the UV-Vis spectra of the polymers in solution (Table 2 and Figure 4b), the absorption maxima related to the π-π* electronic transition of the conjugated polymeric backbone is displayed.

In detail, the HT regioregular derivatives confirm the higher electron-releasing mesomeric effect of oxygen directly linked to the thiophene ring, since a stronger red shift of the maximum wavelength is shown when passing from **1b** to **P2b** (274 nm) compared to the bathochromic effect displayed passing from **1a** to **P2a** (218 nm).

By contrast, as expected, both the λ_{max} values of the HH-TT polymeric bithiophene derivatives (**P4a-b**) are blue-shifted compared to the regioisomeric **P2a-b**, reasonably due to their backbone configurations that disfavor coplanar arrangements of the conjugated aromatic rings.

Moreover, even though an absorption at 345 nm is also shown by the alkoxy bithiophene derivative **P4b**, ascribable to the presence of oligomeric fractions and also suggested by the ^{1}H-NMR spectrum, it is especially noteworthy that its λ_{max} - 522 nm - is strongly red-

shifted compared to both the regioregular sulphur derivatives (**P2-4a**). Indeed, this is a further confirm that the oxygen promotes a strong electron delocalization along the chain, regardless the backbone configuration, since the material is a mixture of regioisomers with an overall regiorandom structure.

Similarly to what observed for the monomers, the maximum absorption values in solution of both the sulphanyl polymeric derivatives are again red shifted with respect to the related maxima of HT (431 nm)[6] and TT-HH P3AT (392 nm)[10] derivatives bearing the same chiral moiety in the side chain.

Although the behaviour of the synthesized chiral polythiophenes has been studied by circular dichroism (CD) spectroscopy, which is based on the absorption phenomena, the investigation of photoluminescence properties could also be useful and interesting to understand better their optical properties. In fact, the obtainment of lower Stokes shift values for the alkoxy polymers with respect to the sulphanyl derivatives (Table 2 and Figure 4b) indicates a reduced energy level difference of the excited states of the formers, thus confirming the increased extent of aromatic resonance and hence coplanarity of the thiophenic rings already deduced by the absorption spectra.

With the purpose to promote a self-assembling and microaggregation of the polymeric chains, starting from the disordered random coil conformation of the macromolecules, solvatochromism experiments were carried out on the chloroform solutions of polymers upon gradual addition of acetonitrile as a poor solvent.

Starting from the regioregular HT polymers, **P2a-b** (Figures 5a-c), a gradual decrease of light absorption with a broadening of the band related to the electronic π-π^* transition, in addition to a slight red-shift of the maximum wavelength (~10 nm) without particularly evident vibronic features, is produced by the addition of acetonitrile to the chloroform solutions. Whereas, taking into account polymer **P4b** (Figure 6c), a similar behaviour to **P2a-b** is displayed as far as the main absorption is concerned, with an expected insensitive change of the absorption at 345 nm, related to oligomers, upon addition of acetonitrile.

For the HH-TT sulphanyl polymer (**P4a**), it is especially interesting the appearance of a new band close to 470 nm at a $CHCl_3/CH_3CN$ composition of 10/90 v/v (Figure 6a) that, regardless the presence of unfavorable HH junctions, suggests the presence of more extended electronic conjugated structures upon aggregation.

The UV-Vis spectra of thin films of polymers, obtained by drop-casting from chlorobenzene solution, are reported in Figures 7 and the related data in Table 2.

In addition to observe a sequence of absorption maxima similar to the chloroform solution, all samples exhibit broader bands and appear red-shifted with respect to those of the aggregated structures obtained from solvatochromism experiments, with **P4a** which confirms the presence in the solid state of multiple aggregated structures.

2.5. CD spectroscopy

As previously said, optical activity of the synthesized chiral materials was studied by circular dichroism (CD) upon aggregation both from the solution - by gradual addition of poor solvent - and as cast films.

The CD spectrum of **P2a** in pure chloroform (Figure 5b) does not display any optical activity in the spectral region related to the π-π* electronic transition of polythiophene, as expected, due to the random coil conformation of the macromolecules; on the other hand, the spectrum of **P2b** (Figure 5d) shows a weak CD signal in correspondence to the UV-Vis absorption, at around 580 nm. In fact, probably due to the increased rigidity of the polymeric backbone induced by the mesomeric effect of the side chain alkoxy group, an intrinsically chiral structure of short main chain sections is suggested, even in dilute solution.

By gradual addition of acetonitrile as a poor solvent, the appearance of bisignate dichroic signals of opposite sign are produced in both **P2a** and **P2b**, with cross-over points at around 520 nm and 580 nm (Table 3), respectively, and thus related to the main chain UV-Vis maxima. While for individual polymer chains with a helical conformation the CD effect is not expected to be bisignated,[6,29] a bisignated CD signal is characteristic of exciton coupling between transition dipole moments of chromophores on adjacent polymer chains in the aggregate state: for this reason, when it is observed in π-conjugated polymers with optically active pendant side chains - such as **P2a** and **P2b** - it is due to the presence of a chiral supramolecular structure of predominantly planar chains.[30]

In particular, in addition to the higher optical activity, a higher chiral anisotropy factor *g* ($\Delta\varepsilon/\varepsilon$) is displayed by the alkoxy derivative **P2b** with respect to **P2a** ($2.0\cdot10^{-3}$ at 651 nm vs. $1.0\cdot10^{-3}$ at 563 nm), which also exhibits a bisignate band and a positive CD signal as a shoulder at around 630 nm. A possible interpretation of these findings, caused by the aggregation of macromolecules, is the supramolecular arrangements of opposite helicity both in **P2b** (*levo*helix sense) and - to a less extent - in **P2a** (*dextro*helix sense), being mixed with aggregates of macromolecules possessing intrinsic chiral structure.

Therefore, the HT regioregular derivative **P2b**, characterized by the presence of higher coplanarity content between thiophene rings with respect to the thioalkyl derivative **P2a**, is able to give chiral supramolecular aggregates upon addition of poor solvent, despite having *g* value about one order of magnitude lower compared to the related HT 3-alkyl derivative poly{3-[(*S*)-(2-methylbutyl)]thiophene}.[6,7]

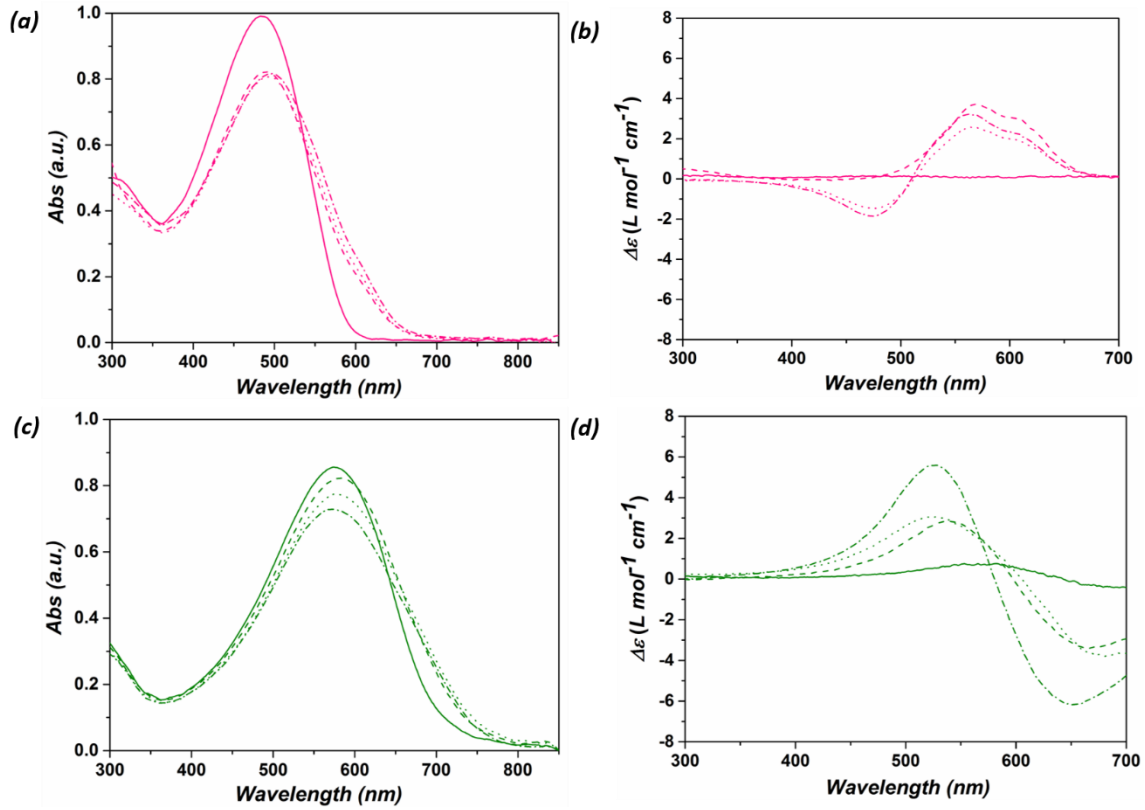

Figure 5. Absorption (a) and CD (b) spectra of **P2a** in $CHCl_3$ (pink solid line), $CHCl_3/CH_3CN$ 40:60 (pink dashed line), $CHCl_3/CH_3CN$ 30:70 (pink dotted line) and $CHCl_3/CH_3CN$ 20:80 (pink dashed-dotted line); absorption (c) and CD (d) spectra of **P2b** in $CHCl_3$ (green solid line), $CHCl_3/CH_3CN$ 60:40 (green dashed line), $CHCl_3/CH_3CN$ 40:60 (green dotted line) and $CHCl_3/CH_3CN$ 20:80 (green dashed-dotted line).

Table 3. CD spectra at 25°C of polymers in the microaggregated state.

Polymers	*$CHCl_3$:CH_3CN (v/v)*	*$\Delta\varepsilon_1$* [a]	*λ_1* [b]	*λ_0* [c]	*$\Delta\varepsilon_2$* [a]	*λ_2* [b]
P2a	20:80	+3.21	563	512	-1.80	474
P2b	20:80	-6.09	651	579	+5.59	523
P4a	10:90	-0.63	523	486	+0.55	458
P4b	20:80	+0.15	561	-	-	-

[a] Δε expressed in L mol^{-1} cm^{-1}; [b] Wavelength (in nm) of the maximum dichroic absorption; [c] Wavelength (in nm) of the cross-over point of dichroic bands.

Similarly to **P2b**, also the CD spectrum (Figure 6b) of the HH regioregular polymeric sulphanyl derivative **P4a** shows a weak signal in pure $CHCl_3$ solution but in the spectral region of 300-400 nm, indicative of the presence of a small amount of chain sections possessing one-handed helical sense. Furthermore, by gradual addition of poor solvent, a moderate but clear bisignate dichroic signal appears, similar and with opposite helicity in respect of that given by **P2a**, probably caused by chiral supramolecular aggregation. In fact, as the cross-over point of the CD spectrum is centred at 486 nm, it corresponds to the wavelength of the shoulder displayed in the corresponding UV-Vis spectrum which is related to aggregated structures (Figure 6a). However, even though the maximum optical activity (g $3.0 \cdot 10^{-4}$ at 522 nm) of **P4a** results to be lower than in **P2a**, it could be mainly a consequence of its lower polymerization degree, that does not promote the formation of large chiral macromolecular aggregates.

Moreover, not only is a shoulder similar to **P2a** - at around 600 nm - present in the CD spectrum, which may be attributed to an optically active aggregated phase constituted by chain sections of one prevailing chirality, but it also appears the possibility of coplanar arrangement of thiophene rings to partially exist even in the case of disfavoring HH connections. It is indeed reported that the extra sulfur atom linked at each thiophene ring could induce self-aggregation via S…S interactions and weak CH…S hydrogen bonding.[16,31] Thanks to the directionality of the above interactions, in addition to the large polarizability of sulfur in thioether fragments, the formation of highly anisotropic supramolecular systems characterized by anti-planar conformations involving reduced steric hindrance between the side chain substituents would be favored.[22]

On the other hand, the CD spectrum in chloroform (Figure 6d) of the alkoxy polymer **P4b**, which possesses a substantially regiorandom configuration, shows weak CD positive signals (g $2.0 \cdot 10^{-4}$ at 555 nm) insensitive to the addition of poor solvent, that are indicative of intrinsic chirality of the backbone and limited to short chain sections. The absence of exciton coupling in the CD spectrum of **P4b**, in contrast to what observed for **P2b**, can be thus attributed to the presence of very short regioregular chain sections that are unable to promote sufficiently extended coplanarity of the thiophene rings in the main chain.

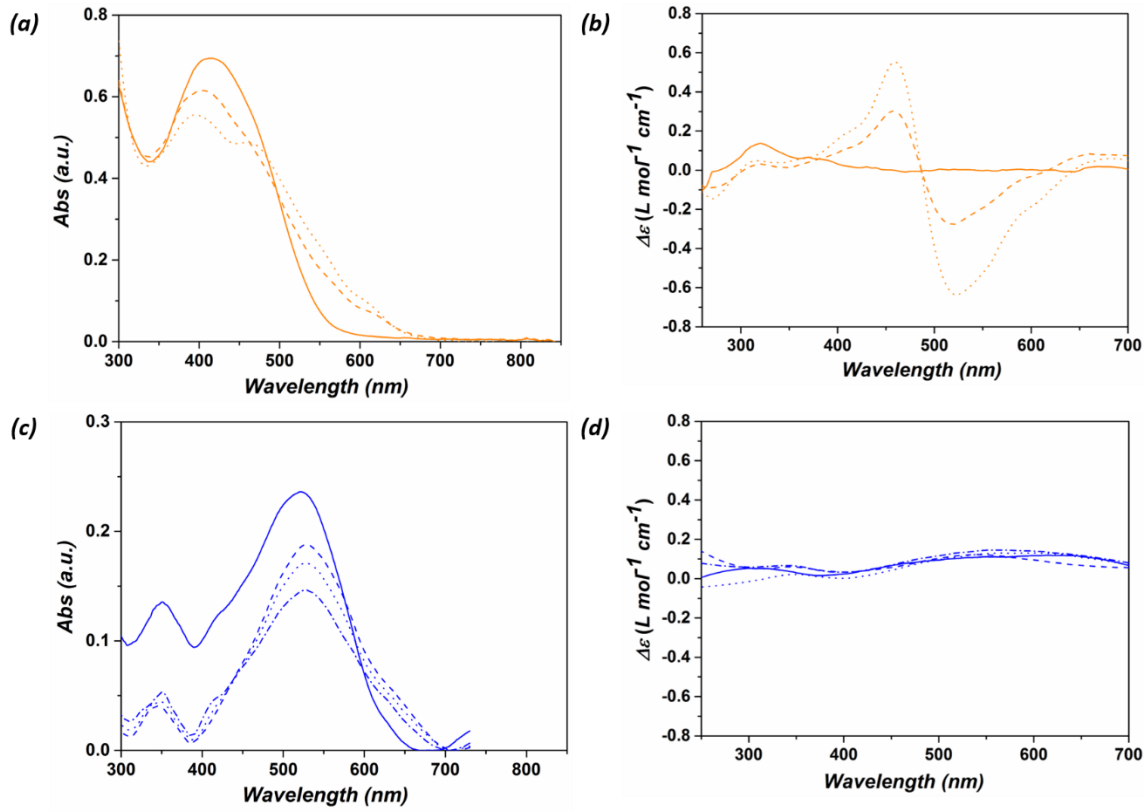

Figure 6. Absorption (a) and CD (b) spectra of **P4a** in $CHCl_3$ (orange solid line), $CHCl_3/CH_3CN$ 30:70 (orange dotted line) and $CHCl_3/CH_3CN$ 10:90 (orange dashed line); absorption (c) and CD (d) spectra of **P4b** in $CHCl_3$ (blue solid line), $CHCl_3/CH_3CN$ 60:40 (blue dashed line), $CHCl_3/CH_3CN$ 40:60 (blue dotted line) and $CHCl_3/CH_3CN$ 20:80 (blue dashed-dotted line).

It appears, however, that experimental procedure of aggregation and composition of the material significantly affect the chiral behaviour of the samples. Indeed, the resulting CD spectra of thin films of polymers - produced by slow evaporation of dilute solutions - usually differ from those obtained from solvatochromism experiments.

In detail, **P2a** (Figure 7b), **P2b** (Figure 7d) and **P4b** (Figure 7h) actually display low optical activity with respect to that given by addition of acetonitrile to the chloroform solution. On the other hand, the CD spectrum of a thin film of **P4a** (Figures 7f) is similar to those given by the microaggregates formed upon acetonitrile addition to the chloroform solution, likely due to its more homogeneous molecular composition (Table 1) with respect to the other derivatives. Therefore, low polydispersity value in addition to regioregularity degree appear as relevant factors affecting the ordering process of the macromolecules from the solution to the solid state.

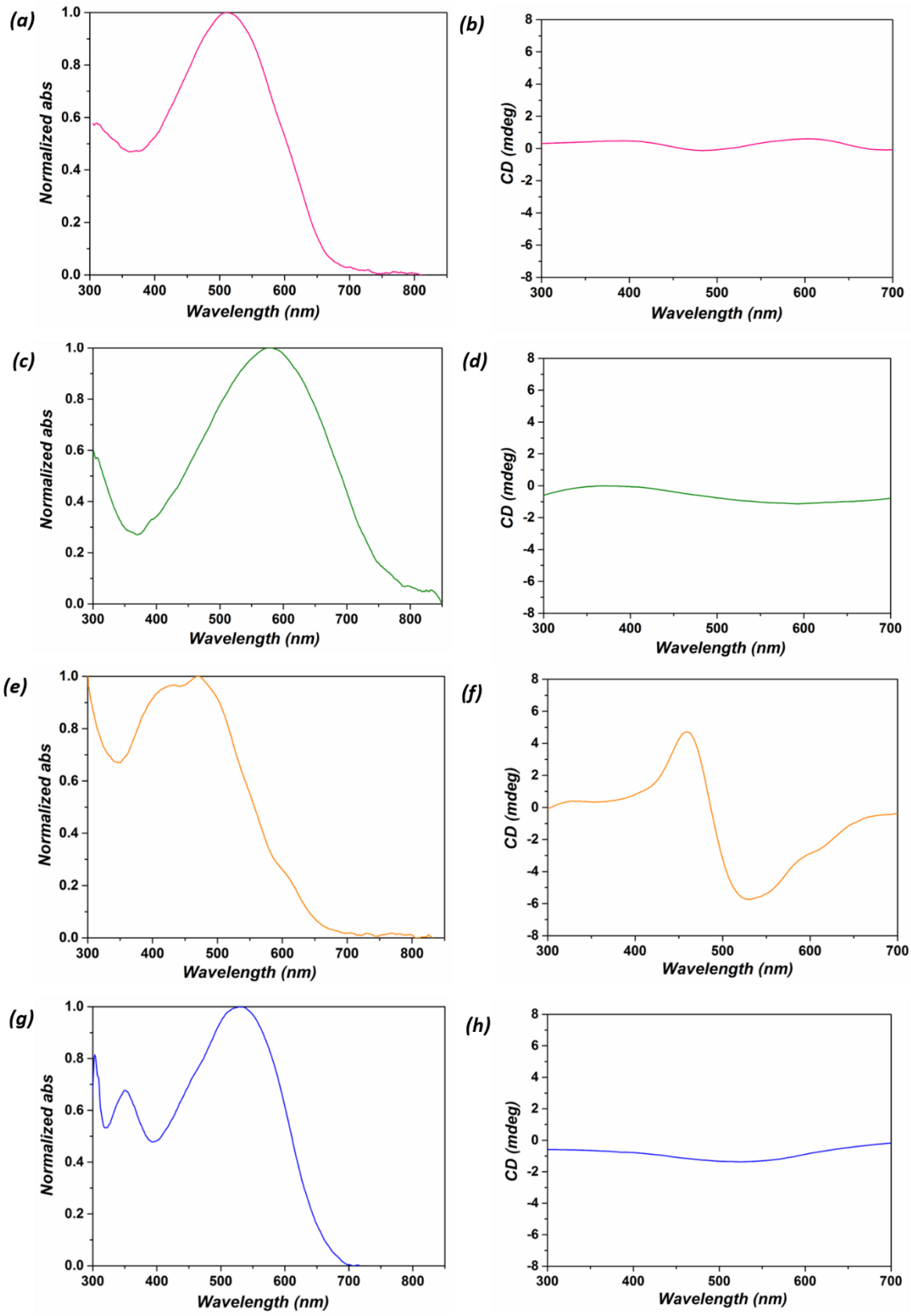

Figure 7. Absorption and CD spectra of **P2a** (a-b), **P2b** (c-d), **P4a** (e-f) and **P4b** (g-h) as films cast from chlorobenzene by drop-casting.

In conclusion, both the HT regioregular derivatives **P2a** and **P2b** are able to display a similar behaviour similar to the related HT poly{3-[(*S*)-(2-methylbutyl)]thiophene} - with formation of chiral supramolecular aggregates upon aggregation from the solution - but with lower optical activity, despite the S or O heteroatom interposed between the chiral residue and the thiophene ring which should enhance coplanarity between the aromatic rings in the backbone.

Regardless the unfavorable regioregularity, even the behaviour of the HH-TT sulphanyl derivative **P4a** appears substantially analogous to that of **P2a** and displays in the microaggregated state a relevant amount of chains with supramolecular chirality with respect to individual macromolecular chains possessing a prevailing one-handed helical sense. In comparison to the previously investigated optically active HH-TT poly(3-alkyl)thiophene - bearing the same (*S*)-(2-methyl)butyl chiral residue directly linked to the thiophene ring - which are characterized by the presence of only helical intrachain conformation,[10] **P4a** appears more prone to produce helical interchain order. This may be attributed to the presence of sulfur which favors a more coplanar arrangement of thiophene rings with respect to the HH-TT poly(3-alkyl)thiophene derivative.

2.6. Conclusions

Novel HT and HH-TT regioregular optically active polythiophenes bearing the (*S*)-(2-methyl)butyl residue linked at position 3 of the thiophene ring through sulfur or oxygen atom were prepared and compared to the related HT and HH-TT P3AT derivatives possessing the same chiral moiety.

With respect to the latters, thanks to the electron releasing properties of the heteroatom and consequent increased possibility of coplanar arrangement of the thiophene rings along the main chain, both the sulphanyl and alkoxy polymers display a red-shifted absorption maxima which is indicative of an enhanced aromatic conjugation in the backbone.

Upon aggregation from the solution by means of poor solvent addition, both the HT polymers – and in particular the HT 3-alkoxy polythiophene – exhibit chiroptical properties indicative of the formation of supramolecular chiral aggregates with chiral anisotropy values quite similar to that of the related HT P3AT derivative. In particular, while the HT 3-sulphanyl derivative also displays the presence of individual chains possessing helical conformation, the HH-TT 3-sulphanyl polythiophene behaves similarly to its HT counterpart, showing a higher tendency to give chiral supramolecular aggregates with respect to the related HH-TT P3AT derivative. On the other hand, the HH-TT 3-alkoxy polythiophene, which is actually constituted by a mixture of HH-TT and HT connections, appears unable to produce relevant chiroptical properties upon aggregation and thus exhibits only the presence of short chain sections possessing chiral conformation in the aggregated state.

It is also to be noted that no relevant chiroptical properties in cast film of these materials are achieved, thus confirming, as previously observed, that the aggregation of these π-conjugated polymers is a multichain event which requires to start from very dilute solutions and to gradually add a weak solvent in order to the process may take place with significant formation of chiral aggregates.

To conclude, in addition to favor the extent of conjugation in the main chain, the presence of oxygen or sulfur as connecting atom between the thiophene ring and the chiral alkyl side chain allows to achieve supramolecular chiral aggregations not dissimilar, or even better, from those obtained with the related chiral P3ATs.

3. Experimental section

3.1. Materials

All commercial reagents and solvents were purchased from Sigma-Aldrich and used as received unless otherwise stated. *N*-Bromosuccinimide (NBS) was recrystallized from hot water and pyridine (Fluka) was freshly distilled before use. Anhydrous solvents were prepared following literature procedures[32] and stored over molecular sieves. All manipulations involving moisture-sensitive reagents were performed under nitrogen in dried glassware.

3.2. Synthesis of monomers

*3.2.1. (+)-(S)-2-Methyl-1-butyl p-toluensulfonate (**R*OTs**)*

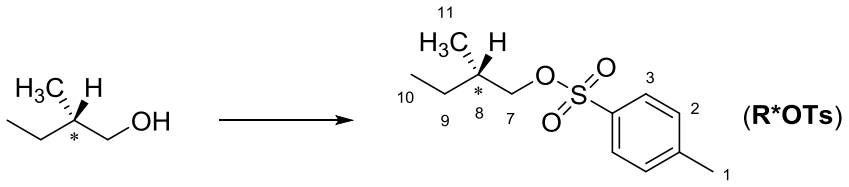

To a three-necked flask containing a solution of (–)-(*S*)-2-methyl-1-butanol (Sigma-Aldrich) (8.50 g, 0.096 mol) in pyridine (15.4 mL) cooled on ice bath, *p*-toluenesulfonyl chloride (20.20 g, 0.106 mol) was slowly added (2h) under inert atmosphere. The mixture was stirred for further 2h at room temperature and then poured into conc. HCl:H_2O = 1:1 (44.0 mL) and water (31.0 mL). The aqueous solution was extracted with chloroform, the organic phase washed with water to neutrality and finally dried over Na_2SO_4. Solvent removal by evaporation under reduced pressure gave 22.18 g (95% yield, $[\alpha]_D^{25}$=+4.5; c=3 in $CHCl_3$) of the ester **R*OTs** as a colorless liquid, without need of further purification.
^{1}H-NMR ($CDCl_3$, ppm): δ 7.78 (d, 2H, 3-H), 7.35 (d, 2H, 2-H), 3.88 (dd, 1H, 7-H_α), 3.82 (dd, 1H, 7-H_β), 2.45 (s, 3H, 1-H), 1.76-1.66 (m, 1H, 8-H), 1.44-1.34 (m, 1H, 9-H_α), 1.20-1.08 (m, 1H, 9-H_β), 0.88 (d, 3H, 11-H), 0.83 (t, 3H, 10-H).

*3.2.2. (+)-(S)-1-Bromo-2-methylbutane (**R*Br**)*

Solid LiBr (42.00 g, 0.483 mol) was slowly added to a solution of (+)-(*S*)-2-methyl-1-butyl *p*-toluensulfonate (22.18 g, 0.092 mol) in acetone (70.0 mL), the mixture stirred at room temperature for 50h, then poured into water and extracted with pentane. The organic phase was washed with water and brine, dried over Na_2SO_4 and finally reduced to small volume at atmospheric pressure. The resulting liquid residue was then distilled to give 7.61 g (55% yield, bp 70-80°C, $[\alpha]_D^{25}$=+4.5; c=2 in $CHCl_3$) of the bromide **R*Br** as a colorless liquid.

^{1}H-NMR ($CDCl_3$, ppm): δ 3.39 (dd, 1H, 1-H_α), 3.34 (dd, 1H, 1-H_β), 1.78-1.66 (m, 1H, 2-H), 1.56-1.44 (m, 1H, 3-H_α), 1.34-1.22 (m, 1H, 3-H_β), 1.05 (d, 3H, 5-H), 0.91 (t, 3H, 4-H).

*3.2.3. 3-Mercapto-thiophene (**TSH**)*

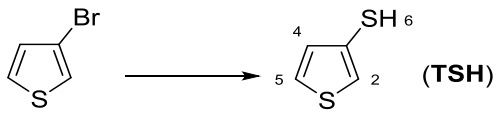

A solution of *n*-butyllithium in hexane 2.5 M (7.4 mL, 18.4 mmol) was added dropwise at –70°C under inert atmosphere to a solution of commercial 3-bromothiophene (3.00 g, 18.4 mmol) in anhydrous diethyl ether (20.0 mL). After stirring at –70°C for 2h, sublimed sulfur (0.589 g, 18.4 mmol) was added and the mixture stirred for further 2 h before quenching with water (100 mL). The thiol was isolated from the reaction mixture by extraction with NaOH 1M followed by acidification of the combined aqueous extracts with aq. HCl 1M. The crude product was finally extracted from the aqueous suspension with CH_2Cl_2 and the organic phase dried over Na_2SO_4. Solvent removal under reduced pressure afforded 1.84 g (86% yield) of the thiol **TSH** as a yellow oil.

^{1}H-NMR ($CDCl_3$, ppm): δ 7.31 (dd, 1H, 5-H), 7.19-7.17 (m, 1H, 2-H), 6.99 (dd, 1H, 4-H), 3.39 (s, 1H, 1-H).

*3.2.4. (S)-(+)-3-[(2'-Methylbutyl)sulphanyl]thiophene (**1a**)*

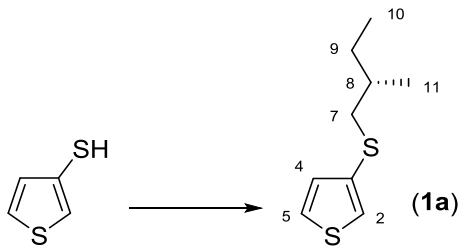

To a two-necked flask containing a solution of potassium tert-butoxide (0.444 g, 4.0 mmol) in anhydrous ethanol (5.0 mL), 3-mercapto-thiophene (0.230 g, 2.0 mmol) was added at 0°C under nitrogen atmosphere and stirring for 30 min. Then, (S)-(+)-1-bromo-2-methylbutane (0.314 g, 2.1 mmol) was slowly added and the mixture heated to 80°C for 2h; after cooling, the reaction mixture was poured into water (50 mL) and extracted with CH_2Cl_2. The combined organic layers were dried over Na_2SO_4 and the solvent removed by evaporation under reduced pressure. The residue was finally purified by column chromatography on silica gel with cyclohexane to obtain 0.246 g (67% yield, $[\alpha]_D^{25}$=+14.8; c=1.2 in $CHCl_3$) of **1a** as a colorless oil.

^{1}H-NMR ($CDCl_3$, ppm): δ 7.30 (dd, 1H, 5-H), 7.09 (dd, 1H, 2-H), 7.02 (dd, 1H, 4-H), 2.87 (dd, 1H, 7-H_α), 2.70 (dd, 1H, 7-H_β), 1.68-1.56 (m, 1H, 8-H), 1.56-1.46 (m, 1H, 9-H_α), 1.32-1.20 (m, 1H, 9-H_β), 1.02 (d, 3H, 11-H), 0.89 (t, 3H, 10-H).

*3.2.5. (+)-2,5-Dibromo-3-[(S)-(2-methylbutyl)sulphanyl]thiophene (**2a**)*

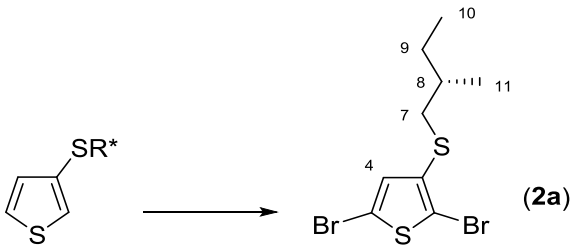

To a two-necked flask containing a solution of 1a (0.246 g, 1.3 mmol) in 7.0 mL of CH_2Cl_2, NBS (0.518 g, 2.9 mmol) was added portion wise under stirring and protection from light. The mixture was heated at 45°C and maintained at this temperature for 24h. After cooling and washing of the organic layer with water, the crude product was purified by column chromatography on silica gel with cyclohexane to obtain 0.419 g (92% yield, $[\alpha]_D^{25}$=+14.1 c=0.5 in $CHCl_3$) of **2a** as a colorless oil.

^{1}H-NMR ($CDCl_3$, ppm): δ 6.90 (s, 1H, 4-H), 2.83 (dd, 1H, 7-H_α), 2.67 (dd, 1H, 7-H_β), 1.62-1.46 (m, 2H, 8-H and 9-H_α), 1.31-1.19 (m, 1H, 9-H_β), 1.01 (d, 3H, 11-H), 0.89 (t, 3H, 10-H).

*3.2.6. 2-Bromo-3-[(S)-(2-methylbutyl)sulphanyl]thiophene (**3a**)*

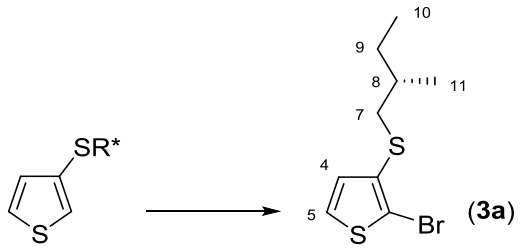

A solution of NBS (0.497 g, 2.8 mmol) in 4.0 mL of DMF was added dropwise at 0°C in 1h, under stirring and in the dark, to a solution of 1a (0.520 g, 2.8 mmol) in 4.0 mL of DMF. The reaction mixture was stirred for 24h protected from the light, then diluted with water and finally extracted with Et_2O. After drying over Na_2SO_4 and solvent evaporation at reduced pressure, the crude product was purified by column chromatography on silica gel with hexane/ethyl acetate 19:1 v/v as eluent, to give 0.723 g (98% yield) of **3a** as a colorless liquid.

^{1}H-NMR ($CDCl_3$, ppm): δ 7.24 (d, 1H, 5-H), 6.92 (d, 1H, 4-H), 2.87 (dd, 1H, 7-H_α), 2.68 (dd, 1H, 7-H_β), 1.60-1.42 (m, 2H, 8-H and 9-H_α), 1.32-1.20 (m, 1H, 9-H_β), 1.00 (d, 3H, 11-H), 0.89 (t, 3H, 10-H).

*3.2.7. (+)-3,3'-Bis[(S)-(2-methylbutyl)sulphanyl]-2,2'-bithiophene (**4a**)*

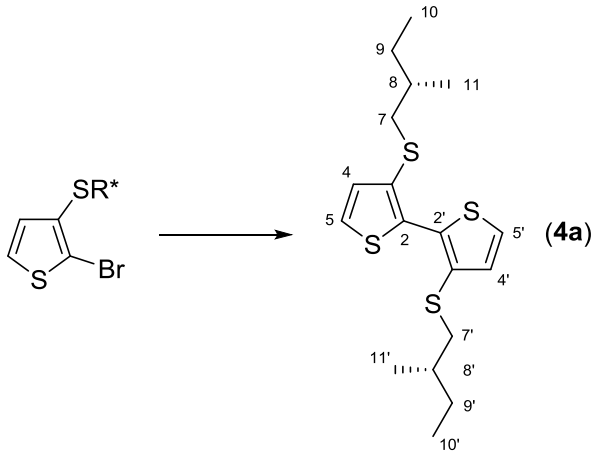

A mixture of 3a (0.342 g, 1.3 mmol), bis(pinacolato)diboron (0.197 g, 0.8 mmol), $Pd(dppf)Cl_2$ (0.053 g, 5% mol) and $NaHCO_3$ (0.325 g, 3.9 mmol) in THF/water 2:1 (3.0 mL) was irradiated by MW at 90°C for 40 min. The reaction mixture was then cooled to room temperature, diluted with dichloromethane and washed with water; the solvent was evaporated under reduced pressure and the product purified by flash chromatography with cyclohexane as eluent to afford 0.433 g (90% yield, $[\alpha]_D^{25}$=+17.3 c=0.3 in $CHCl_3$) of **4a** as a yellowish oil.

^{1}H-NMR ($CDCl_3$, ppm): δ 7.36 (d, 2H, 5-H), 7.08 (d, 2H, 4-H), 2.80 (dd, 2H, 7-H_α), 2.62 (dd, 2H, 7-H_β), 1.60-1.38 (m, 4H, 8-H and 9-H_α), 1.24-1.10 (m, 2H, 9-H_β), 0.92 (d, 6H, 11-H), 0.83 (t, 6H, 10-H).

*3.2.8. (+)-3-[(S)-(2-Methylbutoxy)]thiophene (**1b**)*

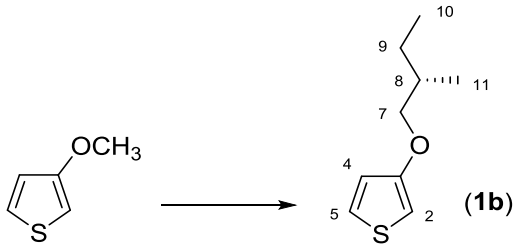

To a solution of 3-methoxythiophene (Alfa Aesar) (0.760 g, 6.7 mmol) in 8.4 mL of toluene, (*S*)-(–)-2-methyl-1-butanol (1.4 mL, 13.3 mmol) and *p*-toluenesulfonic acid monohydrate (0.189 g, 1.0 mmol) were sequentially added under stirring and inert atmosphere. After 24h at reflux, the mixture was cooled to room temperature, poured into 100 mL of water and then extracted with CH_2Cl_2. The organic phase was washed with water, dried over Na_2SO_4 and concentrated by evaporation under reduced pressure. The crude product was purified by column chromatography on silica gel with cyclohexane/CH_2Cl_2 80:20 v/v as eluent to afford 0.764 g (67% yield, $[\alpha]_D^{25}$=+8.7 c=0.4 in $CHCl_3$) of **1b** as a yellow liquid.

^{1}H-NMR ($CDCl_3$, ppm): δ 7.15 (dd, 1H, 5-H), 6.76 (dd, 1H, 4-H), 6.22 (dd, 1H, 2-H), 3.81 (dd, 1H, 7-H_α), 3.73 (dd, 1H, 7-H_β), 1.94-1.88 (m, 1H, 8-H), 1.62-1.50 (m, 1H, 9-H_α), 1.36-1.20 (m, 1H, 9-H_β), 1.01 (d, 3H, 11-H), 0.94 (t, 3H, 10-H).

*3.2.9. (+)-2,5-Dibromo-3-[(S)-2-methylbutoxy]thiophene (**2b**)*

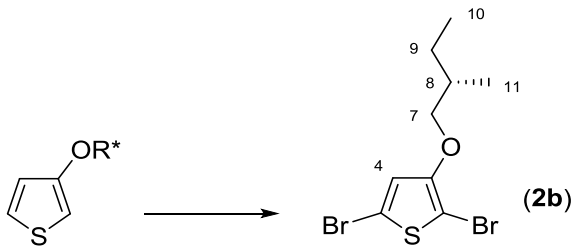

The same procedure described for 2a was followed starting from 1b (0.199 g, 1.2 mmol) and NBS (0.464 g, 2.6 mmol) in CH_2Cl_2 to give 0.328 g (54% yield, $[\alpha]_D^{25}$=+4.0 c=0.6 in $CHCl_3$) of pure **2b** as a colorless oil.

^{1}H-NMR ($CDCl_3$, ppm): δ 6.76 (s, 1H, 4-H), 3.85 (dd, 1H, 7-H$_\alpha$), 3.77 (dd, 1H, 7-H$_\beta$), 1.90-1.76 (m, 1H, 8-H), 1.60-1.48 (m, 1H, 9-H$_\alpha$), 1.32-1.18 (m, 1H, 9-H$_\beta$), 1.01 (d, 3H, 11-H), 0.94 (t, 3H, 10-H).

*3.2.10. 2-Bromo-3-[(S)-2-methylbutoxy]thiophene (**3b**)*

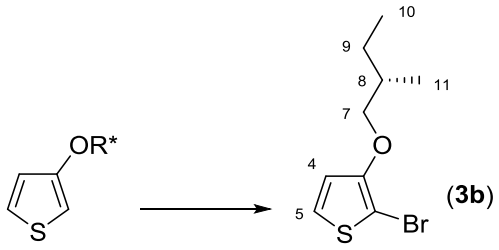

The same procedure described for 3a was followed starting from 1b (0.565 g, 3.3 mmol) and NBS (0.591 g, 3.3 mmol) in DMF obtaining 0.740 g (90% yield) of pure **3b** as a light brown oil.

^{1}H-NMR ($CDCl_3$, ppm): δ 7.18 (d, 1H, 5-H), 6.73 (d, 1H, 4-H), 3.89 (dd, 1H, 7-H$_\alpha$), 3.81 (dd, 1H, 7-H$_\beta$), 1.88-1.78 (m, 1H, 8-H), 1.62-1.50 (m, 1H, 9-H$_\alpha$), 1.32-1.20 (m, 1H, 9-H$_\beta$), 1.01 (d, 3H, 11-H), 0.95 (t, 3H, 10-H).

*3.2.11. (+)-3,3'-Bis[(S)-(2-methylbutoxy)-2,2'-bithiophene (**4b**)*

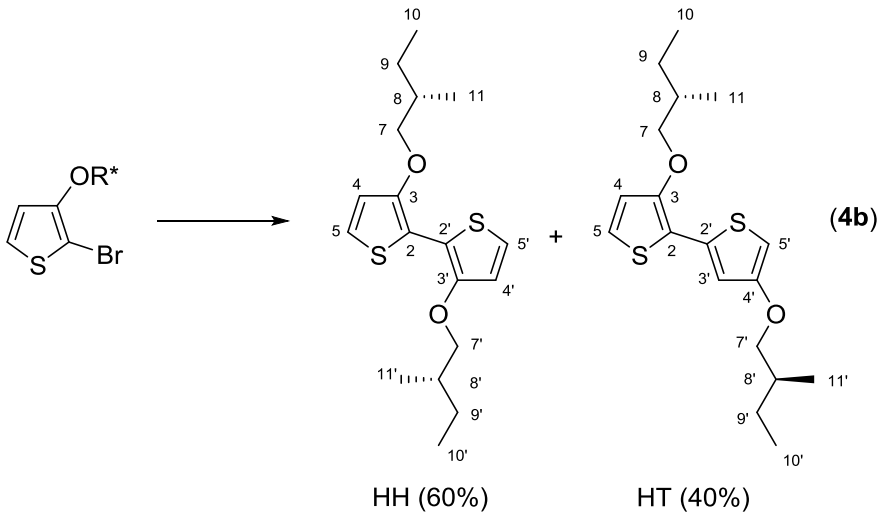

A solution of *n*-butyl lithium in hexane 2.5 M (0.4 mL, 1.0 mmol) was added dropwise under inert atmosphere at –70°C to a solution of 3b (0.215 g, 0.9 mmol) in dry THF (3 mL). After 30 min $Fe(acac)_3$ (Alfa Aesar) (0.494 g, 1.4 mmol) was added to the reaction mixture and the mixture allowed to reach room temperature under stirring overnight before quenching with water. The aqueous phase was extracted with Et_2O and the combined organic phases washed with brine. After drying over Na_2SO_4 and removal of the solvent under reduced pressure, the crude product was purified by column chromatography on silica with hexane as eluent to afford 0.050 g (16% yield, $[\alpha]_D^{25}$=42.7 c=0.4 in $CHCl_3$) of **4b** as a dark green oil constituted by a 60:40 mixture of **HH/HT** regioisomers.

^{1}H-NMR ($CDCl_3$, ppm): δ 7.07 (d, 2H, 5-H and 5'-H, **HH**), 7.02 (d, 1H, 5-H, **HT**), 6.88 (d, 1H, 3'-H, **HT**), 6.83 (d, 2H, 4-H and 4'-H, **HH**), 6.81 (d, 1H, 4-H, **HT**), 6.10 (d, 1H, 5'-H, **HT**), 4.01 and 3.94 (m, 4H, 7- and 7'-H_α and H_β, **HH**), 4.01 and 3.94 (m, 2H, 7-H_α and 7-H_β **HT**), 3.81 and 3.73 (m, 2H, 7'-H_α and 7'-H_β **HT**), 2.00-1.80 (m, 4H, 8-H and 8'-H, **HH** and **HT**), 1.70-1.50 (m, 4H, 9-H_α and 9'-H_α, **HH** and **HT**), 1.44-1.18 (m, 4H, 9-H_β and 9'-H_β, **HH** and **HT**), 1.12-1.06 (m, 12H, 11-H and 11'-H, **HH** and **HT**), 1.02-0.90 (m, 12H, 10-H and 10'-H, **HH** and **HT**).

3.3.Synthesis of polymers

*3.3.1. Poly{3-[(S)-(2-methylbutyl)sulphanyl]thiophene} (**P2a**)*

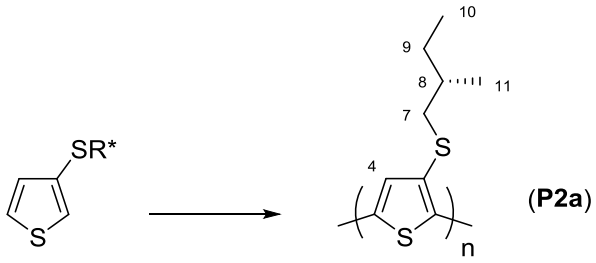

To a three-necked flask containing 2a (0.313 g, 0.9 mmol), dry 2-methyltetrahydrofuran (5 mL) and 2M hexylmagnesium bromide in Et_2O (0.5 mL, 1.0 mmol) were sequentially added under stirring and nitrogen atmosphere. The solution was heated to reflux in the dark for 1h. Then, Ni(dppp)Cl_2 (0.024 g, 5 mol%) was added and the mixture left under stirring and reflux overnight. After cooling, chloroform was added and the mixture washed with water, followed by drying over Na_2SO_4. The organic phase was concentrated to small volume and finally treated with hot MeOH to afford 0.121 g (73% yield) of **P2a** as a dark red solid.

^{1}H-NMR ($CDCl_3$, ppm): δ 7.38 (s, 1H, 4-H), 3.00-2.60 (m, 2H, 7-H), 1.80-1.15 (m, 3H, 8-H and 9-H), 1.10-0.95 (m, 3H, 11-H), 0.95-0.78 (t, 3H, 10-H).

*3.3.2. Poly{3-[(S)-(2-methylbutoxy)]thiophene} (**P2b**)*

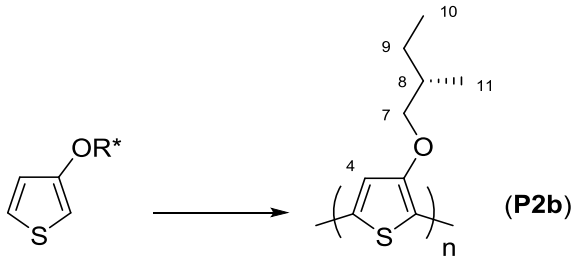

The same procedure described for P2a was followed starting from 2b (0.296 g, 0.9 mmol) and 2M hexylmagnesiumbromide in Et_2O (0.5 mL, 1.0 mmol) in dry 2-methyltetrahydrofuran to give 0.079 g (53% yield) of pure **P2b** as a dark blue powder.

^{1}H-NMR ($CDCl_3$, ppm): δ 7.02-6.80 (bm, 1H, 4-H), 4.10-3.90 (m, 2H, 7-H), 2.08-1.90 (m, 1H, 8-H), 1.78-0.86 (m, 8H, 9-H, 10-H and 11-H).

*3.3.3. Poly{3,3'-bis[(S)-(2-methylbutyl)sulphanyl]-2,2'-bithiophene} (**P4a**)*

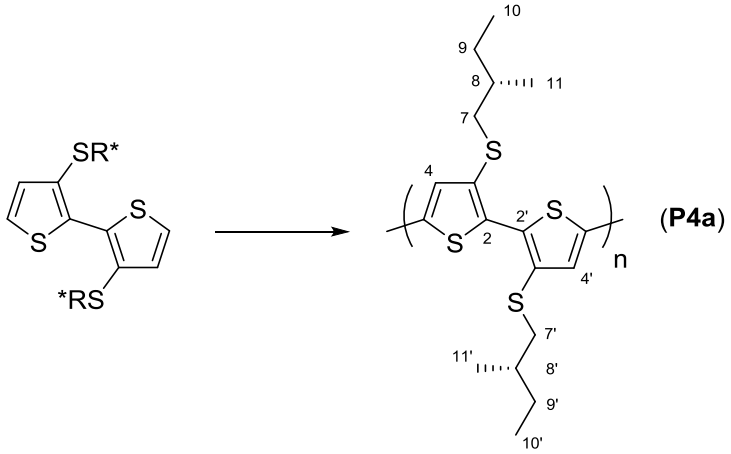

To a solution of 4a (0.075g, 0.2 mmol) in anhydrous $CHCl_3$ (8.1 mL) $FeCl_3$ (0.131 g, 0.8 mmol) was added under a weak stream of nitrogen at room temperature. The suspension was left under stirring for 24h, turning from greenish to dark blue colour. Then, 50 mL of THF and 100 mL of $CHCl_3$ were added, the mixture washed several times with 2% v/v aqueous HCl - up to exhaustive extraction of the iron (III) ion (negative essay with NH_4SCN) - and finally with water to neutrality. The organic phase was dried with $MgSO_4$ and concentrated at reduced pressure. The organic layer was dried over Na_2SO_4, concentrated under reduced pressure and finally treated with MeOH to afford 0.071 g (97% yield) of **P4a** as a brownish waxy solid.

^{1}H-NMR ($CDCl_3$, ppm): δ 7.38 (d, 1H, terminal 5-H), 7.22-7.12 (ms, 2H, backbone 4-H and 4'-H), 7.08 (d, 1H, terminal 4-H), 2.96-2.82 (m, 2H, 7-H_α), 2.76-2.62 (m, 2H, 7-H_β), 1.70-1.40 (m, 2H, 8-H), 1.34-1.10 (m, 2H, 9-H_α), 1.04-0.98 (m, 2H, 9-H_β), 0.98-0.92 (m, 6H, 11-H), 0.92-0.78 (m, 6H, 10-H).

*3.3.4. Poly{3,3'-bis[(S)-(2-methylbutoxy)-2,2'-bithiophene} (**P4b**)*

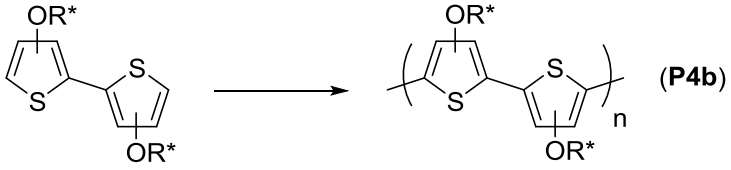

The same procedure described for P4a was followed starting from the H-H/H-T regioisomeric mixture 4b (0.050 g, 0.1 mmol) and $FeCl_3$ (0.065 g, 0.4 mmol) in $CHCl_3$ to obtain 0.032 g (95% yield) of **P4b** as a black solid.

^{1}H-NMR ($CDCl_3$, ppm): δ 7.18-7.08 (m, 2H, 4-H and 3'-H, **HH**), 7.08-6.92 and 6.92-6.68 (m, 2H, 4-H and 3'-H, **HH** and 4-H and 4'-H, **HT**), 4.2-3.6 (m, 4H, 7-H), 2.0-1.8 (m, 2H, 8-H), 1.7-1.5 (m, 2H, 9-H_α), 1.4-1.2 (m, 2H, 9-H_β), 1.1-1.0 (m, 6H, 11-H), 1.0-0.9 (m, 6H, 10-H).

3.4. Methods and characterizations

Microwave (MW) irradiation was performed in a Milestone Microsynth Labstation operating at 2450 MHz and equipped with pressure and temperature sensors.

The ^{1}H-NMR spectra were recorded with a Varian Mercury 400 (400 MHz) spectrometer at room temperature in $CDCl_3$ solutions, using tetramethylsilane as internal reference. Chemical shifts are given in ppm.

Molecular mass and polidispersity index of the polymers were determined by gel permeation chromatography (GPC) in THF solution on a HPLC Lab Flow 2000 apparatus equipped with a Rheodyne 7725i injector, a Phenomenex Phenogel mixed bed 5μ MXL type column and an RI K-2301 KNAUER detector. Calibration curves were obtained by using monodisperse polystyrene standards.

The decomposition temperature (T_d) of the polymers was determined in the 20÷800°C temperature range on a TGA TA Instruments Q600 apparatus operating at a heating rate of 20°C/min under nitrogen atmosphere (mass samples ~10 mg). A DSC TA Instruments Q2000 operating under nitrogen in the –50÷200°C temperature range at a heating rate of 10°C/min was used to determine the glass transition temperature (T_g) of the polymers (mass samples ~10 mg).

UV-Vis and photoluminescence (PL) spectra were carried out on a Perkin Elmer Lambda 20 and Perkin Elmer LS50B spectrophotometer, respectively, at 25°C on 10^{-3}/10^{-4} M $CHCl_3$ solutions in 1 cm quartz cells. Thin film measurements were made on polymer samples cast from chlorobenzene solutions on quartz slides by drop-casting.

IR spectra were carried out on Ge disks using a Perkin-Elmer 1750 or a Spectrum One spectrophotometer.

Optical activities were measured on $CHCl_3$ solutions with a Perkin Elmer 341 digital polarimeter, equipped with a Toshiba sodium bulb, using a cell path length of 0.1 cm. Specific rotation values at the sodium D line are expressed as degree dm^{-1} g^{-1} dL.

The circular dichroism (CD) spectra of the polymers were recorded at room temperature on $CHCl_3$ or $CHCl_3$/CH_3CN solutions by a Jasco 810 dichrograph; Δε values, expressed

as L mol^{-1} cm^{-1}, were calculated by the following equation: $\Delta\varepsilon = [\Theta]/3300$, where the molar ellipticity Θ is in degree cm^2 $dmol^{-1}$.

3.5. ^{1}H-NMR spectra

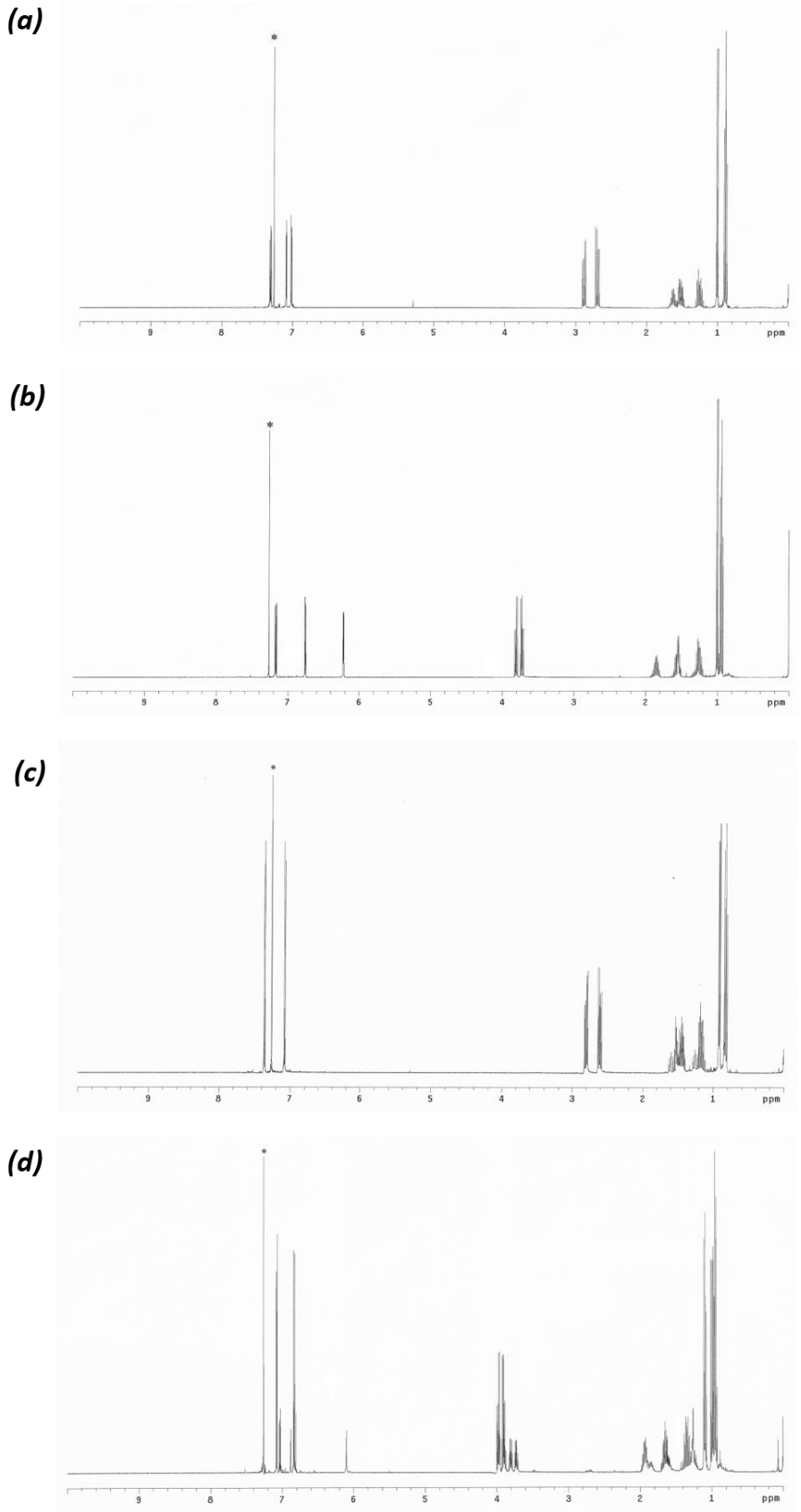

Figure 8. ^{1}H-NMR spectra of **1a** (a), **1b** (b), **4a** (c) and **4b** (d). Asterisk: solvent resonances.

References

[1] L. Pu, *Acta Polymer* **48** (1997) 116-141.
[2] L. A. P. Kane-Maguire, G. G. Wallace, *Chem. Soc. Rev.* **39** (2010) 2545-2576.
[3] M. Lemaire, D. Delabuglise, R. Garreau, A. Guy, J. Roncali, *J. Chem. Soc., Chem. Commun.* **10** (1988) 658-661.
[4] R. D. McCullough, R. D. Lowe, M. Jayaraman, D. L. Anderson, *J. Org. Chem.* **58** (1993) 904-912.
[5] T. A. Chen, R. D. Rieke, *Synth. Met.* **60** (1993) 175-177.
[6] B. M. W. Langeveld-Voss, M. M. Bouman, M. P. T. Christiaans, R. A. J Janssen, E. V. Meijer, *Polym. Prepr.* **37** (1996) 499-500.
[7] M. Catellani, S. Luzzati, F. Bertini, A. Bolognesi, F. Lebon, G. Longhi, S. Abbate, A. Famulari, S. V. Meille, *Chem. Mater.* **14** (2002) 4819-4826.
[8] P. Arosio, A. Famulari, M. Catellani, S. Luzzati, L. Torsi, S. V. Meille, *Macromolecules* **40** (2007) 3-5.
[9] B. M. W. Langeveld-Voss, R. J. M. Waterval, R. A. J. Janssen, E. W. Meijer, *Macromolecules* **32** (1999) 227-230.
[10] L. Angiolini, V. Cocchi, L. Guadagnini, A. Mignani, E. Salatelli, D. Tonelli, *Synth. Met.* **202** (2015) 169-176.
[11] D. Iarossi, A. Mucci, F. Parenti, L. Schenetti, R. Seeber, C. Zanardi, A. Forni, M. Tonelli, *Chem. Eur. J.* **7** (2001) 676-685.
[12] G. Koeckelberghs, M. Vangheluwe, C. Samyn, A. Persoons, T. Verbiest, *Macromolecules* **38** (2005) 5554-5559.
[13] K. Van den Bergh, I. Cosemans, T. Verbiest, G. Koeckelberghs, *Macromolecules* **43** (2010) 3794-3800.
[14] B. M. W. Langeveld-Voss, R. A. J. Janssen, E. W. Meijer, *Journ. Molecular Struct.* **521** (2000) 285-301.
[15] J. R. Matthews, F. Goldoni, H. Kooijman, A. L. Spek, A. P. H. J. Schenning, E. W. Meijer, *Macromol. Rapid Commun.* **28** (2007) 1809-1815.
[16] F. Di Maria, P. Olivelli, M. Gazzano, A. Zanelli, M. Biasiucci, G. Gigli, D. Gentili, P. D'Angelo, M. Cavallini, G. Barbarella, *J. Am. Chem. Soc.* **133** (2011) 8654-8661.
[17] P. Kaszynski, M. Jawdosiuk, *Molecular Crystals and Liquid Crystals Incorporating Nonlinear Optics* **174** (1989) 21-37.
[18] F. Saito, Y. Takeoka, M. Rikukaw, K. Sanni, *Synth. Met.* **153** (2005) 125–128.
[19] B. Xu, S. Noh, B. Thompson, *Macromolecules* **47** (2014) 5029-5039.
[20] R. H. Mitchell, Y.H. Lai, R.V. Williams, *J. Org. Chem.* **44** (1979) 4733-4735.
[21] F. Goldoni, D. Iarossi, A. Mucci, L. Schenetti, M. Zambianchi, *J. Mater. Chem.* **7** (1997) 593-596.
[22] E. Salatelli, M. Marinelli, M. Lanzi, A. Zanelli, S. Dell'Elce, A. Liscio, M. Gazzano, F. Di Maria, *J. Phys.Chem. C.* **122** (2018) 4156-4164.
[23] F. Demanze, A. Yassar, F. Garnier, *Macromolecules* **29** (1996) 4267-4273.
[24] R. S. Loewe, S. M. Khersonsky, R. D. McCullough, *Adv. Mater.* **11** (1999) 250-253.

[25] R. S. Loewe, P. C. Ewbank, J. Liu, L. Zhai, R. D. McCullough, *Macromolecules* **34** (2001) 4324-4333.
[26] X. Hu, L. Xu, *Polym.* **41** (2000) 9147-9154.
[27] Z.-B. Zhang, M. Fujiki, *Polym. J.* **33** (2001) 597-601.
[28] G. Neculqueo, V. R. Fuentes, A. Lopez, R. Matute, S. O. Vasquez, F. Martinez, *Struct. Chem.* **23** (2012) 1751–1760.
[29] D. Beljonne, B. M. W. Langeveld-Voss, Z. Shuai, R. A. J. Janssen, S. C. J. Meskers, E. W. Meijer, J. L. Bredas, *Synth. Met.* **102** (1999) 912-913.
[30] E. Peeters, A. Delmotte, R. A. J. Janssen, E. W. Meijer, *Adv. Mater.* **9** (1997) 493-496.
[31] F. Di Maria, M. Zangoli, M. Gazzano, E. Fabiano, D. Gentili, A. Zanelli, A. Fermi, G. Bergamini, D. Bonifazi, A. Perinot, M. Caironi, R. Mazzaro, V. Morandi, G. Gigli, A. Liscio, G. Barbarella, *Adv. Funct. Mater.* **28** (2018) 1801946.
[32] D. D. Perrin, W. L. F. Armarego, D. R. Perrin, *Purification of Laboratory Chemicals*, Pergamon Press: Oxford, 1966.

Chapter V

Chapter V: BLOCK COPOLYMERS – HOW TO OBTAIN A UNIQUE AGGREGATION BEHAVIOUR

1. Introduction

1.1. Overview

In the last few decades, although many alternatives were developed for the fully synthesis of different conjugated polymers - such as poly(acetylenes), poly(anilines), poly(thiophenes) etc. - most of these synthesis usually go through a step growth mechanism and thus, in addition to provide poor control over the polymerization, they are typically accompanied by a high polydispersity index.

As previously mentioned in the general introductive chapter, only in 2005 Yokozawa and McCullough independently come up with something later has been seen as the foundation for the controlled polymerization of conjugated polymers. They both discovered that the polymerization of poly (3-alkylthiophene) (P3AT) with [1,3-bis(diphenylphosphino)propane]nickel (II) chloride ($Ni(dppp)Cl_2$) as a catalyst proceeds via a controlled chain growth mechanism.[1,2] Indeed, since this mechanism is based on transition metal catalyzed cross-coupling reactions - with control over the chain growth caused by the association of the catalyst with the conjugated π system of the growing polymer chain - it is generally referred to *catalyst transfer condensative polymerization* (CTCP).[3]

In the first place, similarly to a traditional catalyzed reaction cycle, oxidative addition (OA), transmetallation (TM) and reductive elimination (RE) steps are involved; then, thanks to the association of the catalyst that can only undergo to intramolecular OA, transfer reactions are suppressed and the polymerization proceeds in a controlled manner (Figure 1). In fact, in a chain growth polymerization, not only cannot a monomer react with other monomers, but the polymer chain can also only grow from active sites created by an initiator. To stop its polymerization is thus necessary to destroy the active site at the end of the macromolecule (termination step).

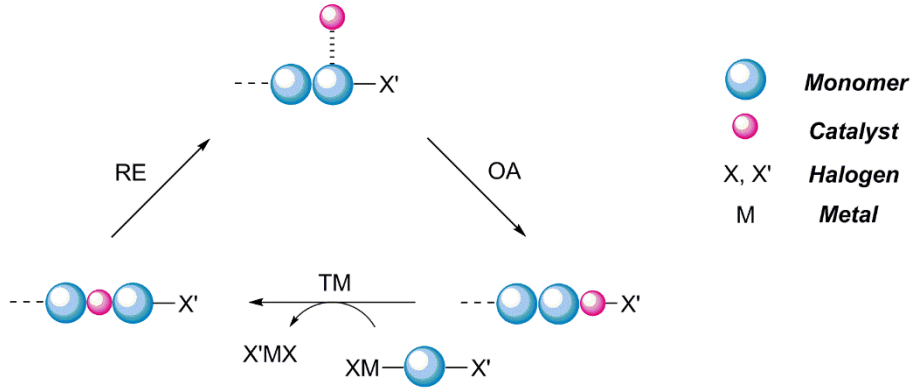

Figure 1. General scheme for a catalyst transfer condensative polymerization (CTCP).

If transfer reactions and termination - when the active site on the polymer chain is not transferred to another species but destroyed - of the polymerization can be prevented, the polymerization is transformed into a so-called living polymerization. In this way, since the polymer chains do not "die" and can keep growing as long as monomer is present, it is also possible to predict the degree of polymerization.

Several advantages are connected to the use of living polymerizations over other polymerization techniques. In addition to the obtainment of generally low polydispersity index and the possibility to control the length of the polymer, by varying the ratio of monomer over initiator, well-defined and reproducible materials can be easily made. Moreover, one of the main advantages of this type of technique is the ability to synthesize block copolymers via sequential monomer addition.

1.2.Suzuki Catalyst Transfer Condensative Polymerization (SCTCP)

Kumada CTCP is by far the most investigated form of controlled polymerization and is based on a Kumada coupling between an organomagnesium halide (or Grignard reagent) and a halide.[3]

As a very electron-rich monomer, thiophene is for sure the reference monomer for KCTCP, since a good association between the catalyst and the conjugated π system is allowed. In addition to poly(3-alkylthiophene)s (P3AT), the synthesis of polymers based on various other monomers - i.e. poly(fluorene) (PF) - through KCTCP have been also reported. However, due to the electron poor nature and much higher dimension of the fluorene than thiophene monomer, the poor association of the catalyst and consequent longer required association time contribute to an insufficient control over the polymerization.[4]

A possible alternative for the synthesis of poly(fluorene) is therefore the Suzuki CTCP, which is based on a Suzuki coupling between an organoborane and a halide.

Not only are boronic acids/esters moisture stable and thus much less reactive than Grignard reagents, but they also are tolerant to a wide variety of functional groups.[5,6] It is a well-known fact that most SCTCP mechanisms work best via a Pd catalyst, instead of Ni, in the presence of a small amount of water.[7] In this way a faster intramolecular transfer is obtained, offering less chance of dissociation and consequently better control over the polymerization.

The hypothesis[8] that Pd(0)/*t*-Bu_3P as external initiator would be able to catalyze a living Suzuki polymerization to prepare poly(fluorene) was first confirmed in 2007 by Yokoyama and coworkers.[9] However, one of the issues that SCTCP has is the proper formation of the Pd-based external catalyst. In fact, even though control over the polymerization is possible, the partial decomposition of the initiator, when dissolved at the start of the polymerization, could produce some fluctuations of polydispersity index.

A possible alternative to overcome this problem has been recently proposed by Zhang and coworkers who, starting from a commercial palladacycle complex [P(*t*-$Bu)_3$Pd G2], have successfully created in situ the 12-electron species (*t*-Bu_3P)Pd(0) required for the properly formation of the initiator (Figure 2).[10,11]

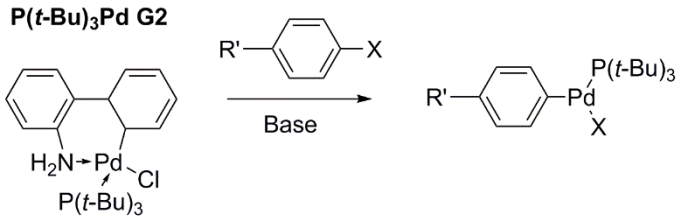

Figure 2. Example of palladacycle complex.

1.3. Controlled synthesis of conjugated block copolymers

Block copolymers, where two blocks with differing supramolecular aggregation may be combined in the same polymer, can be made via indirect and direct synthesis methods. Even though a general overview of all indirect methods that could be adopted for the synthesis of these materials is summarized in Figure 3, only the direct synthesis through sequential monomer addition as method mainly adopted for the synthesis of the compounds presented in this chapter will be discussed.

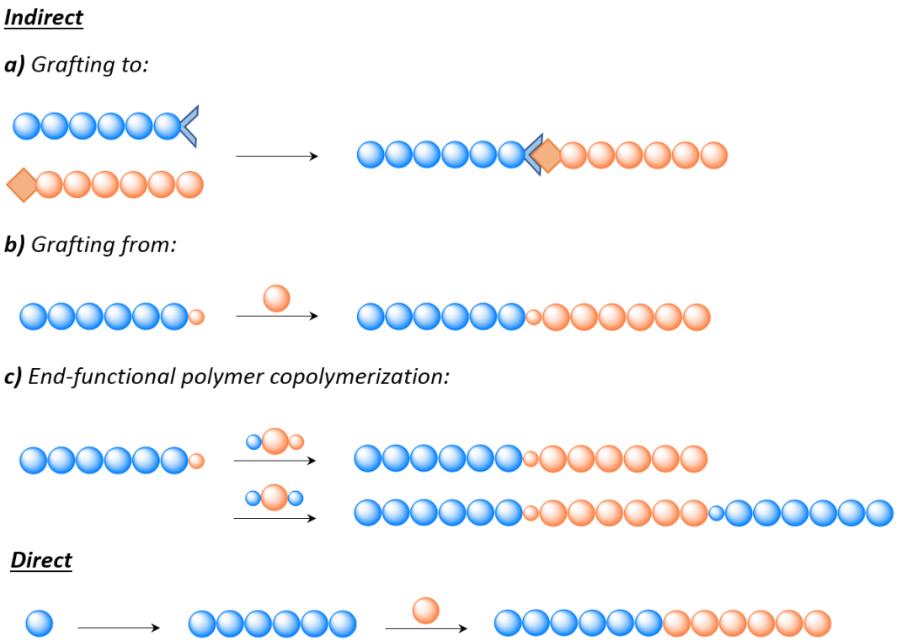

Figure 3. Synthetic methods for block copolymers.

In the first place, many downsides - such as little control over the structure, need to purification and post-polymerization steps - are connected to the employ of indirect methods to make block copolymers. On the other hand, thanks to the use of a living polymerization by sequential monomer addition, a well-defined block copolymer could be obtained since termination does not occur and thus, after full consumption of all first monomer, a second monomer can be added.

As previously discussed in the first chapter of this dissertation, the Grignard metathesis polymerization (GRIM) is basically a CTCP in which the catalyst displays a "ring walking" behaviour, since it remains coordinated to the polymer chain.

The reaction is generally initiated in situ, so without the use of external initiator, via formation of a tail-to-tail bithiophene-Ni complex: because of the two carbon-halogen chain ends, there is no control on which side the catalyst oxidatively inserts. Although this is not a problem for the synthesis of homopolymers, this could be disastrous for the synthesis of block copolymers. In fact, when an AB block copolymer need to be obtained by successive addition of the monomer, the bi-directional chain growth could lead to the formation of BAB' block copolymers, where the length of B and B' depends on polymer to polymer.

Fortunately, bidirectional growth can be avoided by using an external initiator with no active C-Br bond, as the catalyst can still walk over the polymer chain but only inserts in

one chain end. Furthermore, the use of an external initiator also offers the possibility to have functional groups at the start of the polymer chain.[3,12]

As both monomers need to be polymerized under similar conditions, the easiest block copolymers to prepare are block copolymers built from structurally similar monomers in which the order of the monomers does not really play a role. On the other hand, when widely different monomers are used, good polymerization control can only be maintained if the association between catalyst and monomer increases from the first to the second monomer. For this reason, due to the living nature of CTCP - that is based on the association of the catalyst to the growing polymer backbone - the electron-poorer block should always be polymerized first and then followed by the electron-rich monomer.

In details, for the precise synthesis of PF-*b*-P3AT block copolymers, a Suzuki CTCP need to be carried out with fluorene and successive thiophene monomer addition, as reported in 2011 by Yokozawa.[13] By combination of their results with the optimized synthesis of polyfluorene by Zhang and coworkers, in addition to the literature reported for the synthesis of P3AT as homopolymer, the optimized block copolymerization of PF-*b*-P3AT via SCTCP has been obtained.[11,14]

1.4. Aggregation behaviour in copolymers

The fact that the optical rotation of random copolymers, made of chiral and achiral monomers, could result to be distinctly higher than the expected - based on the amount of chiral units built in - was firstly reported by Carlini and coworkers.[15] However, the first description of *"sergeants and soldiers"* principle has been reported only by Green in 1989.[16]

A possible explanation for this effect may be provided by achiral poly(isocyanates) that exist as helical polymers where segments of a certain helix sense are separated by helical reversal states from segments of the other sense.[17] Since introduction of chirality in the monomer unit leads to a preference for one of the helix senses, already a small amount of chiral monomer could induce a preference for a certain sense within each segment. This means that the chiral *"sergeants"* command a certain helical sense to the achiral *"soldiers"*.

It is particularly noteworthy that not only is this effect present in helical polymers, but it is also displayed in other supramolecular structures, such as aggregated stacks of polymers.

For this reason, if a series of random copolymers of chiral and achiral P3ATs are made, the resulting aggregated structures will also show the sergeants and soldiers effect.[18]

Even block copolymers are no exception to this rule and, thus, interesting chiral effects are usually shown. Indeed, when block copolymers are made with a chiral and an achiral block, they typically display the *"first come, first served"* principle: upon aggregation in a chiral way of the first block, which has chiral side chains, the second block aggregates in the same manner independently from the (a)chirality of its side chains.[12]

Fortunately, the validity of both principles is not only true for chiral expression, but it could also be extended to the aggregation/morphology expression of these materials.
In fact, in order to improve existing applications and create new opportunities, it is important to combine materials with different properties (i.e. mechanical properties, thermal stability, processability and hydrophobicity). Although an improvement of the polymer properties could be obtained by the fine-tuning of the chemical structure, also the morphology is of extreme importance for the final characteristics of the material.[19,20,21]
In this framework, block copolymers definitely form an attractive group of materials to accomplish this goal.[22,23,24,25] Indeed, in addition to promote only microphase separation, the covalent bond between the different polymer blocks could allow the obtainment of special morphologies, which cannot be obtained via (blends of) homopolymers, and an even enhancement of the properties.[26,27] Furthermore - since different polymer blocks are chemically linked to each other - not only can they influence each other's properties more easily than in polymer blends, but one polymer block can also transfer its properties to another one for the just mentioned *"first come, first served"* principle.

In fact, thanks to this rule, the first block introduces features in the second block that are not possible in any other way, such as the well-known aggregation in a chiral way. However, despite this principle has been already observed many times, it was always true in block copolymers built up from monomeric units that have similar electronic properties - i.e. thiophene and thiophene - and, therefore, aggregate in the same way.[12,28,29]
On this basis, the possibility to transfer aggregation properties also to polymers with different electronic properties - i.e. PT and PF - results to be a goal particularly interesting to pursue.

The aggregation behaviour of PTs is already well described in literature and depending on the (a)chirality of the side chains, linear or helical stacks of planarized PTs are obtained upon aggregation.[30,31] Whereas, although the aggregation behaviour of PFs is less documented, the existence of three types of phase, i.e. α-, α'- and β-phase, is generally

accepted.[32,33,34] In particular, while in the α- and α'- phase the PF chains aggregate in twisted ribbons, that is possible for PFs with all types of side chains, the β-phase is only possible for PFs with linear octyl (and to a lesser extent heptyl and nonyl) side chains and is obtained when the PF chains aggregate in flat ribbons.[35]

For this reason, taking into account that design a homopolymer in which chirality is combined with β-phase aggregation is impossible since chirality implies branched side chains, it is reasonable to hypothesize the combination of these properties by the design of block copolymers.

1.5. Aim of the chapter

In this context, by combining a PT block with short, chiral side chains with a PF block with a linear octyl side chain, it is probed to obtain a polymer in which chiral expression (arising from the PT with chiral side chains) and β-phase aggregation (arising from the PF with linear octyl side chains) are brought together.

In particular, three block copolymers PF-*b*-PT were synthesized via Suzuki catalyst transfer condensative polymerization (SCTCP) - i.e. poly(9,9-dioctylfluorene)-*b*-poly(3-((*S*)-3,7-dimethyloctyl)thiophene) (**POF-*b*-P3OT***), poly(9,9-dihexylfluorene)-*b*-poly(3-((*S*)-3,7-dimethyloctyl)thiophene) (**PHF-*b*-P3OT***) and poly(9,9-dioctylfluorene)-*b*-poly(3-((*S*)-2-methylbutyl)thiophene) (**POF-*b*-P3BT***) - and their aggregation behavior studied via solvatochromism experiments. In fact, it has been hypothesized that the side chains of the PTs should be short to ensure this block aggregates first in a chiral way (in order to transfer its chirality to the PF block) and that the side chains of the PFs should be 8 C-atoms long to ensure maximal β-phase aggregation.

The work described in the present chapter - which is based on adapted content from "Rational design of poly(fluorene)-*b*-poly(thiophene) block copolymers to obtain a unique aggregation behavior" L. Verheye, K. Janssens, M. Marinelli, E. Salatelli and G. Koeckelberghs, *Macromolecules* **52** (2019) 6578-6584 - is part of a project carried out during a three months stay at the Department of Polymer Chemistry and Materials of the Katholieke Universiteit of Leuven (Belgium), under the supervision of Prof. Dr. Guy Koeckelberghs.

2. Results and discussion

2.1. Synthesis

In order to validate the aforementioned hypotheses, three different block copolymers - i.e. **POF-*b*-P3OT***, **PHF-*b*-P3OT*** and **POF-*b*-P3BT*** (Figure 4) - have been synthesized.

While the aggregation behaviour of the first block copolymer was studied to confirm that the chiral side chain of the thiophene units must be short, in order to obtain an aggregation of the PT block prior to the PF block, **PHF-*b*-P3OT*** has been prepared with the aim to validate the promotion of β-phase aggregation of the PF block by 8 C-atoms long side chains. On the other hand, the third block copolymer was synthesized to confirm that, by choosing the right side chain, is possible to combine chiral expression and β-phase aggregation in one material which displays properties that could never be achieved with homopolymers.

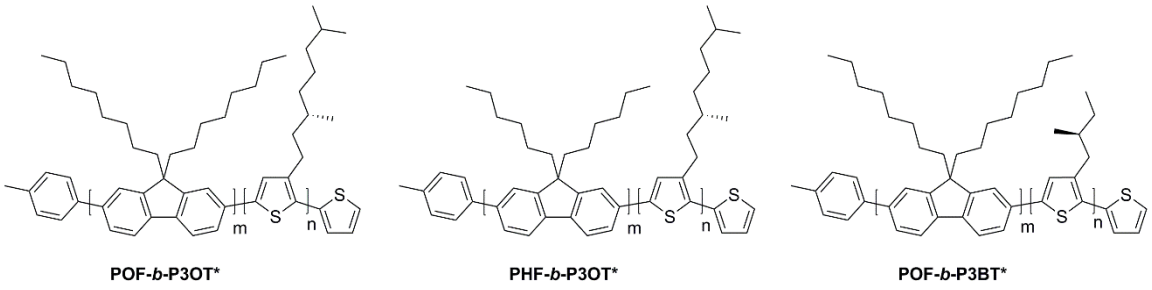

Figure 4. Structure of the synthesized block copolymers.

The organoborano-halide derivatives used as starting monomers for the synthesis of the copolymers were prepared according to adapted literature procedures (details in experimental section).[36,37]

In particular, tri(*tert*-butyl)magnesium lithium·lithium chloride ((*t*Bu)$_3$MgLi·LiCl) and *iso*-propylmagnesiumchloride·lithium chloride (*i*PrMgCl·LiCl) were used, respectively, in the first conversion step of fluorene and thiophene derivatives. Because boronic esters are preferred over boronic acids for stability reasons, 4,4,5,5-tetramethyl-1,3,2-dioxaborolane was then added in the second step, leading to the final monomers.

Since the controlled character was already demonstrated for PFs[11,38,39] as well as for PTs,[7,39,40] the synthesis of the predefined block copolymers was carried out via Suzuki CTCP (Scheme 1).

Taking into account that the fluorene monomer must be polymerized before the thiophene monomer,[13,41] it was chosen to prepare block copolymers in which the PT block has around the double amount of monomer units compared to the PF block. Indeed, as the fluorene monomer is of approximately the double length of the thiophene monomer, the two blocks result to be comparable in length.

With the view to prevent the formation of BAB block copolymers - caused by the random catalyst walking -[12,42,43] and the necessity to determine the chain length of the synthesized block copolymers, an external initiator (**2**) was used by generation in situ from the commercially available palladacycle (**1**) and 4-bromotoluene.[11]

To minimize the influence of end-groups on the final aggregation behaviour of the block copolymer, thiophene-3-boronic pinacol ester (**4**) was used as endcapper. However, a small fraction of the polymerization mixture was also endcapped with **3** before the addition of the second monomer: in this way, the poly(fluorene) block could be analysed separately.

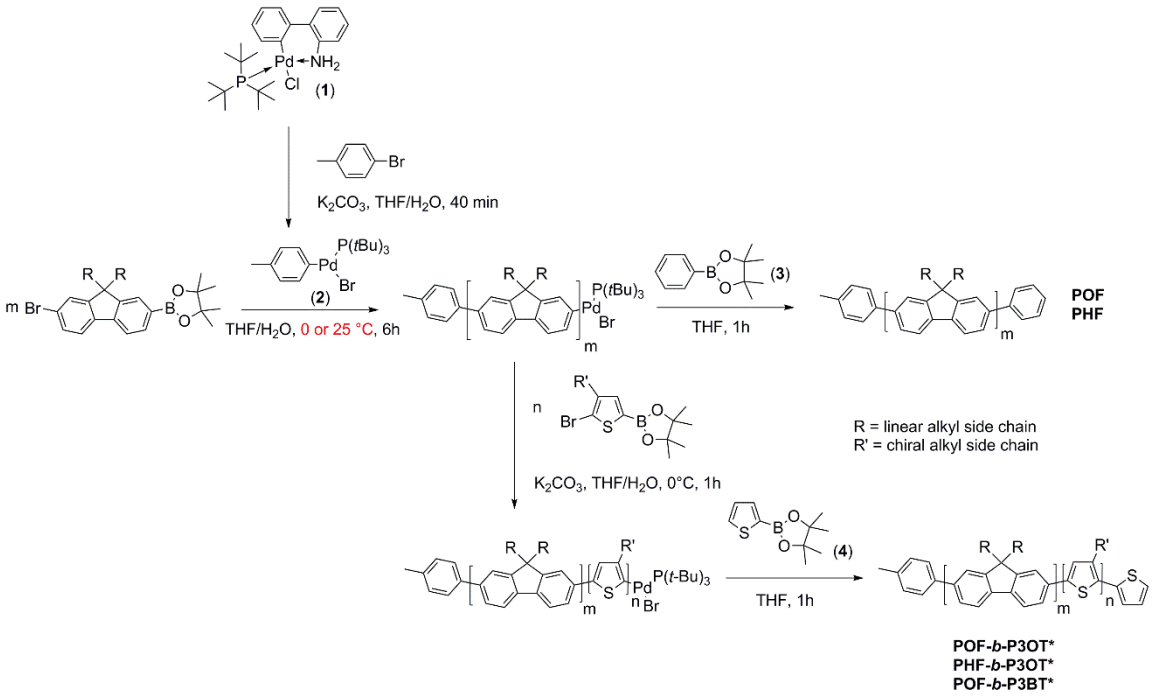

Scheme 1. Synthetic route of copolymerization via SCTCP.

2.1.1. Optimization of POF-*b*-P3OT* synthesis

Despite the successful diblock copolymerization of **POF-*b*-P3BT*** and **PHF-*b*-P3OT*** via SCTCP - previously performed by Koeckelberghs' group - the synthesis of the analogous both octyl side chain functionalized material failed. For this reason, my period at the KU Leuven was basically devoted to the optimization of the synthesis of **POF-*b*-P3OT*** by Suzuki controlled polymerization, in addition to investigate its chiral expression and make a comparison with the two other chiral materials.

In the first place, as deboronation and dehalogenation of the monomer can however occur and optimal reaction conditions depend on the monomer used, the step of conversion from boronic ester to acid of the fluorene monomer was investigated through ^{1}H-NMR spectroscopy. By changing type of THF and increasing the amount of water, which should favor the intramolecular transfer of catalyst, the use of unstabilized THF without changing the ratio of THF/H_2O seemed to lead to a better conversion.

The homopolymerization of the octylfluorene monomer by Suzuki coupling has been directly tested; using different type of THF - the commercial stabilized THF with BHT (butylated hydroxytoluene), the commercial unstabilized THF and unstabilized THF obtained by distillation - the reactions were performed at 0°C, always using P(*t*Bu)$_3$PdG2 as a precatalyst, 4-bromo-toluene as initiator and K_2CO_3 2M as base.

As it is possible to see from the follow-up carried out by gel permeation chromatography (GPC) (Figure 5a), the obtainment already after 2 hours of a polymer - $\overline{Mn}$ = 7.4 kg/mol, $\overline{Mw}$ = 9.7 kg/mol and PDI = 1.3 - with commercial unstabilized THF, confirmed the results previously obtained.

To be sure that the polymerization was actually reproducible, the reaction was performed twice using only commercial unstabilized and stabilized THF. Although the reactions have been carried out in the same condition of the first test, the polymerization made with unstabilized THF failed. However, it appears a clear obtainment of a polymer - $\overline{Mn}$ = 9.4 kg/mol, $\overline{Mw}$ = 13.3 kg/mol and PDI = 1.4 - by the use of stabilized THF but over the night, when the temperature was not controlled anymore (Figure 5b).

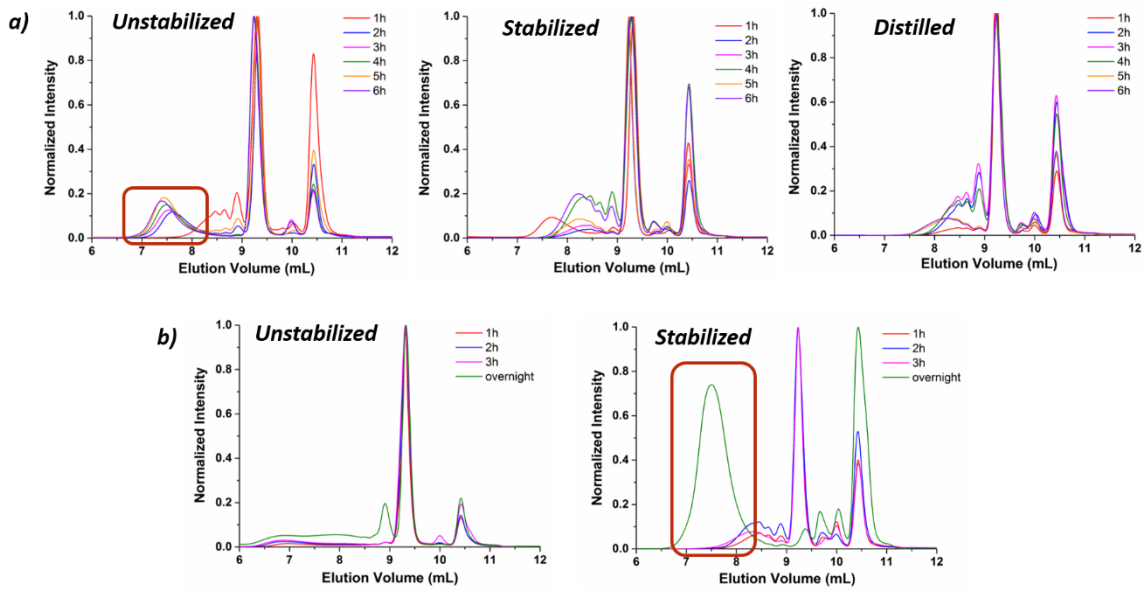

Figure 5. GPC chromatograms of (a) test 1 and (b) test 2 of homopolymerization.

For this reason, I started optimizing the polymerization at room temperature using only stabilized THF. Once established that the polymerization was still living after the night, the successful copolymerization of **POF-*b*-P3OT*** was performed, carrying out the polymerization of the first block (fluorene) and second block (thiophene) respectively at room temperature and at 0°C.

2.2. GPC and ^{1}H-NMR characterization

In order to be sure that only the aggregation behavior of the block copolymers was studied - since a mixture of block copolymers, homopolymers and monomers could also be present - the synthesized materials were purified via Soxhlet extraction and preparative GPC.

After the purification, a GPC analysis has been performed at the maximum absorbance of PF (380 nm) and PT (440 nm) block (Figure 6b). Taking into account that both curves completely overlap for each block copolymer, it can be concluded that all the homopolymer has been successfully removed and only the block copolymers of interest are present. The M_n and polydispersity index (PDI = M_w/M_n) for all the polymers can be found in Table 1.

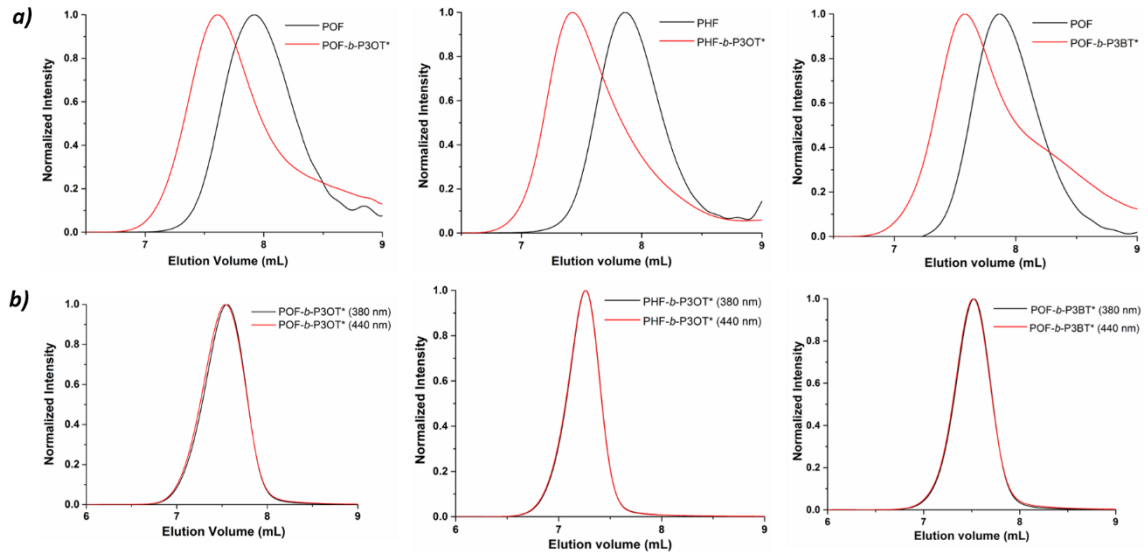

Figure 6. GPC chromatograms of (a) PF and PF-*b*-PT after Soxhlet extraction (detection at 254 nm) and (b) of block copolymers after prep GPC (detection at 380 and 440 nm).

Table 1. Overview of the number average molar mass (M_n), polydispersity (PDI) and degree of polymerization (x_n) of the separate blocks of the synthesized block copolymers

	PF [a]		*PF-b-PT* [b]		x_n [c]	
Copolymers	*Mn (kg/mol)*	*PDI*	*Mn (kg/mol)*	*PDI*	*PF block*	*PT block*
POF-*b*-P3OT*	4.9	1.3	11.7	1.2	10	17
PHF-*b*-P3OT*	5.7	1.2	21.3	1.1	11	27
POF-*b*-P3BT*	6.6	1.4	13.9	1.1	9	18

[a] After purification with Soxhlet extraction; [b] After Soxhlet extraction and preparative GPC; [c] Determined by ^{1}H-NMR.

Since only block copolymer is present after purification, the chain length of both blocks can be determined by ^{1}H-NMR spectroscopy at basis of a difference in chemical shift of both blocks (Figure 7).

In particular, after calibration of the integration values by the use of the methylene group of the initiator (**a**), the degree of polymerization (x_n) has been calculated on the base of the β- and α-methylene protons of the side chains of the fluorene (**b**) and thiophene (**c**) monomer unit, respectively. Even though the polymerization was not completely controlled, the aimed ratio of one fluorene monomer towards two thiophene monomers was still approximately retained. The obtained polymerization degree for each block can also be found in Table 1.

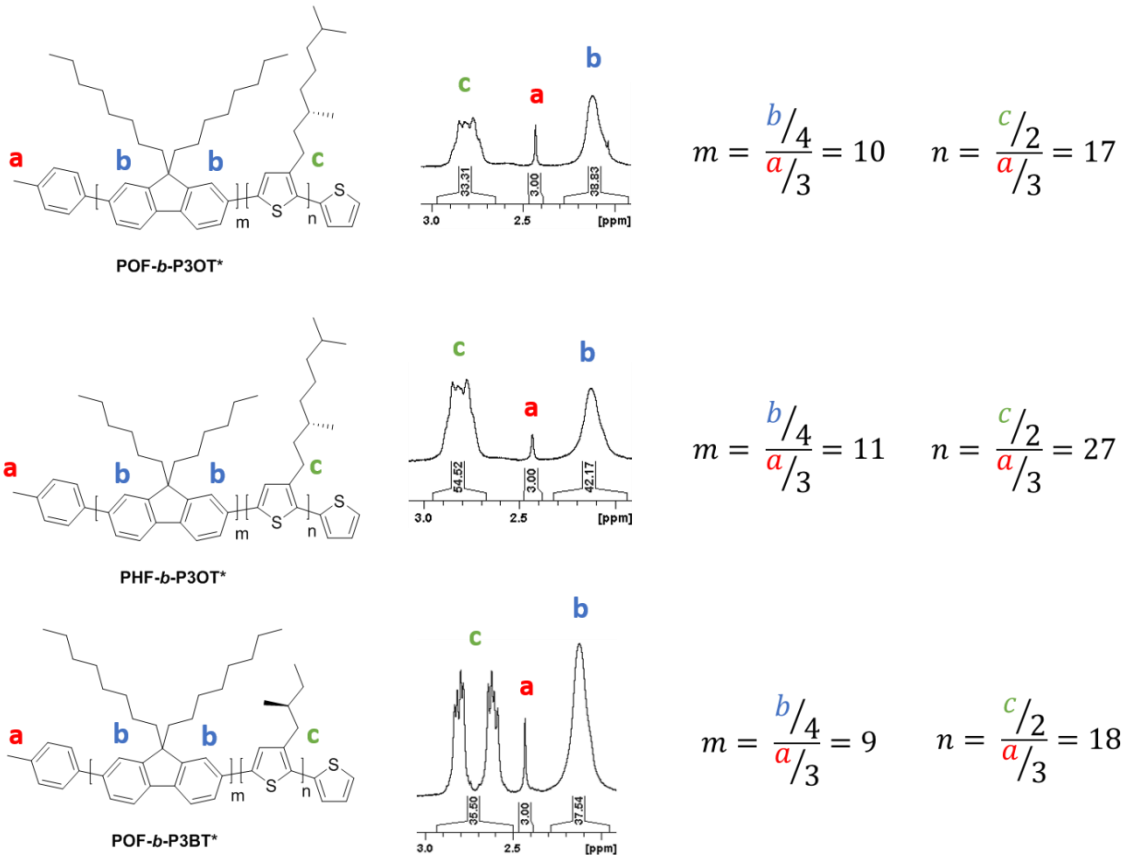

Figure 7. Determination of degree of polymerization for **POF-*b*-P3OT***, **PHF-*b*-P3OT*** and **POF-*b*-P3BT***.

2.3.Solvatochromism and CD spectroscopy

The aggregation behaviour of the polymers was studied via solvatochromism experiments, by gradual addition of poor solvent (methanol) to a chloroform solution of polymer.

In the first place, the main hypothesis that the chiral PT block must aggregate first - in order to transfer its chirality to the PF block - was tested.

With **POF-*b*-P3OT***, due to the long and branched side chains in the PT block which increase the solubility of this block compared to the PF block, the opposite behaviour has been induced (Figure 8a). In particular, the first event is the aggregation (39% MeOH) of the PF block - as β-phase - that is visible in the absorption spectrum, at around 380 nm and 430 nm, as a decrease and appearance of signal, respectively.[44,45] As expected, since the PF block has no chiral side chains, no signal is yet visible in the circular dichroism spectrum (Figure 8b).

Instead, when more MeOH is added, the PT block starts to aggregate (42%); visible as increasing signal in the UV-Vis spectrum, in the region between 500 and 700 nm, a bisignate signal is also displayed in the CD spectrum in the same region. On the other hand, no chiral expression for the PF block is obtained, since the PT chirality cannot be imposed onto the PF block without breaking the previously formed achiral PF aggregates.

From the behaviour displayed by this polymer, it can be assumed that the chiral PT block must aggregate first in order to be able to transfer its chirality to the PF block.

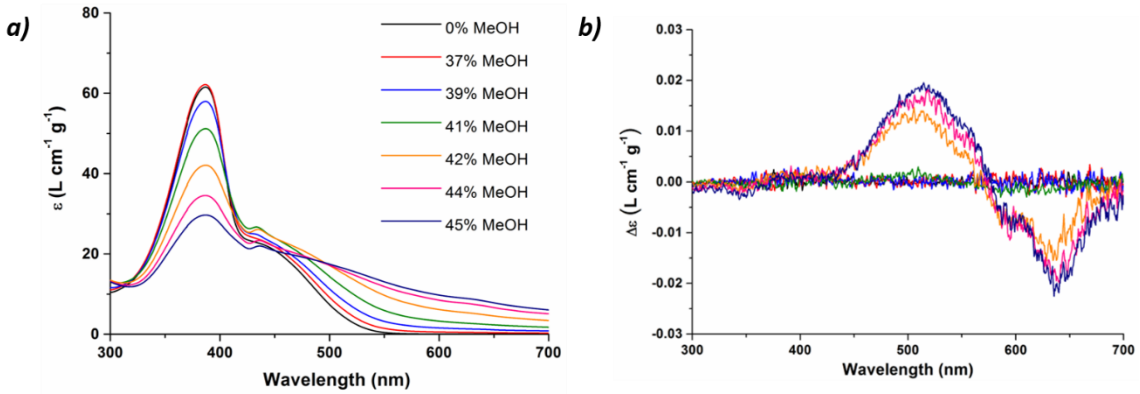

Figure 8. Absorption (a) and CD (b) spectra of the solvatochromism experiments for **POF-*b*-P3OT***.

In order to verify the second hypothesis - the linear side chains of the PF block must be 8 C-atoms long to allow β-phase aggregation - the aggregation behaviour of **PHF-*b*-P3OT*** was studied.

Similarly to **POF-*b*-P3OT***, as it is possible to see from Figure 9, the same sequence of aggregation events in the solvatochromism experiment can be distinguished for **PHF-*b*-P3OT***.

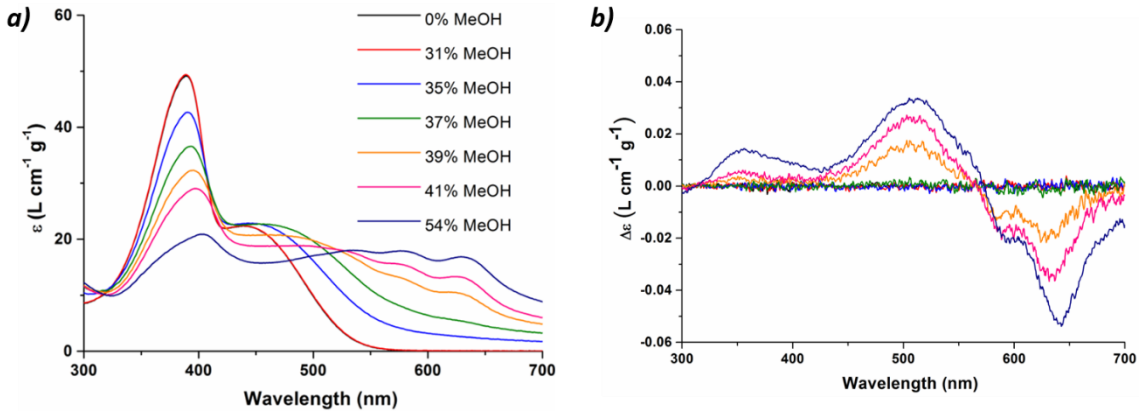

Figure 9. Absorption (a) and CD (b) spectra of the solvatochromism experiments for **PHF-*b*-P3OT***.

Indeed, the PF block starts first to aggregate (35% MeOH), with a visible decrease and broadening of the signal around 380 nm; then, upon the addition of more MeOH (from 39% MeOH), a fine structure between 500 nm and 700 nm in the absorption spectrum and a bisignate signal in the same region in the CD spectrum are shown, due to the PT block aggregation. However, no extra signal around 430 nm was observed upon the aggregation of **PHF-*b*-P3OT***, indicating that no β-phase aggregation occurred.

This result confirms the hypothesis that, in order to obtain β-phase aggregation, the length of the linear side chains of the fluorene units matters.

With the investigation of the first two block copolymers, since the formulated hypotheses were tested only in a negative way - as the criteria are not met - no complete proof of their validity have been actually obtained. For this reason, the aggregation behaviour of the third block copolymer, **POF-*b*-P3BT***, was studied.

Thanks to this polymer, the two previous hypotheses were combined. In fact, not only do short and chiral side chains for the PT block guarantee to be the least soluble block, but with linear octyl side chains for the PF block is also allowed the maximal β-phase aggregation. The first signs of aggregation are visible upon the addition of 33% of MeOH (Figure 10). In details, the aggregation of the PT block is indicated − in the UV spectra − by an increase of the signal between 450 and 650 nm, combined with a small decrease of the signal around 400 nm; the appearance of a bisignate signal in the same region in the CD spectrum confirms this. When gradually more MeOH is added up to 37%, the PT block is almost fully aggregated and the characteristic signal for β-phase aggregation of the PF block, a sharp peak at 430 nm, starts to appear in the absorption spectrum. This is accompanied by the appearance of a bisignate and monosignate signal for the PF block in the CD spectrum.

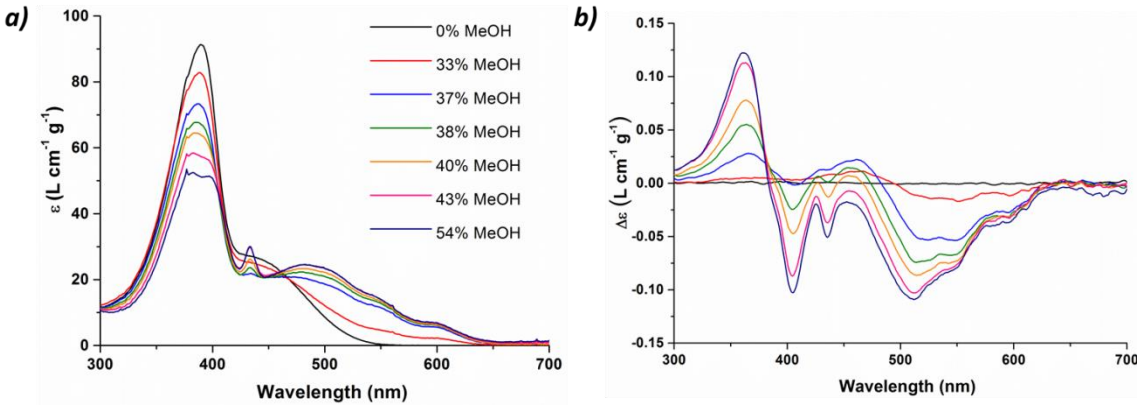

Figure 10. Absorption (a) and CD (b) spectra of the solvatochromism experiments for **POF-*b*-P3BT***.

The sharp monosignate signal at 430 nm points towards a helical transition dipole moment perpendicular to the polymer backbones, which indicates that the different polymer backbones are closely stacked in a helical manner (Figure 11). This is possible in the β-phase, due to the fact that the polymer backbone is planar, and the side chains can intertwine. The bisignate Cotton effect arises from the helical orientation of transition dipole moments along the polymer backbones of (at least two) PF blocks, confirming the helical stacked structure for the PF blocks. This behaviour shows that the PT block is able to transfer its chirality and alter the aggregation behaviour of the PF block.

Furthermore, since a shift towards a more monosignate signal in the PT region can be visible in the CD spectrum, it can be assumed that not only does the PT block influence the aggregation behaviour of the PF block, but that the PF block also influences the supramolecular structure of the aggregated PT block.

Therefore, the aggregation behaviour of this third and last block copolymer proves that it is possible to design materials in which properties can be combined and could never be obtained together with only homopolymers.

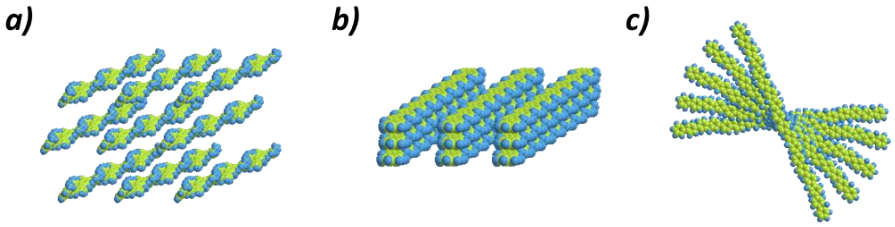

Figure 11. Representation of the packing of PF backbone chains in the α-phase (a), β-phase (b) and helical stacks in **POF-*b*-P3BT*** (c).

2.4. Conclusions

Three different conjugated PF-*b*-PT copolymers were synthesized via Suzuki CTCP and characterized via GPC and ^{1}H-NMR spectroscopy.

With the final aim to confirm the hypothesis that block copolymers can be designed to exhibit a unique set of properties by transferring properties of one block to the other, the aggregation behaviour of the synthesized polymers was studied via solvatochromism experiments.

In particular, the chiral expression and β-phase aggregation of PFs have been chosen as set of properties to be investigated. Indeed, it was probed that those could be combined in PF-*b*-PT copolymers with linear side chains for the PF block and chiral side chains for the PT block, as they allow, respectively, β-phase aggregation and chiral expression.

By the use of a stepwise approach, the hypothesis was verified. With the aggregation behaviour of **POF-*b*-P3OT***, it was elucidated that if the chiral PT block does not aggregate first, it cannot transfer its chirality to the PF block. On the other hand, with the aggregation behaviour of **PHF-*b*-P3OT***, it was confirmed that not just any linear side chain can be used for the PF block to obtain β-phase aggregation. In this way, those two conditions were successfully combined and a polymer − **POF-*b*-P3BT*** − was obtained.

This proves that not only is it possible to design block copolymers which can exhibit properties that transcend the properties of the homopolymers that they consist of, but it is also possible to transfer properties of one block to the other.

3. Experimental section

3.1. Materials

All reagents were purchased and used without further purification. Reagent grade solvents were dried by a solvent purification system MBRAUN SPS 800 (columns with activated alumina).

3.2. Synthesis of monomers

*3.2.1. 2-(7-Bromo-9,9-dioctylfluorene-2-yl)-4,4,5,5-tetramethyl-1,3,2-dioxaborolane (**3a**)*

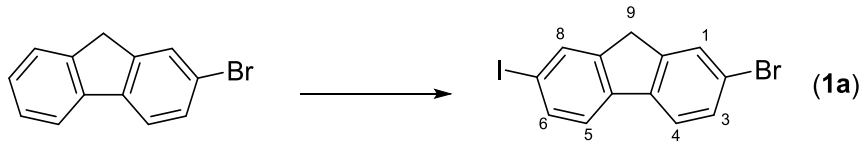

A solution of 2-bromofluorene (50.0 mmol, 12.26 g), I_2 (21.0 mmol, 5.33 g) and KIO_3 (12.0 mmol, 2.57 g) in water (10 mL), CH_3COOH (210 mL) and concentrated H_2SO_4 (5 mL) is stirred for 2 hours at 90°C under a nitrogen atmosphere. The reaction mixture is cooled to room temperature and the crude product as a red powder is formed. After filtration, the crude product was washed with CH_3COOH, water and finally recrystallized from DCM/MeOH to obtain 15.40 g (83% yield) of pure **1a** as a white powder.
^{1}H-NMR ($CDCl_3$, ppm): δ 7.89 (s, 1H, 8-H), 7.72 (d, 1H, 6-H), 7.67 (s, 1H, 1-H), 7.62 (d, 1H, 4-H), 7.50 (m, 2H, 3-H and 5-H), 3.86 (s, 2H, 9-H).

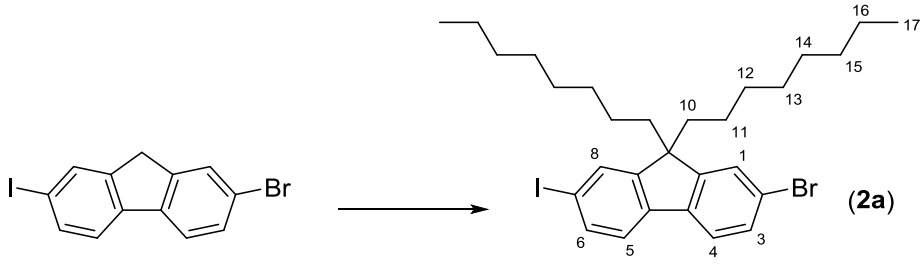

To a solution of 1a (20.0 mmol, 7.42 g) in DMSO (70 mL), purged with argon, a solution of NaOH 50 wt% aq. (9 mL) was added dropwise. Under strong stirring, 1-bromooctane (50.0 mmol, 9 mL) was then added and the reaction mixture is left stirring at room temperature for 24h. After precipitation in ethyl acetate (100 mL) and filtration of salts,

the filtrate was washed successively with a NaOH (20 mol% aq.), $NaHCO_3$ and brine solutions. The organic layer is dried over $MgSO_4$ and concentrated. The crude product is finally purified by recrystallization from isopropanol to afford 7.86 g (66% yield) of pure **2a** as white powder.

^{1}H-NMR ($CDCl_3$, ppm): δ 7.65 (m, 2H, 6-H and 8-H), 7.53 (d, 1H, 5-H), 7.45 (m, 2H, 1-H and 3-H), 7.40 (d, 1H, 4-H), 1.90 (m, 4H, 11-H), 1.25-1.00 (m, 20H, 12-H to 16-H), 0.83 (t, 6H, 17-H), 0.57 (m, 4H, 10-H).

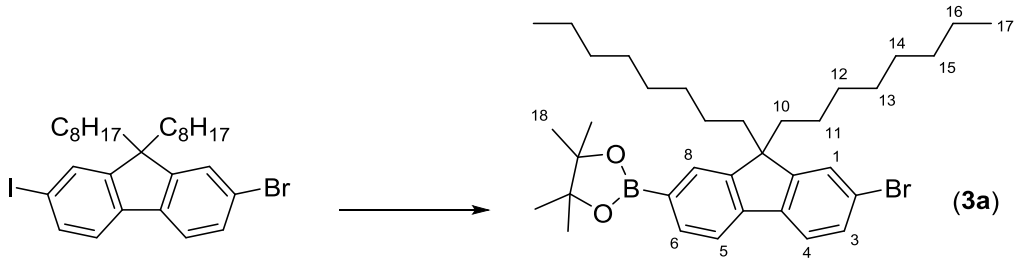

Under inert atmosphere and at 0°C, *t*BuLi (10.0 mmol, 6.67 mL, 1.50 M) was added to a mixture of dry THF (6.7 ml) and *t*BuMgCl (5.00 mmol, 2.94 mL, 1.70 M). This mixture was stirred for 1 hour, where after 1 equivalent (10.0 mmol, 11.1 mL, 0.90 M) was added to 2a (10.0 mmol, 5.95 g) in dry THF (10.0 mL) at 0°C. After 1 hour at 0°C, 2-*iso*propoxy-4,4,5,5-tetramethyl-1,3,2-dioxaborolane (12.0 mmol, 2.45 mL) was added and the resulting mixture was again stirred for 2 hours at 0°C. The reaction mixture was concentrated and poured into cold pentane (0°C). The formed salts were filtered off and the solvent was removed under reduced pressure. The crude product was purified by column chromatography with heptane/dichloromethane (7/3) to produce 3.41 g (57% yield) of pure **3a** as a white solid.

^{1}H-NMR ($CDCl_3$, ppm): δ 7.80 (d, 1H, 6-H), 7.72 (s, 1H, 8-H), 7.66 (d, 1H, 5-H), 7.57 (d, 1H, 3-H), 7.45 (m, 2H, 1-H and 4-H), 1.95 (m, 4H, 11-H), 1.37 (s, 12H, 18-H), 1.10 (m, 20H, 12-H to 16-H), 0.82 (t, 6H, 17-H), 0.56 (m, 4H, 10-H).

*3.2.2. 2-(5-Bromo-4-((S)-3,7-dimethyloctylthiophene-2-yl)-4,4,5,5-tetramethyl-1,3,2-dioxaborolane (**4b**)*

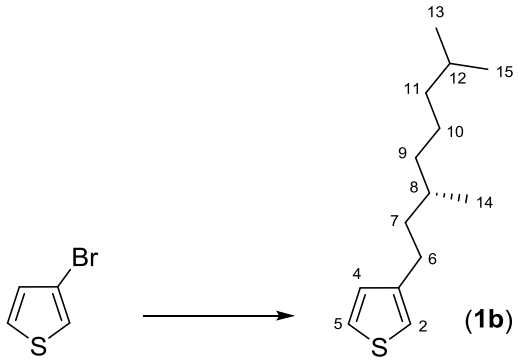

Under argon atmosphere, a solution of (*S*)-1-bromo-3,7-dimethyloctane (76.0 mmol, 16.8 g) in dry diethyl ether (100 mL) is added dropwise to a suspension of Mg curls (80.0 mmol, 1.91 g) in dry diethyl ether (20 mL) and the reaction mixture spontaneously refluxed for 2 hours. This suspension, cooled at room temperature, was then transferred to a solution of 3-bromothiophene (71.5 mmol, 6.7 mL) and Ni(dppp)Cl_2 (0.730 mmol, 301 mg). After 2h of reflux, the reaction mixture is poured into a 2 M HCl solution at 0°C and the salts filtered off. The filtrate is extracted with diethyl ether and the organic layers become washed successively with saturated $NaHCO_3$ solution and brine. After drying over $MgSO_4$, filtration and evaporation, the crude product is purified by vacuum distillation to afford 8.59 g (50% yield) of **1b** as a colorless oil.

^{1}H-NMR ($CDCl_3$, ppm): δ 7.23 (dd, 1H, 4-H), 6.93 (m, 2H, 2-H and 5-H), 2.72-2.52 (m, 2H, 6-H), 1.70-1.60 (m, 1H, 7-H), 1.50-1.40 (m, 3H, 7-H and 8-H and 12-H), 1.38-1.10 (m, 6H, 9-H to 11-H), 0.94 (d, 3H, 14-H), 0.89 (d, 6H, 13-H and 15-H).

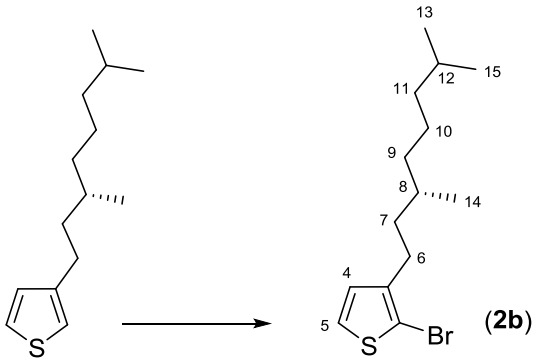

A solution of 1b (38.2 mmol, 8.59 g) in THF (100 mL) is purged with argon, protected from light and cooled to 0°C. NBS (38.2 mmol, 6.70 g) was added portion-wise at 0°C and the reaction mixture was left stirring at room temperature overnight. Water is then added

and the mixture extracted with heptane. The organic layer is successively treated with $NaHSO_3$, NaOH (20 mol% aq.), $NaHCO_3$ and brine solutions. Dried over $MgSO_4$, filtrated and concentrated, the crude product is purified through column chromatography (SiO_2, heptane) to obtain 10.6 g (91% yield) of **2b** as a colorless oil.

^{1}H-NMR ($CDCl_3$, ppm): δ 7.19 (d, 1H, 4-H), 6.80 (d, 1H, 5-H), 2.64-2.49 (m, 2H, 6-H), 1.70-1.10 (m, 10H, 7-H to 12-H), 0.93 (d, 3H, 14-H), 0.87 (d, 6H, 13-H and 15-H).

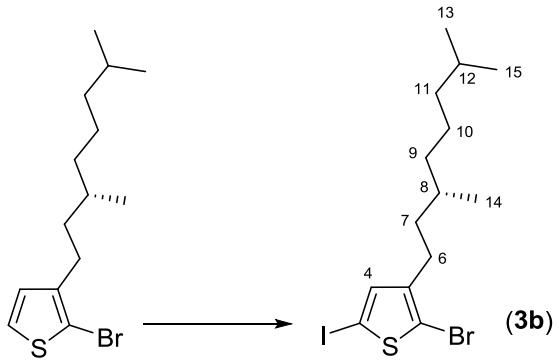

(**3b**)

To a solution of 2b (34.8 mmol, 10.6 g) in DCM (150 mL), purged with argon and cooled to 0°C, I_2 (17.4 mmol, 4.42 g) and (diacetoxyiodine)benzene (17.4 mmol, 5.60 g) are added. The reaction mixture is left stirring at room temperature for 4h and then extracted with diethyl ether. The organic layer is washed with a $NaHSO_3$ and brine solutions, before drying over $MgSO_4$. After filtration and concentration, the crude product is purified through vacuum distillation to obtain 21.6 g (62% yield) of **3b** as a yellow oil.

^{1}H-NMR ($CDCl_3$, ppm): δ 6.96 (s, 1H, 4-H), 2.64-2.44 (m, 2H, 6-H), 1.60-1.47 (m, 2H, 7-H), 1.45-1.05 (m, 8H, 8-H to 12-H), 0.94 (d, 3H, 14-H), 0.89 (d, 6H, 13-H and 15-H).

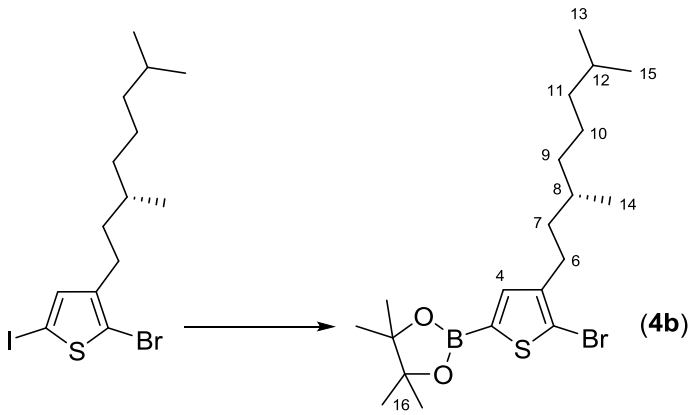

(**4b**)

Under inert atmosphere and at 0°C, a solution of *i*PrMgCl·LiCl in THF (6.90 mmol, 5.60 mL; 1.22 M) was added dropwise to a solution of 3b (6.91 mmol, 2.97 g) in dry THF

(15 mL). After stirring for 30 minutes, 2-*iso*propoxy-4,4,5,5-tetramethyl-1,3,2-dioxaborolane (8.30 mmol, 1.69 mL) was added and the resulting mixture was again stirred for 2 hours at 0°C. The reaction mixture was concentrated and poured into cold pentane (0°C). The formed salts were filtered off and the solvent and impurities were removed under reduced pressure, to afford 2.45 g (83% yield) of pure **4b** as a brown oil.
^{1}H-NMR ($CDCl_3$, ppm): δ 7.32 (s, 1H, 4-H), 2.64-2.47 (m, 2H, 6-H), 1.62-1.08 (m, 22H, 7-H to 12-H and 16-H), 0.92 (d, 3H, 14-H), 0.86 (d, 6H, 13-H and 15-H).

3.3. Synthesis of polymer

*3.3.1. Poly(9,9-dioctylfluorene)-b-poly(3-((S)-3,7-dimethyloctyl)thiophene) (**POF-b-P3OT***)*

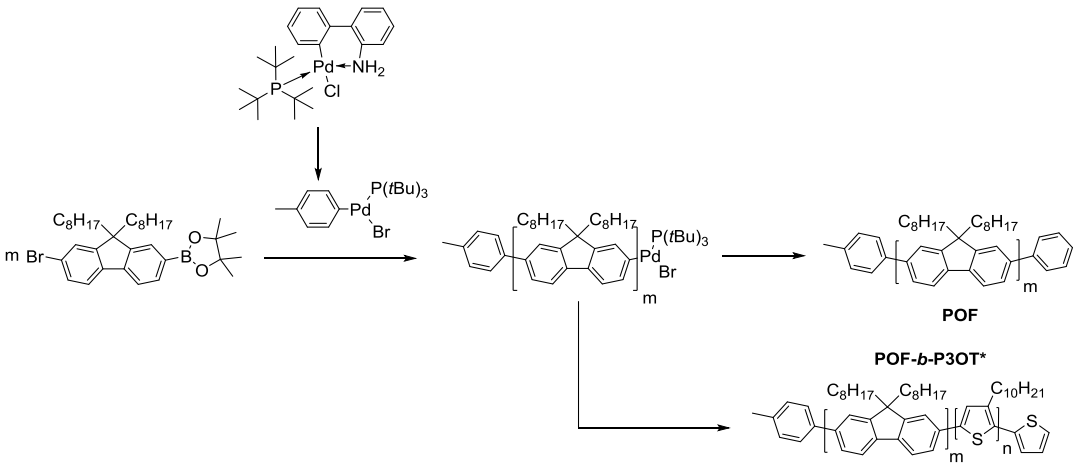

All reagents and solvents are degassed 7 times prior to use. To the palladacycle precatalyst (36.0 µmol, 18.5 mg) in THF (1.5 mL) a 4-bromotoluene solution in THF (60.0 µmol, 240 µL, 0.25 M) and a K_2CO_3 solution in H_2O (2.00 mmol, 1.50 mL, 2.0 M) are added and stirred for 40 minutes at room temperature. Next, a solution of 3a (300 µmol, 179 mg) in THF (15 mL) is added and the mixture is stirred for 6 hours at 25°C. 6.00 mL (100 µmol) is removed from the solution and added to phenyl-boronic ester (100 µmol, 20.4 mg) in THF (2.5 mL) to quench the POF block. This mixture is stirred for 1 hour at room temperature. To the remaining polymerization solution, a solution of 4b (400 µmol, 172 mg) in THF (2 mL) and K_2CO_3 in H_2O (0.100 mmol, 50 µL, 2.0 M) is cannulated. This mixture is stirred for 1 hour at 0°C, where after a solution of thiophene boronic ester (200 µmol, 42.0 mg) in THF (2.5 mL) is added and stirred for another hour to terminate the polymerization. Both terminated polymerization mixtures are concentrated,

precipitated in methanol and purified by Soxhlet extraction with methanol and chloroform consecutively. The chloroform soluble fraction was concentrated and again precipitated in methanol. The block copolymer is further purified via preparative GPC. The final homopolymer (**POF**, 29.7 mg) and the final block copolymer (**POF-*b*-P3OT***, 71.5 mg) have a light green and dark red colour, respectively.

3.4. Methods and characterization

^{1}H-NMR spectra were recorded on a Bruker Avance 400 MHz spectrometer.

Gel permeation chromatography (GPC) measurements were carried out on a Shimadzu LC20 GPC system. The column is a PLgel 5μm mixed-D type column and the detection system consists of a differential refractometer and a UV-vis spectrophotometer. The GPC system is calibrated towards polystyrene standards (purchased from Polymer Laboratories). Before measuring, the polymers are dissolved in THF (c ≈ 1 mg/mL) and filtered over a pore size of 0.2 μm.

The preparative GPC measurements were performed with the same apparatus, but two PL gel 10 μm 500 Å columns were used.

The concentration of the start solution in the solvatochromism experiments was approximately 0.03 mg/mL in chloroform and the methanol was added at a speed of 0.25 mL/min with an automatic infusion pump. The UV-vis spectra were measured on a Perkin Elmer Lambda 900 spectrometer.

CD spectra were recorded on a JASCO J-810 spectrometer.

3.5. ^{1}H-NMR spectra

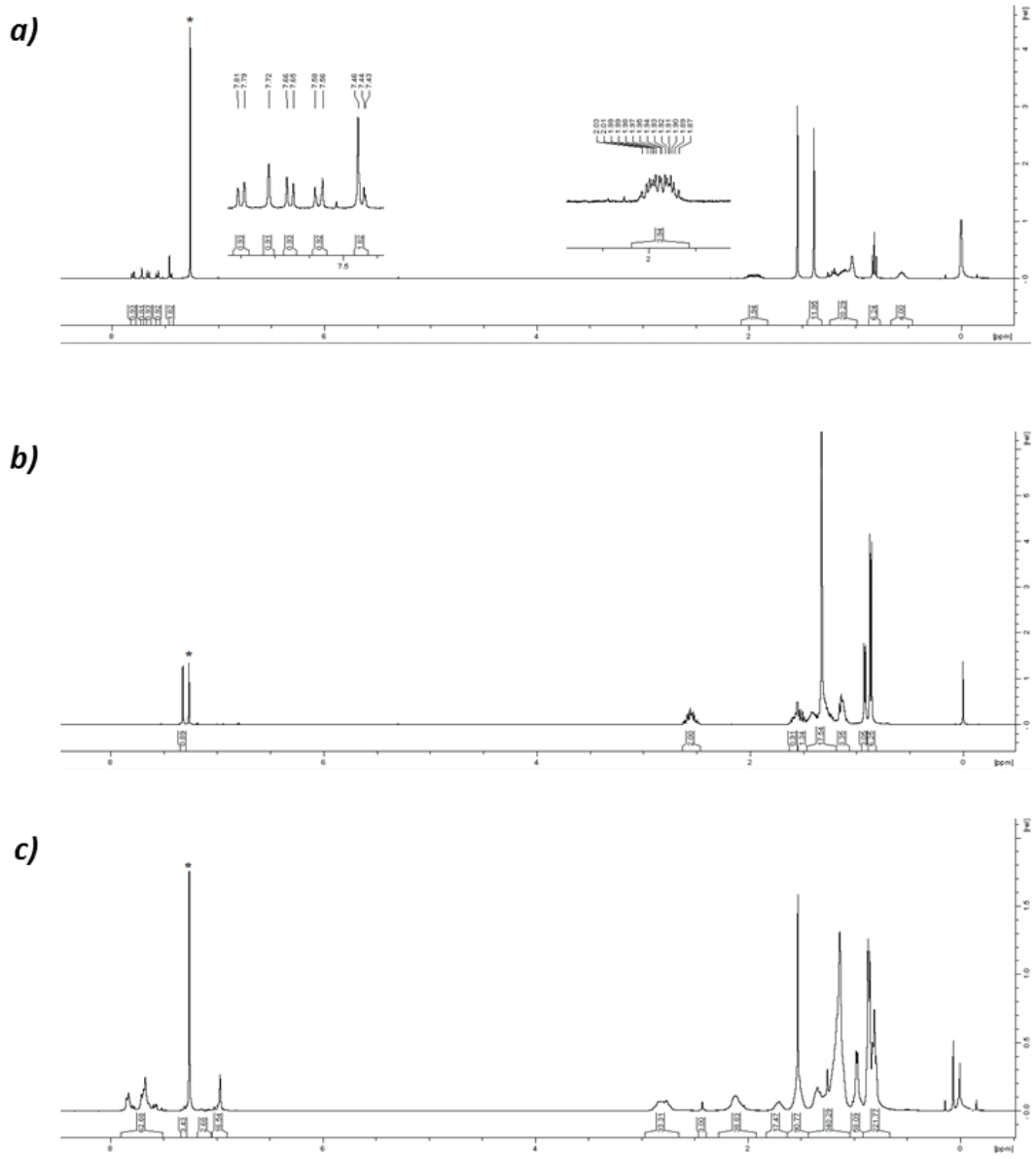

Figure 12. ^{1}H-NMR spectra of **3a** (a), **4b** (b) and **POF-*b*-P3OT*** (c). Asterisk: solvent resonances.

References

[1] A. Yokoyama, R. Miyakoshi, T. Yokozawa, *Macromolecules* **37** (2004) 1169–1171.
[2] E. E. Sheina, J. Liu, M. C. Lovu, D. W. Laird, R. D. McCullough, *Macromolecules* **37** (2004) 3526–3528.
[3] L. Verheyen, P. Leysen, M. P. Van Den Eede, W. Ceunen, T. Hardeman, G. Koeckelberghs, *Polym. Chem.* **108** (2017) 521–546.
[4] L. Huang, S. Wu, Y. Qu, Y. Geng, F. Wang, *Macromolecules* **41** (2008) 8944–8947.
[5] F. Brouwer, J. Alma, H. Valkenier, T. P. Voortman, J. Hillebrand, R. C. Chiechi, J. C. Hummelen, *J. Mater. Chem.* **21** (2011) 1582-1592.
[6] K. B. Seo, I. H. Lee, J. Lee, I. Choi, T. L. Choi, *J. Am. Chem. Soc.* **140** (2018) 4335–4343.
[7] K. Kosaka, Y. Ohta, T. Yokozawa, *Macromol. Rapid Commun.* **36** (2015) 373–377.
[8] C. G. Dong, Q. S. Hu, *J. Am. Chem. Soc.* **127** (2005) 10006–10007.
[9] A. Yokoyama, H. Suzuki, Y. Kubota, K. Ohuchi, H. Higashimura, T. Yokozawa, *J. Am. Chem. Soc.* **129** (2007) 7236–7237.
[10] H. H. Zhang, C. H. Xing, G. B. Tsemo, Q. S. Hu, *ACS Macro Lett.* **2** (2013) 10–13.
[11] H. H. Zhang, W. Peng, J. Dong, Q. S. Hu, *ACS Macro Lett.* **5** (2016) 656–660.
[12] M. Verswyvel, F. Monnaie, G. Koeckelberghs, *Macromolecules* **44** (2011) 9489–9498.
[13] T. Yokozawa, R. Suzuki, M. Nojima, Y. Ohta, A. Yokoyama, *Macromol. Rapid Commun.* **32** (2011) 801–806.
[14] J. K. Lee, S. Ko, Z. Bao, *Macromol. Rapid Commun.* **33** (2012) 938–942.
[15] C. Carlini, F. Ciardelli, P. Pino, *Die Makromol. Chemie* **119** (1968) 244–248.
[16] M. M. Green, M. P. Reidy, R. D. Johnson, G. Darling, D. J. O'Leary, G. Willson, *J. Am. Chem. Soc.* **111** (1989) 6452–6454.
[17] A. J. Bur, L. J. Fetters, *Chem. Rev.* **76** (1976) 727–746.
[18] B. M. W. Langeveld-Voss, R. J. M. Waterval, R. J. Janssen, E. W. Meijer, *Macromolecules* **32** (1999) 227–230.
[19] X. Yang, J. Loos, *Macromolecules* **40** (2007) 1353–1362.
[20] I. Botiz, N. Stingelin, *Materials* **7** (2014) 2273–2300.
[21] J. Huang, S. Lu, P. A. Chen, K. Wang, Y. Hu, Y. Liang, M. Wang, E. Reichmanis, *Macromolecules* **52** (2019) 4749-4756.
[22] F. C. Krebs, M. Jørgensen, *Polym. Bull.* **50** (2003) 359–366.
[23] S. S. Sun, *Sol. Energy Mater. Sol. Cells* **79** (2003) 257–264.
[24] R. A. Segalman, B. McCulloch, S. Kirmayer, J. J. Urban, *Macromolecules* **42** (2009) 9205–9216.
[25] S. B. Darling, *Energy Environ. Sci.* **2** (2009) 1266-1273.
[26] C. Guo, Y. H. Lin, M. D. Witman, K. A. Smith, C. Wang, A. Hexemer, J. Strzalka, E. D. Gomez, R. Verduzco, *Nano Lett.* **13** (2013) 2957–2963.
[27] X. Yu, H. Yang, S. Wu, Y. Geng, Y. Han, *Macromolecules* **45** (2012) 266–274.
[28] K. Van den Bergh, J. Huybrechts, T. Verbiest, G. Koeckelberghs, *Chem. A Eur. J.* **14** (2008) 9122–9125.
[29] K. Van den Bergh, I. Cosemans, T. Verbiest, G. Koeckelberghs, *Macromolecules* **43**

(2010) 3794–3800.
[30] M. M. Bouman, E. E. Havinga, R. A. J. Janssen, E. W. Meijer, *Mol. Cryst. Liq. Cryst. Sci. Technol. Sect. A. Mol. Cryst. Liq. Cryst.* **256** (1994) 439–448.
[31] B. M. W. Langeveld-Voss, M. M. Bouman, M. P. T. Christiaans, R. A. J. Janssen, *Polym. Prepr.* **37** (1996) 499–500.
[32] S. H. Chen, H. L. Chou, A. C. Su, S. A. Chen, *Macromolecules* **37** (2004) 6833–6838.
[33] S. H. Chen, A. G. Su, C. H. Su, S. A. Chen, *Macromolecules* **38** (2005) 379–385.
[34] S. H. Chen, A. C. Su, S. A. Chen, *J. Phys. Chem. B* **109** (2005) 10067–10072.
[35] D. W. Bright, F. B. Dias, F. Galbrecht, U. Scherf, A. P. Monkman, *Adv. Funct. Mater.* **19** (2009) 67–73.
[36] J. Steverlynck, A. De Cattelle, J. De Winter, P. Gerbaux, G. Koeckelberghs, *J. Polym. Sci. Part A Polym. Chem.* **54** (2016) 1252–1258.
[37] A. J. J. Lennox, G. C. Lloyd-Jones, *Chem. Soc. Rev.* **43** (2014) 412–443.
[38] H. Zhang, C. Xing, Q. Hu, *J. Am. Chem. Soc.* **134** (2012) 13156–13159.
[39] K. Kosaka, T. Uchida, K. Mikami, Y. Ohta, T. Yokozawa, *Macromolecules* **51** (2018) 364–369.
[40] J. A. Carrillo, M. J. Ingleson, M. L. Turner, *Macromolecules* **48** (2015) 979–986.
[41] A. Sui, X. Shi, H. Tian, Y. Geng, F. Wang, *Polym. Chem.* **5** (2014) 7072–7080.
[42] R. Tkachov, V. Senkovskyy, H. Komber, J. U. Sommer, A. Kiriy, *J. Am. Chem. Soc.* **132** (2010) 7803–7810.
[43] P. Kohn, S. Huettner, H. Komber, V. Senkovskyy, R. Tkachov, A. Kiriy, R. H. Friend, U. Steiner, W. T. S. Huck, J. U. U. Sommer, *J. Am. Chem. Soc.* **134** (2012) 4790–4805.
[44] D. Neher, *Macromol. Rapid Commun.* **22** (2001) 1365–1385.
[45] U. Scherf, E. J. W. List, *Adv. Mater.* **14** (2002) 477–487.

Chapter VI

Chapter VI: OSCs - SYNTHESIS AND INVESTIGATION OF WATER SOLUBLE CONJUGATED POLYMERS

1. Introduction

1.1. Overview

The development - by means of different approaches - and investigation of several π-conjugated polythiophenes based systems, with related application in organic solar cells, have been the main object of the first part of my PhD project and thus the object of the initial chapters of this dissertation. However, despite the interesting and promising results achieved, it should be recognized that the production of OSCs very often requires the consumption of large amounts of chlorinated and/or aromatic organic toxic solvents. Indeed, there is a clear need for the next generation of photovoltaic technologies to move towards the study of large-scale environmentally friendly techniques.[1]

In this context, due to the effective combination of excellent intrinsic optoelectronic properties with unique solubilities, water/alcohol-soluble conjugated polymers (WSCPs) have attracted increasing attention in recent years.[2]

In the first place, the introduction of oligo(ethylene glycol) patterns in the polymer side chains was used as a first approach aimed to increase the solubility of the active layer materials in more green solvent, such as alcohols or, even more, water. However, since this insertion usually produces a strong reduction in the glass transition temperature and thus a limited stability of the BHJ blend morphology, the introduction of ionic features is usually preferred.[3]

In general, WSCPs are structurally composed of two main components: π-conjugated backbones and surfactant-like side chain groups (i.e. amino, phosphate, quaternary ammonium, anionic carboxyl, sulfonic groups etc.). While the conjugated backbones determine the intrinsic optoelectronic properties of WSCPs, such as their tunable absorption and fluorescence properties, in addition to electrical conductivity, the surfactant-like side groups promote solubilities in highly polar solvents and give rise to a higher dielectric constant.[3,4] In fact, not only do WSCPs show promising features for

application of environmentally friendly processing techniques to the industrial manufacturing of optoelectronic devices, but the charged side chain end groups have also been found to endow materials with extraordinary interface modification functions.[5,6]

Despite the initial research interest in WSCPs mainly focused on their application in highly selective and sensitive chemo-/biosensors,[7] water soluble materials were also successfully employed to optimize both organic light-emitting diodes and organic solar cell technologies. In particular, in addition to show potential as photoactive components in environmentally friendly solvent-processed solar cells, this type of materials can be used as electron/hole-collection layers (ECL/HCL), in order to improve the extraction and collection of charge.[8,9] For example, when WSCPs are employed as ECL, the selectively transport and block of electrons and holes – respectively – is allowed, while the diffusion and reaction between the metal electrode is suppressed.

Taking into account that conjugated backbones and surfactant like pendant groups are essential components of WSCPs, during the past few years the design of new materials has thereby mainly concentrated on two different aspects: (i) tailoring conjugated backbones to tune the intrinsic optoelectronic properties of the resulting materials and (ii) introducing various side groups to obtain desirable self-assembly properties and unique functions for the requested applications.[7]

1.2. Aim of the chapter

In this framework, the last part of my PhD project has been focused on the development and investigation of a series of water-soluble conjugated polymers such as those reported in Figure 1, bearing polar moieties – both neutral and ionic – in the side chain, with the final purpose to test them as photoactive components in OSCs.

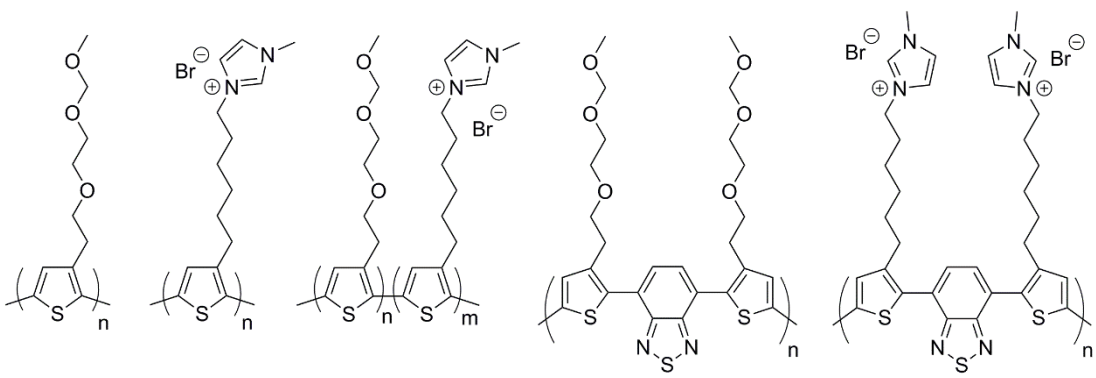

Figure 1. Planned target macromolecules

In particular, in order to fully compare their photoactivity properties with those of similar compounds previously synthesized, these organic electrolytes should have been used as the electron-donor unit in donor-acceptor systems.

Therefore, as a conclusive part of this dissertation, this final chapter will provide a brief description of the main synthetical attempts and results obtained until now.

2. Results and discussion

2.1. Synthesis of polythiophene with multi ethereal functionality in the side chain

Despite a reduction in glass transition temperature is usually displayed as a consequence of this synthetical approach, 2-(2-(methoxymethoxy)ethoxy)ethyl has been chosen as a multi ether side chain to be inserted at position 3 of the thiophene ring.

In detail, by reaction of 2-(2-thienyl)ethanol with the brominated side chain of interest, in presence of DMAP (4-dimethylaminopyridine) and N-ethyl-N-isopropyl-2-propanamine, a first attempt to synthesize 3-(2-(2-(methoxymethoxy)ethoxy)ethyl)thiophene (**1**) as starting monomer was performed.[10] However, compound **1** could only be obtained through nucleophilic substitution by using NaH as a strong base (Scheme 1);[3] moreover, not only a strong production of by-products was obtained, but its purification resulted to be particularly arduous.

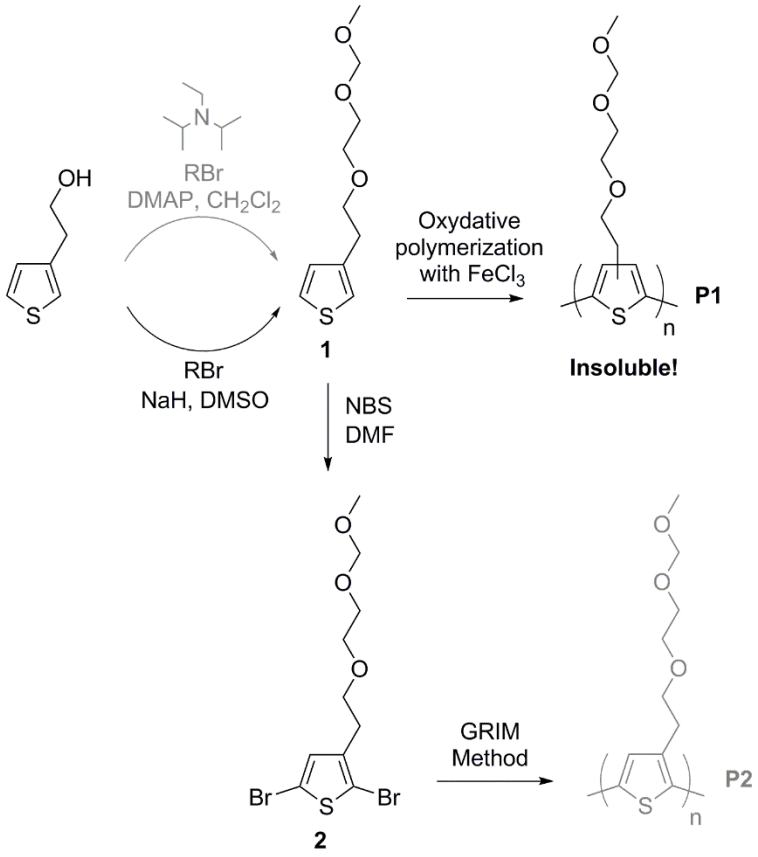

Scheme 1. Attempts to obtain poly[3-(2-(2-(methoxymethoxy)ethoxy)ethyl)thiophene].

In order to prepare the homopolymer, as a first desired target macromolecule, the synthesized material was firstly polymerized by the well-known and established procedure with iron trichloride.[11] Despite several attempts were carried out – by changing time of polymerization, monomer concentration or solvent mixture (i.e. $CHCl_3$ vs. $CHCl_3/CH_3NO_2$) – the obtained polymers (**P1**) resulted to be insoluble in the most common organic solvents as well as in water and alcohol.

Having observed the presence of strong complexation between iron and the numerous oxygen atoms present in the side chains (positive essay of iron with NH_4SCN), that could be the cause of its insolubility, a polymerization attempt of the dibromo derivative (**2**) by GRIM method – and thus in absence of iron – to the related polymeric material **P2** was also performed.[12] Unfortunately, this last method also failed.

For this reason and, most of all, as the preliminary introduction of ionic features is usually preferred, we have decided to move towards the synthesis of materials with charged side chain end groups.

2.2. Synthesis of polythiophene with ionic side chain

To synthesize the ionic homopolymer – poly[1-methyl-3-(6-(thiophen-3-yl)hexyl)-1H-imidazol-3-ium bromide] **PT6I** – we have chosen a stepwise procedure, similar to that one used for the development of double-cable systems (chapter III), involving the preparation of a non-ionic precursor by oxidative coupling with $FeCl_3$ and the subsequent substitution reaction on the bromoalkyl side chains with N-methylimidazole, affording polar 6-(1-methylimidazolium-3-yl)alkyl side chains with bromine counter ions (Scheme 2).

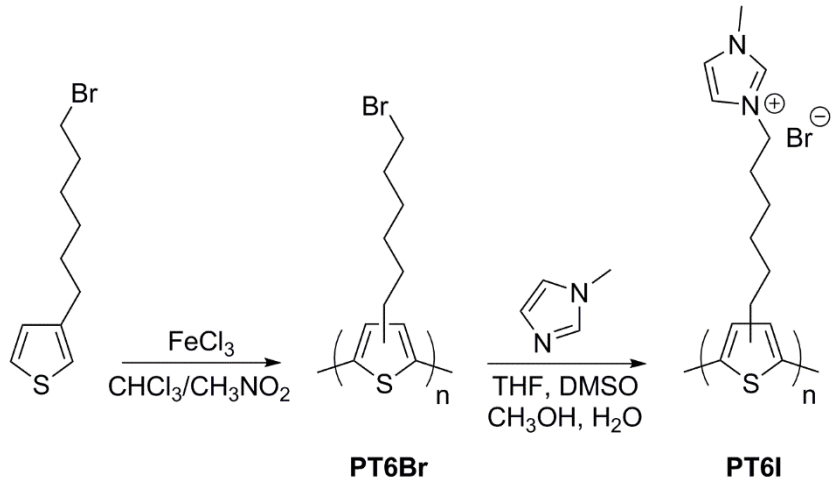

Scheme 2. Synthesis of precursor and ionic homopolymer.

In particular, after addition of N-methylimidazole to a solution of **PT6Br** (Mn = 26000 g/mol, PDI = 1.3) in THF, DMSO, MeOH and water, the functionalization under traditional heating needed 48 h to ensure complete conversion.[13] The resulting ionic polymer **PT6I** was then precipitated in THF, washed several times and used without any further purification. The material was well-soluble in water, MeOH and EtOH. By this approach, the regioregularity of the functionalized polythiophene moiety is pre-determined in the polymeric precursor and is unaffected by the post-functionalization.

2.3. Characterization of PT6I

2.3.1. ^{1}H-NMR and FT-IR spectroscopy

The success of the preparation and the structure/purity of the materials have been evaluated by ^{1}H-NMR spectroscopy: the spectra of **PT6Br** and **PT6I** - which were recorded in $CDCl_3$ and CD_3OD, respectively - are reported in Figure 2.

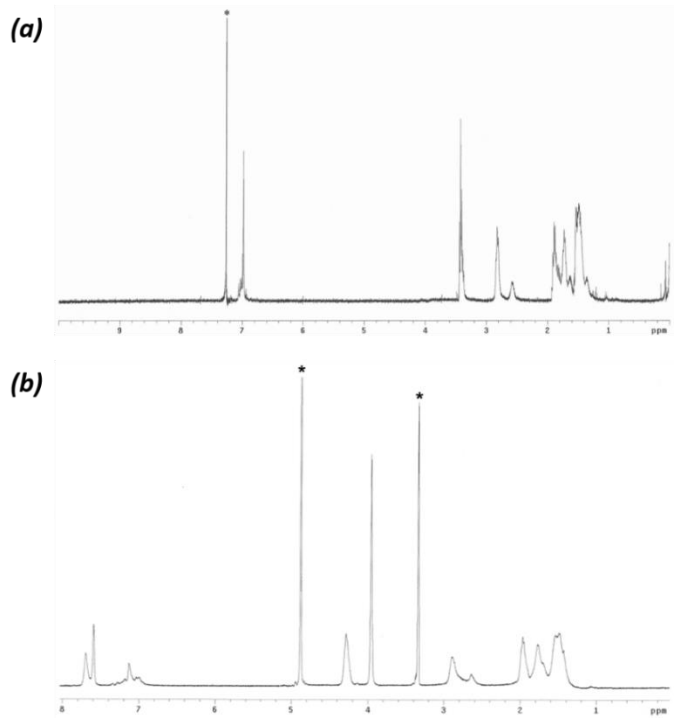

Figure 2. ^{1}H-NMR spectra of **PT6Br** (a) and **PT6I** (b). Asterisk: solvent resonances.

The complete substitution of bromide in the side chain by the 1-methylimidazolium group is first of all indicated by the absence of the signal at 3.43 ppm, related to the methylene group linked to Br. Then, the signals related to the H-protons of the imidazole ring (7.69,

7.59 and 7.11 ppm), in addition to the signal attributable to the methyl group bound to nitrogen (3.95 ppm), are also clearly visible. Moreover, two new multiplets that appear at 4.25 and 1.96 ppm can be assigned, respectively, to the -CH_2- in α and in β position to the imidazole nitrogen.

The regioregularity degree of the precursor polymer, determined by the ratio of the integrated intensities of the signals of the methylene groups linked to the thiophene ring (2.89 and 2.60 ppm), resulted to be around 70% in HT junctions. Taking into account a complete conversion to the ionic derivative, the average molecular weight of **PT6I** can be deduced to be 26200 g/mol, with unvaried PDI = 1.3.

In agreement with NMR characterization, also FT-IR spectroscopy on Ge disks gave further confirm of the identity of the ionic functionalized material synthesized: spectrum and bands, as well as their assignments, are reported in Figure 3 and Table 1.

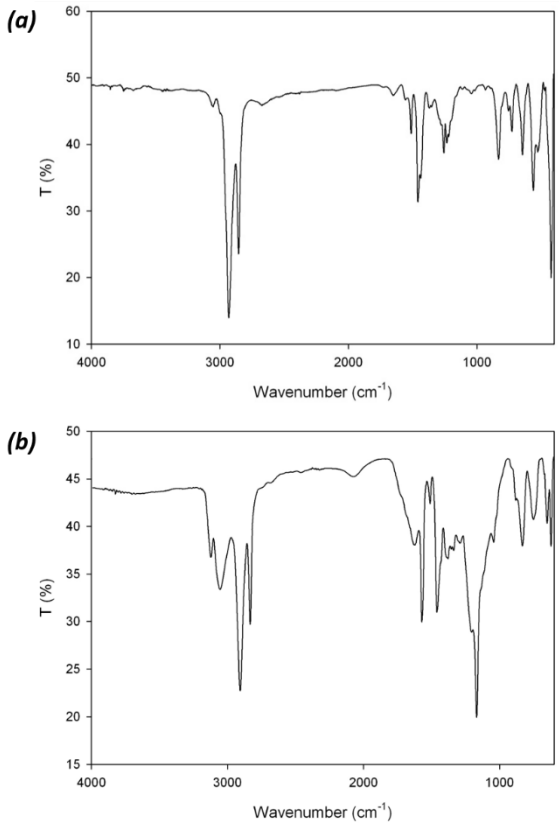

Figure 3. IR spectra of **PT6Br** (a) and **PT6I** (b).

The absence of the bands at 646 and 562 cm^{-1}, that are present in the precursor polymer **PT6Br**, indicate the complete substitution of bromine with the imidazolium moiety. As a further confirmation, the absorption at 3145, 3078, 1627, 1572, 1451, 1178, 1169, 1044 and 752 cm^{-1} which can be assigned to the new functional group, are also visible in the

spectrum of **PT6I**. The remaining absorptions are attributable to the thiophene ring and to the hexamethylene chain.

Table 1. Main IR absorption bands of **PT6Br** and **PT6I**.

Assignment	***PT6Br***	***PT6I***
ν_{as} C-H imidazolium	-	3145
ν C-H α-thiophene	-	-
ν_{s} C-H imidazolium	-	3078
ν C-H β-thiophene	3052	Emb.
ν_{as} CH_2	2931	2930
ν_{s} CH_2	2855	2856
υ_{as} imidazolium ring	-	1627, 1572
υ_{as} C=C thiophene	1512	1511
υ_{sim} C=C thiophene	1460	1461
υ_{s} imidazolium ring	-	1451
υ_{as} N-CH_3	-	1178
υ_{s} N-CH_3	-	1169
δ CH imidazolium	-	1044
γ C-H thiophene tris.	832	832
γ C-H thiophene monos.	-	-
γ -CH imidazolium	-	752
υ C-Br	646, 562	-

2.3.2. Optical properties

Starting from a solution in a good solvent – THF for **PT6Br** and CH_3OH for **PT6I** – the optical properties of both the polymers were evaluated by solvatochromism upon gradual addition of a poor solvent (CH_3OH for **PT6Br** and THF for **PT6I)** in terms of volume fraction (Figure 4a-b).

The wavelength of the maximum absorption (λ_{max}) in pure solvent is pretty similar for both the polymers (438 nm for **PT6Br** and 432 nm for **PT6I**), while the magnitude of the solvatochromic effect is significantly different. Indeed, passing from pure solvent to the maximum non-solvent molar fraction, only a 10 nm of red shift is displayed by **PT6I** compared to a bathochromic shift of 70 nm for **PT6Br**. The latter thus shows an important feature that is the excellent ability to rearrange the polymer chains already in solution, assuming a conformation really similar to the one probably assumed in the solid state.

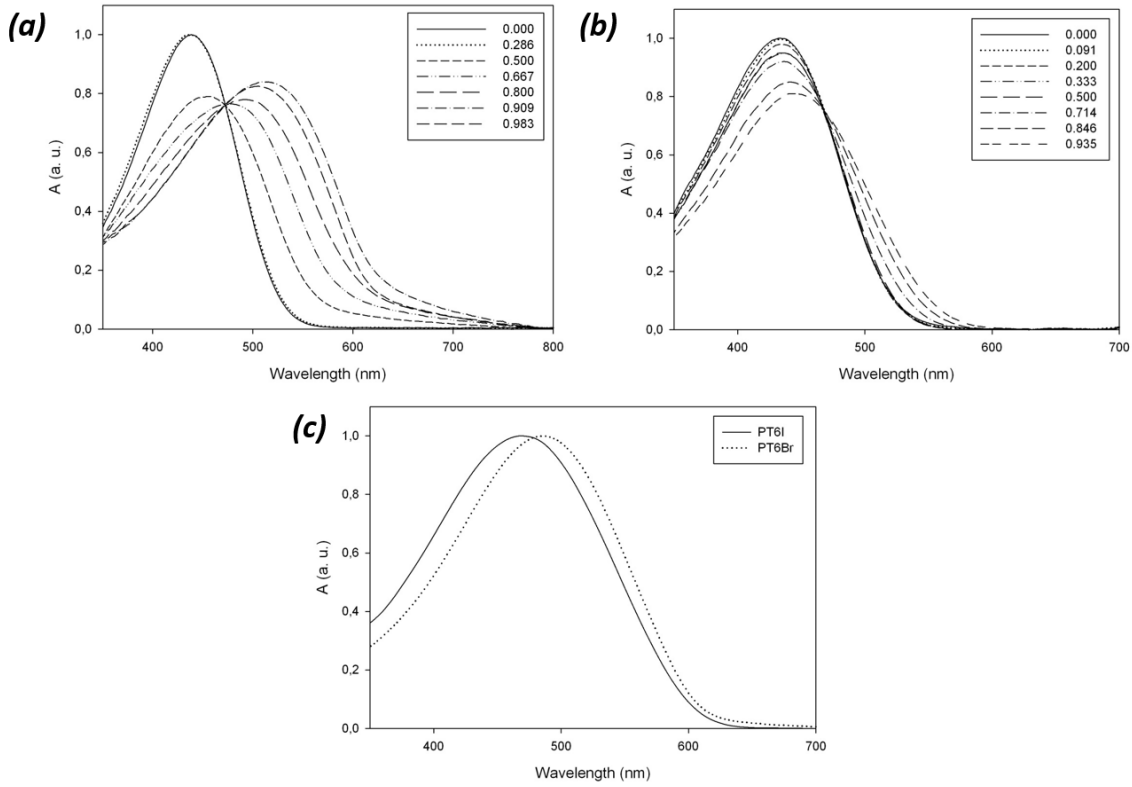

Figure 4. Absorption spectra of the solvatochromism experiments of **PT6Br** (a) and **PT6I** (b); (c) absorption spectra of polymers in thin film.

The UV-Vis spectra of the two synthesized polymers in thin film – deposited by doctor-blade from solutions in pure solvents on a quartz plate – are reported in Figure 4c.

Although it results to be less marked compared to the previously examined solvatochromic effect, a difference in the spectra of the two polymers is again obtained. In details, the absorption maxima of the two polymers are placed at 468 nm and 486 nm, respectively for **PT6I** and **PT6Br**, and correspond to an average conjugation length of 8 and 9 conjugated thiophene rings, respectively.[14]

It can be therefore hypothesized that **PT6I** is somewhat affected by the greater steric hindrance of the substituent in the side chain, which hinders the polymer chains, reducing slightly the achievement of a more planar and ordered conformation.

2.3.3. Photoactivity

The performance of the synthesized ionic polymer as photoactive layer has been investigated by fabrication of a series of organic solar cells having the following structure: ITO (80 nm)/PEDOT:PSS (100 nm)/blend of polymer and $PC_{61}BM$ 1:1 w/w (150 nm)/Al (50 nm).

As a reference cell, a sample of P3HT previously synthesized by oxidative coupling with $FeCl_3$ and having similar regiochemistry and molecular weight characteristics - Mn = 35000, PDI = 1.5 and HT = 71% - comparable to those of the polymers obtained, was used as a blend with PCBM. In particular, the **PT6I** blended with the PCBM was deposited both by chlorobenzene CB (as the reference P3HT) and by methanol, using the doctor blade technique.

In addition to the current density-voltage (J/V) curves of the devices, which are shown in Figure 5, the main photovoltaic parameters such as short-circuit current density (J_{sc}), open-circuit voltage (V_{oc}), fill factor (FF) and above all power conversion efficiency (PCE), are summarized in Table 2.

Table 2. Properties of organic solar cells prepared with blends of **PT6I** with **$PC_{61}BM$**, prepared by doctor-blade technique (preliminary results).

Blends	*J_{sc} (mA/cm^2)* [a]	*V_{oc} (V)* [b]	*FF* [c]	*PCE (%)* [d]
PT6I:$PC_{61}BM$ (from CB)	9.6	0.55	0.50	2.63
PT6I:$PC_{61}BM$ (from MeOH)	14.0	0.62	0.56	4.88
P3HT:$PC_{61}BM$ (from CB)	12.7	0.60	0.55	4.20

[a] Short circuit current density; [b] Open circuit voltage; [c] Fill factor; [d] Photovoltaic cell efficiency.

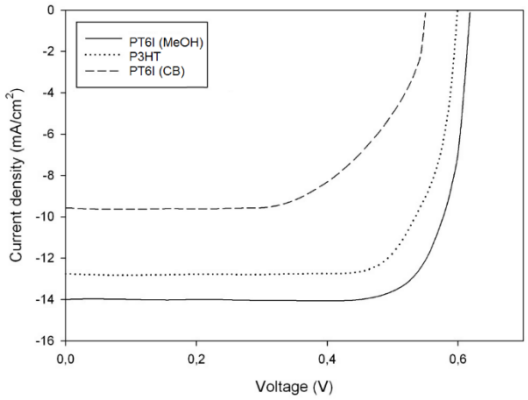

Figure 5. Current density-voltage for cells fabricated with **PT6I** and **P3HT**.

Even though only preliminary tests have been carried out, well promising results were obtained. In fact, it seems that deposition of **PT6I** from MeOH lead to the best conditions for obtaining interesting and good value of efficiency. Moreover, despite the electron-acceptor was only partially soluble in MeOH, a particularly homogeneous film of polymer was obtained by deposition from this solvent. On the other hand, in the case of the cell prepared from chlorobenzene, not only was the obtained film not homogeneous, but a strongly reduced thickness and, thus, affected morphology was produced in some areas.

2.4. Water-soluble SMOSC

As observed above, since the nucleophilic substitution with N-methylimidazolium resulted to be a simple and straightforward post-polymerization functionalization procedure, the synthesis of water soluble main-chain electron/donor acceptor systems by means of this method has been also attempted.

In particular, the final desired target macromolecule (**P3I**) should have a structure like the previous ones reported in chapter II but with ionic features in the side chains (Scheme 3).

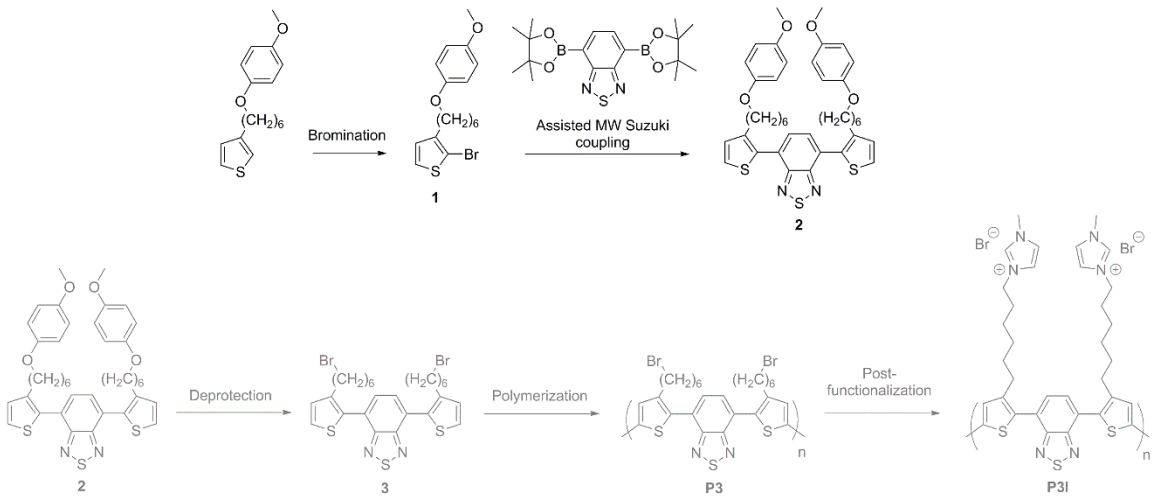

Scheme 3. Plan of synthesis of ionic side chain functionalized SMOSC derivative.

In order to limit as much as possible the chromatographic purification through silica of the brominated intermediate necessary for the cross-coupling reaction, as dehalogenation and elimination reactions could occur, a monobromination was carried out on 3-[6-(p-methoxyphenoxy)hexyl]thiophene. Indeed, the desired product (**1**) as a white precipitate was successfully obtained by extraction and subsequent precipitation at low temperature (details in experimental section).[15]

For the same reason, the Suzuki cross-coupling reaction assisted by microwave - in presence of bis(boronic acid pinacol ester) of 2,1,3-benzothiadiazole and Pd(dppf)Cl_2 as catalyst -[16] was directly carried out on the protected compound, since purification through silica column is usually necessary after this synthetical method.

However, although a first attempt of synthesis of derivative **2** was performed, attempts of purification are still in progress. Indeed, the left part of the planned scheme - as reported in Scheme 3 - will not be part of this dissertation but will be for sure part of future work.

In detail, after deprotection and subsequent polymerization to poly[4,7-bis(3-(6-bromohexyl)thiophen-2-yl)benzo[c][1,2,5]thiadiazolederivative] (**P3**), in order to avoid the formation of insoluble product, the desired ionic compound (**P3I**) should be obtained through the aforementioned post-functionalization procedure with N-methylimidazolium.

2.5. Conclusions and future perspectives

As a final part of my PhD project, water soluble conjugated systems have been studied. In particular, by means of two different synthetical approach, both neutral and ionic side chain functionalized materials were investigated.

Since the insertion of oligo(ethylene glycol) side chains resulted to be unsatisfactory, the synthesis and partial characterization of poly[1-methyl-3-(6-(thiophen-3-yl)hexyl)-1H-imidazol-3-ium bromide] was pursued by post-functionalization of a precursor polymer with 1-methylimidazole.

A preliminary study of the photoactivity of the synthesized material was carried out, obtaining particularly promising and interesting results by deposition from more "green" solvent, such as methanol.

For the future, in addition to better investigate the application in organic solar cells, further characterizations will be carried out, with particular regard to the redox behaviour and morphology of the polymer in the solid state. Moreover, also the development of the analogous imidazolium substituted SMOSC derivative will be for sure object of future study and work.

3. Experimental section

3.1. Materials

All commercial reagents and solvents were used as received unless otherwise stated. *N*-Bromosuccinimide (NBS) (Sigma-Aldrich) was recrystallized from hot water. Anhydrous solvents were prepared following literature procedures[17] and stored over molecular sieves. All manipulations involving air- or moisture-sensitive reagents were performed under nitrogen in dried glassware.

3.2. Synthesis: multi ether side chain approach

*3.2.1. 3-(2-(2-(Methoxymethoxy)ethoxy)ethyl)thiophene (**1**)*

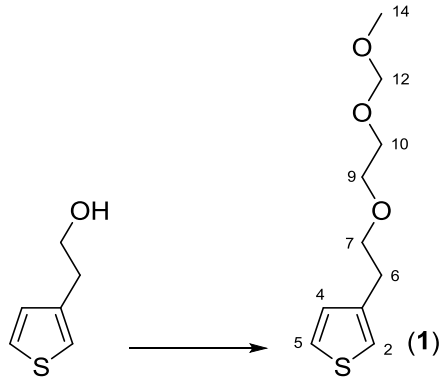

NaH (60% dispersion in mineral oil, 1.18 g, 29.6 mmol) was added to a solution of 2-(thiophen-3-yl)ethanol (1.90 g, 14.8 mmol) in DMSO (60 mL) and the resulting suspension was stirred at rt for 30 min. 1-bromo-2-(methoxymethoxy)ethane (5.00 g, 29.6 mmol) was added drop wise and the mixture was stirred for 8 h at rt. After quench of the reaction by the addition of a saturated NH_4Cl solution (20 mL), water was added, and the reaction mixture was extracted several times with diethyl ether. The organic layer was dried with $MgSO_4$, filtered and evaporated under reduced pressure. The residue was purified on a silica column with CH_2Cl_2/Et_2O 90:10. The pure fractions were collected and evaporated, to afford 1.60 g (50% yield) of **1** as a colorless oil.

^{1}H NMR ($CDCl_3$, ppm): δ 7.14 (dd, 1H, 5-H), 6.93 (dd, 1H, 2-H), 6.85 (dd, 1H, 4-H), 4.67 (t, 2H, 12-H), 3.75–3.69 (m, 4H, 9-H and 10-H), 3.68-3.64 (m, 2H, 7-H), 3.37 (s, 3H, 14-H), 3.13 (t, 2H, 6-H).

*3.2.2. 2,5-Dibromo-3-(2-(2-(methoxymethoxy)ethoxy)ethyl)thiophene (**2**)*

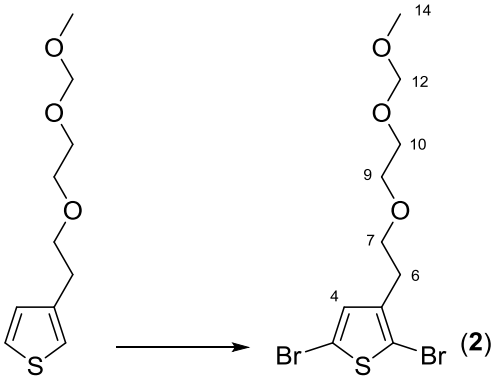

3-(2-(2-(methoxymethoxy)ethoxy)ethyl)thiophene (0.80 g, 3.7 mmol) was dissolved in THF (100 mL), cooled to 0 °C and NBS (2.17 g, 12.2 mmol) was added portion wise. The mixture was stirred at rt for 8 h in the absence of light and then quenched by pouring it into an ice-cold solution of NaOH (1M): the product was extracted with Et_2O. The organic layer was dried with $MgSO_4$, filtered and the solvent was evaporated under reduced pressure. The residue was purified on a silica plug with CH_2Cl_2/Et_2O 90:10 as the eluent. The pure fractions were collected, and the solvent was removed under reduced pressure to afford 1.25 g (90% yield) of **2** as a colorless oil.

^{1}H NMR ($CDCl_3$, ppm): δ 6.87 (s, 1H, 4-H), 4.67 (t, 2H, 12-H), 3.76–3.26 (m, 6H, 7-H, 9-H and 10-H), 3.38 (s, 3H, 14-H), 3.02 (t, 2H, 6-H).

*3.2.3. Poly[3-(2-(2-(methoxymethoxy)ethoxy)ethyl)thiophene] (**P1**) by oxidative coupling with $FeCl_3$*

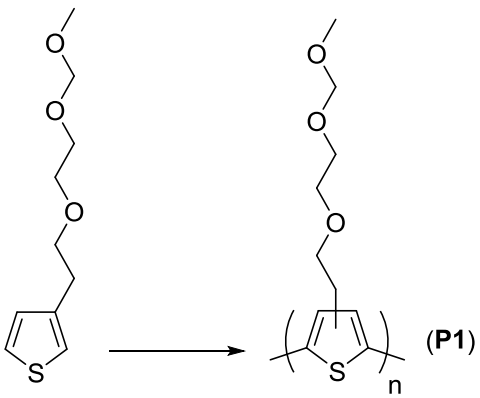

2.40 g (14.8 mmol) of iron trichloride in 15 ml of anhydrous nitromethane was dropped in 20 min, under argon and at room temperature, into a solution of 0.80 g (3.7 mmol) of **1** in 40 ml of anhydrous $CHCl_3$. After the addition was completed, the reaction mixture was

stirred for 2 h at room temperature and then added to 40 ml of THF. Despite the mixture was washed several times with 2% v/v aqueous HCl, no exhaustive extraction of the iron (III) ion was obtained (positive essay with NH_4SCN). The mixture was then poured into 150 ml of a 5% methanolic solution of HCl and the resulting precipitate filtered on a PTFE membrane (0.45 μm pore size) and washed several times with further MeOH. The recovered polymer **P1** results to be insoluble in all solvents.

3.3.Synthesis: ionic side chain approach

*3.3.1. 2-Bromo-3-(6-(4-methoxyphenoxy)hexyl)thiophene (**1**)*

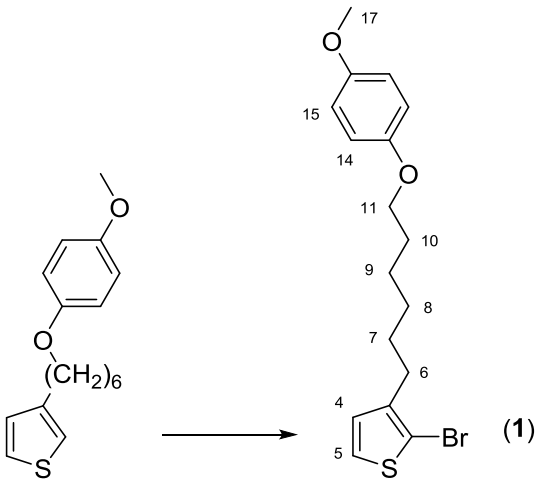

(**1**)

A solution of NBS (0.478 g, 2.69 mmol) in DMF (5 mL) has been added dropwise at -20°C to a solution of 3-(6-(4-methoxyphenoxy)hexyl)thiophene (0.650 g, 2.24 mmol) in DMF (5 mL) over a period of 6h: the solution was left to stir at rm overnight, protected from light. Then it was poured over ice (50 g) and extracted with CH_2Cl_2; the organic layers were washed with water, dried and then concentrated. The residue oil was then extracted with light petroleum and the solution cooled to -80°C to obtain 0.496 g (60% yield) of **1** as a white precipitate, which has been filtered and washed with cool light petroleum.

^{1}H NMR ($CDCl_3$, ppm): δ 7.20 (d, 1H, 5-H), 6.85 (bm, 4H, 14-H and 15-H), 6.80 (d, 1H, 4-H), 3.90 (t, 2H, 11-H), 3.80 (s, 3H, 17-H), 2.60 (t, 2H, 6-H), 1.80-1.30 (bm, 8H, 7-H, 8-H, 9-H and 10-H).

*3.3.2. 4,7-bis(3-(6-(4-methoxyphenoxy)hexyl)thiophen-2-yl)benzo[c][1,2,5]thiadiazole (**2**)*

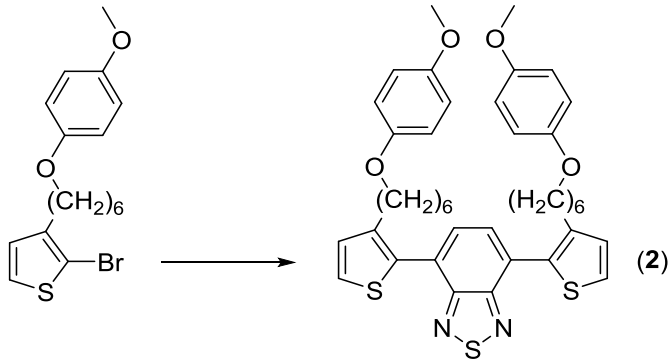

A mixture of 2-bromo-3-(6-(4-methoxyphenoxy)hexyl)thiophene (200 mg, 0.54 mmol), 2,1,3- benzothiadiazole-4,7-bis(boronic acid pinacol ester) (Sigma-Aldrich) (126 mg, 0.32 mmol), $PdCl_2$dppf (Sigma-Aldrich) (22 mg, 5% mol), $NaHCO_3$ (136 mg, 1.63 mmol) in THF/water 2:1 v/v (4.5 ml) was kept under MW irradiation at 80°C for 40 min. The reaction mixture was cooled to room temperature and poured into water (100 ml), extracted with CH_2Cl_2 and finally washed with water. After drying (Na_2SO_4) and solvent evaporation at reduced pressure, efforts of purification by column chromatography of the crude product are still in occur.

*3.3.3. Poly[1-methyl-3-(6-(thiophen-3-yl)hexyl)-1H-imidazol-3-ium bromide] (**PT6I**)*

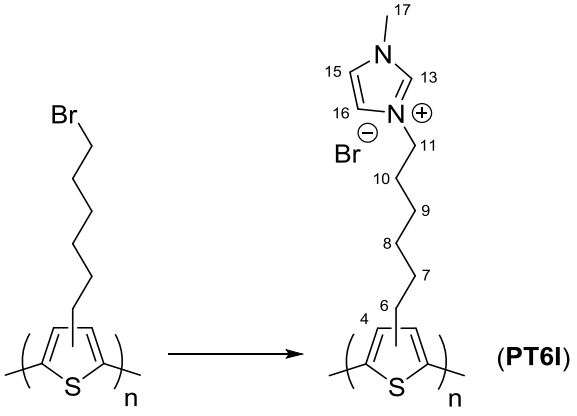

In a three-necked flask, 1.99 g (24.2 mmol) of 1-methylimidazole is added to a solution of PT6Br (0.300 g, 1.21 mmol) in 40 ml of THF, 15 ml of DMSO, 15 ml of CH_3OH and 10 ml of water. The reaction mixture is refluxed (58 ° C) for 2 days and then poured into

400 ml of THF, to obtain a solid. The polymer was filtered and dried carefully, to afford 0.27 g of **PT6I** (yield 90%) as a dark-red powder.

^{1}HNMR (CD_3OD, ppm): δ 7.69 (m, 1H, 13-H), 7.59 (m, 1H, 16-H), 7.11 (m, 1H, 15-H), 7.00 (m, 1H, 4-H), 4.25 (m, 2H, 11-H), 3.95 (s, 3H, 17-H), 2.89 and 2.60 (2m, 2H, 6-H), 1.96 (m, 2H, 10-H), 1.77 (m, 2H, 7-H), 1.60-1.35 (m, 4H, 8-H and 9-H).

3.4.Methods and characterization

Microwave (MW) irradiation was performed in a Milestone Microsynth Labstation operating at 2450 MHz and equipped with pressure and temperature sensors.

^{1}H-NMR spectra were recorded on a Varian Mercury 400 (400 MHz) spectrometer at room temperature. Chemical shifts are given in ppm.

Molecular mass and polidispersity of the precursor polymer was determined in THF by gel permeation chromatography (GPC) on a HPLC Lab Flow 2000 apparatus equipped with a Rheodyne 7725i injector, a Phenomenex Phenogel mixed bed MXL type column and an RI K-2301 KNAUER detector. The calibration curve was obtained using monodisperse polystyrene standards.

UV-Vis spectra were run by using a Perkin Elmer Lambda 20 at room temperature on 1.3 10^{-3} M THF and CH_3OH solutions in 0.1 and 1 cm quartz cells. Solid state measurements were made on polymer samples cast from THF and CH_3OH solutions on quartz slides by the doctor-blade technique.

Organic solar cells were fabricated on commercial ITO-coated glass substrates (2.5 × 2.5 cm, surface resistance 20 Ω/sq) according to the following procedure: the ITO layer was partially etched with acid (aq. HCl 10% wt.) and heated at 60°C for 15 min in order to obtain a final area of 1.5 x 1.0 cm covered by indium tin oxide. The substrate was then cleaned using distilled water followed by 2-propanol, and finally dried by a gentle nitrogen flow. A conductive thin layer of poly(3,4-ethylenedioxythiophene):polystyrene sulfonic acid (Sigma-Aldrich, PEDOT:PSS, 2.8% wt., dispersion in water), diluted 1:1 v/v with isopropanol, was deposited using the doctor blade technique over the previously treated ITO glass and subsequently heated in a Büchi GKR-50 glass oven at 120°C for 2h under vacuum. The active layer constituted by the synthesized polymer sample was cast from chlorobenzene/methanol solution (5 mg/ml) by doctor-blade technique and then annealed under vacuum at 120°C for 30 min. The device fabrication was completed by thermal evaporation of the Al electrode over the active layer through a shadow mask using an

Edwards 6306A coating system operating at 10-6 mmHg (final active area of 1.0 × 1.0 cm). The current-voltage (I-V) characteristics and PCE were measured in air at room temperature using a Keithley 2401 source meter under the illumination of an Abet Technologies LS150 Xenon Arc Lamp Source AM 1.5 Solar Simulator (100 mW/cm2), calibrated with an ILT 1400-BL photometer. The final structure of the device was: ITO (~ 80 nm)/PEDOT:PSS (~ 120 nm)/active layer (~ 100 nm)/Al (~ 50 nm).

3.5. ^{1}H-NMR spectra

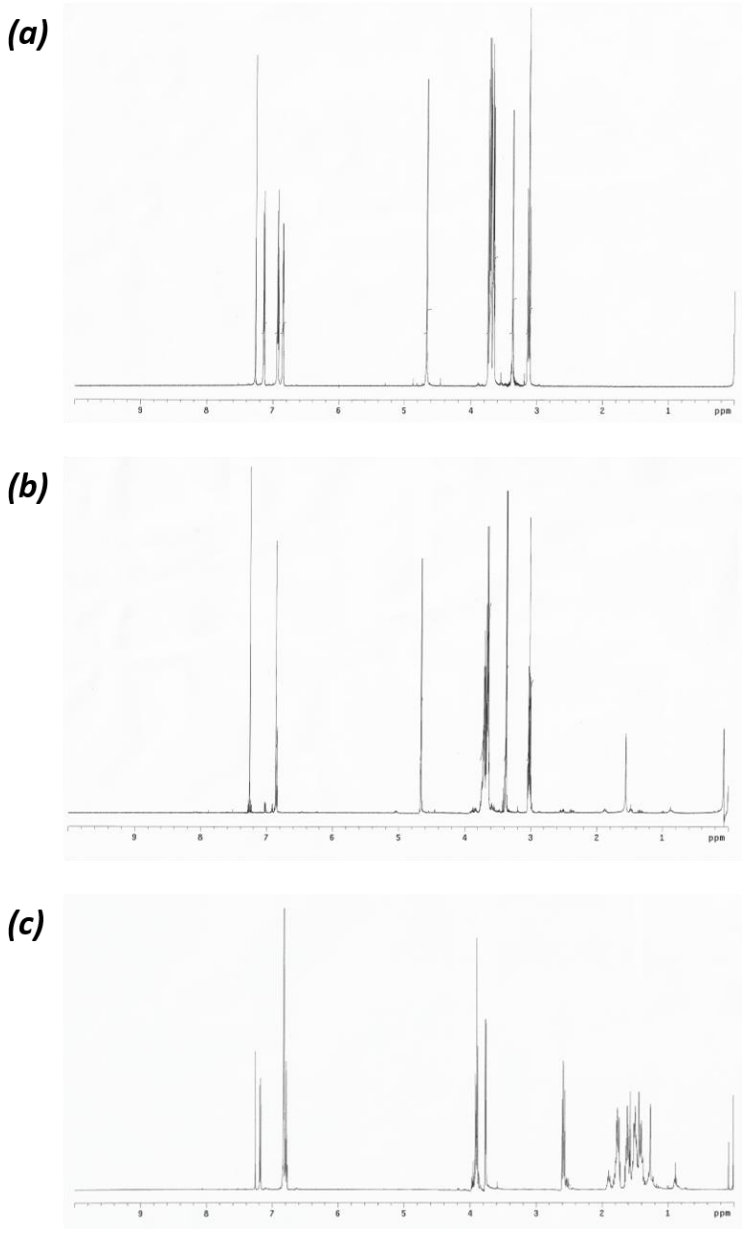

Figure 6. ^{1}HNMR spectra of (a) 3-(2-(2-(methoxymethoxy)ethoxy)ethyl)thiophene, (b) 2-bromo-3-(2-(2-(methoxymethoxy)ethoxy)ethyl)thiophene and (c) 2-bromo-3-(6-(4-methoxyphenoxy)hexyl)thiophene.

References

[1] D. J. Burke, D. J. Lipomi, *Energy Environ Sci* **6** (2013) 2053-2066.
[2] M. Lanzi, E. Salatelli, L. Giorgini, A. Mucci, F. Pierini, F. P. Di Nicola, *European Polymer Journal* **97** (2017) 378-388.
[3] T. Ghoos, J. Brassinne, C. Fustin, J. Gohy, M. Defour, N. Van den Brande, B. Van Mele, L. Lutsen, D. J. Vanderzande, W- Maes, *Polymer* **54** (2013) 6293-6304.
[4] L. J. A. Koster, S. E. Shaheen, J. C. Hummelen, *Adv Energy Mater* **2** (2012) 1246-1253.
[5] F. Huang, H. B. Wu, Y. Cao, *Chem. Soc. Rev.* **39** (2010) 2500–2521.
[6] C. M. Zhong, C. H. Duan, F. Huang, H. B. Wu, Y. Cao, *Chem. Mater.* **23** (2011) 326–340.
[7] C. Duan, K. Zhang, C. Zhong, F. Huang, Y. Cho, *Chem. Soc. Rev.* **42** (2013) 9071-9104.
[8] J. H. Seo, A. Gutacker, Y. M. Sun, H. B. Wu, F. Huang, Y. Cao, U. Scherf, A. J. Heeger, G. C. Bazan, *J. Am. Chem. Soc.* **133** (2011) 8416–8419.
[9] K. Yao, L. Chen, Y. Chen, F. Li, P. Wang, *J. Mater. Chem.* **21** (2011) 13780–13784.
[10] I. Palama, F. Di Maria, I. Viola, E. Fabiano, G. Gigli, C. Bettini, G. Barbarella, *J. Am. Chem. Soc.* **133** (2011) 17777–17785.
[11] P. Costa Bizzarri, F. Andreani, C. Della Casa, M. Lanzi, E. Salatelli, *Synth. Met.* **75** (1995) 141-147.
[12] R. S. Loewe, P. C. Ewbank, J. Liu, L. Zhai, R. McCullough, *Macromolecules* **34** (2001) 4324-4333.
[13] P. Urbanek, A. Di Martino, S. Gladys, I. Kuritka, A. Minarik, E. Pavlova, D. Bondarev, *Synth. Met.* **202** (2015) 16-24.
[14] M. Q. Jiang, Science Press: Beijing, 1980, 184.
[15] A. Iraqi, J. A. Crayston, J. C. Walton, *J. Mater. Chem.* **5** (1995) 1831-1836.
[16] F. Di Maria, G. Barbarella, *J. Sulfur Chem.* **34** (2013) 627-637.
[17] D. D. Perrin, W. L. F. Armarego, D. R. Perrin, *Purification of Laboratory Chemicals*, Pergamon Press: Oxford, 1966.